EFFECTS OF CHANGES IN GLYCOLIPID CELL MEMBRANE COMPOSITION ON THE COMPOSITION OF LIPID RAFTS IN SH-SY5Y HUMAN NEUROBLASTOMA CELL LINE

Zjalić, Milorad

Doctoral thesis / Disertacija

2021

Degree Grantor / Ustanova koja je dodijelila akademski / stručni stupanj: **Josip Juraj Strossmayer University of Osijek, Faculty of Medicine Osijek / Sveučilište Josipa Jurja Strossmayera u Osijeku, Medicinski fakultet Osijek**

Permanent link / Trajna poveznica: https://urn.nsk.hr/urn:nbn:hr:152:053673

JOSIP JURAJ STROSSMAYER UNIVERSITY OF OSIJEK

FACULTY OF MEDICINE OSIJEK

Milorad Zjalić

EFFECTS OF CHANGES IN GLYCOLIPID CELL MEMBRANE COMPOSITION ON THE COMPOSITION OF LIPID RAFTS IN SH-SY5Y HUMAN NEUROBLASTOMA CELL LINE

Doctoral dissertation

Osijek, 2021

JOSIP JURAJ STROSSMAYER UNIVERSITY OF OSIJEK

FACULTY OF MEDICINE OSIJEK

Milorad Zjalić

EFFECTS OF CHANGES IN GLYCOLIPID CELL MEMBRANE COMPOSITION ON THE COMPOSITION OF LIPID RAFTS IN SH-SY5Y HUMAN NEUROBLASTOMA CELL LINE

Doctoral dissertation

Osijek, 2021

Mentor: prof. Marija Heffer, MD, PhD

Co-Mentor: prof. Marianna Pap, MD, PhD

Dissertation contains 188 pages.

The doctoral dissertation was done under the auspice of the Croatian Science Foundation project number HRZZ IP-09-2014-2324 and European Union through the European Regional Development Fund, Operational Program Competitiveness, and Cohesion, grant agreement No. KK.01.1.1.02.0015, Research and diagnostics of malignant, infectious, and rare metabolic diseases based on MALDI TOF technology. The dissertation was done in Laboratory for neurobiology in Department for medical biology and genetics at the Faculty of medicine in Osijek, and in Department for Clinical chemistry and quality control, Clinical Medical Centre Osijek.

Acknowledgements

It is my pleasure to acknowledge several individuals that were instrumental for completion of this PhD thesis.

First of all I would like to express my gratitude to my mentor Marija Heffer, Md, PhD. Without her this thesis most certnainly would not be completed. Thank you for being solver of many obstacles that were thrown in front of me and for all advices you so kindly gave. You are a true mentor and above all a friend.

Also I would like to acknowledge valuable input of my co-mentor Marianna Pap, Md, PhD for her guidance toward experiment upgrade and experiments completion. Additionally I would like to thank for invaluable suggestions you gave me during the writing part of the PhD thesis.

Special thank to the prof Željko Debeljak spec.med.biochem., prof. Dario Mandić spec.med.biochem and bacc.med.lab.diag.Ana Bandjak without whom MALDI-TOF-MS would remain only a dream. Thank you for the patience you shown in teaching me how to operate the MALDI machines and for help in data analysis.

I am gratfull to acknowledge my lab collegues Vedrana Ivić, PhD and Marta Balog PhD for keeping my teaching burden minimal during experiments and for sharing your knowledge of the lab and the life. Additionally I would thank our tehchnitians Nena Arvaj and Darija Balonek Nikolić for being present in times of most need.

The acknowledgment and special gratitude is aimed to my two friends and collegues Monika Berecki and Marina Čović who aided me for many hours with tehcnical part of experiments. You two shined most in the time of darkness.

To my friends Edi Rođak, Aleta Bukvić, Ivana Jelavić, Vjera Ninčević, Tea Omanović and Jelena Jakab I thank you for all given support, endless hours of talk and all good times we had and will have for years to come. You made this journey pleasant and unforgettable.

I am most gracious to my family that unconditionally supported me in this endeavour and pushed me toward completion of this big chapter of my life.

Table of contents

1.INTRODUCTION 1
1.1.The basic structure of the cell membrane 1
1.2.Plasma membrane glycolipids 4
1.2.1.Structure, differentiation, and synthesis of glycolipids 4
1.2.2.Gangliosides 6
1.3.Insulin, insulin receptor and its metabolic pathway 10
1.4.Neuroplastin 16
1.5.Lipid rafts 17
1.6.Neurodegenerative diseases 18
1.6.1.Alzheimer's disease 18
1.6.2.Parkinson’s disease 20
1.6.3.Role of gangliosides in neurodegenerative diseases 21
1.7.SH-SY5Y cell line as a research model of neurodegenerative diseases 22
1.8.Modulation of glycosphingolipid metabolism 23
1.9.Why investigate glycosphingolipid metabolism? 24
2.HYPOTHESIS 25
3.OBJECTIVES 26
4.MATERIALS AND METHODS 27
4.1.Study design 27
4.2.Materials 27
4.3.Methods 27
4.3.1.Cultivation of the cells 27
4.3.2.Preparation of coverslips 28
4.3.3.Collagen type 1 growth surface coating 29
4.3.4.Cell differentiation and general experimental plan 30
4.3.5.Preparation of glycolipid metabolism modulators 31
4.3.6.MTT assay 32
4.3.7.Annexin V staining 33
4.3.8.Immunocytochemistry and histochemical staining 35
4.3.9.MALDI-TOF-MS lipid determination 41
4.3.10.Protein analysis and Western blot method 43
4.4.Statistical analysis 50
5.RESULTS 51
5.1.MTT test of cell viability 51

5.2.Annexin V cell viability stain 57
5.3.Immunocytochemistry 65
5.3.1.Immunocytochemistry of P4-RR treated cells 65
5.3.2.Immunocytochemistry of P4-SS treated cells 72
5.3.3.Immunocytochemistry of MIG treated cells 78
5.3.4.Immunocytochemistry of CBE treated cells 84
5.4.Histochemical staining of the neurites 89
5.5.MALDI-TOF MS total lipidome analysis 95
5.5.1.MALDI-TOF MS total lipidome analysis of the cells treated with insulin 96
5.5.2.MALDI-TOF MS total lipidome analysis of the cells treated with P4-RR 97
5.5.3.MALDI-TOF MS total lipidome analysis of the cells treated with P4-SS 100
5.5.4.MALDI-TOF MS total lipidome analysis of the cells treated with MIG 103
5.5.5.MALDI-TOF MS total lipidome analysis of the cells treated with CBE 107
5.6.Western blot protein analysis 111
5.6.1.Western blot analysis for P4-RR inhibitor 111
5.6.2.Western blot analysis for P4-SS inhibitor 119
5.6.3.Western blot analysis for MIG inhibitor 127
5.6.4.Western blot analysis for CBE inhibitor 135
6.DISCUSSION 143
6.1.Cell viability after inhibitor treatments 143
6.2.Immunocytochemical staining of the cells 145
6.3.Histochemical staining of the cells 149
6.4.MALDI-TOF MS lipidome analysis 151
6.5.Western blot protein analysis 158
6.6.Prospects of the study 165
6.7.Limitations of the study 165
7.CONCLUSIONS 166
8.SUMMARY 167
9.REFERENCES 169
10.BIOGRAPHY 188

Abbreviation list:

AA/Bis,	Acrylamide/bis acrylamide
AD	Alzheimer's disease
Akt	Protein kinase B
AMPA	α-amino-3-hydroxy-5-methyl-4-isoxazole propionic acid
ApoE	Apolipoprotein E
APP	Amyloid precursor protein
ATRA	all-trans-retinoic acid
Aβ	Amyloid-beta
BACE1	β-Site APP cleaving enzyme 1
BAD	BCL antagonist of the cell death
BCL	B-cell lymphoma
BDNF	Brain-derived neurotrophic factor
BSA	Bovine serum albumin
CBE	Conduritol B epoxide
CNS	Central nervous system
CRE	cAMP response element
CREB	cAMP response element-binding protein
DMSO	Dimethyl sulphoxide
DRM	Detergent-resistant microdomains
Elk- 1	E-26-like transcription factor 1
ER	Endoplasmatic reticulum
FITC	Fluorescein isothiocyanate
GalCer	Galactosyl ceramide
GalNAc	N-Acetyl galactosamine
GEF	Guanine nucleotide-exchange factor
GlcCer	Glucosyl ceramide
GLUT4	Glucose transporter 4
GSK3 α+β	Glycogen synthase kinase alpha and beta
HB	Homogenization buffer

IGF1Rβ	Insulin-like growth factor 1 receptor beta subunit
IR	Insulin receptor IR
IRS	Insulin receptor substrate
IRα	Insulin receptor alpha subunit
MAG	Myelin-associated glycoprotein
MALDI-TOF-MS	Matrix-assisted laser desorption/ionization time-of-flight mass spectrometry
MEK	MAPK/extracellular signal-regulated kinase
MIG	Miglustat
Mnk	MAPK-interacting kinase
mTORC-2	Mammalian rapamycin complex-2
NA	Noradrenaline
Neu5Ac	N-acetylneuraminic acid
NP	Neuroplastin
Np65	Neuroplastin 65
P4	D,L-threo-phenyl-2-hexadecanoylamino-3-pyrrolidino-1-propanol
pAkt	Phosphorylated protein kinase B
PBS	Phosphate buffered saline
PD	Parkinson's disease
PDK1	Phosphoinositide-dependent kinase-1
PDMP	D,L-threo-1-phenyl-2-decanoylamino-3-morpholino-1-propanol
PFA	Paraformaldehyde
pGSK3β	Phosphorylated glycogen synthase kinase alpha and beta
PIP3	Phosphatidylinositol (3,4,5)-trisphosphate
PKC	Protein kinase C
PPMP	D,L-threo-1-phenyl-2-hexadecanoylamino-3-morpholino-1-propanol
PrPC	Cellular prion protein
pTAU	Phosphorylated tau protein
RBC	Red blood cells

Rheb	Ras homolog enriched in brain
TSC 1/2	Tuberous sclerosis protein 1/2
αSyn	Alpha synuclein
βAPP	Beta amyloid precursor protein

1. INTRODUCTION

1.1. The basic structure of the cell membrane

Surrounding every living cell is a few nanometers thick, highly organized amphiphilic membrane. Membrane functions are diverse and can be categorized into several parts: setting boundaries of the cell and its organelles, serving as a hub for communication with the outside world, containing cytoplasm, and enabling localized biochemical reactions (1). Building blocks of a cell membrane can vary depending on the type of organism and tissue, or localization within a cell. Lipids are the main constituents of membranes, and several hundred different lipids have been found to make the membranes. Before eukaryotic multicellular organisms evolved, simpler life was vastly present on the Earth. This simpler, early life created a template for all other biological membranes that evolved. Archaea, which are among the oldest living organisms and occupy some of the harshest environments, have a membrane made mainly of cross-connected isoprenoid chains (2). This arrangement was necessary due to their evolution in hydrothermal vents deep under the ocean and hot muddy shales of Precambrian era Earth. Arranging the membrane in this fashion makes it very stable at high temperatures. It is organized as a structural monolayer, otherwise, the membrane would disperse under high heat and pressure (3). As the Earth cooled down, new ecological niches emerged. Occupying less harsh and more manageable biomes allowed the next evolutionary step to occur, and the first true lipid bilayer was observed in bacteria.

Bacterial lipids are primarily characterized by glycerol, which serves as a scaffold for three phosphates linked to fatty acids. Forming a true bilayer allowed diversity and quick adaptation to environmental changes by enabling rapid modification of a cell membrane according to the environmental change (4,5). Further down the evolution lane, significant differences in basic building blocks between eukaryotic and bacterial membranes are observable. If not all eukaryotes, the majority have cholesterol or its derivatives integrated into a cell membrane, but only a handful of bacterial clades contain it (6). Other exceptions regarding membrane lipid composition are endosymbiotic organelles. Even though mitochondria and plastids originated from bacteria, specific changes had to happen to accommodate the symbiotic relationship. In their membranes, specific C-type lipids, cardiolipins, and galactolipids can be found. All those exceptions

and membrane modifications serve to stabilize the membrane, make electron transport chains possible, and enable more complex integration with the rest of the cell (7).

The eukaryotic plasma membrane is the cell's outer-most border and serves as a communication, kinaesthetic, and metabolic interface. The fact that humans and all mammalian experimental models are eukaryotes somewhat simplifies basic research in field of membrane dynamics and oragniasation. Membrane models are extensively used in studies due to their experimental flexibility and a wide range of suitable modifications. One of the first models was the red blood cell (RBC) membrane. Mammalian RBC does not have nuclei or intracellular membranes, making RBCs good candidates for purifying clean outer membranes. Those experiments showed that phospholipid forms a bilayer (8). This early research also had a mission to find which building blocks are included in membrane formation. It was known that membranes behaved partly like lipids and could form micelles, like those previously observed with soaps and detergents, and had to have a polar part. Besides fatty acid chains and glycerol; choline, serine, or ethanolamine is found attached to the glycerol moiety forming a polar part of molecules called phospholipids. Sphingomyelin can be found alongside phospholipids, and those four molecules together form the majority of mammalian biological membranes. Interestingly, the outer part of the membrane is mainly assembled out of phosphatidyl-choline and sphingomyelin. The inner part of the membrane is made of phosphatidyl-ethanolamine and phosphatidyl-serine. Phosphatidyl-inositol takes the smallest portion of all phospholipids in membrane structure, but it has an important role as an endocytosis mediator, cell-to-cell interactions, and cell signaling (7,9).

Besides phospholipids, the membrane integrates glycolipids and cholesterol. Glycolipids are mainly localized on the outer part of the cell membrane and comprise around 2% of total membrane lipids (10). Their role and importance will be discussed in detail when describing gangliosides. Cholesterol serves as a membrane dynamics modifier and stabilizes the membrane. The rigid cyclic structure of cholesterol is the basis for this modifying behavior. Cholesterol cannot create membranes because it lacks a prominent polar group and has one hydroxyl group in its sterol core. This hydroxyl group is just polar enough to enable cholesterol to orientate toward polar phospholipid heads (11). Immediate modification in membrane fluidity by cholesterol is best observed in animals living at extreme temperatures. If the membrane is exposed to temperatures above physiological, cholesterol will position itself between unsaturated fatty acids,

reducing membrane flexibility and preventing membrane dispersion (11–13). Making membrane rigid is important when body temperature physiologically rises due to exercise or it rises to stave off infection. This property can preserve the membrane up to a point. Still, the ultimate survivability of cells at temperatures significantly above physiological is linked to how much energy cell proteins can take before denaturing (14). This is well documented in animals living near hydrothermal vents and in dry equatorial deserts (15). The opposite effect is observed when the membrane is exposed to under-physiologically normal temperatures. In this scenario, cholesterol is interlaced between saturated fatty acids. This is in contrast to its behavior under high temperatures. This cholesterol intervention prevents the crystallization of phospholipids that contain saturated fatty acids (16,17). That said, the cell utilizes cholesterol primarily as a regulator of membrane fluidity. Proper membrane functionality relies on two phospholipid characteristics, as well. The first one is separating water-filled compartments, and the second one exists in semiliquid rather than solid-state. Primary characteristic arises from the fact that fatty acids orient towards each other when forming bilayers. This way, a hydrophobic middle region is created, limiting the diffusion of polar molecules, primarily water and water-soluble molecules. At the same time, polar heads interact with the water creating a water sheet around the membrane (18). This interaction between water and the membrane is essential. If water could not reach the membrane surface and create hydrogen bonds with it, it would prevent water-soluble molecules from getting close enough for interaction with channel proteins. The second property is a result of the order emerging from chaos. In other words, fatty acids of the phospholipids are not all equal, and at least one of the acyl chains has one or more double bonds. Those double bonds prevent the perfect alignment of similar molecules resulting in the prevention of membrane solidification at physiological temperatures (19). The stability of the cell membrane is highly dependent on the ratios of described components, and those ratios are continuously adjusted to suit physiological needs. They can change as a result of the metabolic shift. We can say that phospholipids and cholesterol are constitutive parts of a cell membrane and to keep the membrane and the entire cell balanced, regulative elements should be embedded in a membrane. Groups of molecules that fulfill this function are glycolipids and proteins. Cell-to-cell interaction, the direction of differentiation and cell migration, signaling between different cells – all those functions are mediated through either one or both molecule groups.

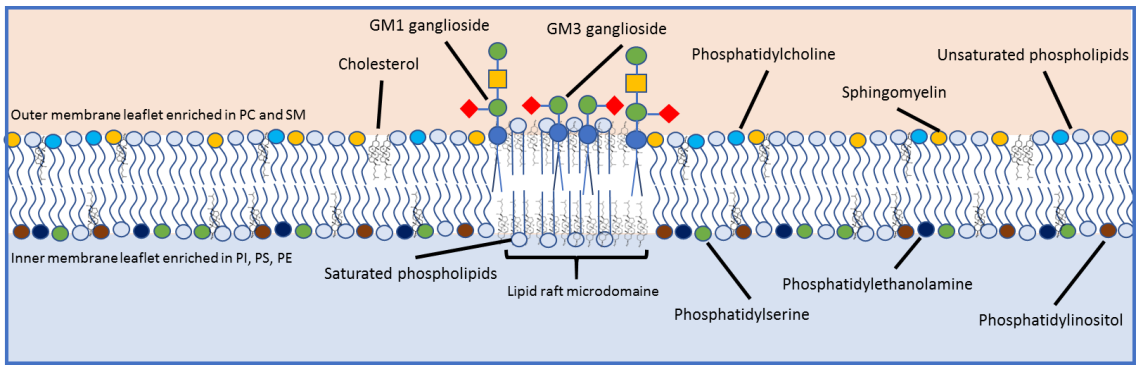

Figure 1.1. Scheme of the mammalian cell membrane representing the spatial organization of specific molecules building the membrane. The figure was made by the author based on references (1-36).

1.2. Plasma membrane glycolipids

1.2.1. Structure, differentiation, and synthesis of glycolipids

Large and diverse. To some scary beyond comprehension to others source of joy and never-ending research inspiration. First discovered and described by Ernst Klenk in brain tissue in 1942 (20). This group of biomolecules is made of two large and diverse compound families – carbohydrates and lipids. They can be described as glycosyl derivatives of lipids with the possibility to modify each component in the molecule either by addition or subtraction of sugars, hydroxyl groups, or double bonds. These modifications will change molecule position within the cell membrane thus altering molecule functionality (10). This diversity is a foundation of glycolipids' importance and emphasizes the need for stable and highly controlled glycolipid metabolism. Internal membranes contain two-thirds of the total glycolipids, rest is found in the cell membrane or the cytosol. Synthesis of glycosphingolipids is carried out by adding sugars one by one to anchor molecule, mainly onto a ceramide or, in some cases, to acetylated or non-acetylated glycerol containing one or more fatty acids (21,22). Ceramide is an amide derivative of sphingosine and one of the long-chain fatty acids. It is synthesized from palmitic acid in the endoplasmatic reticulum (ER) (23). Ceramide derivatives are formed by attaching different molecules onto the first C-atom hydroxyl group in the ceramide structure.

The first step of glycolipid synthesis takes place on the *cis* side of the Golgi apparatus, where the first sugar is transferred primarily to a ceramide. After the first sugar is bound to ceramide, the flippase enzyme rotates the synthesized molecule to the Golgi cisternae lumen. Then, further steps of sugar addition are carried in a lumen of the *trans* part of the Golgi network, where complex branching and addition of functional groups and charged sugars shape the final structure of glycolipid. Once synthesized, glycolipids are transported throughout the cell in small vesicles with bilayer membrane to maintain proper orientation during vesicle fusion with designated cell membranes.

Glycolipids are classified into two major categories: glycoglycerolipids and glycosphingolipids (24). Glycoglicerolipids have one or more sugars attached to a hydroxyl group of glycerol with one or more fatty acids anchoring the structure to the membrane. This group of molecules are quite common in plants, algae, and some bacterial species but can rarely be found in significant abundance in animals. The only exception to this is found in mammalian testes, where seminolipids comprise more than 90% of total lipids (25). Glycosphingolipids are the main glycolipids found in animal tissues, primarily localized in the nervous system. The central anchoring molecule of glycosphingolipids is the ceramide, on top of which are orderly assembled sugars (26). Glycosphingolipids are lipids containing at least one monosaccharide attached to the ceramide moiety. Depending on which sugars and functional groups are attached to ceramide, glycosphingolipids can be further divided into neutral glycosphingolipids and acidic glycosphingolipids. Neutral glycosphingolipids are usually made out of one sugar attached to ceramide.

The most abundant neutral glycosphingolipids are cerebrosides. Two major cerebrosides can be found in mammals: galactosylceramides and glucosylceramides (GalCer and GlcCer, respectively). In the central nervous system (CNS), the most abundant is GalCer, located in a myelin sheath surrounding white matter axons. It also serves as a precursor to more complex structures such as sulfatides and GM4 ganglioside. On the other hand, GlcCer is used mainly as a precursor in the synthesis of gangliosides and globosides. GalCer and GlcCer and their derivatives regulate cell growth, protein trafficking and sorting, cell morphogenesis, and cell adhesion (21,27,28). GlcCer is synthesized by the enzyme glucosylceramide synthase (GCS; GLCT - 1 EC 2.4.1.80) from UDP glucose and ceramide on the cytoplasmatic *cis* side of the Golgi network. Enzyme activity is dependent on concentrations of free ceramide that can be either released by degradation of complex glycolipids or *de novo* synthesized.

Acidic glycosphingolipids use cerebroside structure as the backbone for their synthesis. They have more than one sugar in structure and must have acidic residue in sulfate ester or sialic acid. Sulphoglycosphingolipids, also known as sulfatides, are derived from GalCer and have a distinct sulfatide group attached to the 3' hydroxyl group of galactose with an ester bond. Sulfatides are abundant in brain tissue. They are an essential component of the myelin sheath, serve as modulators in protein trafficking, signal transduction, and differentiate neurons or neuron-like cells. The role of sulfatides has been implied in Alzheimer's disease (AD), where a substantial loss was found in patients' brains (29,30). However, the question remains whether the loss of sulfatides results from disease or is it one of its causes.

1.2.2. Gangliosides

Gangliosides are acidic glycosphingolipids made from an oligosaccharide chain linked by the glycosidic bond to a ceramide anchor. Gangliosides have sialic acid in their motif, which gives them a specific spatial charge depending on the position and number of sialic acids on the oligosaccharide chain. In mammalian tissues, many variances of sialoglycans are found with different lipid components in ceramide moiety. This generates hundreds of different structures with various functions in the range of directing cell migration and cell recognition to regulation of receptor tyrosine kinases' activity (26,31). In the mammalian brain, predominant gangliosides have four sialoglycan sequences. The ceramide structure is quantitatively dominated with stearic acid (C18:0) attached to one of two sphingosines, namely 2-amino-4-octadecene-1,3-diol (d18:1) and 2-amino-4-dodecane-1,3-diol (d20:1) (32). The human brain has almost exclusively N-acetylneuraminic acid (Neu5Ac) with none of the glycosylated forms. Brains of other mammals and non-mammalian brains also have a second variant of sialic acid N-glycolylneuraminic acid (Neu5Gc) in similar proportions as Neu5Ac (33,34). Brain gangliosides in the mammalian brain are synthesized stepwise by a series of enzymes – glycosyltransferases. Galactose is firstly added to GluCer and is typically sialylated at its 3-hydroxyl residue with one Neu5Ac (Figure 1). The addition of Neu5Ac can be furthered by one or two additional Neu5Ac on top of an existing one, connected by an α2–8 link, and this way, GM3, GD3, and GT3 are synthesized. This is a key point in ganglioside biosynthesis. Once N-Acetyl galactosamine (GalNAc) is added to the 4-hydroxyl group of galactose, no further sialic acid additions can occur at the galactose 3-hydroxyl

position. The addition of GalNAc to the existing structure of GM3, GD3, and GT3 will result in the formation of GM2, GD2, and GT2, respectively. Following GalNAc residue, major brain gangliosides have β3-linked galactose added, which can be sialinized with one or two sialic acids on the 3-hydroxyl residue.

Gangliosides from a-series, namely GM1, GD1a, and b-series, GD1b, GT1b, are most abundant in the adult mammalian brain. Gangliosides with no sialic acids at first galactose are named 0-series, those with one sialic acid are a-series, two sialic acids are b-series, and three sialic acids are c-series. The first, 0-series gangliosides, are rare in an adult mammalian brain (Figure 1.2.). The same is true for the c-series or higher, although c-series are abundant in fish and amphibians, most likely because their brains can regenerate in adult life (35–37). For the functionality of gangliosides, orientation in the cell membrane is the key (38). According to detailed conformational studies, ceramide moiety is embedded in the outer layer of the cell membrane. However, a few of them have revealed that the glycan part of both GM1 and GM3 is oriented perpendicular to the membrane due to the glucose-ceramide bond orientation (38–40). The glycan part positioning is essential, and gangliosides are sufficiently large in order to engage with proteins on the lateral cell membrane surface as well as extend outwards from the membrane to interact with adjacent cell membrane proteins.

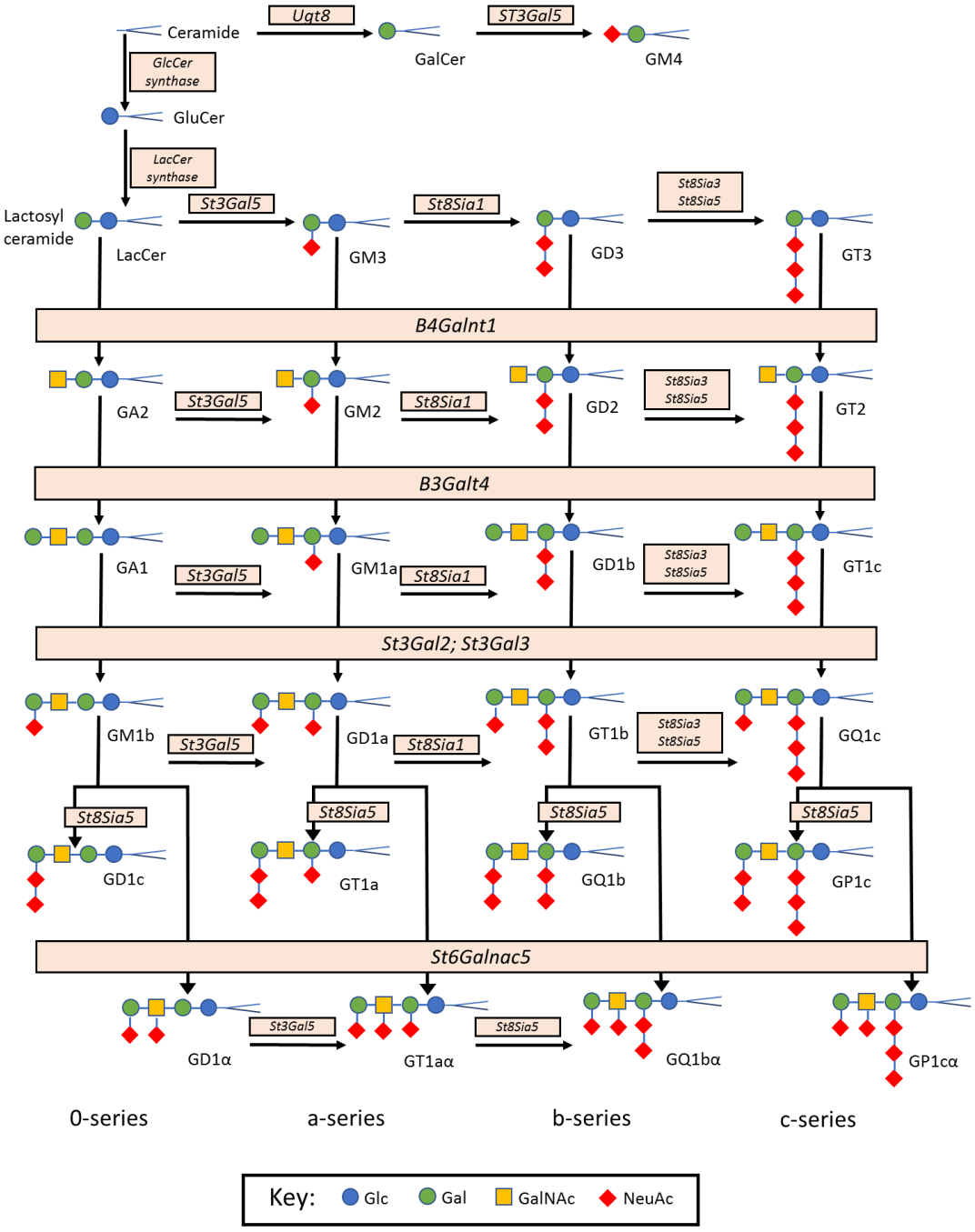

Figure 1.2. Scheme of ganglioside biosynthesis pathway. The author made the figure based on references (20–56); Glc = Glucose, Gal = Galactose, GalNac = N-Acetyl Galactosamine, NeuAc = Sialic acid.

Biological membranes are formed as lipid bilayers that under physiological conditions behave and self-organize into two-dimensional fluids dominated primarily by glycerophospholipids (41,42). The plasma membrane outer leaflet is mainly dominated

by phosphatidylcholine, which accounts for more than half of the total glycerophospholipids. On the other hand, gangliosides represent the most significant minority in the total population of molecules in the outer membrane leaflet (43). Gangliosides, and the rest of the sphingolipids, organize differently within the membrane having large glycan groups and ceramide anchors that drive the lateral association within the bilayer (44). This occurs spontaneously, and together with cholesterol and specific proteins, assembles special membrane microdomains – lipid rafts (45,46). Because of this intrinsic property, gangliosides have been proposed as a molecular marker for lipid rafts. This kinetically driven dynamic self-organization is supported by current findings that nanometer-sized lipid rafts form in eukaryotic cell membranes (47–49). Gangliosides bind to the lipid rafts with high avidity, because of that, created structures rarely dissipate in a living cell. The remaining gangliosides are dispersed across the membrane. This spatial organization gives a small number of gangliosides a wide range of functions – from axon growth regulation to modulation of membrane receptor activity. Axon outgrowth is regulated by gangliosides that serve as control points for nerve cell mechanisms. This regulation is best observed at the axon growth cone, where the interaction of gangliosides with compatible molecules on adjacent cells inhibits the growth. Gangliosides that can negatively affect axonal growth are GD1a and GT1b, after interaction with myelin-associated glycoprotein (MAG). The membrane-associated sialidase *Neu3* cleaves sialic acids from complex gangliosides resulting in GM1. This prevents interaction with other molecules and inhibits axon outgrowth (50–52). A similar increase in *Neu3* activity is observed when the axon is damaged. This is one of the primary mechanisms involved in peripheral axon reparation, but it is not observed in the CNS axons (51). Besides regulating axon growth, gangliosides' essential function within the membrane is regulating receptors' activity, notably receptor tyrosine kinases. It has been observed that lateral association of GM3 with insulin receptor (IR) suppresses downstream signaling cascade *in vitro*. This happens due to IR sequestering upon association with GM3, impairing lateral association with the caveolin required for proper insulin-mediated signaling cascade (53). In addition to GM3's regulation of IR activity and signaling cascade, other gangliosides are involved in the regulation of membrane receptors, as well. GM1 is involved in the activation of Tropomyosin receptor kinase A (TrkA) that prevents apoptosis and stimulates neurite growth (54). It is also important for the proper functioning and stability of the GluR2 subunit of the α-amino-3-hydroxy-5-methyl-4-isoxazole propionic acid (AMPA) receptor within the membrane (55).

Dysregulation of the GluR2 receptor usually leads to intellectual deficits (56). As major cell surface molecules of the vertebrate CNS, gangliosides have multiple roles in maintaining the CNS's proper physiology. With the emergence of new technologies, the relationship between gangliosides and other molecules is being discovered.

Gangliosides are one of the most important cell surface molecules of neurons in the vertebrate nervous system, where they provide molecular signatures for intrinsic (*cis*) and extrinsic (*trans*) molecular interactions. As the knowledge of the multiple roles of gangliosides in physiological and pathological conditions continues to emerge, and the tools for exploring the structure-function relationships and mechanisms of ganglioside-mediated cellular regulation continue to evolve, a better understanding of areas such as axon stability and regeneration, synaptic plasticity, and cellular differentiation in health and disease are to be discovered.

1.3. Insulin, insulin receptor and its metabolic pathway

Insulin is a peptide hormone secreted by pancreatic beta cells in response to increased glucose or amino-acid levels in the blood. It has a relatively simple peptide structure with a total of 51 amino acids. It is made of A and B peptide chains, cross-connected with disulfide bonds to form an active hormone (57). Its primary role is regulating blood glucose levels, but it has a more important secondary role in regulating cell metabolism. Insulin cannot induce any response in targeted cells by itself since it is a peptide and, as such, cannot readily pass across the cell membrane (58). Due to this feature, a localization of a specific cell membrane receptor is required to pass the insulin signal into the cell. As mentioned above, IR belongs to a group of receptor tyrosine kinases. Structurally, the receptor dimer is build up from monomers of A or B isoforms, creating different combinations of homo- and heterodimers (59). Therefore, it is crucial to distinguish receptor A and B monomers from the ones building up the insulin hormone. In both cases, only the nomenclature is the same. Each monomer, regardless of isoform, is made from alpha and beta subunits connected with disulfide bonds.

Additionally, the receptor is assembled by cross-connecting two alpha subunits together with disulfide bonds. The alpha subunits are entirely located outside the cell and serve as docking sites for four insulin molecules. During the activation, insulin ligands first bind to the alpha subunits' leucine-rich domains and then to the fibronectin domains

type I and II. This two-point interaction facilitates the cooperative binding of insulin and reduces the energy necessary for the activation of the receptor (60). The beta subunit is a transmembrane protein, and the majority of its polypeptide chain is located inside the cell. It has a specific autocatalytic domain called the tyrosine kinase domain. The binding of four insulin molecules to the receptor forces monomers to get closer to each other. This movement results in the transphosphorylation of tyrosine residues of the beta subunits and the downstream signaling cascade activation.

The insulin signaling cascade does not encompass just one downstream signaling pathway but several different pathways, simultaneously forming a signaling network that impacts every aspect of the cell (59). The essential part of every metabolic pathway is its auto- or xenoregulation that prevents the signal from spiral out of control. Thus, every step of the vast insulin cascade includes multiple regulatory molecules. The first regulatory mechanism in controlling the insulin signaling network revolves around the receptor. Like other receptor tyrosine kinases, the IR itself can function as a negative regulator by undergoing ligand-induced internalization and subsequent recycling back to the membrane, or degradation in the lysosomes. The recycling process is regulated by 12 amino-acid motifs located at the IR beta subunits juxtamembrane region. Once insulin binds to its receptor and causes conformational changes, this motif is exposed and induces the formation of clathrin-coated pits. Entering IR into the clathrin-coated pits causes its internalization by forming a vesicle (61). The fusion of the primary lysosome with the vesicle changes its pH, which facilitates the release of IR. Once free, the receptor is recycled back to the membrane. Suppose insulin concentration is higher than average and stays high long enough, the abnormality of this recycling process will result in the development of insulin resistance by keeping the majority of receptors internalized (62). This normally happens after a large and sugar-heavy meal, but it is resolved relatively quickly if the organism is healthy. Going downstream from the receptor, signal transduction is handled by kinase and phosphatase enzymes. For each kinase that insulin signal activates, there are often two or more signal quenching phosphatases.

The first step in cytoplasmic signal transduction is phosphorylation and subsequent insulin receptor substrate (IRS) protein activation. To date, four closely related isoforms of IRS have been discovered, which are differentially expressed in different organisms in a tissue-dependent manner. IRS-1 is expressed in most of the cells and regulates body growth. IRS-1 plays a dominant role in skeletal muscle cells by

regulating their insulin response. It is interesting to note that Araki et al. did not found significant deleterious effects on glucose tolerance in IRS-1 knockout mice (63). On the other hand, IRS-2 expression is restricted to specific tissues such as neurons, the pancreatic islet cells, preadipocytes, and hepatocytes. In the cells mentioned above, it regulates either growth or maintains a proper cell function. IRS-3 and -4 expressions have a more restricted tissue and species distribution. In rodents, the majority of IRS-3 protein can be found in adipocytes, lung, and liver cells. The human genome doesn't contain a functional *IRS-3* gene, and consequently, no protein is synthesized. In rodents, IRS-4 protein is found in the kidney, liver, heart, skeletal muscle, and brain cells, where it controls their glucose response (64). In humans, this protein is found only in certain breast tumors acting as an oncogenic driver for mammary glands epithelial cells. That said, only IRS-1 and -2 are relevant when talking about insulin signalization in the majority of human cells, and it is most likely that one of those two is affected in all types of insulin resistance. Regulation of IRS activity relies mainly on its phosphorylation. All IRS isoforms, regardless of animal species, contain the Tyrosine-Any amino acid-Any amino acid-Methionine (YXXM) motif in several places in its amino acid sequence, which is phosphorylated depending on where the signal is coming from and results in the activation of IRS (65). Other amino acid residues regulate IRS. For example, Serine 636 phosphorylation causes the cessation of the above-mentioned part of the insulin signaling cascade. Once the YXXM motif of IRS is phosphorylated, it can lead to two distinct metabolic cascades, one activating mitogen-activated protein kinase (MAPK) pathway and another protein kinase B (Akt) pathway.

The phosphorylated IRS forms a complex with PI3K p85 subunit and Grb2, which recruits guanine nucleotide-exchange factor (GEF), the activator of the Ras small GTPase protein. Ras in a GTP-bound form activates a MAPK cascade. Ras-GTP complex interacts with the Raf protein, phosphorylating and activating the MAPK/extracellular signal-regulated kinase (MEK). MEK, in turn, phosphorylates ERK1/2. ERK1/2 has several targets, including the ribosomal serine kinase and E-26-like transcription factor 1 (Elk-1). It can also phosphorylate and activate the MAPK-interacting kinase (Mnk) 1 and 2, leading to phosphorylation of eukaryotic initiation factor-4e resulting in increased protein synthesis (66).

The other branch of insulin signaling is activated when the SH-2) domain containing regulatory subunit of phosphoinositide 3-kinase (PI3K) - p85 binds to the IRS1

protein. p85 binds to the catalytic subunit of PI3K - p110. For the activation of this signaling cascade in human cells, IRS-1 must be phosphorylated at Tyr^{612} and Tyr^{632} residues. This interaction results in the conformational change and subsequent activation of the PI3K (65,67). In this activated state, the catalytic subunit phosphorylates phosphatidylinositol 4,5-bisphosphate (PIP2) to phosphatidylinositol (3,4,5)-trisphosphate (PIP3) by cleaving one adenosine triphosphate (ATP). PIP3 as a second messenger serves as an activator of phosphoinositide-dependent kinase-1 (PDK1). This kinase has three ligand binding sites; the first one is for ATP, the second one is for PIP3, and the third one is a docking site for interaction with other downstream molecules. In the activated form PDK1 can interact and phosphorylate two protein kinase C (PKC) isoforms λ/ι and ζ to facilitate glucose uptake via insulin-regulated glucose transporter 4 (GLUT4) (68).

The most important substrate for PDK1 is Akt. It behaves as a signaling hub for many major metabolic pathways in the cell, and it is activated by phosphorylation at Ser308, forming pAkt. It can activate the target of rapamycin complex-2 (TORC-2) which in turn phosphorylates Ser^{473} residue on $pAkt^{Ser308}$ and additionally activates it. Fully activated $pAkt^{Ser308/473}$ can now activate the downstream signaling cascade. First in line is tuberous sclerosis protein-1/2 (TSC 1/2), whose phosphorylation inhibits its GTPase activity and enables Ras homolog enriched in brain (Rheb) to remain stable for the activation of TORC1 (69,70). This complex phosphorylates and activates eukaryotic translation initiation factors through MAPK-interacting kinase (Mnk), contributing to protein synthesis. TORC1 complex also activates p70 S6-ribosomal kinase ($p70^{S6K}$), leading to increased elongation of proteins during translation. In addition, TORC1 phosphorylates Unc-51-like kinases 1/2 (Ulk 1/2) as well, resulting in the inhibition of autophagy. $pAkt^{Ser308/473}$ directly phosphorylates Bcl antagonist of the cell death (BAD) and X-linked inhibitor of apoptosis (XIAP), effectively inhibiting apoptosis (71). This outlines the antiapoptotic effect of Akt and insulin as a hormone.

Having activated metabolic pathways for gene transcription, protein translation, and apoptosis inhibition, one can assume that cell growth and division are affected, which is true. This is accomplished by phosphorylation of several different target molecules. The first one is glycogen synthase kinase-3 (GSK-3), and once inactivated by Akt phosphorylation, it allows glycogen synthase to start glycogen deposition in cells. $pAkt^{Ser308/473}$ can also phosphorylate and inactivate phosphodiesterase-3b (PDE3b)

enzyme increasing cyclic adenosine monophosphate (cAMP) levels. cAMP molecules as second messengers activate protein kinase A (PKA), which phosphorylates several proteins, including the cAMP response element-binding protein (CREB) (72,73). GSK-3 phosphorylates CREB protein, causing the transcriptional activation of specific genes by binding to the cAMP response element (CRE) found in the promoter region of these genes. The last and most important for pushing cells into division or keeping cells in the cell cycle is p21 cyclin-dependent kinase inhibitor 1 (p21) and p27 cyclin-dependent kinase inhibitor (p27). Both regulate the cell cycle by inhibiting cyclin D/cyclin dependent kinase 4/6 and cyclin E/cyclin-dependent kinase 2/complexes, consequently trapping cells in the G1 phase of the cell cycle. Once phosphorylated by $pAkt^{Ser308/473}$, both p21 and p27 proteins inactivate, translocate to the cytoplasm, and get tagged for degradation by ubiquitination. This enables the phosphorylation of retinoblastoma protein by cyclin-dependent kinases leading to the transition of cells from the G1 into the S phase of the cell cycle.

The above-described cascade is a one-way, linear pathway (74,75). Inactivation of GSK3β by Akt enables its second catalytic activity, therefore it phosphorylates Ser^{332} of IRS1, changing its conformation and kinase activity, and effectively attenuating signaling cascade (76). Heading further up the insulin network, we get to active ERK1/2, which will eventually lead to the inactivation of IRS1 by phosphorylation of Ser^{312} and Ser^{616} residues leading to a decoupling of IRS1 from PI3K and shutting down the insulin signal (77,78).

An essential part of the regulation of this signaling network is sensing fatty acid levels. Primarily, the synthesis of fatty acids is a clear sign of energy overload within the cell. Therefore, additional energy income via glucose should be stopped, and the regulation of the cytoproliferative effect should be tightly controlled. Protein kinase C theta (PKC θ) is involved in this regulatory step. It gets activated by free fatty acids, and upon activation, phosphorylates Ser^{1101} of IRS1, subsequently attenuating its signal (79,80). This regulatory point could also be responsible for developing insulin resistance and type 2 diabetes or AD. Many other regulatory points of the insulin signaling pathway exist, but those are not investigated or fall beyond this research scope.

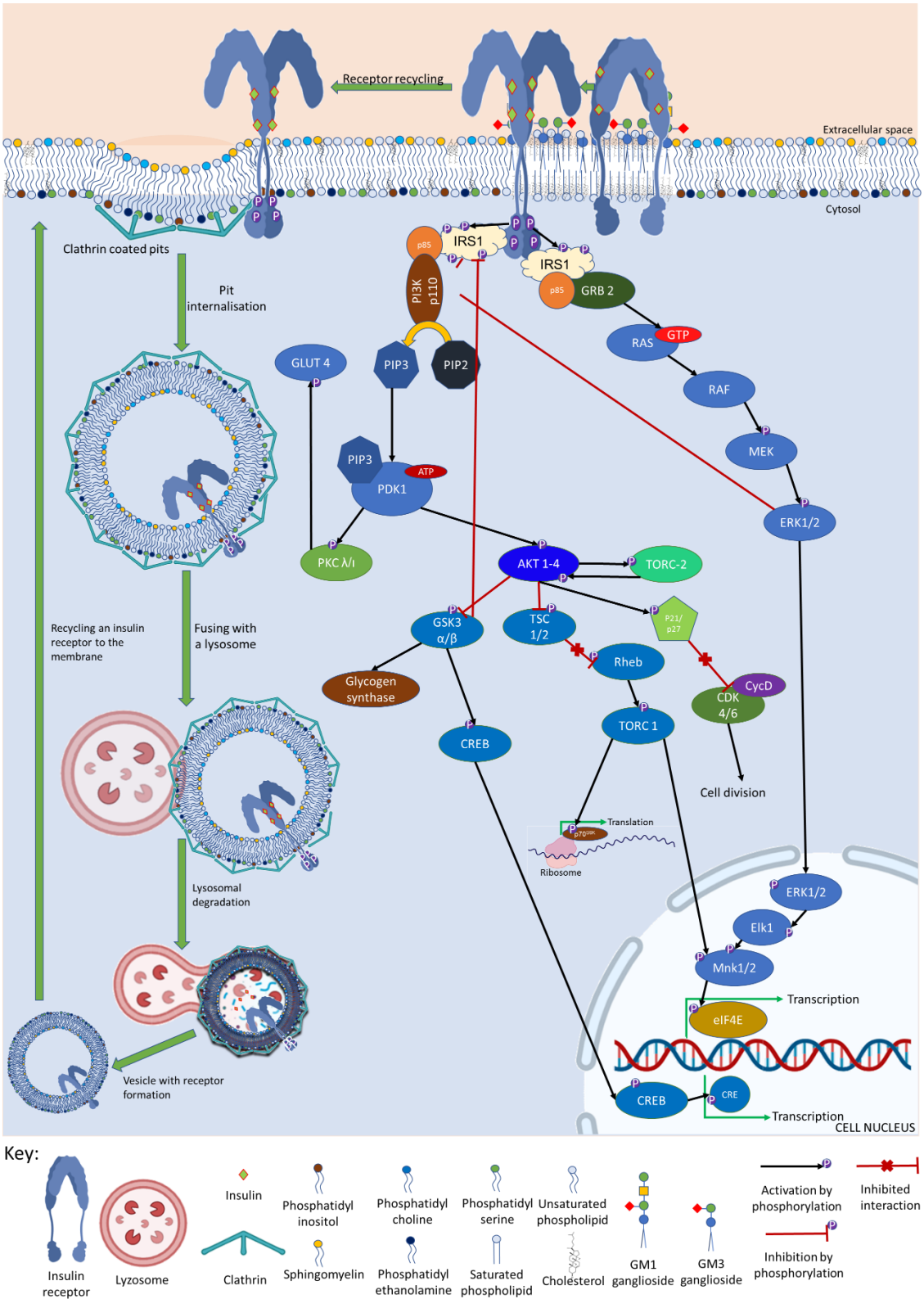

Figure 1.3. Generalized insulin signaling pathway. The figure was made by the author based on references (65-84).

1.4. Neuroplastin

Neuroplastin (NP) belongs to the group of neuronal and synapse enriched immunoglobulins, and it is a part of the cell adhesion molecule superfamily. The proposed roles of NP include various aspects of neuroplasticity, brain development, learning, and memory. The NP precursor gene *NPTN* encodes NP. Alternative splicing of the primary transcript produces two isoforms of NPs termed NP55 and NP65, the latter being specific to neurons. NP65 is expressed in the cortex, hippocampus, and putamen of the human brain. It also appears in high concentrations in the human hypothalamus and cerebellum. Glial cells in the human brain do not express NP65, unlike glial cells found in rodents (81–83). During fetal human brain development, its expression is minimal. The importance of NP becomes obvious during embryonic development, when neuronal network growth and neuronal pruning occur. Lack of functional NP65 usually leads to mental impairments (84). In mice, the absence of NP65 prevents normal synaptogenesis of inner hair cells, this way, normal development of hearing is impaired (85). NP65 regulates neurite outgrowth and dendrite spine formation through ERK 1/2 and p38 MAPK. These two metabolic pathways are the point of crosstalk between the insulin and the NP65 signaling networks. Homophilic interactions of NP65 and activity regulation of these two pathways are essential in long term potentiation and stabilization of AMPA receptors in the membrane (86,87). If NP65 homeostasis within the membrane is disturbed, AMPA receptor subunits internalize, leading to the dissociation of synapses at the dendrite spine, and subsequent memory loss (87).

Cognitive disorders such as dementia are characterized by impairment in memory formation, learning, and short attention span linked to NP65 dysfunctionality. Population genetic studies identified a single nucleotide polymorphism in the *NPTN* gene linked to adolescents' cortical thickness and subsequent decrease in intelligence. It has also been observed that levels of *NPTN* gene expression vary throughout the brain, and it can be higher in one hemisphere or in some regions of the brain where metabolic pressure is higher such as in the hippocampus (84,88,89). Involvement of NP65 dysfunction in the onset or propagation of AD is gaining more evidence. Application of mimetic peptide of NP65 homophilic binding, enplastin, induces activation of p38 MAPK, giving an insight into what physiological conditions look like. The exact process happens when amyloid protein forms plaques, which lead to the phosphorylation of p38 MAPK. Once activated, it hyperphosphorylates tau protein, preventing neuroplasticity and causing subsequent

cell death (90). It has been observed that in the early stages of AD, the expression of NP65 compared to control samples is significantly higher (89). Stabile expression and appropriate regulation of NP65 in the neurons are essential for their proper functioning and represent a target point for treating patients in the early stages of AD.

1.5. Lipid rafts

Following basic research of the cell membrane structure, it has been observed that it is not homogeneous but rather divided into smaller functional subunits. Building blocks of membrane subunits are usually made from mutually similar molecules with a tendency to self-organize and create larger structures. The types of those structures are lipid rafts, which can be described as cholesterol-rich microdomains with integrated proteins and glycosphingolipids. Self-organization in lipid rafts arises from the fact that cholesterol and glycolipids have a higher melting point than the rest of membrane lipids forcing them to stick together. However, the function of lipid rafts is still debated. Simmons and Ikonen have published the first description of lipid rafts as detergent-resistant microdomains (DRM) due to their insolubility in cold 1% Triton™ X-100. Later, similar results have been obtained using other detergents, leaving insoluble DRM in the pellet after ultracentrifugation (42,91,92).

Until the last two decades, the prevailing thought was that lipid rafts are only artifacts created during cell membrane laboratory preparative processes such as detergent mediated isolation or immunocytochemistry, which cannot be considered relevant. This problem was finally solved by Baumgart et al. by the addition of special fluorescently tagged geranyl-geranyl and cholesterol derivatives to the growth medium of living cells. They have used confocal and two-photon microscopy to observe the internalization and distribution of the given compounds across the membrane (93). It was the first accurate observation of lipid raft's existence. Formation of lipid raft follows paradigm in biology: making order from chaos, and whenever possible, breaking the larger functional units into numerous smaller ones. The result of this decomposition is the acquirement of more functions. Neofunctionalization is usually the result of different biochemical properties of building blocks in that structure. For instance, lipid rafts are made from nonpolar cholesterol and its conjugates, which contrasts with amphiphilic phospholipids in the membrane. The nonpolar nature of cholesterol allows for different local chemical properties and the incorporation of proteins and glycolipids with a nonpolar

transmembrane domain. These properties make lipid rafts a good hub for modulation of cell-to-cell interactions and external regulation of metabolism by setting cytokine receptors within the rafts. Several other compounds inside the rafts can modulate cytokine receptor activity, such as leptin and IR.

Besides cholesterol and its derivatives, glycolipids are an essential group of molecules that form functional lipid rafts (94). Glycolipids associate with each other laterally through weak interactions of glycan heads. An association of glycolipids with cholesterol within the membrane happens through hydrophobic interactions with the ceramide saturated fatty acid chains. This spatial arrangement forms tight cholesterol-glycolipid rafts, and it gives a driving force that segregates them from the rest of the membrane phospholipids (95). Within the lipid rafts, all major brain gangliosides can be found, with a predominance of GM1.

The importance of GM1 in the production and propagation of toxic amyloid-beta (Aβ) oligomers is well described. Once GM1 binds to an Aβ, it will induce conformational change and create toxic oligomers (96). Aggregation, production, and neuronal binding of Aβ oligomers are localized within lipid rafts. Sequential cleavage of amyloid precursor protein (APP) occurs by β-Site APP cleaving enzyme 1 (BACE1), the γ-secretase complex. The presence of GM1 and other glycolipids promotes aggregation and the production of soluble oligomers. Once produced, Aβ oligomers bind to cellular prion protein (PrP^{C}) and N-methyl-D-aspartate (NMDA) receptors (97). Glutamate receptors affect the functionality of synapses and long-term memory formation (98). Therefore, the stability of the glycolipid content of lipid rafts is crucial for maintaining the formed synapses and preserving the functionality of neurons.

1.6. Neurodegenerative diseases

1.6.1. Alzheimer's disease

Better living conditions and prolonged lifespan lead to the rise in neurodegenerative diseases in humans. Most neuron division occurs up to the age of 25, and it is significantly tapered off later in life. The majority of brain stem cells can be localized around ventricles and in the hippocampus (99). Regeneration of nervous tissue from these areas is at best limited and cannot serve as a neuronal reservoir to replenish neurodegenerative diseases driven by neuronal death (99–101).

AD is an irreversible and progressive neurodegenerative disease first described by the Bavarian psychiatrist and neuropathologist Alois Alzheimer, who described a neuropathological history of two patients (102). The disease is clinically manifested by memory loss, cognitive decline, as well as changing personality. Neurodegenerative changes in AD include specific areas of the brain and progress over time. Neurodegeneration spreads from the entorhinal cortex, hippocampus, anterior cortex and eventually affects the entire brain (103). The onset of the disease correlates with aging and gender. AD is known to occur in people over 65 years of age, and the majority of patients are women. The disease's molecular mechanisms are not entirely known, but neuronal death and the weakening of synapses have been found in the aforementioned areas of the brain (104). AD is caused by several factors and has familial (less than 1% of cases) and sporadic forms (105). Mutations are associated with the early appearance of senile plaques or β-amyloid deposition, microtubule instability caused by hyperphosphorylation of tau protein, and improper cholesterol metabolism in the case of the ε4 allele of the ApoE protein (106).

Protein aggregation and misfolding is the primary pathophysiological cause of age-related human neurodegenerative diseases (107). It is believed that the primary driver of AD is the formation of extracellular Aβ fibrils, which are the first and most apparent signs of AD. They can further assemble into senile plaques composed of β-amyloid accumulations. β-amyloid is a protein produced by improper processing of the APP. APP is an integral membrane protein expressed in different tissues, mainly in the area of the synapses. It is considered that APP under normal physiological conditions participates in the repair of blood vessels after injury. Also, it is utilized in iron transfer, directing neurons during brain development, and the modulation of synaptic density (108).

APP processing takes place at the cell membranes in two ways. The first is non-pathological, where APP is cleaved by α-secretase and then γ-secretase to form soluble β-amyloids. The second is pathological. It involves cleaving APP with beta-site amyloid precursor protein cleaving enzyme 1 (BACE1) and then with γ-secretase to form insoluble precipitates of β-amyloid – senile plaques (109). Unfortunately, β-amyloids can also create toxic soluble oligomers causing synapses to fail (110,111). Besides the synaptic failure, Aβ oligomers cause insulin resistance, inhibition of axonal transport, oxidative stress, an aberration in tau protein structure, all of which cause neuronal dysfunction and cellular death (112).

Another sign of AD is the formation of neurofibrillary tangles in the brain caused by improper processing of tau protein and its mutations. Tau proteins are cytoplasmic proteins, but they can also act in the cell membrane. Their primary role is to stabilize the microtubules of neuron axons, so they are most pronounced in axons of neurons in the CNS (113). Tau proteins belong to the microtubule-associated proteins stimulating the assembly and stability of microtubules (114). In AD, tau proteins are excessively phosphorylated due to mutations in the encoding *MAPT* gene, resulting in various nonfunctional protein isoforms. As such, altered tau proteins form neurofibrillary tangles, prevent stabilization of axon microtubules and cause neuronal death (113).

The third protein involved in AD is apolipoprotein E (ApoE). ApoE is involved in body fat metabolism and the transfer of lipids, including fat-soluble vitamins, lipoproteins, and cholesterol, through the lymphatic and vascular systems. Although it is synthesized primarily in the liver, its presence has also been found in other tissues – including the brain, kidneys, and spleen. In the CNS, astroglia and microglia are the primary sources of ApoE, while neurons express ApoE receptors. Cholesterol most important role is its involvement in the formation and stability of synapses during brain developments and injuries (115). Impairment in cholesterol levels and overproduction of ApoE leads to the formation of amyloid plaques and tangles. This process is mediated by lipidated ApoE that binds soluble Aβ oligomers, which can now interact with low-density lipoprotein receptor and heparan sulfate proteoglycan inducing its internalization and through lysosome degradation producing insoluble Aβ (116).

1.6.2. Parkinson’s disease

Parkinson's disease (PD) is a chronic, progressive, neurodegenerative disorder predominantly characterized by motor symptoms such as slowness of movement, tremor at rest, stiffness, and loss of mechanisms controlling the upright posture (117). The disease is accompanied by other non-motor and motor symptoms that occur in the late stages, such as falling while changing body position, motoric blocks, speech, and ingestion disorders. Some non-motor symptoms (sleep disorder, depression, paraesthesia, personality disorders, and dementia) may present earlier and be more dominant than motor disturbances. Dementia is a late complication that most commonly affects elderly patients with a chronic course of the disease. PD is a multi-aetiological disorder, the result of the interaction of genetic predisposition and environmental factors (118). So far, 18

genes have been identified that have a role in the etiology of the disease. The most common environmental factors associated with this disease considered in numerous epidemiological studies are gender, age, eating habits, infections, toxins, and trauma (118,119).

Pathophysiological processes in PD include an accumulation of intracellular α-synuclein (α-Sin) fibrils primarily in the substantia nigra of the brain. This protein is encoded by the *SNCA* gene abundantly expressed in presynaptic terminals throughout the CNS. The full scope of functions of α-Sin is not yet apparent, but its importance in synaptic plasticity and neurotransmitter release is known. Studies have shown that elevated neuronal activity increases the release of α-Sin. However, an increase in the release itself does not necessarily lead to the development of PD symptoms. Point mutations, polymorphic variants, and the duplication or triplication of the *SNCA* gene, which encodes α-Sin, represent significant risk factors for developing PD (117).

1.6.3. Role of gangliosides in neurodegenerative diseases

Gangliosides have a different regulatory function in the folding of Aβ and α-Sin proteins. The first ganglioside which has been isolated from Aβ fibrils was GM1. Later on, other major brain gangliosides were discovered to be incorporated in the Aβ structure. Usually, gangliosides are present in submicromolar concentrations, and they appear to facilitate fibrillar aggregation (120–123). Experiments on mice have demonstrated that Aβ strongly binds to GM1 ganglioside. Western blot analysis showed that the detected Aβ protein had a slightly larger mass than expected due to its binding toGM1. Bonds between were so strong that even the denaturation procedure could not dissociate them.

The function of gangliosides in PD is different from their function in AD. Knocking out the *B4galnt1* gene, encoding for the enzyme responsible for the synthesis of complex gangliosides, in mice has shown fewer tyrosine-kinase positive cells and significantly more α-synuclein cells in *substantia nigra* (124,125). This result indicates a physiological role of complex gangliosides in the control of α-synuclein deposition. A similar pattern was observed in human *substantia nigra* samples from PD patients. GM1 ganglioside levels were significantly lower compared to healthy brain samples (126).

1.7. SH-SY5Y cell line as a research model of neurodegenerative diseases

SH-SY5Y cell line is a subclone of the SK-N-SH cell line originating from a bone marrow biopsy of a 4-year old female. The origin of the tumor presumes to be neural crest cells. The cell line can produce S-type cells with the glial phenotype and N-type cells with the neuronal phenotype and can undergo transdifferentiation from one type to another. However, most cells are N-type, with a small percentage of S-type (127). Even though several differentiation protocols have been developed to optimize metabolic properties and profile of SH-SY5Y cells, most of the differentiation protocols utilize all-trans-retinoic acid (ATRA) and can be further advanced with brain-derived neurotrophic factor (BDNF) or with phorbol esters (128).

The initial cell line phenotyping showed moderate activity of dopamine-β-hydroxylase and negligible levels of choline acetyl-transferase, acetylcholinesterase, and butyryl-cholinesterase, basal noradrenaline (NA) release, and tyrosine hydroxylase activity. Tyrosine hydroxylase is a restricting enzyme in the catecholamine synthesis pathway that converts tyrosine to L-dopa, the precursor of dopamine (DA) (128–130). Expression of neuronal nuclear antigen NeuN marks a shift toward mature neuronal phenotype (131). The composition of glycolipids changes and the synthesis of complex gangliosides is several folds upregulated during differentiation (132). Undifferentiated cells have a low metabolic rate. ATRA has known effects on energy metabolism and mitochondrial functionality, primarily upregulating produced energy levels.

Having nearly all genes involved in PD development, the progression preserved SH-SY5Y cell line makes a good model for studying PD (133). Investigating AD in this cell line is oriented to insulin-mediated metabolic abnormalities, tau protein pathophysiology, and APP levels regulation. The cell line is primarily not cholinergic but rather dopaminergic, with some parts of the cholinergic signaling system left intact. (134,135). This makes the cell line less suitable for the investigation of AD, but it is an appropriate model for experiments detecting changes in APP levels, investigating effects of compounds on insulin signaling networks, or assessing cytotoxicity *in vitro* (136). The expression of ganglioside synthases and four major gangliosides, alongside βAPP and αSyn, makes this cell line suitable for the initial evaluation of gangliosides and glycolipids role in maintaining stable metabolic networks and gives us the information necessary for the improvement of predictions for *in vivo* experiments.

1.8. Modulation of glycosphingolipid metabolism

The possibility to tweak and adjust glycolipids levels is essential due to gangliosides' involvement in development, progression, or protection against neurodegenerative diseases. Prevailing outcomes depend on ganglioside levels and the ratio thereof within the cell membrane. Several compounds have been used to investigate the effects of inhibition of glycolipid synthesis on neurodegenerative diseases and to investigate the cellular response to shifting glycolipid balance. A group of three ceramide analog molecules is generally used as an inhibitor of the enzyme that synthesizes ganglioside precursor, GlcCer synthase (E.C. 2.4.1.80): D,L-threo-1-phenyl-2-hexadecanoylamino-3-morpholino-1-propanol (PPMP), D,L-threo-1-phenyl-2-decanoylamino-3-morpholino-1-propanol (PDMP) and D,L-threo-phenyl-2-hexadecanoylamino-3-pyrrolidino-1-propanol (PPPP), also known as P4 (137–139). Inhibition of ganglioside synthesis has demonstrated that lack of gangliosides is not the primary cause of cell death but an accumulation of synthesis precursor ceramide. Ceramide induces apoptosis if accumulated within the cells, which could be avoided if inhibitor compounds are adequately dosed (140,141). One of the currently used inhibitor compounds of GlcCer synthase is N-alkylated imino sugar that behaves as a glucose analog, named miglustat (MIG), trademarked as Zavesca. This drug is used to treat type 1 Gaucher disease patients that can not be treated with enzyme therapy, and it has been the only approved drug to treat Neumann-Pick disease (142,143). The drug has many potentials to treat neurodegenerative diseases since it can readily pass the blood-brain barrier (144).

On the other hand, an overload of gangliosides can be equally informative and give insight into the extent to which energy metabolism is shifted. Conduritol b epoxide (CBE) is used to block the beta-glucosidase enzyme (EC 3.2.1.21) involved in ganglioside degradation. The gene for the enzyme is mutated in patients with Gaucher disease, this way, the disease can be studied on the cell line or animal models. The enzyme can be partially or fully dysfunctional depending on where the mutation occurred, giving a spectrum to the disease (145). The possibility to *in vitro* assesses what different levels of enzyme inhibition can do to the metabolism provide us with insight into the extent to which metabolism has changed to adapt.

1.9. Why investigate glycosphingolipid metabolism?

With an ageing population, neurodegenerative diseases are becoming more prevalent and there is a greater need than ever for appropriate treatment. Disruption of ganglioside synthesis can be a good candidate if taken into consideration the amounts of gangliosides in the brain and their involvement in the development and progression of neurodegenerative diseases. Before testing in living organisms, the effects of glycosphingolipid metabolism modulators must be investigated *in vitro* on models that effectively mimic neurons and have an active majority of intact cytokine signalization. The differentiated SH-SY5Y cell line is a good candidate for this purpose, as it has both neuronal and fibroblastic phenotype, thus fulfilling both prerequisites. The full impact of advanced technologies such as Matrix-Assisted Laser Desorption Ionization Time Of Flight Mass Spectrometry (MALDI-TOF-MS) on metabolic networks can be verified. Knowledge of the metabolic effect in the presence of disruption of ganglioside biosynthesis will provide the opportunity for further *in vivo* and clinical studies.

2. HYPOTHESIS

Inhibition of ganglioside biosynthesis *in vitro* alters the lipid environment of the cell membrane, thereby altering the intracellular signaling cascade of membrane proteins involved in neuroplasticity and neurodegeneration.

3. OBJECTIVES

To determine the influence of changes in glycosphingolipid composition in lipid rafts of differentiated human neuroblastoma cells on membrane placement and intracellular signaling cascade of transmembrane proteins relevant to neuroplasticity and neurodegeneration process: IR, IGF-1R, APP, Np 65.

Specific objectives:

1. immunohistochemically determine the colocalization of lipid raft markers (flotillin) and non-raft markers (transferrin receptor and Na^+/K^+ ATPase) with gangliosides (GM1, GD1a, GD1b, and GT1b) and transmembrane proteins (IR, IGF-1R, APP, Np 65)

2. immunohistochemically determine the colocalization of lipid raft markers (flotillin) and non-raft markers (transferrin receptor and Na^+/K^+ ATPase) with gangliosides (GM1, GD1a, GD1b, and GT1b) and transmembrane proteins (IR, IGF-1R, APP, Np 65) in differentiated human SH-SY5Y neuroblastoma cells after inhibition of synthesis of glycosphingolipids by P4 inhibitors (inhibits GLCT-1 synthase, EC: 2.4.1.80), MIG (inhibits GLCT-1 synthase, EC: 2.4.1.80) and CBE (inhibits beta-galactosidase EC: 3.2.1.23).

3. to determine morphological changes in cell membrane structure caused by the addition of P4, MIG, and CBE by staining the cell membrane using fluorescein isothiocyanate.

4. to MALDI-TOF-MS analyze cellular lipids and test the activation of insulin downstream signaling pathway (GSK3β and pAkt) after modification of glycosphingolipid synthesis using Western blotting method from differentiated human neuroblastoma cells treated with an optimal concentration of P4, MIG, and CBE.

4. MATERIALS AND METHODS

4.1. Study design

The study was structured as a randomized controlled trial.

4.2. Materials

Human neuroblastoma cell line SH-SY5Y, ATCC CRL-2266 (Manassas, Virginia USA) below the 20th passage was used in all experimental procedures. All chemicals used in the procedures were at least analytical grade. Additional chemical properties and manufacturer's details are written in brackets after the first mention.

4.3. Methods

4.3.1. Cultivation of the cells

SH-SY5Y cell line was purchased from Sigma (Sigma-Aldrich, Saint Louis, MO, SAD). DMEM/F12 medium for cell cultivation with added 15 mM HEPES, 4.5 g/L glucose, sodium bicarbonate was bought from Sigma (Sigma-Aldrich, Saint Louis, MO, SAD). The medium was supplemented with 1% of 100x non-essential amino acids, 3 mM of L-glutamine, 1% of 100x penicillin/streptomycin, and 10% fetal bovine serum (FBS). The FBS and penicillin/streptomycin were omitted in experimental growth mediums.

The culturing protocol was following:

1. 9 ml of growth medium was transferred to a 15 mL Falcon tube.
2. The tube with frozen cells was thawed by partially immersing it for 2 minutes in the water bath heated up to 37 °C.
3. The thawed cell suspension was transferred by sterile Pasteur pipette into a growth medium in the Falcon tube.
4. The cell suspension was centrifuged at room temperature at 130g for 5 minutes.
5. The supernatant was discarded, and cells are resuspended in 5 mL of fresh complete growth medium.
6. Cells were counted in the Neubauer chamber.

7. The final concentration of 100 000 cells/mL was prepared, and 7 mL of cell suspension was transferred to each 25 cm^2 flask.
8. The next day, the growth medium was replaced with the same volume of a fresh one.
9. Cells were grown to 85% confluency.
10. After reaching the sufficiently confluent state, the medium was removed, and cells were trypsinized with 2.5 mL of preheated trypsin solution for 3 minutes and lightly shaken until cells were visibly detached from the bottom of the flask.
11. A fresh growth medium (2.5 mL) was added to trypsin/cell suspension to stop the enzymatic reaction. The solution was transferred to a 15 mL Falcon tube and centrifuged at room temperature at 130 g for 5 minutes.
12. The supernatant was discarded, and cells were resuspended in 10 mL of fresh complete growth medium.
13. Cells were counted in the Neubauer chamber.
14. The final concentration of 250 000 cells/mL was prepared, and 12 mL of cell suspension was transferred to each 100 mm Petry dish.
15. Cells were grown to 85 % confluency and then harvested for further experiments.

Since the neuroblastoma cells are adherent type, seeding concentration for experiments is calculated by growth surface area; I found that the optimal concentration is 50 000 cells per square centimeter. Areas per well are 0.32 cm^2 per well of 96-well plates, 9.6 cm^2 per well of 6-well plates, 75 cm^2 per 100 mm Petry dish. Therefore, growth medium volumes per well are 100 µL for each well of 96-well plates, 2000 µL for each well of 6-well plates, 12 mL per 100 mm Petry dish.

4.3.2. Preparation of coverslips

In the production of glass, oils are used to ease glass cutting and handling. Even though most coverslip glass comes prewashed, it is not suitable for cell growth because even a minute amount of oil residue can hinder cell adhesion or change cell metabolism. Therefore, all organic matter must be removed before seeding cells. This was achieved by total oxidation in sulfuric acid fortified with hydrogen peroxide. This also made glass hydrophilic and thus acceptable for later treatments and cell adhesion. The washing

protocol was following: 1 part of 30 % hydrogen peroxide (Kemika, Zagreb, Croatia) was mixed with 9 parts of concentrated (96 %) sulfuric acid (Kemika, Zagreb, Croatia).

1. In 300 mL wide throat Erlenmeyer flask, 100 coverslips were placed (20×20mm square), and a mixture of sulfuric acid and hydrogen peroxide was poured on glass slides.
2. Gentle swirl motion was used to cover all coverslips with the solution, which was repeated at least 3 times during the following 30 minutes.
3. After 30 minutes, under the fume hood, acid was poured from the flask into a 5L-bucket of distilled water to safely dilute it. 200 mL of fresh distilled water was added to the flask with coverslips to dilute leftover acid.
4. Coverslips were rinsed with water, which was then safely discarded into chemical waste, or by dilution with large amounts of tap water.
5. 200 mL of distilled water was poured into a flask and placed on an orbital shaker (100 rpm) for 1 hour.
6. After 1 hour, water was discarded from the flask, and fresh 200 mL of distilled water was added. The washing cycle was repeated another 5 times (in total, 6 hours of washing).
7. After the last wash, distilled water was discarded, and the coverslips were dried by adding 100 mL of ACS or HPLC grade methanol, the flask was swirled for 5 minutes. Methanol was then discarded into chemical waste.
8. Aluminum foil was placed over the flask opening, and coverslips were dry sterilized at 270°C for 5 hours.

4.3.3. Collagen type 1 growth surface coating

Human neuroblastoma is grown on an adhesive surface. For that purpose, collagen is applied in final concentrations of 5.5 µg/cm^2. In addition, different volumes of diluted collagen were used for other multiwell plates to speed up the drying: 30 µL for each well of 96-well plates; 750 µL for each well of 6-well plates, 1000 µL for each 100 mm Petry dish. The coating was done as follows:

1. The necessary volume of collagen stock solution was calculated by dividing the total mass of collagen (in micrograms) by the concentration of collagen stock solution (in micrograms per milliliter) - the given result is expressed in milliliters.

$$V(stock\ solution) = \frac{5.5 \times \sum well\ bottom\ surface\ area}{stock\ concentration}$$

2. The total volume of collagen working solution used for coating was calculated by multiplying the number of wells with the corresponding volume per well (as stated above).

$$V(working\ solution) = n(well) \times V(specifffic\ for\ well\ size)$$

3. The volume of collagen stock solution was subtracted from the total volume of collagen working solution (given number is the volume of 30%-ethanol)

$$V(30\ \%\ ethanol) = V(working\ solution) - V(stock\ solution)$$

4. The 30%-ethanol solution was prepared by mixing 3 parts of 100%-ethanol ASC or HPLC grade (GramMol, Zagreb, Croatia) with 7 parts of distilled water, and the calculated volume of collagen stock solution (Sigma-Aldrich, Saint Louis, MO, SAD) was pipetted.
5. Collagen and ethanol were mixed on a vortex mixer.
6. Inside the laminar flow cabinet, a previously defined volume of diluted collagen solution was pipetted into each well.
7. Once collagen was pipetted, the lids were taken off, the laminar flow turned off, and the cabinet was closed. The UV-C lamp was turned on for 1 hour, after which the lamp was turned off.
8. Everything was left in a laminar flow cabinet to completely dry overnight.
9. The next day, the UV-C lamp was turned on in the laminar flow cabinet for 2 hours to sterilize dried collagen and wells completely.
10. After the proper aseptic procedure, the lids were put back on, and the cell suspension was added.

The protocol for coating coverslips for immunocytochemistry was the same. Before pipetting collagen solution, one coverslip was placed into each well with sterile tweezers. The surface area remained unchanged since properly cleaned coverslips firmly adhered to the bottom of the well.

4.3.4. Cell differentiation and general experimental plan

Cell differentiation protocol was as follows:
Day 0 – cells were seeded in collagenated wells and placed in an incubator (Thermo Fisher scientific Hera Cell 150 Waltham, Massachusetts, United States).

Day 1 – growth medium was replaced with fresh one containing 10 µM of ATRA (Merck, Kenilworth, New Jersey, United States).

Day 3 – growth medium was replaced with a fresh one containing 10 µM of ATRA.

Day 7 – growth medium was replaced with a fresh one containing 10 µM of ATRA.

Day 9 – growth medium was replaced with a fresh one containing ATRA, without FBS.

Notes: Omission of FBS was necessary to avoid the effect of cytokines. During differentiation, cells change their morphology. The presence of significant neurite growth was usually an indication of proper successful differentiation.

Day 10 – growth medium was replaced with a fresh one without FBS, with added inhibitors in three different concentrations and biological triplicates.

Day 12 – further experimental procedures were executed (immunocytochemistry, biochemical analysis, or lipidomic).

4.3.5. Preparation of glycolipid metabolism modulators

Two isomers of P4 were prepared: (*R, R*) D, L-threo-phenyl-2-hexadecanoylamino-3-pyrrolidino-1-propanol (P4-RR) and (*S, S*) D, L-threo-phenyl-2-hexadecanoylamino-3-pyrrolidino-1-propanol (P4-SS), (compounds were a donation from prof. Schnaar, Johns Hopkins University, Baltimore, USA). Both isomers were dissolved in dimethyl sulfoxide (Thermofisher Waltham, Massachusetts, United States) and stored at -20 °C until used.

CBE (Santa Cruz Biotechnology, Dallas, Texas, United States) was measured and dissolved in dimethyl sulfoxide (Thermofisher Waltham, Massachusetts, United States) and stored at -20 °C until used.

MIG was extracted from the Zavesca capsule (Actelion Pharmaceuticals, Basel, Switzerland). Since the active compound is as equally soluble in water as the filler compounds, it could not be dissolved in the water. Instead, acetone was used because MIG dissolves only in it (142,146–152). The isolation protocol was following:

1. The content of the capsule was transferred to a beaker.

2. 100 mL of precooled analytical grade acetone (Thermo Fisher, Waltham, Massachusetts, United States) was poured over, mixed with swirl motion, and left at 4°C overnight to extract the compound.
3. The following day, acetone extract was transferred to a clean glass centrifuge test tube and centrifuged at 1000 g for 20 minutes at 4°C.
4. Clean glass-made test tubes were weighed on an analytical scale.
5. The supernatant was transferred to clean glass-made test tubes, and acetone was evaporated in the stream of nitrogen.
6. Test tubes with MIG were weighed on an analytical scale, and compound mass was calculated
7. MIG was dissolved in 1x phosphate-buffered saline solution (PBS) containing 0.1% of bovine serum albumin (Thermofisher Waltham, Massachusetts, United States) and frozen at -20°C until further use.

All compounds were prepared in 20 mM concentration. For experimental procedures, each compound was diluted in serum-free and antibiotic-free cell growth medium in three concentrations: 40µM, 10µM, and 2.5µM.

4.3.6. MTT assay

MTT assay is extensively used in testing cytotoxicity, cell viability, and cell proliferation. It relies on functional NAD(P)H-dependent oxidoreductase enzymes found in mitochondria of all living cells. These enzymes reduce yellow water-soluble tetrazolium bromide into purple water-insoluble formazan crystals. The amount of produced crystals is usually correlated with the number of live cells.
MTT stock solution was prepared as follows:

1. 100 mg of tetrazolium bromide powder (Cruz chemicals, Dallas, Texas, USA) was weighed.
2. The powder was dissolved in 20 mL of 1× PBS.
   (Note: to speed up the process, an ultrasonic homogenizer Bandelin Sonopuls 2070 (BANDELIN electronic GmbH & Co. KG, Berlin, Germany) set to 70W power was used for 15 seconds duration of the continuous pulse. Falcon tube was placed in the ice bath to keep the solution cold.)

3. The solution was sterilized by filtering it through a 0.2 µm syringe PES filter (Nalgene ™ Thermo Fisher Scientific Waltham, Massachusetts, United States).
4. 1.5 mL aliquots were frozen at -20 °C.

MTT test procedure was following:

1. Cells were sown in a collagenated 96-well plate using previously given instructions and differentiated in at least 6 biological replicas for each experiment.
2. The growth medium was replaced with mediums containing inhibitors in different concentrations, solvent or without any supplements, and incubated for 24 and 48 hours.
   - concentrations of DMSO solvent were 1.12 mM, 0.28 mM, and 0.07 mM
3. The insulin was pipetted into one half of the plate to a final concentration of 2 µg/ml and incubated for 1 hour.
4. After 24 hours, 10 µL of MTT stock solution was pipetted into each well, resulting in 0.5 mg/mL of tetrazolium bromide concentration.
5. The half wells of 96-well plates had 1-hour treatment with insulin in 2 µg/mL concentration.
6. Plates were placed in an incubator for 2 hours to produce formazan crystals.
7. After incubation, 100 µL of MTT solvent was added into each well with MTT stock solution, and formazan crystals were dissolved by repeated pipetting 10 times.
8. 96-well plates were read on the iMark microplate reader (Bio-rad, Hercules, California, United States) at 595 nm.
9. The final result was calculated as OD percentage value against the untreated group.

4.3.7. Annexin V staining

Annexin V staining is used in the detection of apoptotic cells. Together with propidium iodide staining it is suitable to distinguish between viable, necrotic, or apoptotic cells. Phosphatidyl-serine is a membrane phospholipid located in the inner leaflet of the cell membrane. When cells undergo apoptosis phosphatidyl-serine molecules flip outside and positions themselves in the outer leaflet of the cell membrane. Annexin V binds to phosphatidyl-serine, thus marking the cells that undergo apoptosis.

For Annexin V to bind, calcium and magnesium ions are needed, therefore all buffers must contain one or both of the ions (153,154). The procedure was following:

1. Cells were sown in collagenated 12 well plate using previously given instructions and differentiated, at least 6 biological replicas for each concentration, solvent, and untreated control were used.
2. The growth medium was replaced with mediums containing inhibitors in different concentrations, solvent or without any supplements, and incubated for 24 and 48 hours.
3. Annexin V stain working solution was prepared in advance using manufacturer directions, in dilution of 1:100 in Annexin V buffer.
4. The growth medium was removed, and cells were trypsinized with 500 µl of 0.25% trypsin (Sigma-Aldrich, Saint Louis, MO, SAD) for 4 minutes.
5. After 4 minutes, the enzymatic reaction was stopped by pipetting an equal amount of growth medium.
6. Cells were pelleted at 130 g for 5 minutes.
7. The supernatant was removed, and 500 µl of Annexin V stain working solution was pipetted in each tube and incubated for 10 minutes.
8. After incubation, cells were counted on Facs 2 Canto flow cytometer (BD Sciences, Franklin Lakes, New Jersey, USA) with active 488 nm and 633 nm lasers.

Flow cytometry data analysis was performed in FlowLogic software (Miltenyi Biotec, Bergisch Gladbach, Germany). The protocol was following:

1. Fsc files were uploaded into software and grouped by selecting all files and right-clicking. From the drop-down menu "*Group/Add to New"* option was selected.
2. Forward and side scatter plot was drawn in the first file, and all values below 10 of side and forward scatter were gated off from further analysis (Figure 4.1.).
3. The second graph was plotted by double-clicking the selected area and plotting the graph by choosing FITC and PerCP Cy5. Gates for alive cells, early apoptosis, late apoptosis, and dead cells were selected on the graph. By selecting gates in the first graph, they were selected automatically in all other grouped graphs.
4. Data was copied to an Excel spreadsheet and prepared for statistical analysis.

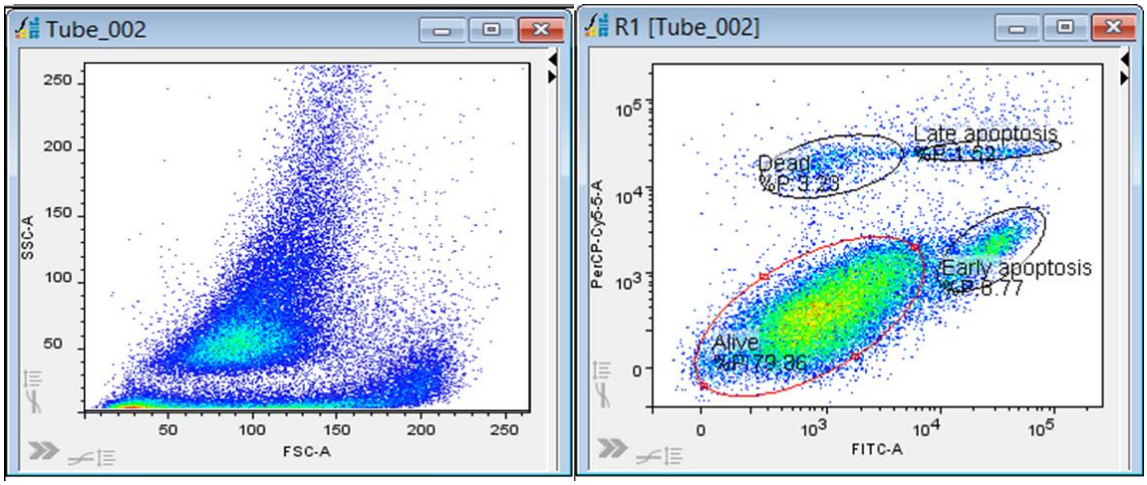

Figure 4.1. The analysis of flow cytometry data in FlowLogic software presenting gate selection for differentiation of alive cells, cells in early and late apoptosis, and dead cells. The figure was made by the author.

4.3.8. Immunocytochemistry and histochemical staining

Immunocytochemistry is a method for the *in situ* visualization of epitopes of interest. Highly specific primary antibodies were used to label epitope positions at or in the cells. A secondary antibody was used to mark and visualize the place of primary antibody binding. The list of solutions used in this set of experiments is listed in Table 4.1. The list of primary and secondary antibodies is listed in Table 4.2. and 4.3. respectively. For all experiments, three biological replicas were used. The protocol was following:

1. Cells were grown and differentiated on previously prepared and collagen type 1 pre-treated glass slides (incubator: Thermo Fisher scientific Hera Cell 150 Waltham, Massachusetts, United States).
2. After differentiation, cells were treated with inhibitors of ganglioside synthesis for 48-hours.
3. After 48 hours, one-half of the cells were treated with insulin in the final concentration of 2 µg/mL and placed in an incubator for 1 hour.
    - The insulin stock solution was prepared in a cell growth medium at a concentration of 12 µg/ml, and 500µl was pipetted into each well of a 6-well plate.

4. After the insulin treatment, the cell growth medium from all plates was removed, and 2 mL of 2% paraformaldehyde (PFA) was pipetted into each well of a 6-well plate.
5. Glass slides were incubated in PFA for 30 minutes at 4°C.
6. After incubation, PFA was removed, and 3 mL of 1x PBS was pipetted in each well.
7. Fixed cells were stored at 4 °C until further use.
8. Before incubation, glass slides were cut to fit the wells of 12-well plates.
9. Cut glass slides were placed in each well of 12-plates in biological triplicates.
10. 500 μL of blocking solution was pipetted in each well and incubated for 4 hours.
11. After incubation, a blocking solution was removed and the solution of two primary antibodies dissolved in the blocking solution was pipetted.
12. Slides were placed at 4°C for 48 hours.
13. After incubation of the primary antibodies, slides were washed three times for 10 minutes with precooled 1x PBS.
14. After washing, appropriate secondary antibodies were prepared in blocking solution in 1:1000 dilution and pipetted in 12-well plates, 500 μL in each well, and incubated for 4 hours at 4 °C.
15. After incubation of the secondary antibodies, slides were washed four times for 10 minutes in precooled 1x PBS. The last wash was with 1x PBS containing 0.05% PFA to fix antibodies and prevent bacterial growth.
16. If secondary antibodies were biotinylated (antibodies raised against goat primary antibody), cells were incubated for 1 hour in a 1:1000 diluted fluorophore-labeled streptavidin.
17. After incubation of streptavidin, slides were washed four times for 10 minutes in precooled 1x PBS. The last wash with 1x PBS contained 0.05% PFA to fix antibodies together and prevent bacterial growth.
18. Slides were mounted in the *Fluorescent mounting medium with DAPI* (Abcam, Cambridge, United Kingdom) and imaged on the Axioskop 2 MOT microscope with mounted Olympus D70 camera controlled through computer program DP Manager 1.2.1.107 and DP Controller 1.2.1.108

Cells used for morphology analysis were grown following the same protocol as for immunocytochemistry. After fixed, cells were stained with FITC dye (Sigma-Aldrich,

Saint Louis, MO, SAD) that covalently binds to the membrane proteins (155). The protocol was following:

1. After fixation, a buffer was removed from the cells, and the FITC solution was pipetted on the cells and incubated for 1 hour at room temperature.
2. Cells were washed 3 times for 10 minutes with 1x PBS to remove the excess dye.
3. Cells were mounted in the *Fluorescent mounting medium with DAPI* (Abcam, Cambridge, United Kingdom) and imaged on the Axioskop 2 MOT microscope with mounted Olympus D70 camera controlled through computer program DP Manager 1.2.1.107 and DP Controller 1.2.1.108

Table 4.1. Solutions used in immunocytochemistry and morphology analysis

Solution name	Abbreviation	Composition of the solution
Insulin stock solution	Ins.Sol.	2 mg/mL of insulin isolated from bovine pancreas (Thermo Fisher Scientific, Waltham, Massachusetts, United States) dissolved in 0.1M hydrochloric acid and stabilized with 0.1% bovine serum albumin; the solution is sterile filtered through 0.2 μm PES filter (Nalgene ™ Thermo Fisher Scientific Waltham, Massachusetts, United States) and stored at -20°C
Phosphate buffered saline	PBS	1x solution contains: 137 mM NaCl, 2.7 mM KCl, 10 mM Na_2HPO_4, 1.8 mM KH_2PO_4 with pH adjusted to 7.40; the solution is filtered through a 0.2 μm PES filter (Nalgene ™ Thermo Fisher Scientific Waltham, Massachusetts, United States)
Paraformaldehyde 2%	PFA	2% PFA (m/v) (Acros organics, Fair Lawn, New Jersey, USA) dissolved in 1x PBS, pH adjusted at 7.40; the solution is filtered through a 0.2 μm PES filter (Nalgene ™ Thermo Fisher Scientific Waltham, Massachusetts, United States).
Paraformaldehyde 0.05%	PFA	2% PFA solution diluted in 1x PBS to a final concentration of 0.05%
Blocking solution	/	1% bovine serum albumin (m/v) (Sigma-Aldrich, St. Louis, MO, SAD) with 2.5% (v/v) of goat serum (Sigma-Aldrich, St. Louis, MO, SAD) and 2.5% (v/v) of horse serum (Sigma-Aldrich, St. Louis, MO, SAD) dissolved and diluted in 1x PBS; the solution is sterile filtered through 0.2 μm PES filter (Nalgene ™ Thermo Fisher Scientific Waltham, Massachusetts, United States)
Fluorescein isothiocyanate solution	FITC	FITC (Sigma-Aldrich, Saint Louis, MO, SAD) was diluted in 1x PBS at the final concentration of 60 μg/mL

Table 4.2. List of primary antibodies used in immunocytochemistry.

Antibody label	Full name of the antibody	Antibody classification	Host species	Manufacturer and catalog number	Dilution
IRα	Anti-Insulin receptor alpha subunit	IgG, polyclonal	Rabbit	Abcam, Cambridge, UK Cat.No. ab5500	1:1000
IGF1Rb	Anti-Insulin-like growth factor receptor – beta subunit	IgG, polyclonal	Rabbit	Santa Cruz, CA, SAD Cat.No. sc-713	1:500
βAPP	Anti-Beta-amyloid precursor protein	IgG, polyclonal	Rabbit	Abcam, Cambridge, UK Cat.No. ab2539	1:500
Np65	Anti-Neuroplastin 65	IgG, polyclonal	Goat	R&D Systems, Minneapolis, MN, SAD, Cat.No. AF5360	1:500
GM1	Anti-GM1 ganglioside	IgG, monoclonal	Mouse	Johns Hopkins, Donation from prof Schnaar	1:1000
GD1a	Anti-GD1a ganglioside	IgG, monoclonal	Mouse	Seikagaku, Tokio, Japan, Cat.No. 370705	1:3000
GD1b	Anti-GD1b ganglioside	IgG, monoclonal	Mouse	Seikagaku, Tokio, Japan	1:3000
GT1b	Anti-GT1b ganglioside	IgG, monoclonal	Mouse	Seikagaku, Tokyo, Japan	1:3000
TFR 1	Anti-Transferrin receptor 1		Mouse	Merck, Darmstadt, Germany Cat.No. MAB Cat.No. S1982	1:1000
Flot1	Anti-flotillin 1	IgG, monoclonal	Mouse	BD Sciences, Franklin Lakes, New Jersey, U.S. Cat.No. Bd 610821	1:1000
Flot2	Anti-flotillin 2	IgG, polyclonal	Rabbit	Santa Cruz, CA, SAD Cat.No. sc25507	1:1000
Na^+/K^+ ATP-ase	Sodium/Potassium ATPase	Polyclonal IgG	Goat	Santa Cruz, CA, SAD Cat.No. sc16052	1:1000

Table 4.3. List of secondary antibodies and tertiary complex used in immunocytochemistry.

Antibody label	Full name of the antibody	Antibody classification	Host species	Manufacturer and catalog number	Dilution
αRB-biotin	anti-rabbit antibody labeled with biotin	IgG	Goat	Jackson immunoresearch West Grove, Pennsylvania, USA Cat.No. 111-065-144	1:1000
αGO-biotin	anti-goat antibody labeled with biotin	IgG	Donkey	Abcam Cat.No. ab6884	1:1000
αMO-FITC	anti-mouse antibody labeled with FITC	IgG	Goat	Jackson immunoresearch West Grove, Pennsylvania, USA Cat.No. 111-095-144	1:600
PE-Cy ™ 5	Streptavidin labeled with PE-Cy ™ 5	-	-	DB Pharmingen Cat.No. 554062	1:1000

Immunocytochemistry data were analyzed a Fiji computer program (156) as follows:

1. After starting the Fiji program, images in TIFF (Tagged Image File Format) were uploaded into the program and sorted into a stack through commands *Image/Stacks/Images to stack.*
2. The images in TIFF format were translated into an 8-bit format which assigns a value to each pixel from 0-255 using the *Menu Toolbar/Image/Type/8-bit* commands.
3. Images were thresholded through commands: *Image/Adjust/Threshold* to automatic settings for each image and *Black background* selected.
4. Aglomerated cell nuclei were separated into individual ones through protocol *Process/Binary/Watershed.*
5. Cell nuclei were counted by protocol: *Analyze/Analyze particles* with settings adjusted as follows: *Size*:250-Infinity; *Circularity:* 0.30-1.00.
6. Following analysis, the *Results* window appears, and it was copied to Excel for further analysis.

Following the counting of the cell nuclei, individual staining intensity had to be measured and analyzed for each channel using a Fiji computer program (156) as follows:

1. After starting the Fiji program, images in TIFF were entered into the program and sorted into a stack through commands *Image/Stacks/Images to stack.*
2. The images in TIFF format were translated into an 8-bit format which assigns a value to each pixel from 0-255 using the *Menu Toolbar/Image/Type/8-bit* commands.
3. Values of all the stack images were measured through the commands *Image/Stack/Measure stack.*
4. *Integrated density values* (IDV) were divided by the number of nuclei per image. Calculated numbers were averaged for each biological replica and used in statistical analysis.
5. Calculated data of IDV per cell is used in further statistical analysis.

Image analysis for colocalization was performed in Python programming language using Spider IDE interface (157). The programming code used for this analysis is listed in Supplement. A short description of the protocol is following:

1. All images were renamed to contain G, R, or B (presenting the green, blue, and red channel, respectively) and a number at the end.
2. First, it was necessary to determine values for negative controls, so the code was run through all channels of negative controls.
3. After values for individual negative control channels were determined, the rest of the images were analyzed.
4. Code had to be adjusted for negative control threshold in *Run/Configuration per file*
   "ext tif -th1 60 -th2 60 -th3 60"
5. Data was written in an Excel spreadsheet and presented as a percentage of red channel colocalizing with the green channel; the percentage was used in further statistical analysis.

Morphology of the treated and stained cells was determined using *ImageJ-Fiji* software with *NeurphologyJHT* plugin following the plugin online protocol (156,158) as follows:

1. Images were transformed into 8-bit through commands *Images/Type/8-bit*.
2. The *NeuronJ* plugin was used to trace neurites.
3. The plugin was started by selecting *Plugins/NeuronJ,* followed by selecting an image for analysis through the toolbar button *Load an image.*

4. Between 35 and 50 neurites were measured in each image by pressing the toolbar button *Add tracings* and selecting the beginning and end of the neurite.
5. Measurement values were obtained by pressing the toolbar button *Measure tracings* and exporting the data into an Excel spreadsheet for further analysis.

4.3.9. MALDI-TOF-MS lipid determination

Matrix-Assisted Laser Desorption/Ionisation Time-Of-Flight Mass Spectrometry (MALDI-TOF-MS) is the method that utilizes biological matrices to ionize the sample loaded onto an electroconductive carrier that can be either glass coated with indium-tin-oxide or a polished steel plate. Only the charged molecules can be easily imaged. Imaging can be performed in either positive or negative mode. In positive mode, the matrix takes an electron from the sample molecules and positively charges them. In negative mode matrix gives an electron to the sample molecule, negatively charging it. The most commonly used matrices are dihydroxybenzoic acid (DHB), for positive mode, and 9-aminoacridine (9-AA) for the negative imaging mode. As a result, neutral or hard-to-ionize molecules will be detected as noise or in low quantities.

For isolation of total lipids, cells were prepared in the same way as for Western blot analysis with the difference in cell washing steps where acetate buffer was used. Cell homogenate was prepared in 0.32 M sucrose in 150 mM ammonium acetate buffer, pH 8.2 with all inhibitors used in the protocol for Western blot analysis. Everything was performed in six biological replicates. Homogenization was performed following the Bligh and Dyer protocol for isolation of total lipids as follows (159):

1. Protein homogenate was diluted to 2.5 µg/µL.
2. 160 µL of homogenate was pipetted into a 1.5 mL Eppendorf tube.
3. 400 µL of HPLC purity methanol (J.T.Baker, Phillipsburg, New Jersey, United States) was added and vortexed.
4. 200 µL of analytical purity chloroform (Carlo Erba, Milan, Italy) was added and vortexed; this amounts to a ratio of 0.8:2:1 (sample: methanol: chloroform).
5. The mixture was left on ice for 10 minutes to complete lipid extraction.
6. After 10 minutes, 200 µL of chloroform and 200 µL of HPLC clean water (Carlo Erba, Milan, Italy) were pipetted.
7. Everything was vortexed for 10 seconds and centrifuged at 20 000 g for 5 minutes at 4 °C.

8. After centrifugation, three phases were visible: upper water, middle protein, and bottom chloroform/methanol phase.
9. The bottom phase was collected and transferred with pipette tips into a dark glass HPLC collection vial, capped, and stored at -20 °C until further use.
10. The remaining phases were discarded into chemical waste.

Both matrices were prepared in a concentration of 10 mg/mL. DHB was dissolved in HPLC purity methanol (J.T.Baker, Phillipsburg, New Jersey, United States) and stored at 4°C. The 9-AA matrix was dissolved in a mixture of acetonitrile (J.T.Baker, Phillipsburg, New Jersey, United States) and isopropanol (Merck, Darmstadt, Germany) in the ratio of 40:60. Both solvents were HPLC grade. The dissolved matrix was stored at 4°C. Matrix was applied as follows:

1. Matrix and sample were mixed in 1:1 ratio total equalling 6 µL for each sample. 2 µL of matrix/sample ratio was applied on a polished steel plate sample carrier and quickly dried with forced air current at room temperature.
2. At one spot, red phosphorus was applied to be used for negative mode calibration. In the case of positive mode, peptide mix (Bruker, Billerica, Massachusetts, United States) was applied.
3. Samples were imaged in the positive and negative mode in the range 500 Da - 2500 Da.

Machine settings for imaging at Bruker UltrafleXtreme MALDI-TOF/TOF MS (Bruker, Billerica, Massachusetts, United States) were identical for positive and negative modes. The sample rate and digitizer were set at 5.00 GS/s, Smartbeam (laser) set to medium, laser frequency 2000 Hz, laser power 90%, 200 shots/pixel, and every measurement was a sum of 15000 shots.

Calibration in positive mode was done with Leucine-Enkephalin (Sigma-Aldrich, Saint Louis, MO, SAD) and Bruker Peptide calibration mix (Bruker, Billerica, Massachusetts, United States). Calibration in negative mode was done with red phosphorus clusters (Sigma-Aldrich, Saint Louis, MO, SAD).

Result of analysis and data extraction were performed in Bruker Flex Analysis software (Bruker, Billerica, Massachusetts, United States) with the following adjustments: Peak detection algorithm was *Snap; s/n threshold* was 6, Smoothing

Algorithm was *SavitzkyGolay* (width 0.2 m/z, cycles 1), Baseline subtraction was done with *TopHat.*

Statistical analysis of the spectrum data was performed in R statistical software (Vienna, Austria) with the following libraries: *matrixTests, roperators, FELLA, KEGGREST, igraph, magrittr, resample* (160).

4.3.10. Protein analysis and Western blot method

Electrophoresis was used to separate proteins in a sample based on their mass. Proteins were denatured with sodium dodecyl sulfate (SDS) and additionally unfolded with dithiothreitol or β-mercaptoethanol. Separation was carried through acrylamide gel that served as a sieve. The gel was made from two separate gels: the top one containing 5% acrylamide/bis-acrylamide (AA/Bis) and the bottom one 12% of AA/Bis concentration. The list of solutions used in the Western blot protocol is listed in table 4.4.

Table 4.4. Prepared solutions used in the Western blot method.

Solution name	Abbreviation	Composition
Phosphate buffered saline 1x	1x PBS	137 mM of NaCl, 2.7 mM of KCl, 10 mM of Na_2HPO_4, 1.8 mM oh KH_2PO_4 (All chemicals from GramMol, Zagreb, Croatia)
Homogenization buffer	HB	1x PBS, 0,32 m sucrose, 1 mM PMSF, 5mM NaF, 1 mM Na_3VO_4, 1 mM EDTA (All chemicals from Sigma-Aldrich, Saint Louis, MO, SAD), 1 tablet of complete mini protease inhibitor per 10 mL of buffer (Roche, Basel Switzerland)
10% SDS	/	10 g of SDS Acrylamide (Sigma-Aldrich, Saint Louis, MO, SAD)/100 mL distilled water
Western blot sample buffer	/	0.35 M Tris-HCl, pH 6.8, 10% SDS, 30% glycerol, 9.3% DTT
3M Tris-HCl	/	36.342 g of Tris base, up to 100 mL of dH2O, pH 8.8
1M Tris-HCl	/	12.114 g of Tris base, up to 100 mL of dH2O, pH 6.8
30% Acrylamide/Bis-acrylamide	AA/Bis	30% Acrylamide(Sigma-Aldrich, Saint Louis, MO, SAD), 2.7% Bis- Acylamide
1.5% Ammonium persulphate	APS	1.5 g Ammonium persulphate (Sigma-Aldrich, Saint Louis, MO, SAD) in 100 mL of distilled water
Electrophoresis buffer	/	25 mM Tris-Base (Fisher Scientific, Waltham, Massachusetts, USA), 192 mM glycine (Fisher Scientific, Waltham, Massachusetts, USA), 0.1% SDS in distilled water
Towbin blotting buffer	/	25 mM Tris-Base, 192 mM glycine, 20% methanol in distilled water
Blocking solution	/	3% BSA (Sigma-Aldrich, Saint Louis, MO, SAD) in 1x PBST

Cells were grown, differentiated, and treated with compounds in 6-well plates to attain 6 biological replicas – two plates were prepared for each concentration of each compound, solvent control, and untreated control – a total of 32 individual 6-well plates. Cells were incubated for 48 hours after treatment application (incubator: Hera Cell 150, Thermo Fisher Scientific Waltham, Massachusetts, United States). In one-half of the 6 well plates, insulin was added in a final concentration of 2 μg/ml, and cells were incubated for 1 hour. This was performed by diluting insulin stock solution in cell growth medium to a concentration of 12 μg/mL, and 500 μL was pipetted in each well of 6-well plate. After this step, everything was done on ice and with precooled solutions. After incubation with insulin, all cells were washed 3 times with 1x PBS. Next, 500 μL of 1x PBS was pipetted in each well, and cells were scraped with a cell scraper. Scraped cells were transferred in a 1.5 mL Eppendorf tube and pelleted in a centrifuge at 130 g for 5 minutes at 4°C (centrifuge: Sigma 1-15 PK, St. Louis, Missouri, United States). The supernatant was removed, and 600 μL of homogenization buffer was added. Cells were homogenized on ice with an ultrasonic homogenizer Bandelin Sonopuls 2070 (BANDELIN electronic GmbH & Co. KG, Berlin, Germany) for 15 seconds, cycle set at 9 and 100% power. Homogenate was centrifuged for 15 minutes at 1000 g at 4°C (centrifuge: Sigma 1-15 PK, St. Louis, Missouri, United States) to remove extracellular matrix and insoluble debris. The supernatant was pipetted in a clean 0.5 mL Eppendorf tube and stored at -80°C until further use.

Before the final preparation of samples for loading on the gel, protein content was measured using Bradford protein assay. Protein measurement with Bradford reagent is based on the reaction of Coomassie blue G 250 in an acidic solution with aromatic groups of amino acids. The dye binding to amino acids shifts the dye absorption maximum from 465 nm to 595 nm (161). The reagent is prepared by dissolving 50 mg of Coomassie blue G 250 powder (Carl Roth Karlsruhe, Germany) in 50 mL of methanol (Carlo Erba, Milan, Italy). After the dye was dissolved, 100 mL of 85% phosphoric acid (Sigma, St. Louis, Missouri, United States) was added and topped with distilled water up to 1 liter. The reagent was filtered through a 0.2 μm PES filter (Nalgene ™ Thermo Fisher Scientific Waltham, Massachusetts, United States) to remove any traces of undissolved dye powder and stored at 4°C.

A calibration curve is prepared and calculated using bovine serum albumin as a standard with known concentrations:

Standard 1 – 10 mg/mL

Standard 2 – 5 mg/mL

Standard 3 – 2.5 mg/mL

Standard 4 – 1.25 mg/mL

Standard 5 – 0.625 mg/mL

Standard 6 – 0.312 mg/mL

Standard 7 – only sample buffer

Samples were pipetted in technical triplicate in a flat-bottom 96-well plate (Thermo Fisher Scientific Waltham, Massachusetts, United States). In each well, 1 µL of the standard sample was pipetted, followed by 250 µL of Bradford reagent. Everything was incubated at room temperature for 15 minutes and analyzed at the iMark microplate reader (Bio-rad, Hercules, California, United States) at 595 nm. The given value of absorption measured in Standard 7 was subtracted from the measured values of the rest of the Standards. A calibration curve was plotted, and a linear equation was calculated.

The concentration of proteins in samples was determined by pipetting 1 µL of the cell homogenate sample in a technical triplicate followed by 250 µL of Bradford reagent. After 15 minutes of incubation at room temperature, absorption was measured on the iMark microplate reader (Bio-rad, Hercules, California, United States) at 595 nm. First, the absorption value measured in Standard 7 was subtracted from the measured values of samples. Then, triplicates were averaged to a single value. Finally, corrected and averaged absorption values were used in a linear equation from which protein concentrations were calculated (Figure 4.5.).

Sample aliquots were diluted to 2.5 mg/mL with 1x PBS buffer and mixed with Western blot sample buffer in a 1:5 buffer to sample ratio. Samples were heated up to 100°C for 5 minutes in a heat block (Eppendorf Thermomixer Compact; Eppendorf, Hamburg, Germany). After heating, samples were cooled down and stored at 4°C until further use.

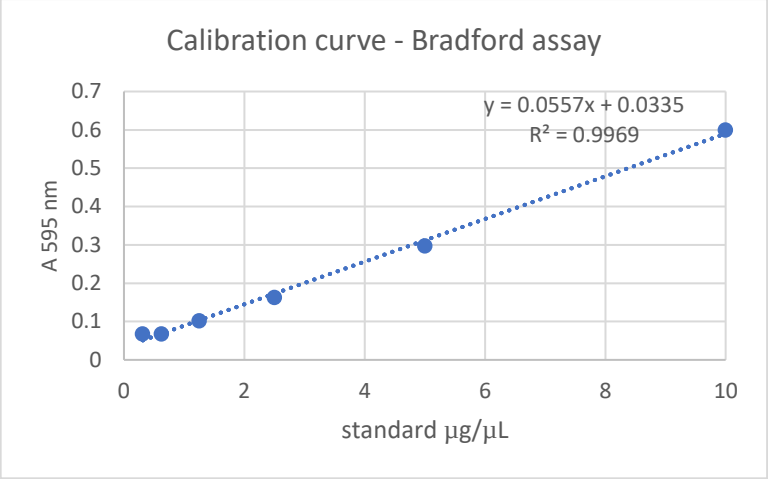

Figure 4.5. Calibration curve of Bradford assay used to calculate linear regression equation for determination of protein content in samples. Figure made by the author.

Gels used in Western blot analysis were the discontinuous type with 5% of AA/Bis in stacking gel and 12% of AA/Bis in resolving gel, prepared in Tris-Glycine buffer with the addition of 1.15% of 2,2,2-Trichloroethanol (Merck, Darmstadt, Germany) for the stain-free method (162,163). Gels were loaded as follows: first well with 5µL of protein standard (SeeBlue 2 Plus, Thermo Fisher Scientific Waltham, Massachusetts, United States) and 10 µL of the sample in each following well of the gel. Thus, the total protein load was equal to 20 µg. Electrophoresis was carried in Hoeffer mighty small electrophoresis system (Hoeffer inc. San Francisco, California, United States) with a continuous current of 15 mA per gel for 3 hours in electrophoresis buffer. The cooling fluid was circulated through the central block to maintain a constant temperature around 4°C.

After electrophoresis, gel cassettes were removed from the electrophoresis system, stacking gel was cut, and bottom stain-free gels were activated in the ChemiDoc™ Imaging system (BioRad Hercules, California, United States) for 45 seconds using automated imaging protocol to visualize proteins within the gel. Detection of proteins is made possible by detecting the amino acid tryptophan to which the gel tri-halo components are attached. Next, the transfer of the proteins from gel to polyvinylidene difluoride (PVDF) membrane of 0.45 µm pore size (Thermo Fisher Scientific Waltham, Massachusetts, United States) was carried out in TE22 Mighty small transfer tank (Hoeffer inc. San Francisco, California, United States) for 2 hours at 200 mA continuous current in Towbin blotting buffer. During blotting, the system was

continuously cooled to 4°C. When the blotting was over, gels were discarded, and PVDF membrane containing proteins from a gel was placed in 1x PBS-T and imaged on ChemiDoc™ Imaging system (BioRad Hercules, California, United States) to visualise proteins on the membrane (Figure 4.6.). The digital images of transfered proteins were saved for later analysis.

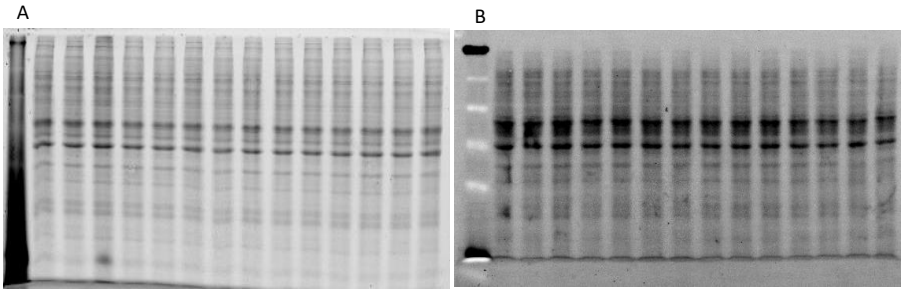

Figure 4.6. The stain-free gel representative image upon activation (A) and the membrane (B) after transferring proteins. Images captured in ChemiDoc™ Imaging system and visualised in the computer program Image Lab (BioRad Hercules, California, United States).

Immunodetection followed transfer of proteins to the membrane. Nonspecific reactions were blocked by a solution of 3% bovine serum albumin in 1x PBS buffer with Tween detergent (PBST). Blocking solution was used for all antibodies and tertiary complex dilutions. After the stepped blocking, the membrane was incubated in the primary antibody solution (IRα, IGF1Rb, βAPP, Np65, paNa/KT, pAkt-Ser 473, GSK3 α+β, pGSK3β, αSyn, pTAU) in the dilutions shown in Table 4.7 on a shaker overnight at 4°C. Membranes were washed 3 times for 10 minutes in PBST buffer followed by incubation in the appropriate secondary antibody (Table 4.8.) conjugated with HRP for 1 hour at room temperature. Membrane probed against Np65 was incubated in a biotinylated secondary antibody followed by washing and incubation in the tertiary streptavidin-HRP complex. Secondary antibodies and streptavidin-HRP complex were washed 3 times for 10 minutes in PBST buffer. According to the manufacturer's instructions, visualization was performed using a chemiluminescent detection solution (Immobilon ® Forte Western HRP Substrate, Millipore Burlington, Massachusetts, USA). According to the manufacturer's instructions, the signal is visualized using the ChemiDoc™ Imaging system (BioRad Hercules, California, United States). The resulting images were stored in digital form for later analysis.

Table 4.7. List of primary antibodies used in the Western blot method.

Antibody label	Full name of the antibody	Antibody classification	Host species	Manufacturer and catalog number	Dilution used for Western blot
IRα	Anti-insulin receptor alpha subunit	IgG, polyclonal	Rabbit	Abcam, Cambridge, UK Cat.No. ab5500	1:1000
IGF1Rb	Anti-insulin-like growth factor receptor – beta subunit	IgG, polyclonal	Rabbit	Santa Cruz, CA, SAD Cat.No. sc-713	1:500
βAPP	Anti-β-amyloid precursor protein	IgG, polyclonal	Rabbit	Abcam, Cambridge, UK Cat.No. ab2539	1:1000
Np65	Anti-neuroplastin 65	IgG, polyclonal	Goat	R&D Systems, Minneapolis , MN, SAD, Cat.No. AF5360	1:1000
Akt	Anti-protein kinase B	IgG monoclonal	Mouse	Cell signalling Danvers, Massachisets, USA Cat.No. 2920S	1:1000
pAkt – Ser 473	Anti-protein kinase B – phosphorylated at serine 473	IgG monoclonal	Rabbit	Cell signaling Danvers, Massachisets, USA Cat.No. 9271S	1:1000
GSK3 α+β	Anti-glycogen synthase kinase 3 alpha + beta	IgG monoclonal	Rabbit	Cell signaling Danvers, Massachisets, USA Cat.No. 5676S	1:1000
pGSK3β	Anti-glycogen synthase kinase 3 beta – phosphorylated as tyrosine 279	IgG polyclonal	Rabbit	Abcam, Cambridge, UK Cat.No. ab75745	1:1000
αSyn	Alpha-synuclein	IgG polyclonal	Rabbit	Cell signaling Danvers, Massachisets, USA Cat.No. 4179P	1:1000
pTAU	Phospho-Tau (Ser202, Thr205)	IgG monoclonal	Mouse	Thermo Fisher Waltham, Massachusetts, United States Cat.No. MN1020	1:1000

Table 4.8. List of secondary antibodies and tertiary complex used in Western blot method.

Antibody label	Full name of the antibody	Antibody classification	Host species	Manufacturer and catalog number	Dilution used for Western blot
αMO- HRP	anti-mouse antibody labeled with HRP	IgG	Donkey	Jackson immunoresearch West Grove, Pennsylvania, USA Cat.No. 715-035-151	1:20000
αRB- HRP	anti-rabbit antibody labeled with HRP	IgG	Goat	Jackson immunoresearch West Grove, Pennsylvania, USA Cat.No. 111-035-144	1:20000
αGO-biotin	anti-goat antibody labeled with biotin	IgG	Donkey	Abcam Cat.No. ab6884	1:5000
Strep-HRP	Streptavidin peroxidase polymer supersensitive	-	-	Sigma-Aldrich, St. Louis, MO, SAD	1:5000

To quantitatively analyze the expression of proteins of interest solution (IRα, IGF1Rb, βAPP, Np65, pan Akt, pAkt-Ser 473, GSK3 α+β, pGSK3β, αSyn, and pTAU), publicly available ImageLab 6.0 computer program compatible with Chemidoc system for visualization was used. In addition, images of total and individual proteins were used for quantitative analysis signals of the investigated proteins. The analysis was performed as follows:

1. An image of total and individual proteins was uploaded into the computer program ImageLab to analyze proteins of interest. Images are uploaded into the program in *.scn* digital format. Command menu toolbar */ File / Open / Select image* was used.

2. The images were prepared for processing by selecting the toolbar command *menu / File / Create Multi-Channel Image*. After opening a new window, the RGB box was unchecked, and two images remained in the window – those of total proteins and individually analyzed protein.

3. *Lane* and *Bands* command in the left part of the toolbar was selected for each image, the widths and heights of the wells were analyzed automatically or manually by the commands *Automatic* or *Manual*.

4. After marking the wells, the protein band signals were analyzed by selecting the command *Bands*. Automatic detection of protein bands was done with the *Detect* command, and manual detection was done using the *Add* tool (manually marks each protein analysis band).

5. The *Analysis Table* command, that prints the obtained data, was selected and data was exported as an Excel spreadsheet.

6. The signal intensity values from the obtained table were used. Intensity value of individually analyzed protein bands were divided by the intensity of total protein tape, and the value obtained was used for further statistical processing.

4.4. Statistical analysis

The statistical program Statistica 12 (TIBCO, Palo Alto, CA USA) was used for statistical analyses. Normality of distribution was tested with the Shapiro-Wilk test. In the case of a normal distribution, a t-test was used to determine the significance of the difference between the two samples. If the distribution of the results was not normal, the conclusion about the differences between the two independent continuous random variables distributions was based on the Mann-Whitney-Wilcoxon test. In the case of more than two samples, and depending on the nature of the results, parametric or nonparametric analysis of variance (ANOVA) was used. The Kruskal-Wallis test was used as a nonparametric analysis for multiple independent samples, and the Friedman test was used for multiple dependent samples. In all analyses, the p-value was determined with $p < 0.05$, $p < 0.005$, and $p < 0.001$. A sample in minimal biological triplicate was used for each statistical analysis.

5. RESULTS

5.1. MTT test of cell viability

P4-RR inhibitor affected cell viability in all three concentrations independently on whether insulin was applied or not. The combined effect of treatment (inhibitors) and insulin is not present after 24 hours (Table 5.1.). After 24 hours, cell viability decreased compared to the control group. Insulin treatment had a prominent effect on cell viability and is best observed at the highest inhibitor concentration, where the viability was nearly doubled compared to the insulin untreated groups. Significant differences can be observed between the highest and lowest concentrations of inhibitor both in insulin treated and non-treated samples (Table 5.6.). After 48 hours, increasing concentrations of the inhibitor resulted the decrease in cell viability. Addition of insulin to the inhibitor treated samples caused similar decline in cell viability (Table 5.1.). Significant reduction in cell viability was observed in samples treated with the highest concentrations of inhibitor regardless of insulin treatment. In addition, there is a significant difference in cell viability between samples treated with the highest inhibitor concentration and the two lower ones (Table 5.7.)

24 hours P4-SS treatment resulted statistically significant effects on cell viability independently from the absence or presence of insulin treatment (Table 5.2.). When compared to the control group, the difference was only observed in samples treated with the highest concentration of inhibitor; cell viability did not change in samples treated the other two inhibitor concentrations (Table 5.8.). 48 hours treatment resulted significant decrease in cell viability only in samples treated with the highest concentrations of the inhibitor both in insulin treated and non-treated samples (Table 5.2). Significant difference between the insulin treated and non-treated samples can be detected only in samples treated with 10 μM concentration (Table 5.9.)

Different concentrations of MIG treatments alone or in combination with the insulin treatment, had no effect on cell viability after 24 hours. A statistically significant decrease in cell viability were observed after 48 hours in samples treated with MIG and insulin (Table 5.3.). The post-HOC analysis found no significant differences between the treated sample groups.

Different concentrations of CBE treatments had effects on cell viability only after 48 hours (Table 5.4.). The post-hoc analysis found no significant difference between the treated sample groups.

DMSO treatment alone (used as the solvent for all 4 inhibitors) had no effect on cell viability in all three concentrations, with or without insulin treatment (Table 5.5.).

Table 5.1. Percentage of cell viability 24 and 48 hours after treatment with P4-RR GlcCer synthesis inhibitor, and insulin of differentiated SH-SY5Y human neuroblastoma cell line measured with MTT test calculated against the control group (Mean; SD).

Duration of treatment	w/o insulin				w insulin				Two-way ANOVA					
	Control	P4-RR 2.5μM	P4-RR 10μM	P4-RR 40μM	Control	P4-RR 2.5μM	P4-RR 10μM	P4-RR 40μM	F values; (degrees of freedom)			p-values		
	Mean; SD	Mean; SD	Mean; SD	Mean; SD	Mean; SD	Mean; SD	Mean; SD	Mean; SD	Insulin	RR	Insulin × RR	Insulin	RR	Insulin × RR
24 h treatment	100.00; 4.71	78.52; 6.86	72.71; 3.32	48.07; 5.03	100.00; 3.75	84.83; 3.96	89.35; 7.35	71.39; 7.73	8.59 (1,40)	17.41 (3,40)	1.71 (3,40)	0.0055	<0.0001	0.1740
48 h treatment	100.00; 3.73	93.61; 7.26	94.62; 6.57	48.82; 2.99	100.00; 2.29	86.20; 2.83	86.71; 3.71	64.37; 3.57	0.00 (1,40)	36.55 (3,40)	3.02 (3,40)	0.9855	<0.0001	0.0406

SD = standard deviation; w/o insulin = without insulin; w insulin = with insulin; P4-RR = (*R, R*) D, L-threo-phenyl-2-hexadecanoylamino-3-pyrrolidino-1-propanol

Table 5.2. Percentage of cell viability 24 and 48 hours after treatment with P4-SS GlcCer synthesis inhibitor and insulin of differentiated SH-SY5Y human neuroblastoma cell line measured with MTT test calculated against the control group (Mean; SD).

Duration of treatment	w/o insulin				w insulin				Two-way ANOVA					
	Control	P4-SS 2.5μM	P4-SS 10μM	P4-SS 40μM	Control	P4-SS 2.5μM	P4-SS 10μM	P4-SS 40μM	F values; (degrees of freedom)			p-values		
	Mean; SD	Mean; SD	Mean; SD	Mean; SD	Mean; SD	Mean; SD	Mean; SD	Mean; SD	Insulin	SS	Insulin × SS	Insulin	SS	Insulin × SS
24 h treatment	100.00; 4.71	94.79; 7.69	92.48; 5.42	26.02; 3.48	100.00; 3.75	106.85; 9.34	106.02; 9.51	28.34; 3.67	2.38 (1,40)	64.74 (3,40)	0.56 (3,40)	0.1308	<0.0001	0.6402
48 h treatment	100.00; 3.73	104.06; 5.41	103.37; 6.70	20.36; 1.95	100.00; 2.29	91.16; 2.14	79.57; 2.27	35.48; 8.68	2.55 (1,40)	103.93 (3,40)	6.18 (3,40)	0.1179	<0.0001	0.0014

SD = standard deviation; w/o insulin = without insulin; w insulin = with insulin; P4-SS = (*S, S*) D, L-threo-phenyl-2-hexadecanoylamino-3-pyrrolidino-1-propanol

Table 5.3. Percentage of cell viability 24 and 48 hours after treatment with MIG GlcCer synthesis inhibitor and insulin of differentiated SH-SY5Y human neuroblastoma cell line measured with MTT test calculated against the control group (Mean; SD).

Duration of treatment	w/o insulin				w insulin				Two-way ANOVA					
	Control	MIG 2.5µM	MIG 10µM	MIG 40µM	Control	MIG 2.5µM	MIG 10µM	MIG 40µM	F values; (degrees of freedom)			p-values		
	Mean; SD	Mean; SD	Mean; SD	Mean; SD	Mean; SD	Mean; SD	Mean; SD	Mean; SD	Insulin	MIG	Insulin × MIG	Insulin	MIG	Insulin × MIG
24 h treatment	100.00; 4.71	86.82; 4.94	82.12; 14.34	92.74; 11.93	100.00; 3.75	94.32; 3.45	91.72; 1.90	99.54; 5.19	1.26 (1,40)	1.19 (3,40)	0.15 (3,40)	0.2672	0.3240	0.9270
48 h treatment	100.00; 3.73	105.48; 5.60	93.67; 3.05	96.50; 10.55	100.00; 2.29	92.94; 3.19	76.42; 3.38	74.33; 2.16	13.66 (1,40)	5.59 (3,40)	1.83 (3,40)	0.0006	0.0026	0.1569

SD = standard deviation; w/o insulin = without insulin; w insulin = with insulin; MIG = miglustat

Table 5.4. Percentage of cell viability 24 and 48 hours after treatment with CBE inhibitor of glycolipid metabolism and insulin of differentiated SH-SY5Y human neuroblastoma cell line measured with MTT test calculated against the control group (Mean; SD).

Duration of treatment	w/o insulin				w insulin				Two-way ANOVA					
	Control	CBE 2.5µM	CBE 10µM	CBE 40µM	Control	CBE 2.5µM	CBE 10µM	CBE 40µM	F values; (degrees of freedom)			p-values		
	Mean; SD	Mean; SD	Mean; SD	Mean; SD	Mean; SD	Mean; SD	Mean; SD	Mean; SD	Insulin	CBE	Insulin × CBE	Insulin	CBE	Insulin × CBE
24 h treatment	100.00; 4.71	98.74; 7.56	86.33; 4.32	88.84; 9.65	100.00; 3.75	106.88; 3.28	97.19; 2.03	95.23; 3.19	2.79 (1,40)	2.18 (3,40)	0.37 (3,40)	0.1021	0.1046	0.7753
48 h treatment	100.00; 3.73	94.36; 4.26	73.22; 1.54	71.52; 3.27	100.00; 2.29	101.65; 9.35	98.20; 14.97	82.11; 16.89	2.83 (1,40)	2.93 (3,40)	0.67 (3,40)	0.0997	0.0448	0.5695

SD = standard deviation; w/o insulin = without insulin; w insulin = with insulin; CBE = Conduritol B epoxide

Table 5.5. Percentage of cell viability 24 and 48 hours after treatment with DMSO solvent and insulin of differentiated SH-SY5Y human neuroblastoma cell line measured with MTT test calculated against the control group (Mean; SD).

Duration of treatment	w/o insulin				w insulin				Two-way ANOVA					
	Control	DMSO 0.07 mM	DMSO 0.28 mM	DMSO 1.12 mM	Control	DMSO 0.07 mM	DMSO 0.28 mM	DMSO 1.12 mM	F values; (degrees of freedom)			p-values		
	Mean; SD	Mean; SD	Mean; SD	Mean; SD	Mean; SD	Mean; SD	Mean; SD	Mean; SD	Insulin	DMSO	Insulin × DMSO	Insulin	DMSO	Insulin × DMSO
24 h treatment	100.00; 4.71	98.55; 2.83	97.55; 2.78	94.44; 6.51	100.00; 3.75	103.44; 3.66	100.18; 4.03	96.69; 2.27	0.73 (1,40)	0.69 (3,40)	0.12 (3,40)	0.3951	0.5634	0.9452
48 h treatment	100.00; 3.73	101.35; 3.13	96.23; 4.92	101.97; 3.01	100.00; 2.29	95.01; 2.97	96.58; 2.03	95.83; 2.01	1.85 (1,40)	0.46 (3,40)	0.69 (3,40)	0.1807	0.7111	0.5608

SD = standard deviation; w/o insulin = without insulin; w insulin = with insulin; DMSO = dimethyl sulfoxi

Table 5.6. Post hoc test of two-way ANOVA results for cell viability 24 hours after treatment with P4-RR GlcCer synthesis inhibitor and insulin of differentiated SH-SY5Y human neuroblastoma cell line presenting significant results

Survivability rate measured with MTT test after 24 hours from treatment				
The first set of variables (A)		The second set of variables (B)		Post hoc Tukey HSD p-value A vs B
Insulin treatment	The concentration of P4-RR	Insulin treatment	The concentration of P4-RR	
w/o insulin	Control	w/o insulin	P4-RR 40μM	0.0001
w/o insulin	Control	w/o insulin	P4-RR 10μM	0.0260
w/o insulin	Control	w insulin	P4-RR 40μM	0.0167
w/o insulin	P4-RR 40μM	w/o insulin	P4-RR 2.5μM	0.0088
w/o insulin	P4-RR 40μM	w insulin	Control	0.0001
w/o insulin	P4-RR 40μM	w insulin	P4-RR 10μM	0.0002
w/o insulin	P4-RR 40μM	w insulin	P4-RR 2.5μM	0.0009
w/o insulin	P4-RR 10μM	w insulin	Control	0.0260
w insulin	Control	w insulin	P4-RR 40μM	0.0167

SD = standard deviation; w/o insulin = without insulin; w insulin = with insulin; P4-RR = (R, R) D, L-threo-phenyl-2-hexadecanoylamino-3-pyrrolidino-1-propanol

Table 5.7. Post hoc test of two-way ANOVA results for cell viability 48 hours after treatment with P4-RR GlcCer synthesis inhibitor and insulin of differentiated SH-SY5Y human neuroblastoma cell line presenting significant results

Survivability rate measured with MTT test after 48 hours from treatment				
The first set of variables (A)		The second set of variables (B)		Post hoc Tukey HSD p-value A vs B
Insulin treatment	The concentration of P4-RR	Insulin treatment	The concentration of P4-RR	
w/o insulin	Control	w/o insulin	P4-RR 40μM	0.0001
w/o insulin	Control	w insulin	P4-RR 40μM	0.0001
w/o insulin	P4-RR 40μM	w/o insulin	P4-RR 10μM	0.0001
w/o insulin	P4-RR 40μM	w/o insulin	P4-RR 2.5μM	0.0001
w/o insulin	P4-RR 40μM	w insulin	Control	0.0001
w/o insulin	P4-RR 40μM	w insulin	P4-RR 10μM	0.0001
w/o insulin	P4-RR 40μM	w insulin	P4-RR 2.5μM	0.0001
w insulin	P4-RR 40μM	w/o insulin	P4-RR 10μM	0.0006
w insulin	P4-RR 40μM	w/o insulin	P4-RR 2.5μM	0.0009
w insulin	P4-RR 40μM	w insulin	Control	0.0001
w insulin	P4-RR 40μM	w insulin	P4-RR 10μM	0.0204
w insulin	P4-RR 40μM	w insulin	P4-RR 2.5μM	0.0253

SD = standard deviation; w/o insulin = without insulin; w insulin = with insulin; P4-RR = (R, R) D, L-threo-phenyl-2-hexadecanoylamino-3-pyrrolidino-1-propanol

Table 5.8. Post hoc test of two-way ANOVA results for cell viability 24 hours with P4-SS GlcCer synthesis inhibitor and insulin of differentiated SH-SY5Y human neuroblastoma cell line presenting significant results

Survivability rate measured with MTT test after 24 hours from treatment				
The first set of variables (A)		The second set of variables (B)		Post hoc Tukey HSD p-value A vs B
Insulin treatment	The concentration of P4-SS	Insulin treatment	The concentration of P4-SS	
w/o insulin	Control	w/o insulin	P4-SS 40µM	0.0001
w/o insulin	P4-SS 40µM	w/o insulin	P4-SS 10µM	0.0001
w/o insulin	P4-SS 40µM	w/o insulin	P4-SS 2.5µM	0.0001

SD = standard deviation; w/o insulin = without insulin; w insulin = with insulin; P4-SS = (S, S) D, L-threo-phenyl-2-hexadecanoylamino-3-pyrrolidino-1-propanol

Table 5.9. Post hoc test of two-way ANOVA results for cell viability 48 hours with P4-SS a GlcCer synthesis inhibitor and insulin of differentiated SH-SY5Y human neuroblastoma cell line presenting significant results

Survivability rate measured with MTT test after 48 hours from treatment				
The first set of variables (A)		The second set of variables (B)		Post hoc Tukey HSD p-value A vs B
Insulin treatment	The concentration of P4-SS	Insulin treatment	The concentration of P4-SS	
w/o insulin	Control	w/o insulin	P4-SS 40µM	0.0001
w/o insulin	Control	w insulin	P4-SS 40µM	0.0001
w/o insulin	P4-SS 40µM	w/o insulin	P4-SS 10µM	0.0001
w/o insulin	P4-SS 40µM	w/o insulin	P4-SS 2.5µM	0.0001
w/o insulin	P4-SS 40µM	w insulin	Control	0.0001
w/o insulin	P4-SS 40µM	w insulin	P4-SS 10µM	0.0001
w/o insulin	P4-SS 40µM	w insulin	P4-SS 2.5µM	0.0001
w/o insulin	P4-SS 10µM	w insulin	P4-SS 40µM	0.0001
w/o insulin	P4-SS 10µM	w insulin	P4-SS 10µM	0.0217
w/o insulin	P4-SS 2.5µM	w insulin	P4-SS 40µM	0.0001
w/o insulin	P4-SS 2.5µM	w insulin	P4-SS 10µM	0.0166
w insulin	Control	w insulin	P4-SS 40µM	0.0001
w insulin	P4-SS 40µM	w insulin	P4-SS 10µM	0.0001
w insulin	P4-SS 40µM	w insulin	P4-SS 2.5µM	0.0001

SD = standard deviation; w/o insulin = without insulin; w insulin = with insulin; P4-SS = (S, S) D, L-threo-phenyl-2-hexadecanoylamino-3-pyrrolidino-1-propanol

5.2. Annexin V cell viability stain

Different concentrations of P4-RR inhibitor treatment had a significant effect on the number of cells will survive. Treatment resulted a dose-dependent decrease in the number of cells alive; lower concentrations of inhibitor resulted higher survival rate (Table 5.10.). The number of apoptotic or dead cells increased by the increasing inhibitor concentrations. This effect can be observed both at 24 or 48 hours after treatments. Insulin showed statistically significant effects in late apoptotic cells (Table 5.15.)

P4-SS effect on cell viability was observable both after 24 and 48 hours. Treatments had no significant effects on early apoptosis, but it significantly affected the numbers of cells in late apoptosis and the dead ones. Insulin did not affect the survival of the cells, but it affected cells in late apoptosis 48 hours after treatment and dead cells 24 and 48 hours after treatment. The mutual effect of insulin and inhibitor treatment was observed in the number of cells in late apoptosis 48 hours after treatment and in the number of dead cells 24 hours after treatment (Table 5.11.). Post hoc analysis showed a dose-dependent effect on late apoptosis, i.e. the higher the inhibitor concentration, the more cells undergo the process. The highest concentration of inhibitor significantly increased cell death after 24 hours, but not after 48 hours (Table 5.16., Table 5.11.).

MIG treatment affected the percentage of live cells, the percentage of cells in early apoptosis and the percentage of dead cells. Insulin treatment alone resulted the decrease of the percentage of early apoptosis cells 48 hours after treatment. The combined effect of insulin and inhibitor treatments was observed in the percentage of dead cells after 24 hours, but not after 48 hours (Table 5.12.). Post hoc analysis showed that MIG treatment did not significantly reduce the number of live cells. A difference in the percentage of cells in early apoptosis was observed when comparing the highest and lowest concentrations. The percentage of dead cells increases with the MIG concentration, but this is also a significant effect of insulin, which, when applied after 24 hours, reduces the lethal effect of MIG. The most notable differences are between the highest concentrations of MIG and the other experimental groups (Table 5.17., Table 5.12.).

CBE treatment alone had effects on the percentage of live cells and cells in early apoptosis, as well as in combinations with insulin treatment, but no observable interaction was observed between the two treatments. The only effect of CBE was observed in the percentage of cells in late apoptosis, but no insulin effect. The percentages are reversed where insulin had an effect, but it is missing when treated with CBE alone (Table 5.13.). Post hoc analysis showed no statistically significant difference between the treated groups.

DMSO had no effect on cell viability. The only effect was observed when cells were treated with insulin. No combined effects of insulin treatment and DMSO treatment was observable (Table 5.14.).

Table 5.10. Percentage of alive, apoptotic, and dead cells 24 and 48 hours after treatment with P4-RR GlcCer synthesis inhibitor measured with Annexin V staining of differentiated SH-SY5Y human neuroblastoma cell. Percentage calculated against the control group (Mean; SD).

Cell status	Expose time	w/o insulin				w insulin				Two-way ANOVA					
		Control	P4-RR 2.5 µM	P4-RR 10 µM	P4-RR 40 µM	Control	P4-RR 2.5 µM	P4-RR 10 µM	P4-RR 40 µM	F values; (degrees of freedom)			p-values		
		Mean; SD	Mean; SD	Mean; SD	Mean; SD	Mean; SD	Mean; SD	Mean; SD	Mean; SD	Insulin	RR	Insulin × RR	Insulin	RR	Insulin × RR
Alive	24 h	87.51; 1.66	90.25; 2.60	78.38; 12.06	64.58; 7.73	91.17; 1.61	93.85; 2.99	81.78; 12.17	63.73; 14.92	0.48 (1,16)	12.75 (3,16)	0.09 (3,16)	0.4972	0.0001	0.9602
	48 h	88.10; 1.91	91.94; 2.88	79.76; 11.89	65.58; 7.45	92.96; 0.59	94.43; 2.94	83.29; 12.07	64.00; 14.79	0.50 (1,16)	13.62 (3,16)	0.16 (3,16)	0.4862	0.0001	0.9206
Early apoptosis	24 h	9.44; 1.13	6.42; 2.68	12.19; 4.42	8.94; 0.59	6.98; 1.11	4.38; 3.20	10.86; 4.80	13.60; 8.83	0.02 (1,16)	2.85 (3,16)	0.94 (3,16)	0.8678	0.0702	0.4405
	48 h	7.85; 0.86	3.59; 2.96	9.94; 4.89	6.86; 0.49	4.16; 1.60	2.60; 2.80	8.30; 5.09	12.28; 9.32	0.01 (1,16)	2.80 (3,16)	1.19 (3,16)	0.9015	0.0722	0.3436
Late apoptosis	24 h	2.01; 0.38	1.89; 0.33	7.20; 7.81	21.81; 5.83	1.54; 0.54	1.35; 0.11	6.69; 7.55	21.25; 5.72	0.06 (1,16)	22.75 (3,16)	0.00 (3,16)	0.7957	<0.0001	0.9999
	48 h	2.37; 0.49	1.86; 0.33	1.86; 0.33	21.86; 0.33	1.86; 1.30	1.95; 0.47	7.23; 7.67	21.90; 5.46	20.83 (1,16)	11.64 (3,16)	12.22 (3,16)	0.0003	0.0002	0.0002
Dead	24 h	1.04; 0.23	1.44; 0.42	2.23; 0.81	4.68; 1.85	0.31; 0.07	0.42; 0.18	0.67; 0.26	1.42; 0.50	27.77 (1,16)	11.66 (3,16)	3.30 (3,16)	<0.0001	0.0002	0.0472
	48 h	1.68; 0.78	1.98; 0.50	2.73; 0.98	5.20; 2.03	1.02; 0.33	1.08; 0.20	1.19; 0.17	1.82; 0.51	9.14 (1,16)	1.34 (3,16)	1.29 (3,16)	0.0080	0.2935	0.3090

SD = standard deviation; w/o insulin = without insulin; w insulin = with insulin; P4-RR = (*R, R*) D, L-threo-phenyl-2-hexadecanoylamino-3-pyrrolidino-1-propanol

Table 5.11. Percentage of alive, apoptotic, and dead cells 24 and 48 hours after treatment with P4-SS GlcCer synthesis inhibitor measured with Annexin V staining of differentiated SH-SY5Y human neuroblastoma cell line. Percentage calculated against the control group (Mean; SD).

Cell status	Expose time	w/o insulin				w insulin				Two-way ANOVA					
		Control	P4-SS 2.5 μM	P4-SS 10 μM	P4-SS 40 μM	Control	P4-SS 2.5 μM	P4-SS 10 μM	P4-SS 40 μM	F values; (degrees of freedom)			p-values		
		Mean; SD	Mean; SD	Mean; SD	Mean; SD	Mean; SD	Mean; SD	Mean; SD	Mean; SD	Insulin	SS	Insulin × SS	Insulin	SS	Insulin × SS
Alive	24 h	87.51; 1.66	89.32; 3.10	88.62; 3.87	83.31; 8.76	86.99; 8.89	91.17; 1.61	92.47; 3.81	92.62; 3.13	2.99 (1,16)	1.61 (3,16)	0.00 (3,16)	0.1029	0.2262	0.9991
	48 h	88.10; 1.91	90.11; 3.73	89.50; 3.45	80.97; 3.76	84.56; 4.51	92.96; 0.59	92.70; 3.64	93.97; 3.52	7.83 (1,16)	9.45 (3,16)	0.13 (3,16)	0.0128	0.0007	0.9384
Early apoptosis	24 h	9.44; 1.13	7.35; 2.64	8.00; 3.48	5.25; 0.74	4.23; 2.10	6.98; 1.11	5.60; 3.54	5.88; 2.71	3.49 (1,16)	2.12 (3,16)	0.09 (3,16)	0.0797	0.1373	0.9593
	48 h	7.85; 0.86	5.71; 3.34	6.11; 3.70	3.43; 0.44	3.42; 1.74	4.16; 1.60	4.06; 3.31	3.69; 3.20	4.14 (1,16)	1.41 (3,16)	0.28 (3,16)	0.0587	0.2739	0.8335
Late apoptosis	24 h	2.01; 0.38	1.92; 0.37	1.94; 0.58	8.66; 6.57	7.99; 6.62	1.54; 0.54	1.50; 0.40	1.10; 0.42	0.19 (1,16)	6.02 (3,16)	0.00 (3,16)	0.6654	0.0060	0.9994
	48 h	2.37; 0.49	2.24; 0.63	2.39; 0.24	12.20; 2.47	10.96; 2.74	1.86; 1.30	2.17; 0.36	1.81; 0.30	1.15 (1,16)	71.28 (3,16)	0.18 (3,16)	0.2981	<0.0001	0.9031
Dead	24 h	1.04; 0.23	1.41; 0.33	1.44; 0.33	2.77; 1.53	0.79; 0.42	0.31; 0.07	0.44; 0.13	0.41; 0.09	23.78 (1,16)	4.01 (3,16)	1.29 (3,16)	0.0001	0.0262	0.3099
	48 h	1.68; 0.78	1.94; 0.40	2.00; 0.58	3.07; 1.35	1.06; 0.29	1.02; 0.33	1.08; 0.11	0.53; 0.09	18.07 (1,16)	1.98 (3,16)	3.68 (3,16)	0.0006	0.1569	0.0342

SD = standard deviation; w/o insulin = without insulin; w insulin = with insulin; P4-SS = (*S, S*) D, L-threo-phenyl-2-hexadecanoylamino-3-pyrrolidino-1-propanol

Table 5.12. Percentage of alive, apoptotic, and dead cells 24 and 48 hours after treatment with MIG GlcCer synthesis inhibitor measured with Annexin V staining of differentiated SH-SY5Y human neuroblastoma cell line. Percentage calculated against the control group (Mean; SD).

Cell status	Expose time	w/o insulin				w insulin				Two-way ANOVA					
		Control	MIG 2.5 µM	MIG 10 µM	MIG 40 µM	Control	MIG 2.5 µM	MIG 10 µM	MIG 40 µM	F values; (degrees of freedom)			p-values		
		Mean; SD	Mean; SD	Mean; SD	Mean; SD	Mean; SD	Mean; SD	Mean; SD	Mean; SD	Insulin	MIG	Insulin × MIG	Insulin	MIG	Insulin × MIG
Alive	24 h	87.51; 1.66	90.77; 0.97	87.87; 1.20	82.16; 5.80	91.17; 1.61	94.50; 0.81	91.24; 1.28	85.80; 5.58	8.31 (1,16)	8.30 (3,16)	0.00 (3,16)	0.0108	0.0014	0.9996
	48 h	88.10; 1.91	91.61; 1.16	88.91; 1.85	83.51; 5.44	92.96; 0.59	95.93; 0.90	92.08; 0.69	87.21; 5.01	11.56 (1,16)	8.67 (3,16)	0.10 (3,16)	0.0036	0.0012	0.9605
Early apoptosis	24 h	9.44; 1.13	6.12; 0.24	9.20; 1.05	13.81; 5.63	6.98; 1.11	3.81; 0.36	7.01; 1.34	11.71; 4.89	4.02 (1,16)	8.06 (3,16)	0.00 (3,16)	0.0620	0.0016	0.9995
	48 h	7.85; 0.86	4.17; 0.91	7.24; 1.52	11.72; 4.89	4.16; 1.60	1.56; 0.92	5.10; 1.33	9.41; 4.40	6.73 (1,16)	9.32 (3,16)	0.11 (3,16)	0.0195	0.0008	0.9509
Late apoptosis	24 h	2.01; 0.38	1.86; 0.85	1.88; 0.23	2.41; 0.34	1.54; 0.54	1.33; 0.50	1.45; 0.40	2.01; 0.73	4.34 (1,16)	1.61 (3,16)	0.01 (3,16)	0.0533	0.2241	0.9963
	48 h	2.37; 0.49	2.24; 0.96	2.25; 0.32	2.78; 0.60	1.86; 1.30	1.80; 0.79	2.09; 0.50	2.60; 0.79	1.37 (1,16)	1.19 (3,16)	0.10 (3,16)	0.2588	0.3438	0.9543
Dead	24 h	1.04; 0.23	1.24; 0.02	1.05; 0.12	1.62; 0.17	0.31; 0.07	0.36; 0.03	0.30; 0.05	0.48; 0.04	340.89 (1,16)	13.77 (3,16)	3.92 (3,16)	<0.0001	0.0001	0.0281
	48 h	1.68; 0.78	1.98; 0.10	1.60; 0.31	2.00; 0.15	1.02; 0.33	0.70; 0.29	0.73; 0.45	0.78; 0.20	33.29 (1,16)	3.42 (3,16)	6.04 (3,16)	<0.0001	0.0428	0.0059

SD = standard deviation; w/o insulin = without insulin; w insulin = with insulin; MIG = miglustat

Table 5.13. Percentage of alive, apoptotic, and dead cells 24 and 48 hours after treatment with CBE inhibitor of glycolipid metabolism measured with Annexin V staining of differentiated SH-SY5Y human neuroblastoma cell line. Percentage calculated against the control group (Mean; SD).

Cell status	Expose time	w/o insulin				w insulin				Two-way ANOVA					
		Control	CBE 2.5 µM	CBE 10 µM	CBE 40 µM	Control	CBE 2.5 µM	CBE 10 µM	CBE 40 µM	F values; (degrees of freedom)			p-values		
		Mean; SD	Mean; SD	Mean; SD	Mean; SD	Mean; SD	Mean; SD	Mean; SD	Mean; SD	Insulin	CBE	Insulin × CBE	Insulin	CBE	Insulin × CBE
Alive	24 h	87.51; 1.66	83.68; 2.52	83.23; 3.00	81.78; 4.61	91.17; 1.61	87.06; 2.42	86.87; 3.31	84.93; 4.77	7.03 (1,16)	3.78 (3,16)	0.01 (3,16)	0.0174	0.0317	0.9989
	48 h	88.10; 1.91	84.53; 1.89	83.67; 3.21	82.85; 4.85	92.96; 0.59	88.17; 2.22	88.40; 3.55	86.51; 5.43	9.44 (1,16)	3.38 (3,16)	0.06 (3,16)	0.0073	0.0442	0.9808
Early apoptosis	24 h	9.44; 1.13	12.69; 2.13	13.37; 2.46	13.40; 2.90	6.98; 1.11	10.64; 2.42	11.27; 3.44	11.62; 3.45	4.13 (1,16)	3.79 (3,16)	0.01 (3,16)	0.0589	0.0313	0.9964
	48 h	7.85; 0.86	10.67; 0.85	12.04; 2.46	11.42; 3.14	4.16; 1.60	8.36; 1.82	8.84; 3.91	9.04; 4.43	7.03 (1,16)	3.58 (3,16)	0.09 (3,16)	0.0174	0.0372	0.9624
Late apoptosis	24 h	2.01; 0.38	2.25; 0.25	2.18; 0.49	3.41; 1.36	1.54; 0.54	1.92; 0.07	1.52; 0.38	3.05; 1.31	2.18 (1,16)	4.93 (3,16)	0.06 (3,16)	0.1585	0.0129	0.9787
	48 h	2.37; 0.49	2.82; 0.55	2.49; 0.70	3.78; 1.84	1.86; 1.30	2.53; 0.16	1.92; 0.56	3.70; 1.15	0.96 (1,16)	4.07 (3,16)	0.09 (3,16)	0.3412	0.0250	0.9635
Dead	24 h	1.04; 0.23	1.38; 0.22	1.22; 0.51	1.42; 0.51	0.31; 0.07	0.37; 0.02	0.34; 0.13	0.40; 0.16	59.13 (1,16)	0.78 (3,16)	0.33 (3,16)	<0.0001	0.5198	0.8026
	48 h	1.68; 0.78	1.97; 0.49	1.79; 0.62	1.95; 0.65	1.02; 0.33	0.94; 0.46	0.84; 0.13	0.74; 0.32	14.73 (1,16)	1.12 (3,16)	2.62 (3,16)	0.0014	0.3691	0.0864

SD = standard deviation; w/o insulin = without insulin; w insulin = with insulin; CBE = Conduritol B epoxide

Table 5.14. Percentage of alive, apoptotic, and dead cells 24 and 48 hours after treatment with DMSO solvent measured with Annexin V staining of differentiated SH-SY5Y human neuroblastoma cell line. Percentage calculated against the control group (Mean; SD).

Cell status	Expose time	w/o insulin				w insulin				Two-way ANOVA					
		Control	DMSO 0.07 mM	DMSO 0.28 mM	DMSO 1.2 mM	Control	DMSO 0.07 mM	DMSO 0.28 mM	DMSO 1.2 mM	F values; (degrees of freedom)			p-values		
		Mean; SD	Mean; SD	Mean; SD	Mean; SD	Mean; SD	Mean; SD	Mean; SD	Mean; SD	Insulin	DMSO	Insulin × DMSO	Insulin	DMSO	Insulin × DMSO
Alive	24 h	87.51; 1.66	87.90; 0.60	86.48; 0.43	87.67; 1.68	91.17; 1.61	91.96; 0.53	90.74; 0.31	91.69; 1.54	66.90 (1,16)	1.40 (3,16)	0.10 (3,16)	<0.0001	0.2847	0.9768
	48 h	88.10; 1.91	87.57; 0.27	86.93; 0.13	88.52; 1.87	92.96; 0.59	94.00; 0.26	92.89; 0.43	93.43; 1.25	127.00 (1,16)	0.90 (3,16)	0.60 (3,16)	<0.0001	0.4692	0.6092
Early apoptosis	24 h	9.44; 1.13	10.22; 0.31	10.28; 0.70	9.31; 0.14	6.98; 1.11	8.83; 0.43	7.79; 0.69	6.85; 0.41	58.79 (1,16)	5.76 (3,16)	0.88 (3,16)	<0.0001	0.5198	0.4715
	48 h	7.85; 0.86	9.11; 0.46	8.91; 0.51	8.12; 0.91	4.16; 1.60	5.76; 0.36	5.33; 0.47	4.01; 0.57	147.39 (1,16)	5.78 (3,16)	0.27 (3,16)	<0.0001	0.3691	0.8417
Late apoptosis	24 h	2.01; 0.38	2.10; 0.45	1.93; 0.49	1.97; 0.44	1.54; 0.54	1.81; 0.46	1.47; 0.17	1.86; 0.09	4.02 (1,16)	0.51 (3,16)	0.24 (3,16)	0.0621	0.6761	0.8621
	48 h	2.37; 0.49	2.76; 0.29	2.56; 0.83	2.30; 0.43	1.86; 1.30	2.03; 0.29	2.06; 0.67	2.07; 0.57	4.06 (1,16)	0.29 (3,16)	0.19 (3,16)	0.0474	0.8289	0.8966
Dead	24 h	1.04; 0.23	0.85; 0.35	1.40; 0.50	1.07; 0.49	0.31; 0.07	0.31; 0.01	0.30; 0.03	0.35; 0.06	43.26 (1,16)	0.87 (3,16)	0.95 (3,16)	<0.0001	0.4734	0.4389
	48 h	1.68; 0.78	1.75; 0.49	1.58; 0.09	1.62; 0.43	1.02; 0.33	1.18; 0.45	1.09; 0.27	1.24; 0.38	3.57 (1,16)	1.28 (3,16)	1.05 (3,16)	0.0769	0.3136	0.3939

SD = standard deviation; w/o insulin = without insulin; w insulin = with insulin; DMSO = dimethyl sulfoxide

Table 5.15. Post hoc test of two-way ANOVA results for cell viability with Annexin V staining 24 and 48 hours after treatment with P4-RR GlcCer synthesis inhibitor and insulin of differentiated SH-SY5Y human neuroblastoma cell line presenting significant results

Cell status	Expose time	The first set of variables (A)		The second set of variables (B)		Post hoc Tukey HSD p-value A vs B
		Insulin treatment	The concentration of the P4-RR	Insulin treatment	The concentration of the P4-RR	
Alive	24 hours	w/o insulin	RR 40 µM	w/o insulin	RR 2.5 µM	0.0357
	48 hours	w/o insulin	RR 40 µM	w/o insulin	RR 2.5 µM	0.0281
Late apoptosis	24 hours	w/o insulin	Control	w/o insulin	RR 40 µM	0.0024
		w/o insulin	RR 40 µM	w/o insulin	Control	0.0024
		w/o insulin	RR 40 µM	w/o insulin	RR 10 µM	0.0310
		w/o insulin	RR 40 µM	w/o insulin	RR 2.5 µM	0.0023
	48 hours	w/o insulin	Control	w/ insulin	RR 40 µM	0.0002
		w/o insulin	RR 40 µM	w/ insulin	RR 40 µM	0.0001
		w/o insulin	RR 10 µM	w/ insulin	RR 40 µM	0.0001
		w/o insulin	RR 2.5 µM	w/ insulin	RR 40 µM	0.0001
		w/ insulin	Control	w/ insulin	RR 40 µM	0.0001
		w/ insulin	RR 10 µM	w/ insulin	RR 40 µM	0.0013
		w/ insulin	RR 2.5 µM	w/ insulin	RR 40 µM	0.0001
Dead	24 hours	w/o insulin	Control	w/o insulin	RR 40 µM	0.0006
		w/o insulin	RR 10 µM	w/o insulin	RR 40 µM	0.0205
		w/o insulin	RR 2.5 µM	w/o insulin	RR 40 µM	0.0018
		w/ insulin	Control	w/o insulin	RR 40 µM	0.0002
		w/ insulin	RR 40 µM	w/o insulin	RR 40 µM	0.0017
		w/ insulin	RR 10 µM	w/o insulin	RR 40 µM	0.0003
		w/ insulin	RR 2.5 µM	w/o insulin	RR 40 µM	0.0002

SD = standard deviation; w/o insulin = without insulin; w insulin = with insulin; P4-RR = (R, R) D, L-threo-phenyl-2-hexadecanoylamino-3-pyrrolidino-1-propanol

Table 5.16. Post hoc test of two-way ANOVA results for cell viability with Annexin V staining 24 and 48 hours after treatment with P4-SS GlcCer synthesis inhibitor and insulin of differentiated SH-SY5Y human neuroblastoma cell line presenting significant results

Cell status	Expose time	The first set of variables (A)		The second set of variables (B)		Post hoc Tukey HSD p-value A vs B
		Insulin treatment	The concentration of the P4-SS	Insulin treatment	The concentration of the P4-SS	
Late apoptosis	48 hours	w/o insulin	Control	w/o insulin	SS 40 µM	0.0001
		w/o insulin	SS 40 µM	w/o insulin	SS 10 µM	0.0001
		w/o insulin	SS 40 µM	w/o insulin	SS 2.5 µM	0.0001
Dead	24 hours	w/o insulin	Control	w/o insulin	SS 40 µM	0.0401
	48 hours	w/o insulin	SS 40 µM	w/ insulin	SS 40 µM	0.0150

SD = standard deviation; w/o insulin = without insulin; w insulin = with insulin; P4-RR = (R, R) D, L-threo-phenyl-2-hexadecanoylamino-3-pyrrolidino-1-propanol

Table 5.17. Post hoc test of two-way ANOVA results for cell viability with Annexin V staining 24 and 48 hours after treatment with MIG GlcCer synthesis inhibitor and insulin of differentiated SH-SY5Y human neuroblastoma cell line presenting significant results

Cell status	Expose time	The first set of variables (A)		The second set of variables (B)		Post hoc Tukey HSD p-value A vs B
		Insulin treatment	The concentration of the MIG	Insulin treatment	The concentration of the MIG	
Dead	24 hours	w/o insulin	Control	w/o insulin	MIG 40 µM	0.0004
		w/o insulin	Control	w/ insulin	Control	0.0001
		w/o insulin	Control	w/ insulin	MIG 40 µM	0.0005
		w/o insulin	Control	w/ insulin	MIG 10 µM	0.0001
		w/o insulin	Control	w/ insulin	MIG 2.5 µM	0.0002
		w/o insulin	MIG 40 µM	w/o insulin	Control	0.0004
		w/o insulin	MIG 40 µM	w/o insulin	MIG 10 µM	0.0005
		w/o insulin	MIG 40 µM	w/o insulin	MIG 2.5 µM	0.0195
		w/o insulin	MIG 40 µM	w/ insulin	Control	0.0001
		w/o insulin	MIG 40 µM	w/ insulin	MIG 40 µM	0.0001
		w/o insulin	MIG 40 µM	w/ insulin	MIG 10 µM	0.0001
		w/o insulin	MIG 40 µM	w/ insulin	MIG 2.5 µM	0.0001
		w/o insulin	MIG 40 µM	w/o insulin	MIG 40 µM	0.0005
		w/o insulin	MIG 40 µM	w/ insulin	Control	0.0001
		w/o insulin	MIG 40 µM	w/ insulin	MIG 40 µM	0.0005
		w/o insulin	MIG 40 µM	w/ insulin	MIG 10 µM	0.0001
		w/o insulin	MIG 40 µM	w/ insulin	MIG 2.5 µM	0.0002
		w/o insulin	MIG 2.5 µM	w/o insulin	MIG 40 µM	0.0195
		w/o insulin	MIG 2.5 µM	w/ insulin	Control	0.0001
		w/o insulin	MIG 2.5 µM	w/ insulin	MIG 40 µM	0.0001
		w/o insulin	MIG 2.5 µM	w/ insulin	MIG 10 µM	0.0001
		w/o insulin	MIG 2.5 µM	w/ insulin	MIG 2.5 µM	0.0001

SD = standard deviation; w/o insulin = without insulin; w insulin = with insulin; MIG = miglustat

5.3. Immunocytochemistry

5.3.1. Immunocytochemistry of P4-RR treated cells

Treating cells with P4-RR inhibitor *in situ* caused changes in the expression levels of several epitopes. The expression levels of IRα and Np65 were decreased by the inhibitor treatment. In the combination of inhibitor treatment with insulin levels of Np65 dropped, and levels of IR rised when treated with 10 and 40 µM. GM1 levels increased with the treatment but decreased after insulin application. The same pattern occurred for GD1a and GD1b (Table 5.18.).

Colocalization analysis showed significant difference in percentages of colocalization of βAPP, GM1, GD1b and GT1b with lipid raft markers showing epitope reduction in raft area (Table 5.22.). At the same time analysis showed that IGF1-Rβ, GM1 and GD1a are getting more accumulated in non raft area of the cells (Table 5.23.)

The post hoc analysis for IRα showed a significant difference only between the control group and the treatment with the lowest concentration of inhibitor (Table 5.19.).

The post hoc analysis for Np 65 showed a significant decrease in the low and middle concentration treated groups. The addition of insulin significantly reduced Np 65 levels in the low and high concentration treatment groups (Table 5.20.).

GM1 levels increased with the addition of insulin and were significantly higher in all treated groups compared to the insulin control. Addition of insulin and treatment with the inhibitor caused a reduction in GM1 levels compared to the insulin treated control group (Table 5.21.).

Post hoc analysis of colocalization showed that GT1b was significantly increased in lipid rafts when cells were treated with low concentration of inhibitor and significantly decreased in all inhibitor and insulin treated groups compared to the insulin treated control (Table 5.24.).

The highest value of GD1a was found when cells were treated with low a concentration of inhibitor and was significantly higher than in all other groups (Table 5.25.).

Table 5.18. The integrated density value of immunocytochemical staining of Differentiated SH-SY5Yhuman neuroblastoma cells treated 48 hours with P4-RR, a GlcCer synthesis inhibitor. Data are presented as integrated density values per cell. Statistical significance was tested with two-way ANOVA

Epitope	w/o insulin				w insulin				Two-way ANOVA					
	Control	P4-RR 2.5 µM	P4-RR 10 µM	P4-RR 40 µM	Control	P4-RR 2.5 µM	P4-RR 10 µM	P4-RR 40 µM	F values; (degrees of freedom)			p-values		
	Mean; SD	Mean; SD	Mean; SD	Mean; SD	Mean; SD	Mean; SD	Mean; SD	Mean; SD	Insulin	RR	Insulin × RR	Insulin	RR	Insulin × RR
βAPP	351769; 113703	50896; 9207	517391; 188371	315682; 89182	285842; 44657	186284; 70335	260653; 86163	399897; 78705	0.09 (1, 43)	1.86 (3, 43)	1.27 (3, 43)	0.7635	0.1491	0.2965
IGF1-Rβ	987948; 84329	783112; 286823	915838; 183158	973933; 204780	1724030; 748935	1132583; 314611	209284; 76201	522149; 159192	0.00 (1, 45)	2.08 (3, 45)	1.83 (3, 45)	0.9851	0.1157	0.1541
IRα	843864; 47466	43768; 6924	577281; 205316	613209; 157512	243148; 77939	124501; 39789	580708; 210997	655374; 232417	0.36 (1, 42)	3.88 (3, 42)	2.82 (3, 42)	0.5506	0.0154	0.0499
NP65	229369; 64570	156577; 44145	202632; 39699	427767; 47196	540101; 164500	186141; 23308	269211; 19226	122847; 22064	0.32 (1, 47)	3.27 (3, 47)	6.01 (3, 47)	0.5703	0.0291	0.0014
GM1	836326; 105238	679744; 80622	1253001; 125970	1378036; 344532	3236956; 348564	963919; 125176	720050; 187903	1247526; 376222	8.76 (1, 40)	9.94 (3, 40)	14.65 (3, 40)	0.0051	<0.0001	<0.0001
GD1a	722619; 128660	810246; 103621	701811; 50023	1131906; 135368	1294780; 375421	1246978; 255129	542773; 91124	1109459; 83719	2.54 (1, 40)	2.89 (3, 40)	1.84 (3, 40)	0.1188	0.0471	0.1546
GD1b	416644; 46406	780897; 178084	673692; 73579	638080; 54958	597870; 62536	1517894; 490275	1042644; 224440	1061293; 64456	7.72 (1, 46)	3.12 (3, 46)	0.60 (3, 46)	0.0078	0.0348	0.6158
GT1b	406755; 83516	3162272; 2191210	665317; 28951	482732; 55941	786112; 49734	716065; 131921	1047343; 63234	735114; 84322	0.40 (1, 47)	1.30 (3, 47)	1.56 (3, 47)	0.5268	0.2851	0.2109

SD = standard deviation w/o insulin = without insulin; w insulin = with insulin; P4-RR = (*R, R*) D, L-threo-phenyl-2-hexadecanoylamino-3-pyrrolidino-1-propanol; βAPP = beta amyloid precursor protein; IGF1-Rβ = beta subunit of receptor for insulin like growth factor; NP65 = neuroplastin 65; IRα = insulin receptor alpha subunit; GM1 = GM1 ganglioside; GD1a = GD1a ganglioside; GD1b = GD1b ganglioside; GT1b = GT1b ganglioside

Table 5.19. Post hoc analysis of immunocytochemical ANOVA data for IRα epitope in cells treated P4-RR GlcCer inhibitor.

The first set of variables (A)		The second set of variables (B)		Post hoc Tukey HSD p-value A vs B
Insulin treatment	The concentration of P4 - RR	Insulin treatment	The concentration of P4 - RR	
w/o insulin	Control	w insulin	P4-RR 2.5μM	0.0289

SD = standard deviation w/o insulin = without insulin; w insulin = with insulin; P4-RR = (*R*, *R*) D, L-threo-phenyl-2-hexadecanoylamino-3-pyrrolidino-1-propanol.

Table 5.20. Post hoc analysis of immunocytochemical ANOVA data for NP65 epitope in cells treated P4-RR GlcCer inhibitor.

Expression of NP65				
The first set of variables (A)		The second set of variables (B)		Post hoc Tukey HSD p-value A vs B
Insulin treatment	The concentration of P4 - RR	Insulin treatment	The concentration of P4 - RR	
w insulin	Control	w/o insulin	P4-RR 2.5μM	0.0072
w insulin	Control	w/o insulin	P4-RR 10μM	0.0266
w insulin	Control	w insulin	P4-RR 2.5μM	0.0169
w insulin	Control	w insulin	P4-RR 40μM	0.0026

SD = standard deviation w/o insulin = without insulin; w insulin = with insulin; P4-RR = (*R*, *R*) D, L-threo-phenyl-2-hexadecanoylamino-3-pyrrolidino-1-propanol.

Table 5.21. Post hoc analysis of immunocytochemical ANOVA data for GM1 epitope in cells treated P4-RR GlcCer inhibitor.

The first set of variables (A)		The second set of variables (B)		Post hoc Tukey HSD p-value A vs B
Insulin treatment	The concentration of P4 - RR	Insulin treatment	The concentration of P4 - RR	
w/o insulin	Control	w insulin	Control	0.0001
w insulin	Control	w/o insulin	P4-RR 2.5μM	0.0001
w insulin	Control	w/o insulin	P4-RR 10μM	0.0001
w insulin	Control	w/o insulin	P4-RR 40μM	0.0001
w insulin	Control	w insulin	P4-RR 2.5μM	0.0001
w insulin	Control	w insulin	P4-RR 10μM	0.0001
w insulin	Control	w insulin	P4-RR 40μM	0.0001

SD = standard deviation w/o insulin = without insulin; w insulin = with insulin; P4-RR = (*R*, *R*) D, L-threo-phenyl-2-hexadecanoylamino-3-pyrrolidino-1-propanol

Table 5.22. Colocalization percentage of selected epitopes with flotillin 1 or 2 (F1, F2) lipid raft markers in Differentiated SH-SY5Yhuman neuroblastoma cells treated 48 hours with P4-RR, a GlcCer synthesis inhibitor. Data are presented as integrated density values per cell. Statistical significance was tested with two-way ANOVA

Epitope	w/o insulin				w insulin				Two-way ANOVA					
	Control	P4-RR 2.5 µM	P4-RR 10 µM	P4-RR 40 µM	Control	P4-RR 2.5 µM	P4-RR 10 µM	P4-RR 40 µM	F values; (degrees of freedom)			p-values		
	Mean; SD	Mean; SD	Mean; SD	Mean; SD	Mean; SD	Mean; SD	Mean; SD	Mean; SD	Insulin	RR	Insulin × RR	Insulin	RR	Insulin × RR
F1-bAPP	4.45; 3.44	0.35; 0.25	0.61; 0.43	1.46; 0.32	6.06; 2.34	0.35; 0.21	0.02; 0.00	5.07; 1.97	0.09 (1, 16)	4.30 (3, 16)	0.65 (3, 16)	0.3355	0.0208	0.5898
F1-IGF1Rb	0.62; 0.16	0.09; 0.09	0.32; 0.31	0.11; 0.10	11.36; 7.11	0.38; 0.16	0.33; 0.24	0.17; 0.15	2.42 (1, 16)	2.61 (3, 16)	2.22 (3, 16)	0.1390	0.0871	0.1248
F1-IRα	0.04; 0.03	0.01; 0.01	0.05; 0.01	0.00; 0.00	1.22; 1.19	0.00; 0.00	0.04; 0.04	0.02; 0.02	0.96 (1, 16)	1.03 (3, 16)	0.97 (3, 16)	0.3395	0.4030	0.4303
F1-NP65	0.13; 0.13	0.02; 0.01	0.21; 0.21	0.02; 0.02	0.03; 0.03	0.02; 0.02	0.00; 0.00	0.00; 0.00	1.70 (1, 16)	0.57 (3, 16)	0.60 (3, 16)	0.2096	0.6371	0.6227
F2-GM1	3.00; 0.90	0.28; 0.14	0.00; 0.00	0.01; 0.01	3.38; 2.12	0.00; 0.00	0.02; 0.00	0.01; 0.00	0.00 (1, 16)	7.43 (3, 16)	0.05 (3, 16)	0.9619	0.0024	0.9829
F2-GD1a	0.02; 0.01	0.08; 0.08	0.25; 0.16	0.03; 0.01	1.68; 1.68	0.02; 0.01	0.01; 0.01	0.00; 0.00	0.63 (1, 16)	0.87 (3, 16)	1.11 (3, 16)	0.4388	0.4732	0.3705
F2-GD1b	2.43; 1.27	2.80; 1.25	0.00; 0.00	0.07; 0.04	1.19; 0.47	0.32; 0.19	0.00; 0.00	0.02; 0.01	4.13 (1, 16)	4.35 (3, 16)	1.59 (3, 16)	0.0589	0.0200	0.2289
F2-GT1b	2.78; 0.71	9.43; 0.41	0.05; 0.05	0.01; 0.00	3.16; 1.41	0.00; 0.00	0.01; 0.00	0.09; 0.07	30.40 (1, 16)	32.04 (3, 16)	34.37 (3, 16)	<0.0001	<0.0001	<0.0001

SD = standard deviation w/o insulin = without insulin; w insulin = with insulin; P4-RR = (*R, R*) D, L-threo-phenyl-2-hexadecanoylamino-3-pyrrolidino-1-propanol; βAPP = beta amyloid precursor protein; IGF1-Rβ = beta subunit of receptor for insulin like growth factor; NP65 = neuroplastin 65; IRα = insulin receptor alpha subunit; GM1 = GM1 ganglioside; GD1a = GD1a ganglioside; GD1b = GD1b ganglioside; GT1b = GT1b ganglioside; F1 = flotillin 1, F2 = flotillin 2

Table 5.23. Colocalization percentage of selected epitopes with transferrin receptor (TfR) or sodium/potassium ATPase (Na/K ATPase) lipid non-raft markers in Differentiated SH-SY5Yhuman neuroblastoma cells treated 48 hours with P4-RR, a GlcCer synthesis inhibitor. Data are presented as integrated density values per cell. Statistical significance was tested with two-way ANOVA

Epitope	w/o insulin				w insulin				Two-way ANOVA					
	Control	P4-RR 2.5 μM	P4-RR 10 μM	P4-RR 40 μM	Control	P4-RR 2.5 μM	P4-RR 10 μM	P4-RR 40 μM	F values; (degrees of freedom)			p-values		
	Mean; SD	Mean; SD	Mean; SD	Mean; SD	Mean; SD	Mean; SD	Mean; SD	Mean; SD	Insulin	RR	Insulin × RR	Insulin	RR	Insulin × RR
TfR-bAPP	0.82; 0.76	1.15; 0.35	0.94; 0.43	1.19; 0.60	0.11; 0.11	0.04; 0.03	0.00; 0.00	0.26; 0.24	10.27 (1, 16)	0.18 (3, 16)	0.08 (3, 16)	0.0055	0.9061	0.9682
TfR-IGF1Rb	0.86; 0.41	23.23; 2.76	4.83; 3.12	4.33; 2.15	0.34; 0.27	12.70; 7.72	3.25; 1.74	0.79; 0.72	3.05 (1, 16)	11.71 (3, 16)	0.94 (3, 16)	0.0994	0.0002	0.4399
TfR-IRα	1.20; 1.17	1.31; 0.05	4.83; 2.21	2.44; 2.33	1.15; 1.11	1.31; 0.40	3.53; 3.50	9.28; 6.56	0.43 (1, 16)	1.22 (3, 16)	0.79 (3, 16)	0.5167	0.3333	0.5128
Tfr-NP65	0.86; 0.46	0.33; 0.04	1.74; 0.88	0.15; 0.15	1.44; 0.76	0.02; 0.02	0.34; 0.24	0.00; 0.00	0.98 (1, 16)	3.07 (3, 16)	1.64 (3, 16)	0.3348	0.0575	0.2185
Na/K-GM1	8.64; 1.11	14.96; 4.16	6.52; 2.73	12.52; 1.31	2.61; 0.42	11.37; 3.31	10.94; 4.25	19.99; 0.19	0.09 (1, 16)	6.22 (3, 16)	2.89 (3, 16)	0.7674	0.0052	0.0677
Na/K-GD1a	3.46; 1.87	11.23; 0.85	2.20; 0.79	1.11; 0.57	1.06; 0.94	0.28; 0.16	2.66; 1.35	0.64; 0.45	22.13 (1, 16)	8.49 (3, 16)	13.46 (3, 16)	0.0002	0.0013	0.0001
Na/K-GD1b	1.01; 0.51	0.01; 0.00	0.01; 0.00	0.02; 0.01	0.22; 0.14	1.46; 0.93	0.27; 0.27	0.01; 0.00	0.69 (1, 16)	1.62 (3, 16)	2.82 (3, 16)	0.4172	0.2232	0.0717
Na/K-GT1b	1.59; 1.58	0.17; 0.08	0.02; 0.01	0.55; 0.28	1.24; 0.86	0.02; 0.00	0.36; 0.31	0.62; 0.59	0.00 (1, 16)	1.52 (3, 16)	0.09 (3, 16)	0.9636	0.2455	0.9640

SD = standard deviation w/o insulin = without insulin; w insulin = with insulin; P4-RR = (*R, R*) D, L-threo-phenyl-2-hexadecanoylamino-3-pyrrolidino-1-propanol; βAPP = beta amyloid precursor protein; IGF1-Rβ = beta subunit of receptor for insulin like growth factor; NP65 = neuroplastin 65; IRα = insulin receptor alpha subunit; GM1 = GM1 ganglioside; GD1a = GD1a ganglioside; GD1b = GD1b ganglioside; GT1b = GT1b ganglioside; TfR=transferrin receptor, Na/K=sodium/potassium ATPase

Table 5.24. Post hoc analysis of immunocytochemical ANOVA data for colocalization analysis results of F2-GT1b epitopes in cells treated P4-RR GlcCer inhibitor

The first set of variables (A)		The second set of variables (B)		Post hoc Tukey HSD p-value A vs B
Insulin treatment	The concentration of P4 - RR	Insulin treatment	The concentration of P4 - RR	
w/o insulin	Control	w/o insulin	P4-RR 2.5μM	0.0001
w/o insulin	P4-RR 10μM	w/o insulin	P4-RR 2.5μM	0.0001
w/o insulin	P4-RR 40μM	w/o insulin	P4-RR 2.5μM	0.0001
w insulin	Control	w/o insulin	P4-RR 2.5μM	0.0001
w insulin	P4-RR 2.5μM	w/o insulin	P4-RR 2.5μM	0.0001
w insulin	P4-RR 10μM	w/o insulin	P4-RR 2.5μM	0.0001
w insulin	P4-RR 40μM	w/o insulin	P4-RR 2.5μM	0.0001
w insulin	Control	w/o insulin	P4-RR 10μM	0.0256
w insulin	Control	w/o insulin	P4-RR 40μM	0.0231
w insulin	Control	w insulin	P4-RR 2.5μM	0.0231
w insulin	Control	w insulin	P4-RR 10μM	0.0232
w insulin	Control	w insulin	P4-RR 40μM	0.0283

w/o insulin = without insulin; w insulin = with insulin; P4-RR = (*R, R*) D, L-threo-phenyl-2-hexadecanoylamino-3-pyrrolidino-1-propanol

Table 5.25. Post hoc analysis of immunocytochemical ANOVA data for colocalization analysis results of Na/K-GD1a epitopes in cells treated P4-RR GlcCer inhibitor

The first set of variables (A)		The second set of variables (B)		Post hoc Tukey HSD p-value A vs B
Insulin treatment	The concentration of P4 - RR	Insulin treatment	The concentration of P4 - RR	
w/o insulin	Control	w/o insulin	P4-RR 2.5μM	0.0011
w/o insulin	P4-RR 10μM	w/o insulin	P4-RR 2.5μM	0.0003
w/o insulin	P4-RR 40μM	w/o insulin	P4-RR 2.5μM	0.0002
w insulin	Control	w/o insulin	P4-RR 2.5μM	0.0002
w insulin	P4-RR 2.5μM	w/o insulin	P4-RR 2.5μM	0.0001
w insulin	P4-RR 10μM	w/o insulin	P4-RR 2.5μM	0.0005
w insulin	P4-RR 40μM	w/o insulin	P4-RR 2.5μM	0.0001

w/o insulin = without insulin; w insulin = with insulin; P4-RR = (*R, R*) D, L-threo-phenyl-2-hexadecanoylamino-3-pyrrolidino-1-propanol

5.3.2. Immunocytochemistry of P4-SS treated cells

Treatment of the cells with P4-SS caused significant changes in IGF1-Rβ, GM1 GD1a and GT1b levels. The effect of insulin on the expression of epitope levels was observed for IRα, Np 65, GTM1, GD1a and GT1b, but the combined effects of insulin and inhibitor treatment was observed for GM1, GD1a and GT1b. Post hoc analysis showed significant differences only for GM1, GD1a and GT1b epitopes (Table 5.26.).

Post hoc analysis of ICC data for GM1 showed that only treatment with insulin increased significantly theGM1 level. Treatment with inhibitor and insulin reduced GM1 level in a dose dependent manner (Table 5.27.).

The level of GD1a was significantly higher when cells were treated with the highest concentration of inhibitor compared to all other groups, both insulin-treated and untreated samples (Table 5.28.).

Colocalization analysis showed a significant difference in the levels of GM1 and GT1b in lipid rafts, and this was reduced by the inhibitor treatment (Table 5.3.2.5.). In the non-raft area insulin treatment reduced the levels of βAPP and IR and increased levels of GM1 (table 5.31.)

Post hoc analysis of GT1b showed that the highest concentration of inhibitor reduced epitope levels compared to the other groups, but not significantly more than the control. Insulin and inhibitor combination treatment significantly reduced epitope levels at low and middle concentrations but increased fourfold when treated with the highest inhibitor concentrations (Table 5.29.).

Post hoc analysis of colocalization showed that the low concentration of inhibitor had the greatest effect on the shifting APP into the non-raft area and this was significantly higher compared to the other treatments (Table 5.32.)

Treatment of cells with medium inhibitor concentration and insulin had the most profound effect on the shift of GM1into the non-raft area and it was comparably higher than in the other treatment groups (Table 5.33.)

Table 5.26. The integrated density value of immunocytochemical staining of differentiated SH-SY5Y human neuroblastoma cells treated 48 hours with P4-SS, a GlcCer synthesis inhibitor. Data are presented as integrated density values per cell. Statistical significance was tested with two-way ANOVA

Epitope	w/o insulin				w insulin				Two-way ANOVA					
	Control	P4-SS 2.5 µM	P4-SS 10 µM	P4-SS 40 µM	Control	P4-SS 2.5 µM	P4-SS 10 µM	P4-SS 40 µM	F values; (degrees of freedom)			p-values		
	Mean; SD	Mean; SD	Mean; SD	Mean; SD	Mean; SD	Mean; SD	Mean; SD	Mean; SD	Insulin	SS	Insulin × SS	Insulin	SS	Insulin × SS
βAPP	351769; 113703	421692; 140819	312284; 60033	555325; 79563	285842; 44657	200520; 50818	322977; 118062	371793; 76126	1.04 (1, 43)	1.80 (3, 43)	0.54 (3, 43)	0.3129	0.1609	0.6527
IGF1-Rβ	987948; 84329	193330; 70128	297687; 138147	763247; 248499	1724030; 748935	233055; 51417	368643; 110307	692201; 187328	0.57 (1, 39)	4.54 (3, 39)	0.60 (3, 39)	0.4535	0.0079	0.6148
IRα	843864; 47466	634005; 100836	421858; 89446	769600; 253968	243148; 77939	12104; 503	284553; 127867	48979; 6561	22.79 (1, 34)	1.35 (3, 34)	1.21 (3, 34)	<0.0001	0.2741	0.3179
NP65	229369; 64570	162611; 42935	127055; 20581	365213; 51493	540101; 164500	164777; 52569	411150; 58275	348294; 132123	5.59 (1, 45)	2.74 (3, 45)	2.07 (3, 45)	0.0223	0.0538	0.1165
GM1	836326; 105238	1328158; 415228	1254237; 533719	1010204; 221466	3236956; 348564	1035697; 159234	1103972; 200723	752827; 176884	3.34 (1, 37)	4.68 (3, 37)	8.75 (3, 37)	0.0754	0.0071	0.0001
GD1a	722619; 128660	1161244; 225029	1691761; 208099	5147854; 1907391	1294780; 375421	705209; 33899	820265; 76504	1374974; 252734	5.17 (1, 40)	4.94 (3, 40)	3.50 (3, 40)	0.0283	0.0051	0.0239
GD1b	416644; 46406	3176197; 1687297	890030; 181554	742223; 147779	597870; 62536	413920; 29371	406223; 67342	861919; 102346	2.85 (1, 47)	1.82 (3, 47)	2.54 (3, 47)	0.0978	0.1549	0.0673
GT1b	406755; 83516	528712; 95628	559793; 67581	508334; 70952	786112; 49734	521412; 35815	608666; 52098	5151175; 2362391	4.48 (1, 47)	3.27 (3, 47)	3.44 (3, 47)	0.0394	0.0291	0.0241

SD = standard deviation w/o insulin = without insulin; w insulin = with insulin; P4-SS = (*S, S*) D, L-threo-phenyl-2-hexadecanoylamino-3-pyrrolidino-1-propanol; βAPP = beta amyloid precursor protein; IGF1-Rβ = beta subunit of receptor for insulin like growth factor; NP65 = neuroplastin 65; IRα = insulin receptor alpha subunit; GM1 = GM1 ganglioside; GD1a = GD1a ganglioside; GD1b = GD1b ganglioside; GT1b = GT1b ganglioside

Table 5.27. Post hoc analysis of immunocytochemical ANOVA data for GM1 epitope in cells treated with P4-SS GlcCer inhibitor.

The first set of variables (A)		The second set of variables (B)		Post hoc Tukey HSD p-value A vs B
Insulin treatment	The concentration of P4 - SS	Insulin treatment	The concentration of P4 - SS	
w insulin	Control	w/o insulin	Control	0.0001
w insulin	Control	w/o insulin	P4-SS 2.5μM	0.0024
w insulin	Control	w/o insulin	P4-SS 10μM	0.0015
W insulin	Control	w/o insulin	P4-SS 40μM	0.0003
w insulin	Control	w insulin	P4-SS 2.5μM	0.0004
w insulin	Control	w insulin	P4-SS 10μM	0.0006
w insulin	Control	w insulin	P4-SS 40μM	0.0011

w/o insulin = without insulin; w insulin = with insulin; P4-SS = (*S*, *S*) D, L-threo-phenyl-2-hexadecanoylamino-3-pyrrolidino-1-propanol

Table 5.28. Post hoc analysis of immunocytochemical ANOVA data for GD1a epitope in cells treated with P4-SS GlcCer inhibitor.

The first set of variables (A)		The second set of variables (B)		Post hoc Tukey HSD p-value A vs B
Insulin treatment	The concentration of P4 - SS	Insulin treatment	The concentration of P4 - SS	
w/o insulin	Control	w/o insulin	P4-SS 40μM	0.0017
w/o insulin	P4-SS 2.5μM	w/o insulin	P4-SS 40μM	0.0058
w/o insulin	P4-SS 10μM	w/o insulin	P4-SS 40μM	0.0250
w insulin	Control	w/o insulin	P4-SS 40μM	0.0085
w insulin	P4-SS 2.5μM	w/o insulin	P4-SS 40μM	0.0016
w insulin	P4-SS 10μM	w/o insulin	P4-SS 40μM	0.0022
w insulin	P4-SS 40μM	w/o insulin	P4-SS 40μM	0.0106

w/o insulin = without insulin; w insulin = with insulin; P4-SS = (*S*, *S*) D, L-threo-phenyl-2-hexadecanoylamino-3-pyrrolidino-1-propanol

Table 5.29. Post hoc analysis of immunocytochemical ANOVA data for GD1b epitope in cells treated with P4-SS GlcCer inhibitor.

The first set of variables (A)		The second set of variables (B)		Post hoc Tukey HSD p-value A vs B
Insulin treatment	The concentration of P4 - SS	Insulin treatment	The concentration of P4 - SS	
w/o insulin	Control	w insulin	P4-SS 40μM	0.0057
w/o insulin	P4-SS 2.5μM	w insulin	P4-SS 40μM	0.0077
w/o insulin	P4-SS 10μM	w insulin	P4-SS 40μM	0.0082
w/o insulin	P4-SS 40μM	w insulin	P4-SS 40μM	0.0098
w insulin	Control	w insulin	P4-SS 40μM	0.0141
w insulin	P4-SS 2.5μM	w insulin	P4-SS 40μM	0.0075
w insulin	P4-SS 10μM	w insulin	P4-SS 40μM	0.0093

w/o insulin = without insulin; w insulin = with insulin; P4-SS = (*S*, *S*) D, L-threo-phenyl-2-hexadecanoylamino-3-pyrrolidino-1-propanol

Table 5.30. Colocalization percentage of selected epitopes with flotillin 1 or 2 (F1, F2) lipid raft markers in differentiated SH-SY5Y human neuroblastoma cells treated 48 hours with P4-SS, a GlcCer synthesis inhibitor. Data are presented as integrated density values per cell. Statistical significance was tested with two-way ANOVA

Epitope	w/o insulin				w insulin				Two-way ANOVA					
	Control	P4-SS 2.5 μM	P4-SS 10 μM	P4-SS 40 μM	Control	P4-SS 2.5 μM	P4-SS 10 μM	P4-SS 40 μM	F values; (degrees of freedom)			p-values		
	Mean; SD	Mean; SD	Mean; SD	Mean; SD	Mean; SD	Mean; SD	Mean; SD	Mean; SD	Insulin	SS	Insulin × SS	Insulin	SS	Insulin × SS
F1-βAPP	4.45; 3.44	3.95; 0.66	2.32; 1.62	0.76; 0.20	6.06; 2.34	0.17; 0.07	1.43; 0.69	5.23; 2.87	0.06 (1, 16)	1.32 (3, 16)	1.70 (3, 16)	0.7988	0.3014	0.2068
F1-IGF1Rb	0.62; 0.16	0.21; 0.21	4.39; 3.61	0.51; 0.37	11.36; 7.11	0.01; 0.01	0.11; 0.11	0.04; 0.04	0.52 (1, 16)	1.87 (3, 16)	2.62 (3, 16)	0.4783	0.1746	0.0861
F1-IRα	0.04; 0.03	0.02; 0.00	0.02; 0.01	0.00; 0.00	1.22; 1.19	0.00; 0.00	0.01; 0.01	0.00; 0.00	0.93 (1, 16)	1.07 (3, 16)	0.98 (3, 16)	0.3491	0.3866	0.4239
F1-NP65	0.13; 0.13	0.01; 0.01	0.13; 0.13	0.00; 0.00	0.03; 0.03	0.49; 0.49	0.02; 0.01	0.00; 0.00	0.26 (1, 16)	0.64 (3, 16)	1.13 (3, 16)	0.6104	0.5981	0.3642
F2-GM1	3.00; 0.90	0.13; 0.08	0.00; 0.00	0.09; 0.09	3.38; 2.12	0.00; 0.00	0.01; 0.01	0.10; 0.08	0.01 (1, 16)	7.41 (3, 16)	0.03 (3, 16)	0.9106	0.0024	0.9908
F2-GD1a	0.02; 0.01	0.00; 0.00	0.00; 0.00	0.01; 0.01	1.68; 1.68	0.02; 0.01	0.01; 0.01	0.01; 0.00	1.00 (1, 16)	1.00 (3, 16)	0.97 (3, 16)	0.3308	0.4168	0.4268
F2-GD1b	2.43; 1.27	0.09; 0.09	0.00; 0.00	1.45; 1.34	1.19; 0.47	0.67; 0.64	0.20; 0.13	0.00; 0.00	0.89 (1, 16)	2.21 (3, 16)	1.02 (3, 16)	0.3594	0.1260	0.4095
F2-GT1b	2.78; 0.71	0.05; 0.03	0.00; 0.00	0.02; 0.02	3.16; 1.41	0.05; 0.02	0.00; 0.00	0.01; 0.01	0.05 (1, 16)	13.97 (3, 16)	0.05 (3, 16)	0.8161	<0.0001	0.9809

SD=standard deviation w/o insulin = without insulin; w insulin = with insulin; P4-SS = (*S, S*) D, L-threo-phenyl-2-hexadecanoylamino-3-pyrrolidino-1-propanol;; βAPP = beta amyloid precursor protein; IGF1-Rβ = beta subunit of receptor for insulin like growth factor; ; NP65 = neuroplastin 65; IRα = insulin receptor alpha subunit; GM1 = GM1 ganglioside; GD1a = GD1a ganglioside; GD1b = GD1b ganglioside; GT1b = GT1b ganglioside; F1 = flotillin 1, F2 = flotillin 2

Table 5.31. Colocalization percentage of selected epitopes with transferrin receptor (TfR) or sodium/potassium ATPase (Na/K ATPase) lipid non-raft markers in differentiated SH-SY5Y human neuroblastoma cells treated 48 hours with P4-SS, a GlcCer synthesis inhibitor. Data are presented as integrated density values per cell. Statistical significance was tested with two-way ANOVA

Epitope	w/o insulin				w insulin				Two-way ANOVA					
	Control	P4-SS 2.5 µM	P4-SS 10 µM	P4-SS 40 µM	Control	P4-SS 2.5 µM	P4-SS 10 µM	P4-SS 40 µM	F values; (degrees of freedom)			p-values		
	Mean; SD	Mean; SD	Mean; SD	Mean; SD	Mean; SD	Mean; SD	Mean; SD	Mean; SD	Insulin	SS	Insulin × SS	Insulin	SS	Insulin × SS
TfR-βAPP	0.82; 0.76	4.06; 0.93	1.16; 1.14	0.12; 0.09	0.11; 0.11	0.07; 0.04	0.11; 0.06	0.80; 0.56	8.38 (1, 16)	3.13 (3, 16)	5.01 (3, 16)	0.0105	0.0544	0.0122
TfR-IGF1Rb	0.86; 0.41	3.15; 1.75	2.87; 0.33	0.70; 0.62	0.34; 0.27	0.37; 0.01	0.18; 0.17	4.04; 1.69	1.05 (1, 16)	1.28 (3, 16)	4.91 (3, 16)	0.3192	0.3139	0.0131
TfR-IRα	1.20; 1.17	4.68; 1.74	0.51; 0.30	1.62; 1.14	1.15; 1.11	9.72; 4.20	2.79; 0.25	1.64; 0.39	2.13 (1, 16)	5.28 (3, 16)	0.92 (3, 16)	0.1635	0.0100	0.4509
TfR-NP65	0.86; 0.46	0.15; 0.13	0.12; 0.12	0.15; 0.06	1.44; 0.76	0.70; 0.45	0.36; 0.22	0.11; 0.08	1.69 (1, 16)	3.13 (3, 16)	0.32 (3, 16)	0.2114	0.0545	0.8098
Na/K-GM1	8.64; 1.11	12.71; 2.20	2.85; 1.90	11.59; 5.00	2.61; 0.42	9.67; 3.02	21.92; 1.49	2.02; 0.13	0.00 (1, 16)	3.74 (3, 16)	14.45 (3, 16)	0.9512	0.0326	<0.0001
Na/K-GD1a	3.46; 1.87	0.62; 0.30	3.30; 1.85	0.57; 0.16	1.06; 0.94	3.08; 1.70	0.74; 0.56	0.34; 0.24	0.66 (1, 16)	0.94 (3, 16)	1.97 (3, 16)	0.4282	0.4419	0.1590
Na/K-GD1b	1.01; 0.51	0.02; 0.01	1.75; 1.74	0.04; 0.04	0.22; 0.14	0.01; 0.01	0.00; 0.00	0.00; 0.00	1.99 (1, 16)	0.90 (3, 16)	0.81 (3, 16)	0.1767	0.4595	0.5063
Na/K-GT1b	1.59; 1.58	0.00; 0.00	0.70; 0.42	0.08; 0.07	1.24; 0.86	1.15; 1.15	1.21; 0.63	0.35; 0.34	0.47 (1, 16)	0.80 (3, 16)	0.29 (3, 16)	0.5018	0.5107	0.8290

SD=standard deviation; w/o insulin = without insulin; w insulin = with insulin; P4-SS = (*S, S*) D, L-threo-phenyl-2-hexadecanoylamino-3-pyrrolidino-1-propanol; βAPP = beta amyloid precursor protein; IGF1-Rβ = beta subunit of receptor for insulin like growth factor; NP65 = neuroplastin 65; IRα = insulin receptor alpha subunit; GM1 = GM1 ganglioside; GD1a = GD1a ganglioside; GD1b = GD1b ganglioside; GT1b = GT1b ganglioside ; TfR=transferrin receptor, Na/K=sodium/potassium ATPase

Table 5.32. Post hoc analysis of immunocytochemical ANOVA data for colocalization analysis results of TFR-βAPP epitopes in cells treated with P4-SS GlcCer inhibitor

The first set of variables (A)		The second set of variables (B)		Post hoc Tukey HSD p-value A vs B
Insulin treatment	The concentration of P4 - SS	Insulin treatment	The concentration of P4 - SS	
w/o insulin	Control	w/o insulin	P4-SS 2.5μM	0.0320
w/o insulin	P4-SS 40μM	w/o insulin	P4-SS 2.5μM	0.0069
w insulin	Control	w/o insulin	P4-SS 2.5μM	0.0068
w insulin	P4-SS 2.5μM	w/o insulin	P4-SS 2.5μM	0.0061
w insulin	P4-SS 10μM	w/o insulin	P4-SS 2.5μM	0.0066
w insulin	P4-SS 40μM	w/o insulin	P4-SS 2.5μM	0.0306

w/o insulin = without insulin; w insulin = with insulin; P4-SS = (*S*, *S*) D, L-threo-phenyl-2-hexadecanoylamino-3-pyrrolidino-1-propanol

Table 5.33. Post hoc analysis of immunocytochemical ANOVA data for colocalization analysis results of Na/K-GM1 epitopes in cells treated with P4-SS GlcCer inhibitor

Expression of Na/K-GM1				
The first set of variables (A)		The second set of variables (B)		Post hoc Tukey HSD p-value A vs B
Insulin treatment	The concentration of P4 - SS	Insulin treatment	The concentration of P4 - SS	
w/o insulin	Control	w insulin	P4-SS 10μM	0.0215
w/o insulin	P4-SS 10μM	w insulin	P4-SS 10μM	0.0009
w insulin	Control	w insulin	P4-SS 10μM	0.0008
w insulin	P4-SS 2.5μM	w insulin	P4-SS 10μM	0.0383
w insulin	P4-SS 40μM	w insulin	P4-SS 10μM	0.0006

w/o insulin = without insulin; w insulin = with insulin; P4-SS = (*S*, *S*) D, L-threo-phenyl-2-hexadecanoylamino-3-pyrrolidino-1-propanol

5.3.3. Immunocytochemistry of MIG treated cells

Treatment of the cells with the MIG inhibitor caused changes in IGF1-Rβ, GD1a and GD1b levels. Insulin treatment caused significant changes in GD1a, GD1b and GT1b levels, while the combined effect of inhibitor treatment and insulin was only observed for Np 65, GD1b and GT1b (Table 5.34.). Post hoc analysis revealed significant differences for Np 65, GD1b and GT1b levels.

Colocalization analysis showed no difference in the repositioning of the epitopes in or out of lipid rafts (Table 5.38.). Significant differences were found in the colocalization of βAPP, IFG1-Rβ and GM1 with non-raft markers (Table 5.39.).

Post hoc analysis for Np 65 found a significant reduction in epitope levels when cells were treated with low and medium concentrations of inhibitor and insulin compared to the insulin treated control (Table 5.35.).

GD1b levels increased with inhibitor concentration and were significantly higher in the insulin untreated groups. Treatment of the cells with insulin reduced epitope levels in the control, medium and high concentration treated cells compared to the medium concentration treated group (Table 5.36.).

In the case of GT1b epitope, a significant increase was observed only in the insulin-treated samples. The same was observed for the highest concentration of inhibitor (Table 5.37.).

Post hoc analysis of βAPP colocalization showed that there was a significant increase with the highest concentration of inhibitor treatment and insulin, and it was significantly higher from all other groups regardless of inhibitor concentration or insulin treatment (Table 5.40.).

IGF1-Rβ showed the largest shift into non-raft areas when treated with low concentration of inhibitor and insulin and it was the highest compared to all other groups (Table 5.41.).

The GM1 post hoc analysis showed that treatment decreased colocalizations with non-raft at high and medium concentrations compared to the control, but it increased at the lowest concentrations, which caused the highest number of shifts and it was statistically more than for the other groups (Table 5.42.).

Table 5.34. The integrated density value of immunocytochemical staining of differentiated SH-SY5Y human neuroblastoma cells treated 48 hours with MIG, a GlcCer synthesis inhibitor.

Epitope	w/o insulin				w insulin				Two-way ANOVA					
	Control	MIG 2.5 µM	MIG 10 µM	MIG 40 µM	Control	MIG 2.5 µM	MIG 10 µM	MIG 40 µM	F values; (degrees of freedom)			p-values		
	Mean; SD	Mean; SD	Mean; SD	Mean; SD	Mean; SD	Mean; SD	Mean; SD	Mean; SD	Insulin	MIG	Insulin × MIG	Insulin	MIG	Insulin × MIG
βAPP	351769; 113703	330688; 87517	369438; 117604	359733; 166050	285842; 44657	209268; 74333	242699; 82922	398289; 135950	3.10 (1, 47)	1.99 (3, 47)	0.26 (3, 47)	0.0844	0.1278	0.8521
IGF1-Rβ	987948; 84329	462325; 78860	364404; 90072	535589; 175718	1724030; 748935	869180; 121244	317850; 51700	162351; 52134	1.02 (1, 47)	5.88 (3, 47)	1.25 (3, 47)	0.3164	0.0017	0.2991
IRα	820119; 48631	600703; 204053	512451; 149162	395617; 147923	201280; 77784	247051; 60135	461001; 62202	122075; 40171	16.68 (1, 39)	1.96 (3, 39)	2.22 (3, 39)	0.0002	0.1353	0.1003
NP65	229369; 64570	435150; 94218	212221; 55045	239130; 58652	540101; 164500	134913; 37736	131261; 35784	310708; 125944	0.01 (1, 46)	1.96 (3, 46)	4.31 (3, 46)	0.9065	0.1323	0.0091
GM1	836326; 105238	2780216; 1069374	2070692; 492117	838467; 237795	3236956; 348564	1060034; 175715	485028; 61593	812112; 54770	2.18 (1, 39)	0.81 (3, 39)	4.02 (3, 39)	0.1473	0.4920	0.0137
GD1a	722619; 128660	1135850; 128181	664957; 85253	847407; 73647	1294780; 375421	1873835; 300853	650467; 108003	1206221; 368568	6.44 (1, 40)	4.55 (3, 40)	0.99 (3, 40)	0.0151	0.0077	0.4053
GD1b	416644; 46406	913446; 184212	1109670; 159366	656273; 110089	597870; 62536	694476; 77688	354133; 41406	333082; 36891	14.07 (1, 47)	4.29 (3, 47)	6.71 (3, 47)	0.0004	0.0093	0.0007
GT1b	406755; 83516	423360; 53849	503791; 52220	340072; 15683	786112; 49734	442165; 35651	468206; 16657	732223; 192302	9.87 (1, 47)	1.44 (3, 47)	3.63 (3, 47)	0.0028	0.2412	0.0193

SD=standard deviation; w/o insulin = without insulin; w insulin = with insulin; MIG=miglustat; βAPP = beta amyloid precursor protein; IGF1-Rβ = beta subunit of receptor for insulin like growth factor; NP65 = neuroplastin 65; IRα = insulin receptor alpha subunit; GM1 = GM1 ganglioside; GD1a = GD1a ganglioside; GD1b = GD1b ganglioside; GT1b = GT1b ganglioside

Table 5.35. Post hoc analysis of immunocytochemical ANOVA data for NP65 epitope in cells treated MIG, a GlcCer inhibitor.

The first set of variables (A)		The second set of variables (B)		Post hoc Tukey HSD p-value A vs B
Insulin treatment	The concentration of MIG	Insulin treatment	The concentration of MIG	
w/ insulin	Control	w/ insulin	MIG 2.5µM	0.0419
w/ insulin	Control	w/ insulin	MIG 10µM	0.0389

w/o insulin = without insulin; w insulin = with insulin; MIG = miglustat

Table 5.36. Post hoc analysis of immunocytochemical ANOVA data for GD1b epitope in cells treated MIG, a GlcCer inhibitor.

The first set of variables (A)		The second set of variables (B)		Post hoc Tukey HSD p-value A vs B
Insulin treatment	The concentration of MIG	Insulin treatment	The concentration of MIG	
w/o insulin	Control	w/o insulin	MIG 2.5µM	0.0323
w/o insulin	Control	w/o insulin	MIG 10µM	0.0007
w/o insulin	MIG 2.5µM	w/ insulin	MIG 10µM	0.0102
w/o insulin	MIG 2.5µM	w/ insulin	MIG 40µM	0.0068
w/o insulin	MIG 10µM	w/ insulin	Control	0.0247
w/o insulin	MIG 10µM	w/ insulin	MIG 10µM	0.0002
w/o insulin	MIG 10µM	w/ insulin	MIG 40µM	0.0002

w/o insulin = without insulin; w insulin = with insulin; MIG=miglustat

Table 5.37. Post hoc analysis of immunocytochemical ANOVA data for GT1b epitope in cells treated MIG, a GlcCer inhibitor.

The first set of variables (A)		The second set of variables (B)		Post hoc Tukey HSD p-value A vs B
Insulin treatment	The concentration of MIG	Insulin treatment	The concentration of MIG	
w/ insulin	Control	w/o insulin	Control	0.0422
w/ insulin	Control	w/o insulin	MIG 40µM	0.0176

w/o insulin = without insulin; w insulin = with insulin; MIG = miglustat

Table 5.38. Colocalization percentage of selected epitopes with flotillin 1 or 2 (F1, F2) lipid raft markers in differentiated SH-SY5Y human neuroblastoma cells treated 48 hours with MIG, a GlcCer synthesis inhibitor. Data are presented as integrated density values per cell. Statistical significance was tested with two-way ANOVA

Epitope	w/o insulin				w insulin				Two-way ANOVA					
	Control	MIG 2.5 µM	MIG 10 µM	MIG 40 µM	Control	MIG 2.5 µM	MIG 10 µM	MIG 40 µM	F values; (degrees of freedom)			p-values		
	Mean; SD	Mean; SD	Mean; SD	Mean; SD	Mean; SD	Mean; SD	Mean; SD	Mean; SD	Insulin	MIG	Insulin × MIG	Insulin	MIG	Insulin × MIG
F1-βAPP	4.45; 3.44	0.17; 0.07	5.63; 3.29	7.87; 3.49	6.06; 2.34	0.39; 0.31	1.02; 0.41	1.24; 0.56	2.16 (1, 16)	1.89 (3, 16)	1.48 (3, 16)	0.1604	0.1718	0.2551
F1-IGF1Rb	0.62; 0.16	3.39; 2.20	0.01; 0.01	0.29; 0.10	11.36; 7.11	1.51; 1.26	0.10; 0.07	0.69; 0.67	1.51 (1, 16)	2.03 (3, 16)	2.25 (3, 16)	0.2354	0.1497	0.1211
F1-IRα	0.04; 0.03	1.79; 1.79	0.16; 0.15	0.01; 0.00	1.22; 1.19	0.39; 0.36	0.02; 0.02	0.08; 0.08	0.01 (1, 16)	0.81 (3, 16)	0.93 (3, 16)	0.8946	0.5043	0.4463
F1-NP65	0.13; 0.13	0.00; 0.00	0.01; 0.01	0.02; 0.02	0.03; 0.03	0.08; 0.08	0.47; 0.23	0.00; 0.00	2.29 (1, 16)	2.12 (3, 16)	3.22 (3, 16)	0.1489	0.1373	0.0507
F2-GM1	3.00; 0.90	2.31; 2.09	9.44; 4.74	3.39; 3.32	3.38; 2.12	6.10; 3.07	0.03; 0.02	0.45; 0.23	1.27 (1, 16)	0.46 (3, 16)	2.40 (3, 16)	0.2761	0.7096	0.1055
F2-GD1a	0.02; 0.01	4.57; 4.19	4.97; 4.92	0.00; 0.00	1.68; 1.68	0.02; 0.02	1.17; 1.16	0.01; 0.00	0.97 (1, 16)	0.66 (3, 16)	0.77 (3, 16)	0.3387	0.5841	0.5239
F2-GD1b	2.43; 1.27	4.15; 1.46	1.59; 0.34	1.19; 0.53	1.19; 0.47	1.15; 0.52	0.02; 0.02	2.68; 1.39	2.82 (1, 16)	1.39 (3, 16)	2.13 (3, 16)	0.1119	0.2793	0.1360
F2-GT1b	2.78; 0.71	4.78; 0.06	2.81; 1.16	3.87; 2.15	3.16; 1.41	3.98; 1.99	0.04; 0.03	1.99; 0.82	1.97 (1, 16)	1.77 (3, 16)	0.56 (3, 16)	0.1791	0.1918	0.6436

SD=standard deviation; w/o insulin = without insulin; w insulin = with insulin; MIG=miglustat; βAPP = beta amyloid precursor protein; IGF1-Rβ = beta subunit of receptor for insulin like growth factor; NP65 = neuroplastin 65; IRα = insulin receptor alpha subunit; GM1 = GM1 ganglioside; GD1a = GD1a ganglioside; GD1b = GD1b ganglioside; GT1b = GT1b ganglioside ; F1 = flotillin 1, F2 = flotillin 2

Table 5.39. Colocalization percentage of selected epitopes with transferrin receptor (TfR) or sodium/potassium ATPase (Na/K ATPase) lipid non-raft marker in differentiated SH-SY5Y human neuroblastoma cells treated 48 hours with MIG, a GlcCer synthesis inhibitor. Data are presented as integrated density values per cell. Statistical significance was tested with two-way ANOVA

Epitope	w/o insulin				w insulin				Two-way ANOVA					
	Control	MIG 2.5 µM	MIG 10 µM	MIG 40 µM	Control	MIG 2.5 µM	MIG 10 µM	MIG 40 µM	F values; (degrees of freedom)			p-values		
	Mean; SD	Mean; SD	Mean; SD	Mean; SD	Mean; SD	Mean; SD	Mean; SD	Mean; SD	Insulin	MIG	Insulin × MIG	Insulin	MIG	Insulin × MIG
TfR-βAPP	0.82; 0.76	0.64; 0.49	0.02; 0.01	0.02; 0.00	0.11; 0.11	0.00; 0.00	1.70; 1.04	11.14; 2.87	12.92 (1, 16)	10.04 (3, 16)	12.41 (3, 16)	0.0024	0.0005	0.0001
TfR-IGF1Rb	0.86; 0.41	0.42; 0.16	0.00; 0.00	0.99; 0.37	0.34; 0.27	5.63; 1.80	0.30; 0.17	0.04; 0.04	4.41 (1, 16)	7.49 (3, 16)	8.81 (3, 16)	0.0517	0.0023	0.0011
TfR-IRα	1.20; 1.17	1.82; 1.53	4.19; 3.63	0.76; 0.61	1.15; 1.11	0.32; 0.18	0.06; 0.03	1.03; 0.32	1.57 (1, 16)	0.26 (3, 16)	0.86 (3, 16)	0.2280	0.8520	0.4808
TfR-NP65	0.86; 0.46	1.86; 1.84	0.70; 0.69	0.31; 0.27	1.44; 0.76	0.37; 0.36	2.21; 2.15	0.02; 0.01	0.01 (1, 16)	0.52 (3, 16)	0.69 (3, 16)	0.9178	0.6699	0.5693
Na/K-GM1	8.64; 1.11	10.70; 1.41	0.39; 0.12	0.98; 0.39	2.61; 0.42	1.42; 0.38	2.11; 0.63	4.34; 1.68	15.14 (1, 16)	12.49 (3, 16)	21.28 (3, 16)	0.0012	0.0001	<0.0001
Na/K-GD1a	3.46; 1.87	1.06; 1.06	0.32; 0.32	6.91; 2.01	1.06; 0.94	1.67; 0.52	10.11; 5.00	3.80; 2.00	0.61 (1, 16)	1.70 (3, 16)	3.61 (3, 16)	0.4446	0.2055	0.0364
Na/K-GD1b	1.01; 0.51	2.09; 0.59	0.28; 0.14	0.06; 0.01	0.22; 0.14	0.05; 0.05	0.76; 0.55	2.52; 2.47	0.00 (1, 16)	0.30 (3, 16)	2.08 (3, 16)	0.9648	0.8235	0.1419
Na/K-GT1b	1.59; 1.58	0.15; 0.09	0.00; 0.00	0.02; 0.01	1.24; 0.86	1.22; 0.61	0.01; 0.01	0.46; 0.38	0.35 (1, 16)	1.65 (3, 16)	0.39 (3, 16)	0.5573	0.2229	0.7597

SD=standard deviation; w/o insulin = without insulin; w insulin = with insulin; MIG=miglustat; βAPP = beta amyloid precursor protein; IGF1-Rβ = beta subunit of receptor for insulin like growth factor; NP65 = neuroplastin 65; IRα = insulin receptor alpha subunit; GM1 = GM1 ganglioside; GD1a = GD1a ganglioside; GD1b = GD1b ganglioside; GT1b = GT1b ganglioside; TfR=transferrin receptor, Na/K=sodium/potassium ATPase

Table 5.40. Post hoc analysis of immunocytochemical ANOVA data for colocalization analysis results of TFR-βAPP epitopes in cells treated MIG, a GlcCer inhibitor

The first set of variables (A)		The second set of variables (B)		Post hoc Tukey HSD p-value A vs B
Insulin treatment	The concentration of MIG	Insulin treatment	The concentration of MIG	
w/o insulin	Control	w insulin	MIG 40μM	0.0003
w/o insulin	MIG 2.5μM	w insulin	MIG 40μM	0.0002
w/o insulin	MIG 10μM	w insulin	MIG 40μM	0.0002
w/o insulin	MIG 40μM	w insulin	MIG 40μM	0.0002
w insulin	Control	w insulin	MIG 40μM	0.0002
w insulin	MIG 2.5μM	w insulin	MIG 40μM	0.0002
w insulin	MIG 10μM	w insulin	MIG 40μM	0.0005

w/o insulin = without insulin; w insulin = with insulin; MIG = miglustat

Table 5.41. Post hoc analysis of immunocytochemical ANOVA data for colocalization analysis results of TFR-IFG1-Rβ epitopes in cells treated MIG, a GlcCer inhibitor

The first set of variables (A)		The second set of variables (B)		Post hoc Tukey HSD p-value A vs B
Insulin treatment	The concentration of MIG	Insulin treatment	The concentration of MIG	
w/o insulin	Control	w insulin	MIG 2.5μM	0.0028
w/o insulin	MIG 2.5μM	w insulin	MIG 2.5μM	0.0012
w/o insulin	MIG 10μM	w insulin	MIG 2.5μM	0.0006
w/o insulin	MIG 40μM	w insulin	MIG 2.5μM	0.0036
w insulin	Control	w insulin	MIG 2.5μM	0.0010
w insulin	MIG 10μM	w insulin	MIG 2.5μM	0.0010
w insulin	MIG 40μM	w insulin	MIG 2.5μM	0.0006

w/o insulin = without insulin; w insulin = with insulin; MIG = miglustat

Table 5.42. Post hoc analysis of immunocytochemical ANOVA data for colocalization analysis results of GM1-IFG1-Rβ epitopes in cells treated MIG, a GlcCer inhibitor

The first set of variables (A)		The second set of variables (B)		Post hoc Tukey HSD p-value A vs B
Insulin treatment	The concentration of MIG	Insulin treatment	The concentration of MIG	
w/o insulin	MIG 10μM	w/o insulin	Control	0.0003
w/o insulin	MIG 40μM	w/o insulin	Control	0.0006
w insulin	Control	w/o insulin	Control	0.0057
w insulin	MIG 2.5μM	w/o insulin	Control	0.0011
w insulin	MIG 10μM	w/o insulin	Control	0.0028
w/o insulin	MIG 10μM	w/o insulin	MIG 2.5μM	0.0001
w/o insulin	MIG 40μM	w/o insulin	MIG 2.5μM	0.0001
w insulin	Control	w/o insulin	MIG 2.5μM	0.0004
w insulin	MIG 2.5μM	w/o insulin	MIG 2.5μM	0.0002
w insulin	MIG 10μM	w/o insulin	MIG 2.5μM	0.0003
w insulin	MIG 40μM	w/o insulin	MIG 2.5μM	0.0036

w/o insulin = without insulin; w insulin = with insulin; MIG = miglustat

5.3.4. Immunocytochemistry of CBE treated cells

Treatment of the cells with CBE caused significant changes in IGF1-Rβ, IRα and Np65 levels. The effect of insulin was observed only in IRα and GD1a epitopes and a combined effect was observed only in IRα and GM1 epitopes (Table 5.43.).

CBE caused a significant shift from the raft only for the GT1b epitope, the other epitopes were not affected (Table 5.45.). The only significant shift to the non-raft area was for IGF1-Rβ, where the treatment caused an increased shift of epitope to the non-raft regions (Table 5.46.).

Post hoc analysis showed that application of inhibitors and insulin caused a significant decrease in IRα levels in all groups compared to controls, regardless of insulin treatment (Table 5.44.).

Post hoc analysis of colocalization showed a significant influx of IGF1-Rβ into the non-raft area regardless of treatment concentration and compared to the control group (5.47.).

Table 5.43. The integrated density value of immunocytochemical staining of differentiated SH-SY5Y human neuroblastoma cells treated 48 hours with MIG, a glycolipid degradation inhibitor.

Epitope	w/o insulin				w insulin				Two-way ANOVA					
	Control	CBE 2.5 µM	CBE 10 µM	CBE 40 µM	Control	CBE 2.5 µM	CBE 10 µM	CBE 40 µM	F values; (degrees of freedom)			p-values		
	Mean; SD	Mean; SD	Mean; SD	Mean; SD	Mean; SD	Mean; SD	Mean; SD	Mean; SD	Insulin	CBE	Insulin × CBE	Insulin	CBE	Insulin × CBE
βAPP	351769; 113703	409947; 107779	362335; 96827	307874; 105692	285842; 44657	360680; 100908	378272; 87815	241769; 87380	0.19 (1, 47)	0.76 (3, 47)	0.07 (3, 47)	0.6608	0.5172	0.9749
IGF1-Rβ	987948; 84329	164646; 62592	927252; 140611	1194669; 394397	1724030; 748935	617068; 190794	1218303; 131899	1057083; 81242	2.09 (1, 45)	3.41 (3, 45)	0.63 (3, 45)	0.1551	0.0251	0.5975
IRα	843864; 47466	277406; 41269	263386; 39791	222177; 83635	243148; 77939	331654; 79023	192586; 76148	237185; 77237	9.88 (1, 42)	10.40 (3, 42)	10.89 (3, 42)	0.0030	<0.0001	<0.0001
Np65	229369; 64570	177460; 28109	222159; 71156	356699; 70534	540101; 164500	96073; 17294	234811; 89619	215971; 76107	0.33 (1, 46)	3.07 (3, 46)	2.62 (3, 46)	0.5662	0.0367	0.0618
GM1	836326; 105238	1984241; 286233	757467; 121773	1562704; 675676	3236956; 348564	1045580; 389690	1444220; 372473	1294026; 40643	3.61 (1, 40)	2.45 (3, 40)	8.59 (3, 40)	0.0645	0.0767	0.0001
GD1a	722619; 128660	411201; 87649	501366; 113844	790358; 72827	1294780; 375421	1130095; 274360	1419579; 475168	1132667; 206545	12.35 (1, 40)	0.33 (3, 40)	0.44 (3, 40)	0.0011	0.7978	0.7205
GD1b	416644; 46406	653776; 175670	691465; 136264	354303; 57165	597870; 62536	499680; 121766	494015; 96104	466388; 125157	0.06 (1, 46)	0.91 (3, 46)	1.32 (3, 46)	0.8025	0.4409	0.2789
GT1b	406755; 83516	886269; 258435	457148; 50210	791745; 162853	786112; 49734	726882; 130734	563934; 61474	642679; 73461	0.18 (1, 47)	2.06 (3, 47)	1.97 (3, 47)	0.6669	0.1177	0.1303

SD=standard deviation; w/o insulin = without insulin; w insulin = with insulin; Conduritol B epoxide; βAPP = beta amyloid precursor protein; IGF1-Rβ = beta subunit of receptor for insulin like growth factor; Np 65 = neuroplastin 65; IRα = insulin receptor alpha subunit; GM1 = GM1 ganglioside; GD1a = GD1a ganglioside; GD1b = GD1b ganglioside; GT1b = GT1b ganglioside

Table 5.44. Post hoc analysis of immunocytochemical ANOVA data for IR α epitope in cells treated with CBE glycolipid degradation inhibitor.

The first set of variables (A)		The second set of variables (B)		Post hoc Tukey HSD p-value A vs B
Insulin treatment	The concentration of CBE	Insulin treatment	The concentration of CBE	
w/o insulin	Control	w/o insulin	CBE 2.5μM	0.0001
w/o insulin	Control	w/o insulin	CBE 10μM	0.0001
w/o insulin	Control	w/o insulin	CBE 40μM	0.0001
w/o insulin	Control	w insulin	Control	0.0001
w/o insulin	Control	w insulin	CBE 2.5μM	0.0001
w/o insulin	Control	w insulin	CBE 10μM	0.0001
w/o insulin	Control	w insulin	CBE 40μM	0.0001

w/o insulin = without insulin; w insulin = with insulin; CBE = conduritol B epoxide

Table 5.45. Colocalization percentage of selected epitopes with flotillin 1 or 2 (F1, F2) lipid raft markers in differentiated SH-SY5Y human neuroblastoma cells treated 48 hours with CBE, a glycolipid degradation inhibitor.

Epitope	w/o insulin				w insulin				Two-way ANOVA					
	Control	CBE 2.5 µM	CBE 10 µM	CBE 40 µM	Control	CBE 2.5 µM	CBE 10 µM	CBE 40 µM	F values; (degrees of freedom)			p-values		
	Mean; SD	Mean; SD	Mean; SD	Mean; SD	Mean; SD	Mean; SD	Mean; SD	Mean; SD	Insulin	CBE	Insulin × CBE	Insulin	CBE	Insulin × CBE
F1-βAPP	4.45; 3.44	2.22; 0.25	2.71; 2.09	0.27; 0.15	6.06; 2.34	1.82; 1.04	1.42; 0.78	3.19; 1.36	0.31 (1, 16)	1.75 (3, 16)	0.57 (3, 16)	0.5821	0.1968	0.6390
F1-IGF1Rb	0.62; 0.16	1.23; 0.61	0.01; 0.01	0.09; 0.09	11.36; 7.11	5.16; 4.74	6.60; 6.50	0.35; 0.19	4.00 (1, 16)	0.76 (3, 16)	0.67 (3, 16)	0.0627	0.5286	0.5794
F1-IRα	0.04; 0.03	0.04; 0.04	0.03; 0.01	0.01; 0.01	1.22; 1.19	0.35; 0.21	0.06; 0.05	0.23; 0.13	2.03 (1, 16)	0.73 (3, 16)	0.68 (3, 16)	0.1727	0.5465	0.5721
F1-Np 65	0.13; 0.13	0.01; 0.01	0.30; 0.16	0.31; 0.28	0.03; 0.03	0.01; 0.01	9.31; 9.21	1.42; 1.33	1.15 (1, 16)	0.95 (3, 16)	0.88 (3, 16)	0.2979	0.4372	0.4715
F2-GM1	3.00; 0.90	0.03; 0.02	0.04; 0.02	0.01; 0.01	3.38; 2.12	2.83; 2.83	0.27; 0.15	0.03; 0.01	0.88 (1, 16)	2.60 (3, 16)	0.50 (3, 16)	0.3605	0.0876	0.6814
F2-GD1a	0.02; 0.01	1.12; 0.82	2.42; 1.29	1.49; 0.94	1.68; 1.68	1.31; 0.05	1.81; 1.02	3.22; 1.89	0.83 (1, 16)	0.78 (3, 16)	0.49 (3, 16)	0.3756	0.5221	0.6889
F2-GD1b	2.43; 1.27	2.89; 2.79	0.37; 0.36	0.04; 0.02	1.19; 0.47	5.31; 5.30	1.70; 1.63	0.05; 0.02	0.15 (1, 16)	1.18 (3, 16)	0.24 (3, 16)	0.6969	0.3482	0.8608
F2-GT1b	2.78; 0.71	0.05; 0.05	0.00; 0.00	0.31; 0.31	3.16; 1.41	0.73; 0.71	0.86; 0.83	0.00; 0.00	0.68 (1, 16)	7.47 (3, 16)	0.28 (3, 16)	0.4204	0.0023	0.8380

SD = standard deviation; w/o insulin = without insulin; w insulin = with insulin; CBE=conduritol B epoxide; βAPP = beta amyloid precursor protein; IGF1-Rβ = beta subunit of receptor for insulin like growth factor; NP65 = neuroplastin 65; IRα = insulin receptor alpha subunit; GM1 = GM1 ganglioside; GD1a = GD1a ganglioside; GD1b = GD1b ganglioside; GT1b = GT1b ganglioside; F1 = flotillin 1, F2 = flotillin 2

Table 5.46. Colocalization percentage of selected epitopes with transferrin receptor (TfR) or sodium/potassium ATPase (Na/K ATPase) lipid non-raft markers in differentiated SH-SY5Y human neuroblastoma cells treated 48 hours with CBE, a glycolipid degradations inhibitor.

Epitope	w/o insulin				w insulin				Two-way ANOVA					
	Control	CBE 2.5 µM	CBE 10 µM	CBE 40 µM	Control	CBE 2.5 µM	CBE 10 µM	CBE 40 µM	F values; (degrees of freedom)			p-values		
	Mean; SD	Mean; SD	Mean; SD	Mean; SD	Mean; SD	Mean; SD	Mean; SD	Mean; SD	Insulin	CBE	Insulin × CBE	Insulin	CBE	Insulin × CBE
TfR-βAPP	0.82; 0.76	0.04; 0.02	0.15; 0.08	1.58; 1.30	0.11; 0.11	1.40; 0.14	2.44; 1.31	0.79; 0.52	1.08 (1, 16)	0.57 (3, 16)	2.18 (3, 16)	0.3132	0.6419	0.1295
TfR-IGF1Rb	0.86; 0.41	9.69; 1.37	3.93; 0.69	13.43; 2.76	0.34; 0.27	9.16; 1.28	9.74; 2.61	3.35; 1.84	1.28 (1, 16)	11.33 (3, 16)	7.78 (3, 16)	0.2737	0.0003	0.0019
TfR-IRα	1.20; 1.17	0.22; 0.08	0.53; 0.46	1.31; 0.05	1.15; 1.11	0.37; 0.34	0.48; 0.37	2.38; 0.45	0.37 (1, 16)	2.39 (3, 16)	0.34 (3, 16)	0.5485	0.1067	0.7901
TfR-Np65	0.86; 0.46	3.13; 1.33	0.66; 0.55	0.21; 0.12	1.44; 0.76	1.27; 0.99	1.61; 1.50	1.03; 0.46	0.03 (1, 16)	1.11 (3, 16)	1.12 (3, 16)	0.8454	0.3703	0.3668
Na/K-GM1	8.64; 1.11	0.97; 0.13	4.52; 2.31	1.06; 0.94	2.61; 0.42	3.38; 1.22	2.69; 2.56	1.67; 1.04	1.39 (1, 16)	3.33 (3, 16)	3.19 (3, 16)	0.2547	0.0462	0.0518
Na/K-GD1a	3.46; 1.87	4.79; 3.76	1.25; 0.88	3.44; 1.90	1.06; 0.94	1.13; 0.53	4.13; 3.96	8.92; 8.68	0.04 (1, 16)	0.45 (3, 16)	0.65 (3, 16)	0.8320	0.7198	0.5910
Na/K-GD1b	1.01; 0.51	0.08; 0.07	0.28; 0.18	0.06; 0.03	0.22; 0.14	2.02; 1.74	0.01; 0.00	0.19; 0.07	0.30 (1, 16)	0.93 (3, 16)	1.66 (3, 16)	0.5897	0.4480	0.2135
Na/K-GT1b	1.59; 1.58	0.01; 0.01	0.00; 0.00	0.00; 0.00	1.24; 0.86	0.00; 0.00	0.17; 0.16	0.00; 0.00	0.01 (1, 16)	2.34 (3, 16)	0.05 (3, 16)	0.9185	0.1110	0.9810

SD = standard deviation; w/o insulin = without insulin; w insulin = with insulin; CBE = conduritol B epoxide; βAPP = beta amyloid precursor protein; IGF1-Rβ = beta subunit of receptor for insulin like growth factor; ; NP65 = neuroplastin 65; IRα = insulin receptor alpha subunit; GM1 = GM1 ganglioside; GD1a = GD1a ganglioside; GD1b = GD1b ganglioside; GT1b = GT1b ganglioside; TfR = transferrin receptor, Na/K = sodium/potassium ATPase

Table 5.47. Post hoc analysis of immunocytochemical ANOVA data for colocalization analysis results of TFR-IGF1-Rβ epitopes in cells treated CBE a glycolipid degradation inhibitor

Expression of TfR-IGF1Rb				
The first set of variables (A)		The second set of variables (B)		Post hoc Tukey HSD p-value A vs B
Insulin treatment	The concentration of CBE	Insulin treatment	The concentration of CBE	
w/o insulin	CBE 2.5µM	w/o insulin	Control	0.0285
w/o insulin	CBE 40µM	w/o insulin	Control	0.0014
w insulin	CBE 2.5µM	w/o insulin	Control	0.0440
w insulin	CBE 10µM	w/o insulin	Control	0.0273
w/o insulin	CBE 40µM	w/o insulin	CBE 2.5µM	0.0164
w insulin	Control	w/o insulin	CBE 40µM	0.0009
w insulin	CBE 40µM	w/o insulin	CBE 40µM	0.0102
w insulin	CBE 2.5µM	w insulin	Control	0.0289
w insulin	CBE 10µM	w insulin	Control	0.0178

w/o insulin = without insulin; w insulin = with insulin; CBE = conduritol B epoxide

5.4. Histochemical staining of the neurites

All four inhibitors had a significant effect on the length of the neurites. Higher concentrations of both isoforms of P4 caused more prominent shortening and opposite was observed with MIG and CBE. Insulin treatment alone resulted a prominent decrease in the length of neurites in comparison to the non-treated control samples. Insulin treatment in combination with all inhibitors except MIG also affected the neurite length (Table 5.48.).

Post hoc analysis of data from cells treated with P4-RR showed a significant reduction in length when treated with either the highest or the lowest inhibitor concentration compared to the control. Insulin treatment regardless of the inhibitor concentration resulted significant reduction in the length of neurites compared to both control groups (Table 5.49., Table 5.48. Figure 5.1).

Post hoc analysis of the data from cells treated with the P4-SS inhibitor showed a shortening effect compared to the control group at all three concentrations. The application of insulin significantly increased the length of neurites when comparing the treated groups. An opposite effect was observed in the control groups, where the application of insulin shortened the neurites (Table 5.50., Table 5.48., Figure 5.2.).

MIG treatment alone and in combination with insulin affected neurite length, but no interaction was observed between the two treatments (Table 5.48.). Post hoc analysis

showed significance only between insulin-treated and untreated control groups, where insulin treatment shortened the neurite length. The same effect was observed only in cell treated with the highest concentrations of inhibitor, where neurite length was significantly reduced following insulin treatment (Table 5.51., Table 5.48., Figure 5.3.).

Post hoc analysis of data from CBE treated cells showed a significant effect of the two lower CBE concentrations on neurite shortening. However, no effect was observable at the highest concentrations. Treatment with CBE and insulin, neurites were significantly longer compared to the non-insulin treated groups (Table 5.52., Table 5.48., Figure 5.4.).

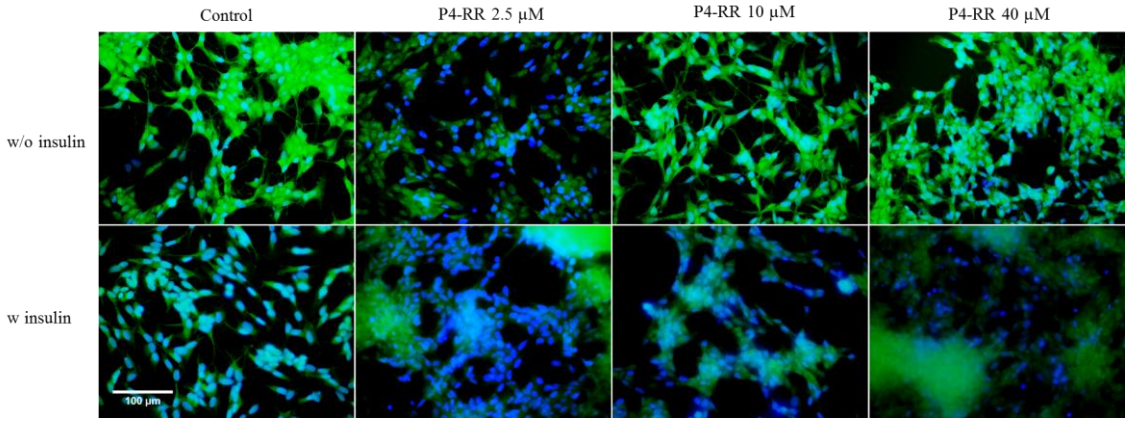

Figure 5.1. FITC dye histochemical staining of differentiated SH-SY5Y human neuroblastoma cell line treated with three concentrations of P4-RR GlcCer synthesis inhibitor and additionally with insulin. The author made the figure. Green = FITC stain, blue = cell nuclei, w/o insulin = without insulin; w insulin = with insulin; P4-RR = (*R*, *R*) D, L-threo-phenyl-2-hexadecanoylamino-3-pyrrolidino-1-propanol; scale 100 micrometers.

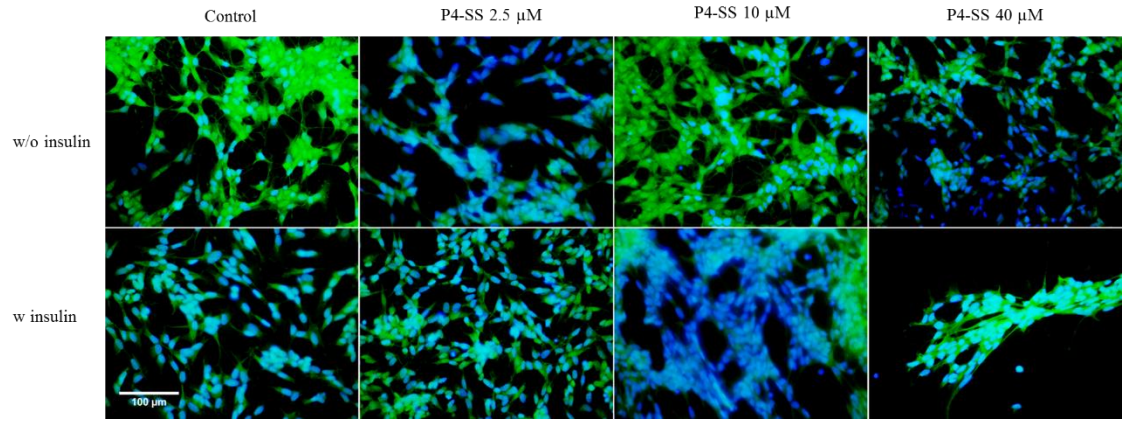

Figure 5.2. FITC dye histochemical staining of differentiated SH-SY5Y human neuroblastoma cell line treated with three concentrations of P4-SS GlcCer synthesis inhibitor and additionally with insulin. The author made the figure. Green = FITC stain, blue = cell nuclei, w/o insulin = without insulin; w insulin = with insulin; P4-SS = (*S*, *S*) D, L-threo-phenyl-2-hexadecanoylamino-3-pyrrolidino-1-propanol; scale 100 micrometers.

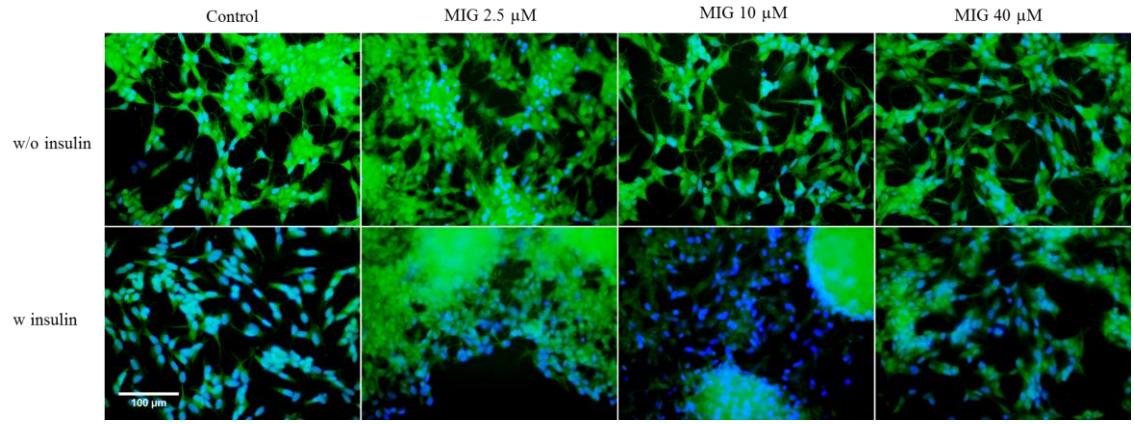

Figure 5.3. FITC dye histochemical staining of differentiated SH-SY5Y human neuroblastoma cell line treated with three concentrations of miglustat GlcCer synthesis inhibitor and additionally with insulin. The author made the figure. Green = FITC stain, blue = cell nuclei, w/o insulin = without insulin; w insulin = with insulin; MIG = miglustat; scale 100 micrometers.

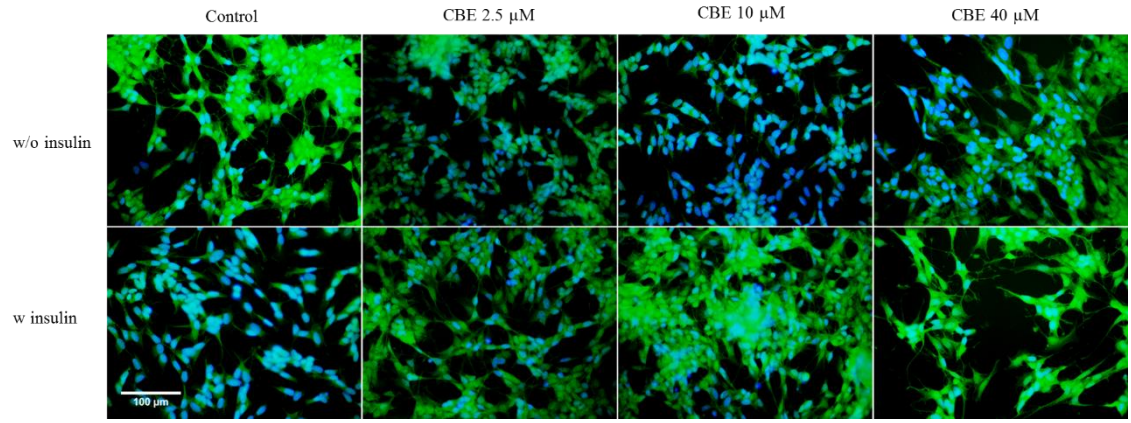

Figure 5.4. FITC dye histochemical staining of differentiated SH-SY5Y human neuroblastoma cell line treated with three concentrations of conduritol B epoxide, a glycosphingolipid degradation inhibitor, and additionally with insulin. The author made the figure. Green = FITC stain, blue = cell nuclei, w/o insulin = without insulin; w insulin = with insulin; CBE = conduritol B epoxide; scale 100 micrometers.

Table 5.48. Neurite length of differentiated SH-SY5Y human neuroblastoma cell line at 48 hours after treatment with P4-RR, P4-SS, MIG or CBE inhibitors in the absence or presence of insulin. Length is measured and presented in micrometers. Statistical significance was tested with two-way ANOVA.

Treatment (Treat.)	w/o insulin				w insulin				Two-way ANOVA					
	Control	2.5µM	10µM	40µM	Control	2.5µM	10µM	40µM	F values; (degrees of freedom)			p-values		
	Mean; SD	Mean; SD	Mean; SD	Mean; SD	Mean; SD	Mean; SD	Mean; SD	Mean; SD	Insulin	Treat.	Insulin × Treat.	Insulin	Treat.	Insulin × Treat.
P4-RR	42.46; 4.91	23.71; 3.33	39.02; 1.57	27.06; 1.88	28.38; 1.50	18.83; 3.24	15.40; 2.21	9.73; 2.16	51.07 (1,53)	14.26 (3,53)	3.29 (3,53)	<0.0001	<0.0001	0.0273
P4-SS	42.46; 4.91	22.62; 2.15	22.57; 1.72	18.46; 0.97	28.38; 1.50	25.99; 1.60	35.98; 3.94	33.07; 3.32	5.42 (1,56)	7.97 (3,56)	14.08 (3,56)	0.0234	0.0001	<0.0001
MIG	42.46; 4.91	35.18; 1.29	40.18; 2.19	53.98; 4.79	28.38; 1.50	23.27; 0.80	24.76; 0.89	35.69; 2.56	37.90 (1,47)	7.02 (3,47)	0.27 (3,47)	<0.0001	0.0005	0.8438
CBE	42.46; 4.91	25.76; 0.84	28.43; 2.32	41.12; 1.55	28.38; 1.50	47.23; 0.81	41.86; 3.80	65.60; 3.28	23.87 (1,40)	14.59 (3,40)	19.54 (3,40)	<0.0001	<0.0001	<0.0001

SD = standard deviation; w/o insulin = without insulin; w insulin = with insulin; P4-RR = (*R, R*) D, L-threo-phenyl-2-hexadecanoylamino-3-pyrrolidino-1-propanol; P4-SS = (*S, S*) D, L-threo-phenyl-2-hexadecanoylamino-3-pyrrolidino-1-propanol; MIG = miglustat; CBE = Conduritol B epoxide

Table 5.49. Post hoc test of two-way ANOVA results for neurite length 48 hours after treatment with P4-RR, a GlcCer synthesis inhibitor and additionally with insulin of differentiated SH-SY5Y human neuroblastoma cell line presenting significant results;

The first set of variables (A)		The second set of variables (B)		Post hoc Tukey HSD p-value A vs B
Insulin treatment	The concentration of P4-RR	Insulin treatment	The concentration of P4-RR	
w/o insulin	Control	w/o insulin	P4-RR 40μM	0.0028
w/o insulin	Control	w/o insulin	P4-RR 2.5μM	0.0003
w/o insulin	Control	w insulin	Control	0.0049
w/o insulin	Control	w insulin	P4-RR 40μM	0.0001
w/o insulin	Control	w insulin	P4-RR 10μM	0.0001
w/o insulin	Control	w insulin	P4-RR 2.5μM	0.0002
w/o insulin	P4-RR 40μM	w/o insulin	P4-RR 10μM	0.0203
w/o insulin	P4-RR 40μM	w insulin	P4-RR 40μM	0.0088
w/o insulin	P4-RR 10μM	w/o insulin	P4-RR 2.5μM	0.0017
w/o insulin	P4-RR 10μM	w insulin	Control	0.0368
w/o insulin	P4-RR 10μM	w insulin	P4-RR 40μM	0.0001
w/o insulin	P4-RR 10μM	w insulin	P4-RR 10μM	0.0001
w/o insulin	P4-RR 10μM	w insulin	P4-RR 2.5μM	0.0009
w insulin	Control	w insulin	P4-RR 40μM	0.0025
w insulin	Control	w insulin	P4-RR 10μM	0.0297

w/o insulin = without insulin; w insulin = with insulin; P4-RR = (*R*, *R*) D, L-threo-phenyl-2-hexadecanoylamino-3-pyrrolidino-1-propanol

Table 5.50. Post hoc test of two-way ANOVA results for neurite length 48 hours after treatment with P4-SS, a GlcCer synthesis inhibitor and additionally with insulin of differentiated SH-SY5Y human neuroblastoma cell line presenting significant results

Neurite length				
The first set of variables (A)		The second set of variables (B)		Post hoc Tukey HSD p-value A vs B
Insulin treatment	The concentration of P4-SS	Insulin treatment	The concentration of P4-SS	
w/o insulin	Control	w/o insulin	P4-SS 40μM	0.0001
w/o insulin	Control	w/o insulin	P4-SS 10μM	0.0001
w/o insulin	Control	w/o insulin	P4-SS 2.5μM	0.0001
w/o insulin	Control	w insulin	Control	0.0023
w/o insulin	Control	w insulin	P4-SS 2.5μM	0.0007
w/o insulin	P4-SS 40μM	w insulin	P4-SS 40μM	0.0071
w/o insulin	P4-SS 40μM	w insulin	P4-SS 10μM	0.0014
w/o insulin	P4-SS 10μM	w insulin	P4-SS 10μM	0.0260
w/o insulin	P4-SS 2.5μM	w insulin	P4-SS 10μM	0.0480

w/o insulin = without insulin; w insulin = with insulin; P4-SS = (*S*, *S*) D, L-threo-phenyl-2-hexadecanoylamino-3-pyrrolidino-1-propanol

Table 5.51. Post hoc test of two-way ANOVA results for neurite length 48 hours after treatment with miglustat, a GlcCer synthesis inhibitor and additionally with insulin of differentiated SH-SY5Y human neuroblastoma cell line presenting significant results;

The first set of variables (A)		The second set of variables (B)		Post hoc Tukey HSD p-value A vs B
Insulin treatment	The concentration of MIG	Insulin treatment	The concentration of MIG	
w/o insulin	Control	w insulin	Control	0.0148
w/o insulin	MIG 40μM	w insulin	MIG 40μM	0.0108

w/o insulin = without insulin; w insulin = with insulin; MIG = miglustat

Table 5.52. Post hoc test of two-way ANOVA results for neurite length 48 hours after treatment with CBE glycosphingolipid degradation inhibitor and additionally with insulin of differentiated SH-SY5Y human neuroblastoma cell line presenting significant results

The first set of variables (A)		The second set of variables (B)		Post hoc Tukey HSD p-value A vs B
Insulin treatment	The concentration of CBE	Insulin treatment	The concentration of CBE	
w/o insulin	Control	w/o insulin	CBE-P4 10μM	0.0182
w/o insulin	Control	w/o insulin	CBE-P4 2.5μM	0.0172
w/o insulin	Control	w insulin	Control	0.0057
w/o insulin	Control	w insulin	CBE-P4 40μM	0.0002
w/o insulin	CBE-P4 40μM	w insulin	CBE-P4 40μM	0.0003
w/o insulin	CBE-P4 10μM	w insulin	CBE-P4 40μM	0.0001
w/o insulin	CBE-P4 10μM	w insulin	CBE-P4 2.5μM	0.0064
w/o insulin	CBE-P4 2.5μM	w insulin	CBE-P4 40μM	0.0001
w/o insulin	CBE-P4 2.5μM	w insulin	CBE-P4 2.5μM	0.0056
w insulin	Control	w insulin	CBE-P4 40μM	0.0001
w insulin	Control	w insulin	CBE-P4 2.5μM	0.0027
w insulin	CBE-P4 40μM	w insulin	CBE-P4 10μM	0.0008
w insulin	CBE-P4 40μM	w insulin	CBE-P4 2.5μM	0.0166

w/o insulin = without insulin; w insulin = with insulin; MIG = miglustat

5.5. MALDI-TOF MS total lipidome analysis

Analysis of total lipidome on inhibitor-treated cells revealed that all treatments had an effect but each to a different degree. Positive imaging mode was used, and data is presented in the form of a table with affected metabolic modules and individual compounds, all with statistical significance of the affected metabolic constituent. In individual compounds, p-value presents statistical difference calculated with t-test from data of control end experimental group comparing the number of hits in each group-specific m/z. KEGG analysis p score represents the probability that metabolic module is affected comparing closeness of each molecule to one another and considering the total number of molecules in pathway/module. It is interpreted in the same way as the p-value of any other statistical test, where H_0 means there is no change. Presented data is from

positive imaging mode. The negative imaging mode gave no statistically significant results and thus is not presented in further text.

5.5.1. MALDI-TOF MS total lipidome analysis of the cells treated with insulin

Treatment of the cells with insulin caused changes in biosynthetic pathways of ceramide and cholesterol biosynthesis, all downregulated compared to the control group (Table 5.53. and 5.54.).

Table 5.53. Effects of insulin on metabolic compounds in differentiated SH-SY5Y human neuroblastoma cell line data was generated after KEGGREST analysis significant signals procured by MALDI-TOF MS imaging in positive mode.

KEGG id	m/z	p-value	t score	adduct	compound name
C20972	530.30	0.0112	3.553631	M+NH4	Angiotensin
C00319	599.55	<0.0001	-11.724	2M+H	Sphingosine;
C02934	599.55	<0.0001	-11.724	2M+H	3-Dehydrosphinganine;
C16512	599.55	<0.0001	-11.724	2M+H	Palmitoylethanolamide;
C01069	659.20	0.0074	-4.351	2M+H	Desulfoglucotropeolin
C05113	659.20	0.0074	-4.351	2M+K	Porphyrin
C16692	659.20	0.0074	-4.351	2M+K	Mannopine
C21480	768.55	0.0001	-10.8144	M+H	1-Octadecanoyl-2-(5Z,8Z,11Z,14Z-eicosatetraenoyl)-sn-glycero-3-phosphoethanolamine
C05103	835.70	<0.0001	-12.9664	2M+K	4- alpha-Methylzymosterol
C08813	835.70	<0.0001	-12.9664	2M+K	Brassicasterol
C15777	835.70	<0.0001	-12.9664	2M+K	Episterol
C15781	835.70	<0.0001	-12.9664	2M+K	24-Methylenecholesterol
C22112	895.60	<0.0001	-12.9664	2M+K	4alpha-Carboxy-5alpha-cholesta-8,24-dien-3beta-ol

m/z = mass-to-charge ratio

Table 5.54. Effects of insulin on differentiated SH-SY5Y human neuroblastoma cell line data was generated after KEGGREST analysis and FELLA enrichment of significant signals procured by MALDI-TOF MS imaging in positive mode presenting affected biochemical modules

KEGG ID	KEGG name	p score
M00094	Ceramide biosynthesis	0.0001
M00099	Sphingosine biosynthesis	0.0001
M00101	Cholesterol biosynthesis, squalene 2,3-epoxide	0.0001
M00917	Phytosterol biosynthesis, squalene 2,3-epoxide	0.0010

5.5.2. MALDI-TOF MS total lipidome analysis of the cells treated with P4-RR

Treatment of the cells with 2.5 μM P4-RR caused a decrease in the biosynthesis of ceramides and sphingosine and an increase in purine metabolism. The 10 μM P4-RR treatment caused even greater reduction in sphingolipid metabolism but introduced further changes in upregulation of cholesterol biosynthesis. The 40 μM P4-RR treatment caused further changes in metabolism. The upregulation of ceramide and sphingosine biosynthesis was followed by an increase in triglyceride levels, a levelling off of retinoic acid derivatives and a shift in bile acid metabolism (Table 5.55., 5.56.).

Addition of insulin and treatment with 2.5 μM P4-RR caused a 13-to-14-fold significant decrease in the biosynthesis of metabolic precursors of sphingosine and ceramide. At the same time, cholesterol biosynthesis was upregulated along with the metabolic pathways for tetrahydrobiopterin. Treatment of cells with 10 μM P4-RR also resulted the accumulation of iodine compounds and a shift in folate biosynthesis. The combination of 40 μM P4-RR treatment and insulin upregulated cholesterol metabolism and significantly reduced the metabolism of sphingolipids, while tetrahydrobiopterin metabolism remained upregulated as at the previous concentration (Table 5.57., 5.58.).

Table 5.55. Effects of P4-RR 48 hours post-treatment on metabolic compounds in differentiated SH-SY5Y human neuroblastoma cell line data was generated after KEGGREST of significant signals procured by MALDI-TOF MS imaging in positive mode

Compound identifiers				P4-RR 2.5μM		P4-RR 10μM		P4-RR 40μM	
Compound name	KEGG ID	m/z	adduct	p-value	t score	p-value	t score	p-value	t score
all-trans-13,14-Dihydroretinol	C15492	577.50	2M+H					0.0268	3.10
Retinol	C00473	595.45	2M+Na					<0.0001	17.50
11-cis-Retinol	C00899	595.45	2M+Na					<0.0001	17.50
9-cis-Retinol	C16682	595.45	2M+Na					<0.0001	17.50
Sphingosine	C00319	599.55	2M+H					<0.0001	17.50
3-Dehydrosphinganin	C02934	599.55	2M+H	0.0001	-10.14	<0.0001	-12.10	<0.0001	17.50
Palmitoylethanolamide	C16512	599.55	2M+H	0.0001	-10.14	<0.0001	-12.10	<0.0001	17.50
Sphingosine	C00319	599.60	2M+H					0.0002	10.24
3-Dehydrosphinganine	C02934	599.60	2M+H					0.0002	10.24
Palmitoylethanolamide	C16512	599.60	2M+H					0.0002	10.24
CMP-N-glycolylneuraminate	C03691	631.15	M+H					0.0258	-3.13
N-Acetylaspartylglutamate	C12270	631.15	2M+Na					0.0258	-3.13

Compound identifiers				P4-RR 2.5μM		P4-RR 10μM		P4-RR 40μM	
Compound name	KEGG ID	m/z	adduct	p-value	t score	p-value	t score	p-value	t score
Porphyrin	C05113	659.20	2M+K	0.0074	-4.35	0.0074	-4.35		
UDP-N-acetylmuramoyl-L-alanine	C01212	733.15	M+H-H2O	0.0047	4.84			<0.0001	15.07
1-(5'-Phosphoribosyl)-5-formamido-4-imidazolecarboxamide	C04734	733.15	2M+H	0.0047	4.84			<0.0001	15.07
1-Octadecanoyl-2-(5Z,8Z,11Z,14Z-eicosatetraenoyl)-sn-glycero-3-phosphoethanolamine	C21480	768.55	M+H	0.0001	-10.81	0.0001	-10.81	0.0001	-10.81
N-Oleoyl dopamine	C12272	835.70	2M+H			0.0233	2.77		
4-alpha-Methylzymosterol	C05103	835.70	2M+K			0.0233	2.77		

P4-RR = (*R*, *R*) D, L-threo-phenyl-2-hexadecanoylamino-3-pyrrolidino-1-propanol; m/z = mass-to-charge ratio

Table 5.56. Effects of P4-RR 48 hours post-treatment on differentiated SH-SY5Y human neuroblastoma cell line data was generated after KEGGREST analysis and FELLA enrichment of significant signals procured by MALDI-TOF MS imaging in positive mode presenting affected biochemical modules

Module identifiers		P4-RR 2.5μM	P4-RR 10μM	P4-RR 40μM
KEGG ID	KEGG name	p score	p score	p score
M00094	Ceramide biosynthesis	<0.0001	<0.0001	<0.0001
M00099	Sphingosine biosynthesis	<0.0001	<0.0001	<0.0001
M00101	Cholesterol biosynthesis, squalene 2,3-epoxide		<0.0001	
M00102	Ergocalciferol biosynthesis, squalene 2,3-epoxide		<0.0001	
M00106	Conjugated bile acid biosynthesis, cholate => taurocholate/glycocholate			0.0138
M00089	Triacylglycerol biosynthesis			<0.0001
M00048	Inosine monophosphate biosynthesis, PRPP + glutamine => IMP	0.0001		<0.0001

P4-RR = (*R*, *R*) D, L-threo-phenyl-2-hexadecanoylamino-3-pyrrolidino-1-propanol

Table 5.57. Effects of P4-RR 48 hours post-treatment and insulin on metabolic compounds in differentiated SH-SY5Y human neuroblastoma cell line data was generated after KEGGREST of significant signals procured by MALDI-TOF MS imaging in positive mode

Compound identifiers				P4-RRI 2.5μM		P4-RRI 10μM		P4-RRI 40μM	
Compound name	KEGG ID	m/z	adduct	p-value	t score	p-value	t score	p-value	t score
1-Octadecanoyl-sn-glycero-3-phosphoethanolamine	C21484	504.30	M+Na	<0.0001	-14.08	<0.0001	-14.08	0.0001	-7.55
Sphingosyl-phosphocholine	C03640	504.30	M+K	<0.0001	-14.08	<0.0001	-14.08	0.0001	-7.55
Cholesterol	C18043	505.25	M+K	0.0003	5.74	0.0013	4.43	0.0037	3.77
Tetrahydrobiopterin	C00272	505.25	2M+Na	0.0003	5.74	0.0013	4.43	0.0037	3.77
L-threo-Tetrahydrobiopterin	C20264	505.25	2M+Na	0.0003	5.74	0.0013	4.43	0.0037	3.77
Iodine	C01382	508.60	2M+H	0.0273	3.08	0.0251	3.15		
Sphingosine	C00319	599.55	2M+H	<0.0001	-13.39	<0.0001	-13.39	<0.0001	-13.39
3-Dehydrosphinganine	C02934	599.55	2M+H	<0.0001	-13.39	<0.0001	-13.39	<0.0001	-13.39
Palmitoylethanolamide	C16512	599.55	2M+H	<0.0001	-13.39	<0.0001	-13.39	<0.0001	-13.39
Sphingosine	C00319	599.60	2M+H	<0.0001	13.11	0.0001	10.31	0.0001	12.56
3-Dehydrosphinganine	C02934	599.60	2M+H	<0.0001	13.11	0.0001	10.31	0.0001	12.56
Palmitoylethanolamide	C16512	599.60	2M+H	<0.0001	13.11	0.0001	10.31	0.0001	12.56
Porphyrin	C05113	659.20	2M+K	0.0074	-4.35	0.0074	-4.351	0.0067	-4.14
UDP-N-acetylmuramoyl-L-alanine	C01212	733.15	M+H-H2O	<0.0001	22.44	0.0043	4.93	0.0002	10.13
1-(5'-Phosphoribosyl)-5-formamido-4-imidazolecarboxamide	C04734	733.15	2M+H	<0.0001	22.44	0.0043	4.93	0.0002	10.13
(R)-S-Lactoylglutathione	C03451	759.20	2M+H	0.0267	3.10	<0.0001	32.27	0.0285	3.04
1-Octadecanoyl-2-(5Z,8Z,11Z,14Z-eicosatetraenoyl)-sn-glycero-3-phosphoethanolamine	C21480	768.55	M+H	0.0001	-10.81	0.0001	-10.81	0.0001	-14.37
N-Oleoyl dopamine	C12272	835.70	2M+H	<0.0001	-12.96				
4-alpha-Methylzymosterol	C05103	835.70	2M+K	<0.0001	-12.96				

P4-RRI = (*R*, *R*) D, L-threo-phenyl-2-hexadecanoylamino-3-pyrrolidino-1-propanol + insulin; m/z = mass-to-charge ratio

Table 5.58. Effects of P4-RR 48 hours post-treatment and insulin on differentiated SH-SY5Y human neuroblastoma cell line data was generated after KEGGREST analysis and FELLA enrichment of significant signals procured by MALDI-TOF MS imaging in positive mode

Module identifiers		P4-RRI 2.5μM	P4-RRI 10μM	P4-RRI 40μM
KEGG ID	KEGG name	p score	p score	p score
M00842	Tetrahydrobiopterin biosynthesis, GTP => BH4	0.0370	0.0435	0.0135
M00843	L-threo-Tetrahydrobiopterin biosynthesis, GTP => L-threo-BH4	<0.0001	<0.0001	<0.0001
M00048	Inosine monophosphate biosynthesis, PRPP + glutamine => IMP	<0.0001	0.0008	<0.0001
M00094	Ceramide biosynthesis	<0.0001	<0.0001	<0.0001
M00099	Sphingosine biosynthesis	<0.0001	<0.0001	<0.0001
M00043	Thyroid hormone biosynthesis, tyrosine => triiodothyronine/thyroxine	<0.0001	<0.0001	
M00101	Cholesterol biosynthesis, squalene 2,3-epoxide	<0.0001		
M00102	Ergocalciferol biosynthesis, squalene 2,3-epoxide	<0.0001		
M00840	Tetrahydrofolate biosynthesis		<0.0001	

P4-RRI = (*R, R*) D, L-threo-phenyl-2-hexadecanoylamino-3-pyrrolidino-1-propanol + insulin

5.5.3. MALDI-TOF MS total lipidome analysis of the cells treated with P4-SS

Treatment of the cells with 2.5 μM P4-SS caused a significant decrease in sphingolipid metabolism and an upregulation of cholesterol metabolism and biosynthesis. At this concentration, an increase in tetrahydrobiopterin synthesis was also observed. The 10 μM P4-SS treatment caused an even greater decrease in ceramide and sphingosine biosynthesis, and the upregulation of the cholesterol and tetrahydrobiopterin biosynthesis was more pronounced. The highest concentration decreased the level of CMP-N-glycolylneuraminate, but no effect on cholesterol biosynthesis was observed (Table 5.59., 5.60.).

The addition of insulin to the cells treated with 2.5 μM P4-SS resulted in a 13-14-fold reduction in sphingolipid and ceramide metabolism, a downregulation in cholesterol biosynthesis, and an upregulation of vitamin K metabolism and iodine compounds accumulation compared to controls. Treatment with 10 μM P4-SS and insulin inhibited sphingolipid and ceramide metabolism and upregulation of cholesterol levels but decreased metabolites levels and increased tetrahydrobiopterin metabolism. In response to 40 μM P4-SS and insulin treatment, sphingosine and ceramide biosynthesis remained inhibited, as well as cholesterol metabolism, but no change in cholesterol levels was observed (Table 5.61., 5.62.).

Table 5.59. Effects of P4-SS 48 hours post-treatment on metabolic compounds in differentiated SH-SY5Y human neuroblastoma cell line data was generated after KEGGREST of significant signals procured by MALDI-TOF MS imaging in positive mode

Compound identifiers				P4-SS 2.5μM		P4-SS 10μM		P4-SS 40μM	
Compound name	KEGG ID	m/z	adduct	p-value	t score	p-value	t score	p-value	t score
1-Octadecanoyl-sn-glycero-3-phosphoethanolamine	C21484	504.30	M+Na	0.0023	-4.48	0.0277	-2.58		
Sphingosyl-phosphocholine	C03640	504.30	M+K	0.0023	-4.48	0.0277	-2.58		
Cholesterol	C18043	505.25	M+K	0.0124	3.50	0.0022	4.39	0.0420	2.34
Tetrahydrobiopterin	C00272	505.25	2M+Na	0.0124	3.50	0.0022	4.39	0.0420	2.34
L-threo-Tetrahydrobiopterin	C20264	505.25	2M+Na	0.0124	3.50	0.0022	4.39	0.0420	2.34
Sphingosine	C00319	599.55	2M+H	<0.0001	-13.39	0.0092	3.26	<0.0001	-7.75
3-Dehydrosphinganine	C02934	599.55	2M+H	<0.0001	-13.39	<0.0001	-10.97	<0.0001	-7.75
Palmitoylethanolamide	C16512	599.55	2M+H	<0.0001	-13.39	<0.0001	-10.97	<0.0001	-7.75
Sphingosine	C00319	599.60	2M+H	0.0003	8.72	<0.0001	-10.97		
3-Dehydrosphinganine	C02934	599.60	2M+H	0.0003	8.72	0.0259	3.13		
Palmitoylethanolamide	C16512	599.60	2M+H	0.0003	8.72	0.0259	3.13		
CMP-N-glycoloylneuraminate	C03691	631.15	M+H					0.0257	-3.13
N-Acetylaspartylglutamate	C12270	631.15	2M+Na					0.0257	-3.13
Dehypoxanthine	C17010	631.15	2M+K					0.0257	-3.13
Porphyrin	C05113	659.20	2M+K	0.0074	-4.35	0.0114	-3.26		
UDP-N-acetylmuramoyl-L-alanine	C01212	733.15	M+H-H2O	<0.0001	27.01	<0.0001	30.28		
1-(5'-Phosphoribosyl)-5-formamido-4-imidazolecarboxamide	C04734	733.15	2M+H	<0.0001	27.01	<0.0001	30.28		
1-Octadecanoyl-2-(5Z,8Z,11Z,14Z-eicosatetraenoyl)-sn-glycero-3-phosphoethanolamine	C21480	768.55	M+H	0.0001	-10.81	0.0001	-10.81	<0.0001	-14.37
1-Octadecanoyl-2-(7Z,10Z,13Z,16Z-docosatetraenoyl)-sn-glycero-3-phosphoethanolamine	C21481	796.60	M+H					0.0398	2.75
N-Oleoyl dopamine	C12272	835.70	2M+H	0.0222	-2.96	0.0364	-2.57		
4 alpha-Methylzymosterol	C05103	835.70	2M+K	0.0222	-2.96	0.0364	-2.57		

P4-SS = (*S*,*S*) D, L-threo-phenyl-2-hexadecanoylamino-3-pyrrolidino-1-propanol; m/z = mass-to-charge ratio

Table 5.60. Effects of P4-SS 2.5 μM 48 hours post-treatment on differentiated SH-SY5Y human neuroblastoma cell line data was generated after KEGGREST analysis and FELLA enrichment of significant signals procured by MALDI-TOF MS imaging in positive mode

Module identifiers		P4-SS 2.5μM	P4-SS 10μM	P4-SS 40μM
KEGG ID	KEGG name	p score	p score	p score
M00094	Ceramide biosynthesis	<0.0001	<0.0001	<0.0001
M00099	Sphingosine biosynthesis	<0.0001	<0.0001	<0.0001
M00842	Tetrahydrobiopterin biosynthesis, GTP => BH4	0.0216	0.0344	0.0062
M00843	L-threo-Tetrahydrobiopterin biosynthesis, GTP => L-threo-BH4	<0.0001		<0.0001
M00048	Inosine monophosphate biosynthesis, PRPP + glutamine => IMP	0.0001	0.0004	
M00101	Cholesterol biosynthesis, squalene 2,3-epoxide	<0.0001	<0.0001	
M00102	Ergocalciferol biosynthesis, squalene 2,3-epoxide	<0.0001	<0.0001	

P4-SS=(*S*,*S*) D, L-threo-phenyl-2-hexadecanoylamino-3-pyrrolidino-1-propanol

Table 5.61. Effects of P4-SS 48 hours post-treatment and insulin on metabolic compounds in differentiated SH-SY5Y human neuroblastoma cell line data was generated after KEGGREST of significant signals procured by MALDI-TOF MS imaging in positive mode

Compound identifiers				P4-SSI 2.5μM		P4-SSI 10μM		P4-SSI 40μM	
Compound name	KEGG ID	m/z	adduct	p-value	t score	p-value	t score	p-value	t score
1-Octadecanoyl-sn-glycero-3-phosphoethanolamine	C21484	504.30	M+Na	<0.0001	-14.08	<0.0001	-14.08	0.0118	-3.4
Sphingosyl-phosphocholine	C03640	504.30	M+K	<0.0001	-14.08	<0.0001	-14.08	0.0118	-3.48
Cholesterol	C18043	505.25	M+K			0.0397	2.36		
Tetrahydrobiopterin	C00272	505.25	2M+Na			0.0397	2.36		
L-threo-Tetrahydrobiopterin	C20264	505.25	2M+Na			0.0397	2.36		
Vitamin K1 epoxide	C05849	505.30	M+K	0.0287	3.04				
Iodine	C01382	508.60	2M+H	<0.0001	14.37				
Sphingosine	C00319	599.55	2M+H	<0.0001	-13.39	<0.0001	-13.39	<0.0001	-13.10
3-Dehydrosphinganine	C02934	599.55	2M+H	<0.0001	-13.39	<0.0001	-13.39	<0.0001	-13.10
Palmitoylethanolamide	C16512	599.55	2M+H	<0.0001	-13.39	<0.0001	-13.39	<0.0001	-13.10
Sphingosine	C00319	599.60	2M+H	<0.0001	13.70	0.0008	7.29	0.0084	4.20
3-Dehydrosphinganine	C02934	599.60	2M+H	<0.0001	13.70	0.0008	7.29	0.0084	4.20
Palmitoylethanolamide	C16512	599.60	2M+H	<0.0001	13.70	0.0008	7.29	0.0084	4.20
Porphyrin	C05113	659.20	2M+K	0.0074	-4.351	0.0074	-4.35	0.0236	-2.69
UDP-N-acetylmuramoyl-L-alanine	C01212	733.15	M+H-H2O	<0.0001	23.32	0.0011	6.78	0.0046	4.86
1-(5'-Phosphoribosyl)-5-formamido-4-imidazolecarboxamide	C04734	733.15	2M+H	<0.0001	23.32	0.0011	6.78	0.0046	4.86

Compound identifiers				P4-SSI 2.5μM		P4-SSI 10μM		P4-SSI 40μM	
Compound name	KEGG ID	m/z	adduct	p-value	t score	p-value	t score	p-value	t score
2,5-Diamino-6-(5-phospho-D-ribitylamino)pyrimidin-4(3H)-one	C18910	733.15	2M+Na	<0.0001	23.32	0.0011	6.78	0.0046	4.86
(R)-S-Lactoylglutathione	C03451	759.20	2M+H	0.0269	3.09				
1-Octadecanoyl-2-(5Z,8Z,11Z,14Z-eicosatetraenoyl)-sn-glycero-3-phosphoethanolamine	C21480	768.55	M+H	0.0001	-10.81	0.0001	-10.81	<0.0001	-14.37
N-Oleoyl dopamine	C12272	835.70	2M+H	<0.0001	-12.96	<0.0001	-12.96	<0.0001	-16.77
4-alpha-Methylzymosterol	C05103	835.70	2M+K	<0.0001	-12.96	<0.0001	-12.96	<0.0001	-16.77

P4-SS = (*S*,*S*) D, L-threo-phenyl-2-hexadecanoylamino-3-pyrrolidino-1-propanol + insulin; m/z = mass-to-charge ratio

Table 5.62. Effects of P4-SS 48 hours post-treatment and insulin on differentiated SH-SY5Y human neuroblastoma cell line data was generated after KEGGREST analysis and FELLA enrichment of significant signals procured by MALDI-TOF MS imaging in positive mode

Module identifiers		P4-SSI 2.5μM	P4-SSI 10μM	P4-SSI 40μM
KEGG ID	KEGG name	p score	p score	p score
M00048	Inosine monophosphate biosynthesis, PRPP + glutamine => IMP	0.0003	0.0001	<0.0001
M00094	Ceramide biosynthesis	<0.0001	<0.0001	<0.0001
M00099	Sphingosine biosynthesis	<0.0001	<0.0001	<0.0001
M00101	Cholesterol biosynthesis, squalene 2,3-epoxide	<0.0001	<0.0001	<0.0001
M00102	Ergocalciferol biosynthesis, squalene 2,3-epoxide	<0.0001	<0.0001	<0.0001
M00842	Tetrahydrobiopterin biosynthesis, GTP => BH4		0.0243	
M00843	L-threo-Tetrahydrobiopterin biosynthesis, GTP => L-threo-BH4		<0.0001	
M00043	Thyroid hormone biosynthesis, tyrosine => triiodothyronine/thyroxine	<0.0001		

P4-SS=(*S*,*S*) D, L-threo-phenyl-2-hexadecanoylamino-3-pyrrolidino-1-propanol + insulin

5.5.4. MALDI-TOF MS total lipidome analysis of the cells treated with MIG

Treatment of cells with 2.5 μM MIG caused changes in sphingosine and ceramide biosynthesis as well as downregulated the cholesterol metabolism. Treatment caused the upregulation of tetrahydrofolate biosynthesis. Treatment of the cells with 10 μM MIG downregulated ceramide and sphingosine biosynthesis. Simultaneously, tetrahydrobiopterin metabolism was upregulated. The same effect was observed with the

highest inhibitor concentration, but no significant effect on cholesterol metabolism was observed (Table 5.63., 5.64.).

The addition of insulin to the 2.5 μM MIG treatment caused significant changes in sphingosine and ceramide biosynthesis. An accumulation of iodine compounds was also observed, which affected its metabolic pathway. Cholesterol biosynthesis decreased at least 12-foldcompared to the control group. When 10 μM MIG and insulin were administered, there was a significant sixfold decrease in the sphingolipid pathway metabolite – sphingosyl phosphocholine. The decrease in cholesterol biosynthesis was similar to that observed at the previous concentration, in addition to affecting ergocalciferol biosynthesis. At 40 μM MIG treatment, sphingosyl phosphocholine level decreased 15-fold compared to the control group. The other ceramide and sphingosine biosynthetic pathways were also affected. There was a further decrease in cholesterol biosynthesis and upregulation of iodine compound accumulation were observed. No effect was observed for ergocalciferol at this concentration (Table 5.65., 5.66.).

Table 5.62. Effects of MIG 48 hours post-treatment on metabolic compounds in differentiated SH-SY5Y human neuroblastoma cell line data was generated after KEGGREST of significant signals procured by MALDI-TOF MS imaging in positive mode

Compound identifiers				MIG 2.5μM		MIG 10μM		MIG 40μM	
Compound name	KEGG ID	m/z	adduct	p-value	t score	p-value	t score	p-value	t score
1-Octadecanoyl-sn-glycero-3-phosphoethanolamine	C21484	504.30	M+Na	0.0190	-2.92			0.0452	-2.35
Sphingosyl-phosphocholine	C03640	504.30	M+K	0.0190	-2.92			0.0452	-2.35
Cholesterol	C18043	505.25	M+K	0.0011	4.61	0.0316	2.80	0.0073	3.35
Tetrahydrobiopterin	C00272	505.25	2M+Na	0.0011	4.61	0.0316	2.80	0.0073	3.35
L-threo-Tetrahydrobiopterin	C20264	505.25	2M+Na	0.0011	4.61	0.0316	2.80	0.0073	3.35
Nicotinamide-beta-riboside	C03150	511.20	2M+H	0.0315	2.95				
7,8-Dihydroneopterin	C04874	511.20	2M+H	0.0315	2.95				
7,8-Dihydromonapterin	C21008	511.20	2M+H	0.0315	2.95				
Biotin	C00120	511.20	2M+Na	0.0315	2.95				
Sphingosine	C00319	599.55	2M+H	<0.0001	-13.39	<0.0001	-9.91	0.0001	-6.79
3-Dehydrosphinganine	C02934	599.55	2M+H	<0.0001	-13.39	<0.0001	-9.91	0.0001	-6.79
Palmitoylethanolamide	C16512	599.55	2M+H	<0.0001	-13.39	<0.0001	-9.91	0.0001	-6.79
Sphingosine	C00319	599.60	2M+H	0.0004	8.34				
3-Dehydrosphinganine	C02934	599.60	2M+H	0.0004	8.34				
Palmitoylethanolamide	C16512	599.60	2M+H	0.0004	8.34				

Compound identifiers				MIG 2.5μM		MIG 10μM		MIG 40μM	
Compound name	KEGG ID	m/z	adduct	p-value	t score	p-value	t score	p-value	t score
3',5'-Cyclic AMP	C00575	659.15	2M+H					0.0103	4.00
2',3'-Cyclic AMP	C02353	659.15	2M+H					0.0103	4.00
Porphyrin	C05113	659.20	2M+K	0.0074	-4.35			0.0074	-4.35
Nicotinamide	C00455	707.10	2M+K					0.0251	3.16
UDP-N-acetylmuramoyl-L-alanine	C01212	733.15	M+H-H2O	<0.0001	31.61	0.0070	4.40	0.0251	3.15
1-(5'-Phosphoribosyl)-5-formamido-4-imidazolecarboxamide	C04734	733.15	2M+H	<0.0001	31.61	0.0070	4.40	0.0251	3.15
2,5-Diamino-6-(5-phospho-D-ribitylamino)pyrimidin-4(3H)-one	C18910	733.15	2M+Na	<0.0001	31.61	0.0070	4.40	0.0251	3.15
1-Octadecanoyl-2-(5Z,8Z,11Z,14Z-eicosatetraenoyl)-sn-glycero-3-phosphoethanolamine	C21480	768.55	M+H	0.0273	3.08	0.0001	-10.81	0.0001	-10.81
1-Octadecanoyl-2-(7Z,10Z,13Z,16Z-docosatetraenoyl)-sn-glycero-3-phosphoethanolamine	C21481	796.60	M+H			0.0409	2.73	0.0264	3.11
N-Oleoyl dopamine	C12272	835.70	2M+H	0.0026	-4.55				
4alpha-Methylzymosterol	C05103	835.70	2M+K	0.0026	-4.55				

MIG = miglustat; m/z = mass-to-charge ratio

Table 5.63. Effects of MIG 48 hours post-treatment on differentiated SH-SY5Y human neuroblastoma cell line data was generated after KEGGREST analysis and FELLA enrichment of significant signals procured by MALDI-TOF MS imaging in positive mode

Module identifiers		MIG 2.5μM	MIG 10μM	MIG 40μM
KEGG ID	KEGG name	p score	p score	p score
M00094	Ceramide biosynthesis	<0.0001	<0.0001	<0.0001
M00099	Sphingosine biosynthesis	<0.0001	<0.0001	<0.0001
M00101	Cholesterol biosynthesis, squalene 2,3-epoxide	<0.0001		
M00102	Ergocalciferol biosynthesis, squalene 2,3-epoxide	<0.0001		
M00126	Tetrahydrofolate biosynthesis, GTP => THF	0.0006		
M00843	L-threo-Tetrahydrobiopterin biosynthesis, GTP => L-threo-BH4	<0.0001	<0.0001	<0.0001
M00048	Inosine monophosphate biosynthesis, PRPP + glutamine => IMP		<0.0001	0.0001
M00842	Tetrahydrobiopterin biosynthesis, GTP => BH4		0.0038	0.0241

MIG = miglustat

Table 5.64. Effects of MIG 48 hours post-treatment and insulin on metabolic compounds on differentiated SH-SY5Y human neuroblastoma cell line data was generated after KEGGREST of significant signals procured by MALDI-TOF MS imaging in positive mode

Compound identifiers				MIGI 2.5μM		MIGI 10μM		MIGI 40μM	
Compound name	KEGG ID	m/z	adduct	p-value	t score	p-value	t score	p-value	t score
1-Octadecanoyl-sn-glycero-3-phosphoethanolamine	C21484	504.30	M+Na	<0.0001	-14.08	0.0002	-6.15	<0.0001	-15.84
Sphingosyl-phosphocholine	C03640	504.30	M+K	<0.0001	-14.08	0.0002	-6.15	<0.0001	-15.84
Cholesterol	C18043	505.25	M+K	<0.0001	7.64	<0.0001	10.76		
Tetrahydrobiopterin	C00272	505.25	2M+Na	<0.0001	7.64	<0.0001	10.76		
L-threo-Tetrahydrobiopterin	C20264	505.25	2M+Na	<0.0001	7.64	<0.0001	10.76		
Iodine	C01382	508.60	2M+H	0.0310	2.97			<0.0001	27.68
5-(3'-Carboxy-3'-oxopropenyl)-4,6-dihydroxypicolinate	C05641	545.00	2M+K					0.0378	-2.68
Sphingosine	C00319	599.55	2M+H	<0.0001	-13.39	<0.0001	-13.39	<0.0001	-13.39
3-Dehydrosphinganine	C02934	599.55	2M+H	<0.0001	-13.39	<0.0001	-13.39	<0.0001	-13.39
Palmitoylethanolamide	C16512	599.55	2M+H	<0.0001	-13.39	<0.0001	-13.39	<0.0001	-13.39
Sphingosine	C00319	599.60	2M+H	<0.0001	21.73	0.0001	10.91	<0.0001	23.91
3-Dehydrosphinganine	C02934	599.60	2M+H	<0.0001	21.73	0.0001	10.91	<0.0001	23.91
Palmitoylethanolamide	C16512	599.60	2M+H	<0.0001	21.73	0.0001	10.91	<0.0001	23.91
Porphyrin	C05113	659.20	2M+K	0.0074	-4.35	0.0133	-3.27	0.0061	-4.56
4-(4-Deoxy-alpha-D-gluc-4-enuronosyl)-D-galacturonate	C06118	705.10	2M+H	0.0047	4.84			0.0130	-3.12
UDP-N-acetylmuramoyl-L-alanine	C01212	733.15	M+H-H2O	0.0047	4.85	<0.0001	33.16	<0.0001	19.92
1-(5'-Phosphoribosyl)-5-formamido-4-imidazolecarboxamide	C04734	733.15	2M+H	0.0047	4.85	<0.0001	33.16	<0.0001	19.92
(R)-S-Lactoylglutathione	C03451	759.20	2M+H	0.0049	4.79				
1-Octadecanoyl-2-(5Z,8Z,11Z,14Z-eicosatetraenoyl)-sn-glycero-3-phosphoethanolamine	C21480	768.55	M+H	0.0001	-10.81	0.0001	-10.81	<0.0001	-14.37
N-Oleoyl dopamine	C12272	835.70	2M+H	<0.0001	-12.96	<0.0001	-12.96	<0.0001	-16.77
4alpha-Methylzymosterol	C05103	835.70	2M+K	<0.0001	-12.96	<0.0001	-12.96	<0.0001	-16.77

MIGI = miglustat + insulin; m/z = mass-to-charge ratio

Table 5.65. Effects of MIG 48 hours post-treatment and insulin on differentiated SH-SY5Y human neuroblastoma cell line data was generated after KEGGREST analysis and FELLA enrichment of significant signals procured by MALDI-TOF MS imaging in positive mode

Module identifiers		MIGI 2.5μM	MIGI 10μM	MIGI 40μM
KEGG ID	KEGG name	p score	p score	p score
M00048	Inosine monophosphate biosynthesis, PRPP + glutamine => IMP	0.0023	0.0008	0.0003
M00094	Ceramide biosynthesis	<0.0001	<0.0001	<0.0001
M00099	Sphingosine biosynthesis	<0.0001	<0.0001	<0.0001
M00101	Cholesterol biosynthesis, squalene 2,3-epoxide	0.0001	<0.0001	<0.0001
M00102	Ergocalciferol biosynthesis, squalene 2,3-epoxide	<0.0001	<0.0001	<0.0001
M00843	L-threo-Tetrahydrobiopterin biosynthesis, GTP => L-threo-BH4	<0.0001	<0.0001	
M00043	Thyroid hormone biosynthesis, tyrosine => triiodothyronine/thyroxine	<0.0001		<0.0001
M00842	Tetrahydrobiopterin biosynthesis, GTP => BH4		0.0446	

MIGI = miglustat + insulin

5.5.5. MALDI-TOF MS total lipidome analysis of the cells treated with CBE

Treatment of the cells with 2.5 μM CBE caused a decrease in sphingolipid and ceramide biosynthesis for all the compounds listed and involved in this biosynthesis. A decrease in CMP-N-glycolylneuraminate level was observed. At 10 μM, further decrease in cholesterol biosynthesis, sphingolipid and ceramide biosynthesis were observed, but no changes in CMP-N-glycolylneuraminate level was detected. Treatment of the cells with 40 μM CBE affected ceramide and sphingosine biosynthesis and downregulated cholesterol biosynthesis, similar to previous concentrations (Table 5.66., 5.67.).

Treatment of the cells with 2.5 μM CBE and insulin downregulated the synthesis of sphingosine, ceramide, and cholesterol. Folate biosynthesis and biopterin biosynthesis was upregulated as well as the nicotinamide metabolism (Table 5.68., 5.69.). .). The treatment with 10 μM CBE and insulin affected the same pathways as the treatment with the lower concentration. At the highest CBE concentration, a threefold increase in N-Acetylneuraminate accumulation was observed compared to the control group, in addition to effects on cholesterol, sphingolipid and ceramide biosynthesis. Accumulation of iodine metabolites also occurred, which affected its metabolism (Table 5.68., 5.69.).

Table 5.66. Effects of CBE 48 hours post-treatment on metabolic compounds in differentiated SH-SY5Y human neuroblastoma cell line data was generated after KEGGREST of significant signals procured by MALDI-TOF MS imaging in positive mode

Compound identifiers				CBE 2.5μM		CBE 10μM		CBE 40μM	
Compound name	KEGG ID	m/z	adduct	p-value	t score	p-value	t score	p-value	t score
1-Octadecanoyl-sn-glycero-3-phosphoethanolamine	C21484	504.30	M+Na	0.0461	-2.37	0.0061	-3.77		
Sphingosyl-phosphocholine	C03640	504.30	M+K	0.0461	-2.37	0.0061	-3.77		
Sphingosine	C00319	599.55	2M+H	<0.0001	-9.26	<0.0001	-12.35	<0.0001	-13.07
3-Dehydrosphinganine	C02934	599.55	2M+H	<0.0001	-9.26	<0.0001	-12.35	<0.0001	-13.07
Palmitoylethanolamide	C16512	599.55	2M+H	<0.0001	-9.26	<0.0001	-12.35	<0.0001	-13.07
Sphingosine	C00319	599.60	2M+H			0.0152	3.62	0.0068	4.43
3-Dehydrosphinganine	C02934	599.60	2M+H			0.0152	3.62	0.0068	4.43
Palmitoylethanolamide	C16512	599.60	2M+H			0.0152	3.62	0.0068	4.43
CMP-N-glycoloylneuraminate	C03691	631.15	M+H	0.0437	-2.46				
N-Acetylaspartylglutamate	C12270	631.15	2M+Na	0.0437	-2.46				
Dehypoxanthine futalosine	C17010	631.15	2M+K	0.0437	-2.46				
Desulfoglucotropeolin	C01069	659.20	2M+H	0.0106	-3.35				
Porphyrin	C05113	659.20	2M+K	0.0106	-3.35	0.0074	-4.35	0.0190	-2.82
UDP-N-acetylmuramoyl-L-alanine	C01212	733.15	M+H-H2O					0.0052	4.73
1-(5'-Phosphoribosyl)-5-formamido-4-imidazolecarboxamide	C04734	733.15	2M+H					0.0052	4.73
1-Octadecanoyl-2-(5Z,8Z,11Z,14Z-eicosatetraenoyl)-sn-glycero-3-phosphoethanolamin	C21480	768.55	M+H	0.0006	7.54	0.0001	-10.81	0.0001	-10.81
N-Oleoyl dopamine	C12272	835.70	2M+H			0.0001	-6.87	<0.0001	-12.96
4alpha-Methylzymosterol	C05103	835.70	2M+K			0.0001	-6.87	<0.0001	-12.96

CBE = conduritol B epoxide; m/z = mass-to-charge ratio

Table 5.67. Effects of CBE 2.5 μM 48 hours post-treatment on differentiated SH-SY5Y human neuroblastoma cell line data was generated after KEGGREST analysis and FELLA enrichment of significant signals procured by MALDI-TOF MS imaging in positive mode

Module identifiers		CBE 2.5μM	CBE 10μM	CBE 40μM
KEGG ID	KEGG name	p score	p score	p score
M00094	Ceramide biosynthesis	<0.0001	<0.0001	<0.0001
M00099	Sphingosine biosynthesis	<0.0001	<0.0001	<0.0001
M00101	Cholesterol biosynthesis, squalene 2,3-epoxide		<0.0001	<0.0001
M00102	Ergocalciferol biosynthesis, squalene 2,3-epoxide		<0.0001	<0.0001
M00048	Inosine monophosphate biosynthesis, PRPP + glutamine => IMP			<0.0001

CBE = conduritol B epoxide

Table 5.68. Effects of CBE 48 hours post-treatment and insulin on metabolic compounds in differentiated SH-SY5Y human neuroblastoma cell line data was generated after KEGGREST of significant signals procured by MALDI-TOF MS imaging in positive mode

Compound identifiers				CBEI 2.5μM		CBEI 10μM		CBEI 40μM	
Compound name	KEGG ID	m/z	adduct	p-value	t score	p-value	t score	p-value	t score
1-Octadecanoyl-sn-glycero-3-phosphoethanolamine	C21484	504.30	M+Na	<0.0001	-7.78	0.03071	2.98	<0.0001	-14.08
Sphingosyl-phosphocholine	C03640	504.30	M+K	<0.0001	-7.78	0.03071	2.98	<0.0001	-14.08
Cholesterol	C18043	505.25	M+K	0.0017	4.56	0.00201	-5.37		
Tetrahydrobiopterin	C00272	505.25	2M+Na	0.0017	4.56	0.00201	-5.37		
L-threo-Tetrahydrobiopterin	C20264	505.25	2M+Na	0.0017	4.56	0.00201	-5.37		
Iodine	C01382	508.60	2M+H					0.0001	10.83
5-(3'-Carboxy-3'-oxopropenyl)-4,6-dihydroxypicolinate	C05641	545.00	2M+K					0.0256	-3.14
5-(3'-Carboxy-3'-oxopropenyl)-4,6-dihydroxypicolinate	C05641	545.05	2M+K					0.0104	3.99
Nicotinamide-beta-riboside	C03150	511.25	2M+H	0.0276	3.07				
Sphingosine	C00319	599.55	2M+H	<0.0001	-13.39	<0.0001	-13.39	<0.0001	-13.39
3-Dehydrosphinganine	C02934	599.55	2M+H	<0.0001	-13.39	<0.0001	-13.39	<0.0001	-13.39
Palmitoylethanolamide	C16512	599.55	2M+H	<0.0001	-13.39	<0.0001	-13.39	<0.0001	-13.39
Sphingosine	C00319	599.60	2M+H	0.0005	7.83	0.0210	3.32	0.0001	10.81
3-Dehydrosphinganine	C02934	599.60	2M+H	0.0005	7.83	0.0210	3.32	0.0001	10.81
Palmitoylethanolamide	C16512	599.60	2M+H	0.0005	7.83	0.0210	3.32	0.0001	10.81
N-Acetylneuraminate	C00270	657.15	2M+K					0.0257	3.13

Compound identifiers				CBEI 2.5μM		CBEI 10μM		CBEI 40μM	
Compound name	KEGG ID	m/z	adduct	p-value	t score	p-value	t score	p-value	t score
Porphyrin	C05113	659.20	2M+K	0.0074	-4.35	0.0165	-3.04	0.0074	-4.35
4-(4-Deoxy-alpha-D-gluc-4-enuronosyl)-D-galacturonate	C06118	705.15	2M+H			0.0352	2.86	0.0054	4.68
4-Methylthiobutyl-desulfoglucosinolate	C17248	705.15	2M+Na			0.0352	2.86	0.0054	4.68
UDP-N-acetylmuramoyl-L-alanine	C01212	733.15	M+H-H2O	0.0049	4.80	0.0056	4.63	0.0315	2.96
1-(5'-Phosphoribosyl)-5-formamido-4-imidazolecarboxamide	C04734	733.15	2M+H	0.0049	4.80	0.0056	4.63	0.0315	2.96
(R)-S-Lactoylglutathione	C03451	759.20	2M+H	0.0054	4.68			0.0044	4.92
1-Octadecanoyl-2-(5Z,8Z,11Z,14Z-eicosatetraenoyl)-sn-glycero-3-phosphoethanolamine	C21480	768.55	M+H	0.0001	-10.81	0.0001	-10.81	0.0001	-10.81
N-Oleoyl dopamine	C12272	835.70	2M+H	<0.0001	-12.96	<0.0001	-12.96	<0.0001	-12.96
4-alpha-Methylzymosterol	C05103	835.70	2M+K	<0.0001	-12.96	<0.0001	-12.96	<0.0001	-12.96

CBEI = conduritol B epoxide + insulin; m/z = mass-to-charge ratio

Table 5.69. Effects of CBE 48 hours post-treatment and insulin on differentiated SH-SY5Y human neuroblastoma cell line data was generated after KEGGREST analysis and FELLA enrichment of significant signals procured by MALDI-TOF MS imaging in positive mode

Module identifiers		CBEI 2.5μM	CBEI 10μM	CBEI 40μM
KEGG ID	KEGG name	p score	p score	p score
M00048	Inosine monophosphate biosynthesis, PRPP + glutamine => IMP	0.0009	<0.0001	0.0014
M00094	Ceramide biosynthesis	<0.0001	<0.0001	<0.0001
M00099	Sphingosine biosynthesis	<0.0001	<0.0001	<0.0001
M00101	Cholesterol biosynthesis, squalene 2,3-epoxide	<0.0001	<0.0001	<0.0001
M00102	Ergocalciferol biosynthesis, squalene 2,3-epoxide	<0.0001	<0.0001	<0.0001
M00126	Tetrahydrofolate biosynthesis, GTP => THF	0.0004	0.0242	
M00840	Tetrahydrofolate biosynthesis, mediated by ribA and trpF, GTP => THF	0.0059		
M00842	Tetrahydrobiopterin biosynthesis, GTP => BH4	0.0468	<0.0001	
M00843	L-threo-Tetrahydrobiopterin biosynthesis, GTP => L-threo-BH4	<0.0001		
M00043	Thyroid hormone biosynthesis, tyrosine => triiodothyronine/thyroxine			<0.0001

CBEI = conduritol B epoxide + insulin

5.6. Western blot protein analysis

5.6.1. Western blot analysis for P4-RR inhibitor

Treatment of the cells with P4-RR inhibitor caused changes in AKT, IGF1-Rβ, Np 65, βAPP, αSyn and pTAU protein levels. Insulin affected the levels of all epitopes tested, but the interaction of insulin treatment with inhibitor treatment was only observed for AKT, IRα, Np 65, GSK3β and αSyn (Table 5.70., Figure 5.5., Figure 5.6.).

Post hoc analysis Akt data showed a significant decrease in Akt levels when cells were treated with insulin alone. The same effect was observed with the highest and the lowest inhibitor concentrations and insulin treatment compared to the untreated control (Table 5.70, Table 5.71.).

pAkt levels increase with insulin treatment, but no significant difference was found between treatments (Table 5.70, Table 5.72.).

Post hoc analysis of IRα expression showed that insulin administration increases the receptor levels, which was observed in the groups treated with medium inhibitor concentration. The same was noticed when cells were treated with medium and low concentrations of inhibitor and insulin compared to the insulin-treated control group (Table 5.70, Table 5.73.).

Post hoc analysis of IGF1-Rβ showed a significant decrease in epitope levels when cells were treated with any concentration of inhibitor in addition to insulin, as well as in the control group. Significant increase in IGF1-Rβ level was noticed when cells were treated with the lowest concentration of inhibitor and no insulin compared to the control (Table 5.70., Table 5.74.).

P4-RR had a range of effects on the Np 65 levels. Treatment of the cells with the middle and lowest concentrations of the inhibitor caused a significant increase in Np 65 concentrations. The addition of insulin significantly reduced Np 65 levels in the control group, but treatment caused a dose-dependent increase in the same way as in the groups without insulin, with levels peaking at the lowest inhibitor concentration (Table 5.70., Table 5.75.).

Post hoc test of GSK3β levels showed that insulin significantly reduced GSK3β levels in the control group and in the high and medium inhibitor concentrations compared

to the non-insulin treated control group. The same effect was observed in the groups treated with the highest inhibitor concentration, but the opposite effect was observed at the lowest inhibitor concentration (Table 5.70., Table 5.76.).

Post hoc analysis of pGSK3β levels showed no specific significance between the groups. Post hoc analysis for βAPP showed that levels were significantly reduced by insulin treatment compared to the control group (Table 5.70., Table 5.77.).

αSyn levels are significantly increased with the highest and lowest concentrations of inhibitor compared to the control. Combined treatment with insulin significantly increased the αSyn levels in the control and all treatments compared to the untreated control group. The same effect was observed in the medium and lowest concentration of inhibitor compared to the insulin treated group (Table 5.70., Table 5.78.).

Insulin upregulated on the pTAU epitope in the control group and in all treated groups compared to the untreated control (Table 5.70., Table 5.79.).

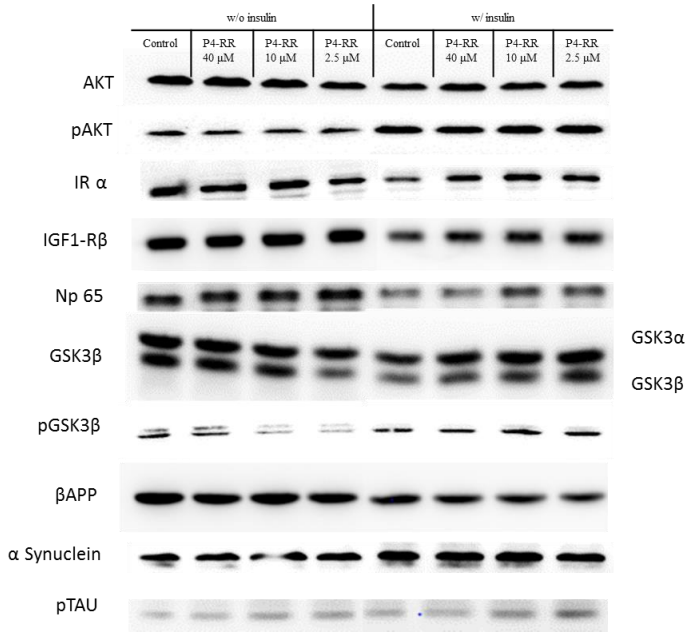

Figure 5.5 Western blots of differentiated SH-SY5Y human neuroblastoma cells treated with P4-RR a GlcCer synthesis inhibitor for 48 hours; w/o insulin = without insulin; w insulin = with insulin; P4-RR = (*R, R*) D, L-threo-phenyl-2-hexadecanoylamino-3-pyrrolidino-1-propanol; Akt = protein kinase B; pAkt = protein kinase b phosphorylated at tyrosine 473; IRα = insulin receptor alpha subunit; IGF1-Rβ = beta subunit of receptor for insulin like growth factor; NP65 = neuroplastin 65; GSK3β = glycogen synthase kinase beta; GSK3α = glycogen synthase kinase alpha; pGSK3β = glycogen synthase kinase beta phosphorylated at tyrosine 216; βAPP = beta amyloid precursor protein; αSyn = alpha synuclein; pTAU = tau protein phosphorylated at Ser202 and Thr 205.

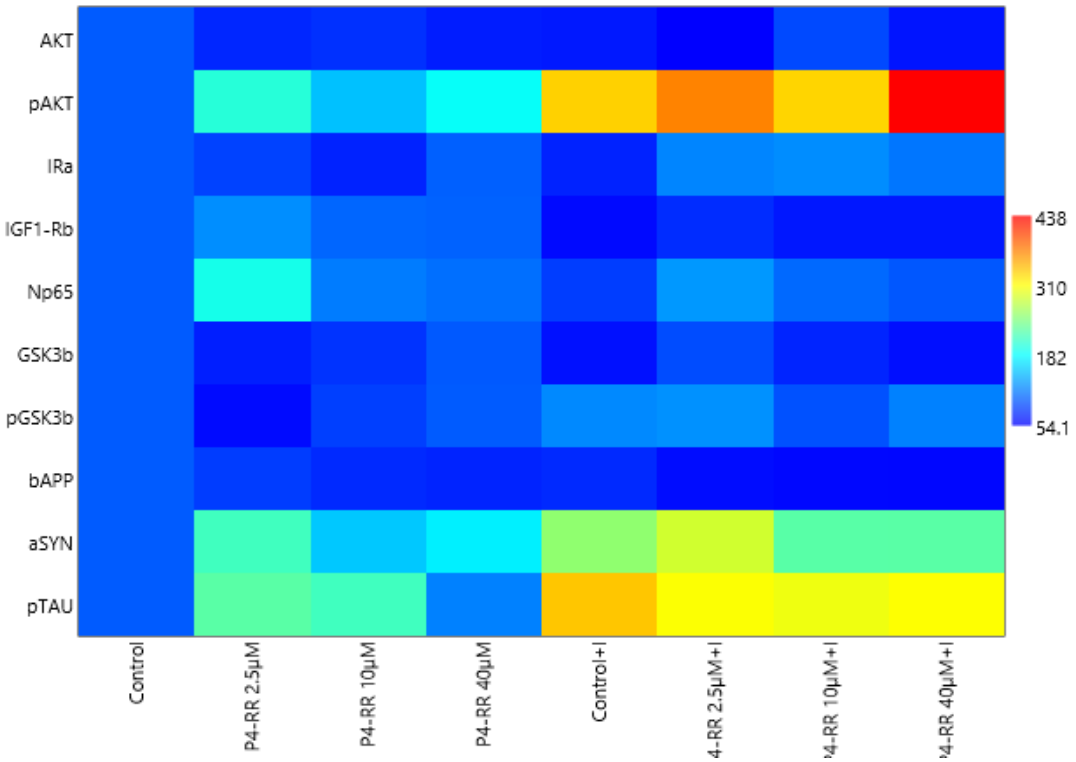

Figure 5.6. Matrix plot made from Western blots of differentiated SH-SY5Y human neuroblastoma cells treated with P4-RR a GlcCer synthesis inhibitor for 48 hours; data are presented as percentage of intensity calculated against the control group; + I = with insulin; P4-RR = (*R, R*) D, L-threo-phenyl-2-hexadecanoylamino-3-pyrrolidino-1-propanol; Akt = protein kinase B; pAkt = protein kinase b phosphorylated at tyrosine 473; IRα = insulin receptor alpha subunit; IGF1-Rβ = beta subunit of receptor for insulin like growth factor; NP65 = neuroplastin 65; GSK3β = glycogen synthase kinase beta; GSK3α = glycogen synthase kinase alpha; pGSK3β = glycogen synthase kinase beta phosphorylated at tyrosine 216; βAPP = beta amyloid precursor protein; αSyn = alpha synuclein; pTAU = tau protein phosphorylated at Ser202 and Thr 205.

Table 5.70. Protein signal intensity calculated as a percentage against the control group from Western blot for differentiated SH-SY5Y human neuroblastoma cells treated 48 hours with P4-RR, a GlcCer synthesis inhibitor.

Epitope	w/o insulin				w insulin				Two-way ANOVA					
	Control	P4-RR 2.5 µM	P4-RR 10 µM	P4-RR 40 µM	Control	P4-RR 2.5 µM	P4-RR 10 µM	P4-RR 40 µM	F values; (degrees of freedom)			p-values		
	Mean; SD	Mean; SD	Mean; SD	Mean; SD	Mean; SD	Mean; SD	Mean; SD	Mean; SD	Insulin	RR	Insulin × RR	Insulin	RR	Insulin × RR
AKT	100.00; 7.25	73.61; 3.30	78.60; 3.44	68.46; 4.03	66.18; 10.91	54.14; 4.67	90.78; 10.89	64.52; 6.88	5.09 (1,24)	4.74 (3,24)	3.94 (3,24)	0.0333	0.0097	0.0201
pAKT	100.00; 17.56	201.27; 40.76	151.06; 52.27	185.42; 47.15	332.94; 23.76	371.80; 15.92	331.04; 29.57	437.76; 43.18	66.63 (1,24)	2.82 (3,24)	0.60 (3,24)	<0.0001	0.0599	0.6168
IRα	100.00; 7.52	87.29; 5.92	71.28; 15.13	102.20; 6.78	71.54; 5.16	120.85; 10.33	124.68; 11.05	113.15; 12.22	6.21 (1,24)	1.89 (3,24)	6.43 (3,24)	0.0199	0.1575	0.0023
IGF1-Rβ	100.00; 2.32	125.30; 6.62	105.3; 6.13	103.50; 3.68	58.67; 4.49	76.32; 3.54	66.08; 2.43	65.97; 2.70	188.95 (1,24)	7.86 (3,24)	0.71 (3,24)	<0.0001	0.0007	0.5518
Np65	100.00; 2.26	192.70; 1.79	116.4; 2.61	109.90; 1.96	84.75; 2.84	130.30; 3.76	106.60; 1.88	97.67; 3.29	179.52 (1,24)	268.38 (3,24)	45.34 (3,24)	<0.0001	<0.0001	<0.0001
GSK3β	100.00; 0.98	69.40; 1.56	80.04; 1.74	98.89; 2.34	62.60; 5.22	92.27; 2.48	72.60; 3.52	61.45; 9.83	22.876 (1,24)	0.53 (3,24)	21.58 (3,24)	0.0002	0.6643	<0.0001
pGSK3β	100.00; 14.97	59.48; 5.82	85.69; 14.19	100.00; 15.31	122.90; 8.87	126.70; 11.67	94.82; 20.46	118.90; 18.35	8.39 (1,24)	1.14 (3,24)	1.60 (3,24)	0.0078	0.3493	0.2154
βAPP	100.00; 5.02	84.34; 7.38	74.69; 3.20	71.75; 0.83	74.67; 9.19	60.40; 7.05	57.75; 7.81	57.52; 6.11	20.01 (1,24)	5.29 (3,24)	0.35 (3,24)	0.0031	0.0099	0.7846
αSyn	100.00; 7.83	214.3; 16.42	154.10; 17.27	174.40; 13.43	254.30; 22.53	286.00; 17.58	226.00; 9.00	226.8; 11.71	66.51 (1,24)	8.84 (3,24)	4.48 (3,24)	<0.0001	0.0003	0.0123
pTAU	100.00; 14.01	226.80; 42.43	214.30; 59.98	118.60; 21.63	338.60; 62.26	308.00; 38.26	301.80; 70.05	309.00; 51.94	28.05 (1,24)	0.91 (3,24)	1.89 (3,24)	<0.0001	0.4545	0.1706

w/o insulin = without insulin; w insulin = with insulin; P4-RR = (*R, R*) D, L-threo-phenyl-2-hexadecanoylamino-3-pyrrolidino-1-propanol; Akt = protein kinase B; pAkt = protein kinase b phosphorylated at tyrosine 473; IRα = insulin receptor alpha subunit; IGF1-Rβ = beta subunit of receptor for insulin like growth factor; NP65 = neuroplastin 65; GSK3β = glycogen synthase kinase beta; GSK3α = glycogen synthase kinase alpha; pGSK3β = glycogen synthase kinase beta phosphorliated at tyrosine 216; βAPP = beta amyloid precursor protein; αSyn = alpha synuclein; pTAU = tau protein phosphorylated at Ser202 and Thr 205.

Table 5.71. Post hoc Tukey HSD test of two-way ANOVA results for Western blot against AKT epitope on differentiated SH-SY5Y human neuroblastoma cells treated 48 hours with P4-RR, a GlcCer synthesis inhibitor. Data are presented as a percentage calculated against the control group. Statistical significance was tested with two-way ANOVA.

The first set of variables (A)		The second set of variables (B)		Post hoc Tukey HSD p-value A vs B
Insulin treatment	The concentration of P4 - RR	Insulin treatment	The concentration of P4 - RR	
w/o insulin	Control	w insulin	Control	0.0423
w/o insulin	Control	w insulin	P4-RR 40 μM	0.0293
w/o insulin	Control	w insulin	P4-RR 2.5 μM	0.0026

w/o insulin = without insulin; w insulin = with insulin; P4-RR = (*R*, *R*) D, L-threo-phenyl-2-hexadecanoylamino-3-pyrrolidino-1-propanol.

Table 5.72. Post hoc Tukey HSD test of two-way ANOVA results for Western blot against pAkt epitope on differentiated SH-SY5Y human neuroblastoma cells treated 48 hours with P4-RR, a GlcCer synthesis inhibitor. Data are presented as a percentage calculated against the control group.

The first set of variables (A)		The second set of variables (B)		Post hoc Tukey HSD p-value A vs B
Insulin treatment	The concentration of P4 - RR	Insulin treatment	The concentration of P4 - RR	
w/o insulin	Control	w insulin	Control	0.0028
w/o insulin	P4-RR 40 μM	w insulin	P4-RR 40 μM	0.0012
w/o insulin	P4-RR 10 μM	w insulin	P4-RR 10 μM	0.0320
w/o insulin	P4-RR 2.5 μM	w insulin	P4-RR 2.5 μM	0.0480

w/o insulin = without insulin; w insulin = with insulin; P4-RR = (*R*, *R*) D, L-threo-phenyl-2-hexadecanoylamino-3-pyrrolidino-1-propanol

Table 5.73. Post hoc Tukey HSD test of two-way ANOVA results for Western blot against IRα epitope on differentiated SH-SY5Y human neuroblastoma cells treated 48 hours with P4-RR a GlcCer synthesis inhibitor. Data are presented as a percentage calculated against the control group. Statistical significance was tested with two-way ANOVA.

The first set of variables (A)		The second set of variables (B)		Post hoc Tukey HSD p-value A vs B
Insulin treatment	The concentration of P4 - RR	Insulin treatment	The concentration of P4 - RR	
w/o insulin	P4-RR 10 μM	w insulin	P4-RR 10 μM	0.0151
w insulin	Control	w insulin	P4-RR 10 μM	0.0158
w insulin	Control	w insulin	P4-RR 2.5 μM	0.0296

w/o insulin = without insulin; w insulin = with insulin; P4-RR = (*R*, *R*) D, L-threo-phenyl-2-hexadecanoylamino-3-pyrrolidino-1-propanol.

Table 5.74. Post hoc Tukey HSD test of two-way ANOVA results for Western blot against IGF1-Rβ epitope on differentiated SH-SY5Y human neuroblastoma cells treated 48 hours with P4-RR, a GlcCer synthesis inhibitor. Data are presented as a percentage calculated against the control group.

Expression of IGF1-Rβ				
The first set of variables (A)		The second set of variables (B)		Post hoc Tukey HSD p-value A vs B
Insulin treatment	The concentration of P4 - RR	Insulin treatment	The concentration of P4 - RR	
w/o insulin	Control	w/o insulin	P4-RR 2.5 μM	0.0328
w/o insulin	Control	w insulin	Control	0.0001
w/o insulin	P4-RR 40 μM	w insulin	P4-RR 40 μM	0.0002
w/o insulin	P4-RR 10 μM	w insulin	P4-RR 10 μM	0.0001
w/o insulin	P4-RR 2.5 μM	w insulin	P4-RR 2.5 μM	0.0001

w/o insulin = without insulin; w insulin=with insulin; P4-RR = (*R*, *R*) D, L-threo-phenyl-2-hexadecanoylamino-3-pyrrolidino-1-propanol.

Table 5.75. Post hoc Tukey HSD test of two-way ANOVA results for Western blot against NP65 epitope on differentiated SH-SY5Y human neuroblastoma cells treated 48 hours with P4-RR, a GlcCer synthesis inhibitor. Data are presented as a percentage calculated against the control group. Statistical significance was tested with two-way ANOVA.

The first set of variables (A)		The second set of variables (B)		Post hoc Tukey HSD p-value A vs B
Insulin treatment	The concentration of P4 - RR	Insulin treatment	The concentration of P4 - RR	
w/o insulin	Control	w/o insulin	P4-RR 10 μM	0.0039
w/o insulin	Control	w/o insulin	P4-RR 2.5 μM	0.0001
w/o insulin	P4-RR 40 μM	w/o insulin	P4-RR 2.5 μM	0.0001
w/o insulin	P4-RR 10 μM	w/o insulin	P4-RR 2.5 μM	0.0001
w/o insulin	Control	w insulin	Control	0.0084
w/o insulin	Control	w insulin	P4-RR 2.5 μM	0.0001
w/o insulin	P4-RR 40 μM	w insulin	Control	0.0001
w/o insulin	P4-RR 40 μM	w insulin	P4-RR 2.5 μM	0.0004
w/o insulin	P4-RR 10 μM	w insulin	Control	0.0001
w/o insulin	P4-RR 10 μM	w insulin	P4-RR 40 μM	0.0009
w/o insulin	P4-RR 10 μM	w insulin	P4-RR 2.5 μM	0.0203
w/o insulin	P4-RR 2.5 μM	w insulin	Control	0.0001
w/o insulin	P4-RR 2.5 μM	w insulin	P4-RR 40 μM	0.0001
w/o insulin	P4-RR 2.5 μM	w insulin	P4-RR 10 μM	0.0001
w/o insulin	P4-RR 2.5 μM	w insulin	P4-RR 2.5 μM	0.0001
w insulin	Control	w insulin	P4-RR 40 μM	0.0355
w insulin	Control	w insulin	P4-RR 10 μM	0.0002
w insulin	Control	w insulin	P4-RR 2.5 μM	0.0001
w insulin	P4-RR 40 μM	w insulin	P4-RR 2.5 μM	0.0001
w insulin	P4-RR 10 μM	w insulin	P4-RR 2.5 μM	0.0001

w/o insulin = without insulin; w insulin = with insulin; P4-RR = (*R*, *R*) D, L-threo-phenyl-2-hexadecanoylamino-3-pyrrolidino-1-propanol

Table 5.76. Post hoc Tukey HSD test of two-way ANOVA results for Western blot against GSK3β epitope on differentiated SH-SY5Y human neuroblastoma cells treated 48 hours with P4-RR, a GlcCer synthesis inhibitor. Data are presented as a percentage calculated against the control group.

The first set of variables (A)		The second set of variables (B)		Post hoc Tukey HSD p-value A vs B
Insulin treatment	The concentration of P4 - RR	Insulin treatment	The concentration of P4 - RR	
w/o insulin	Control	w insulin	Control	0.0005
w/o insulin	Control	w insulin	P4-RR 40 μM	0.0004
w/o insulin	Control	w insulin	P4-RR 10 μM	0.0080
w/o insulin	P4-RR 40 μM	w insulin	P4-RR 40 μM	0.0005
w/o insulin	P4-RR 2.5 μM	w insulin	P4-RR 2.5 μM	0.0329

w/o insulin = without insulin; w insulin = with insulin; P4-RR = (*R*, *R*) D, L-threo-phenyl-2-hexadecanoylamino-3-pyrrolidino-1-propanol.

Table 5.77. Post hoc Tukey HSD test of two-way ANOVA results for Western blot against βAPP epitope on differentiated SH-SY5Y human neuroblastoma cells treated 48 hours with P4-RR, a GlcCer synthesis inhibitor. Data are presented as a percentage calculated against the control group.

The first set of variables (A)		The second set of variables (B)		Post hoc Tukey HSD p-value A vs B
Insulin treatment	The concentration of P4 - RR	Insulin treatment	The concentration of P4 – RR	
w/o insulin	Control	w insulin	P4-RR 40 μM	0.0044
w/o insulin	Control	w insulin	P4-RR 10 μM	0.0046
w/o insulin	Control	w insulin	P4-RR 2.5 μM	0.0082

w/o insulin = without insulin; w insulin = with insulin; P4-RR = (*R*, *R*) D, L-threo-phenyl-2-hexadecanoylamino-3-pyrrolidino-1-propanol.

Table 5.78. Post hoc Tukey HSD test of two-way ANOVA results for Western blot against αSyn epitope on differentiated SH-SY5Y human neuroblastoma cells treated 48 hours with P4-RR, a GlcCer synthesis inhibitor. Data are presented as a percentage calculated against the control group.

The first set of variables (A)		The second set of variables (B)		Post hoc Tukey HSD p-value A vs B
Insulin treatment	The concentration of P4 – RR	Insulin treatment	The concentration of P4 – RR	
w/o insulin	Control	w/o insulin	P4-RR 40 μM	0.0356
w/o insulin	Control	w/o insulin	P4-RR 2.5 μM	0.0005
w/o insulin	Control	w insulin	Control	0.0001
w/o insulin	Control	w insulin	P4-RR 40 μM	0.0002
w/o insulin	Control	w insulin	P4-RR 10 μM	0.0002
w/o insulin	Control	w insulin	P4-RR 2.5 μM	0.0001
w/o insulin	P4-RR 40 μM	w insulin	Control	0.0201
w/o insulin	P4-RR 40 μM	w insulin	P4-RR 2.5 μM	0.0006

The first set of variables (A)		The second set of variables (B)		Post hoc Tukey HSD p-value A vs B
Insulin treatment	The concentration of P4 – RR	Insulin treatment	The concentration of P4 – RR	
w/o insulin	P4-RR 10 µM	w insulin	Control	0.0022
w/o insulin	P4-RR 10 µM	w insulin	P4-RR 40 µM	0.0428
w/o insulin	P4-RR 10 µM	w insulin	P4-RR 10 µM	0.0466
w/o insulin	P4-RR 10 µM	w insulin	P4-RR 2.5 µM	0.0001
w/o insulin	P4-RR 2.5 µM	w insulin	P4-RR 2.5 µM	0.0473

w/o insulin = without insulin; w insulin = with insulin; P4-RR = (*R, R*) D, L-threo-phenyl-2-hexadecanoylamino-3-pyrrolidino-1-propanol.

Table 5.79. Post hoc Tukey HSD test of two-way ANOVA results for Western blot against pTAU epitope on differentiated SH-SY5Y human neuroblastoma cells treated 48 hours with P4-RR, a GlcCer synthesis inhibitor. Data are presented as a percentage calculated against the control group.

The first set of variables (A)		The second set of variables (B)		Post hoc Tukey HSD p-value A vs B
Insulin treatment	The concentration of P4 - RR	Insulin treatment	The concentration of P4 – RR	
w/o insulin	Control	w insulin	Control	0.0115
w/o insulin	Control	w insulin	P4-RR 40 µM	0.0316
w/o insulin	Control	w insulin	P4-RR 10 µM	0.0403
w/o insulin	Control	w insulin	P4-RR 2.5 µM	0.0327

w/o insulin = without insulin; w insulin = with insulin; P4-RR = (*R, R*) D, L-threo-phenyl-2-hexadecanoylamino-3-pyrrolidino-1-propanol

5.6.2. Western blot analysis for P4-SS inhibitor

Treatment of the cells with P4-SS inhibitor caused significant changes in levels of pAKT, IRα, IGF1-Rβ, Np 65, βAPP and αSyn. Insulin treatment affected levels of almost all molecules tested except AKT, IRα and βAPP. The interaction between the inhibitor treatments and insulin was observed for all molecules except pAkt (Table 5.80., Figure 5.7., Figure 5.8.).

Post hoc analysis showed only one significant effect of insulin in cells treated with medium concentration of inhibitor, where application of insulin increased IRα levels (Table 5.80., Table 5.81.)

pAKT levels were significantly increased in all three concentrations of inhibitor and insulin treated groups compared to untreated controls. Also when the control was treated with insulin, there was a significant threefold increase in pAKT level. Only one significant effect of inhibitor treatment was observed at the 10µM concentration, which increased pAkt levels compared to the control group (Table 5.80. Table 5.82.).

Post hoc analysis of pAkt levels showed no specific significance between the groups.

Post hoc analysis of IRα levels showed a difference between the control group and the groups treated with the highest or lowest concentrations of inhibitor only in the insulin treated groups, where there was an increase in IRα levels (Table 5.80. Table 5.83.).

Treatment of the cells with P4-SS reduced IGF1-Rβ levels, which was most pronounced at medium and low inhibitor concentrations compared to the control group. There was also a significant difference between the high and low concentration groups, with the latter group having less IGF1-Rβ. Although application of insulin significantly increased the receptor level in the inhibitor treated cells compared to the insulin-treated control group, it was still lower than in the untreated control group. The same pattern was observed in the high concentration inhibitor-treated group, where IGF1-Rβ levels were significantly higher than in the all insulin-treated groups (Table 5.80. Table 5.84.).

Treatment with high and medium concentrations of P4-SS caused a significant increase in Np 65 levels, while low concentration caused a significant decrease compared to the control group. There was a noticeable difference between treatments, with the medium concentration causing a threefold increase in Np65 level compared to the low concentration. Inhibitor treatments at all concentrations in combinations with insulin increased Np65 levels in contrast to samples treated with insulin alone. The decrease in Np65 levels was significant in all insulin-treated groups and only for the medium concentration of inhibitor (Table 5.80. Table 5.85.).

The use of insulin caused a significant reduction in GSK3β levels in the control groups. An opposite effect was observed between the insulin-treated and untreated groups, where application of insulin significantly increased GSK3β levels. The same observation was made when the insulin-treated control groups were compared with the groups treated with both insulin and inhibitor (Table 5.80. Table 5.86.).

Post hoc analysis of the pGSK3β data showed a significant increase in pGSK3β levels only in cells treated with insulin and high or low concentrations of inhibitor (Table 5.80. Table 5.87.).

There was only one significant difference for βAPP, where the medium inhibitor concentration significantly reduced the epitope level (Table 5.80. Table 5.88.).

Treatment with the P4-SS inhibitor caused a significant increase in αSyn levels compared to the control group and independent of concentration. The same was true for

insulin itself in the insulin-treated control group and in the combined inhibitor and insulin-treated groups, regardless of concentration compared to the untreated control group. At high an medium concentrations, αSyn levels were significantly lower than in the insulin-treated samples. Medium concentration of inhibitor and insulin treatment caused a significant increase in epitope levels compared to the insulin-treated control group or the low concentration inhibitor group (Table 5.80. Table 5.89.).

There was a significant threefold increase in pTAU levels when insulin was applied, but no other significant observations were found (Table 5.80. Table 5.90.).

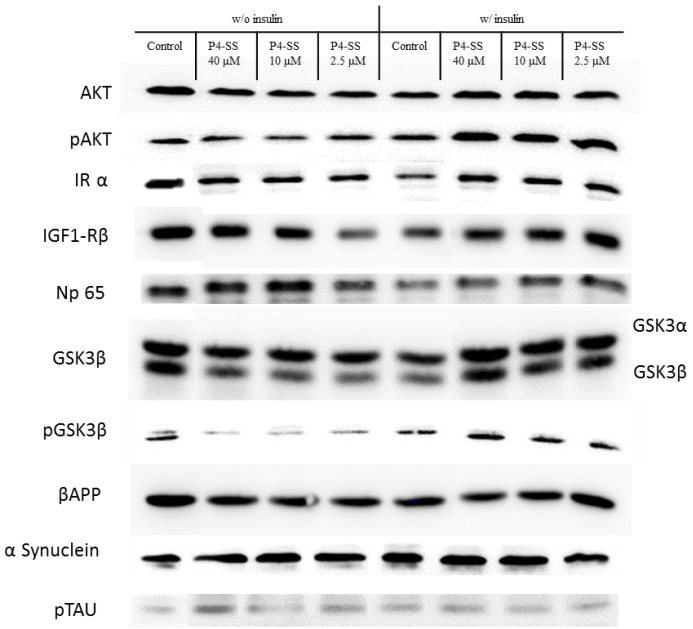

Figure 5.7. Western blots of differentiated SH-SY5Y human neuroblastoma cells treated with P4-SS a GlcCer synthesis inhibitor for 48 hours; w/o insulin = without insulin; w insulin = with insulin; P4-SS=(*S, S*) D, L-threo-phenyl-2-hexadecanoylamino-3-pyrrolidino-1-propanol; Akt = protein kinase B; pAkt = protein kinase b phosphorylated at tyrosine 473; IRα = insulin receptor alpha subunit; IGF1-Rβ = beta subunit of receptor for insulin like growth factor; NP65 = neuroplastin 65; GSK3β = glycogen synthase kinase beta; GSK3α = glycogen synthase kinase alpha; pGSK3β = glycogen synthase kinase beta phosphorylated at tyrosine 216; βAPP = beta amyloid precursor protein; αSyn = alpha synuclein; pTAU = tau protein phosphorylated at Ser202 and Thr 205.

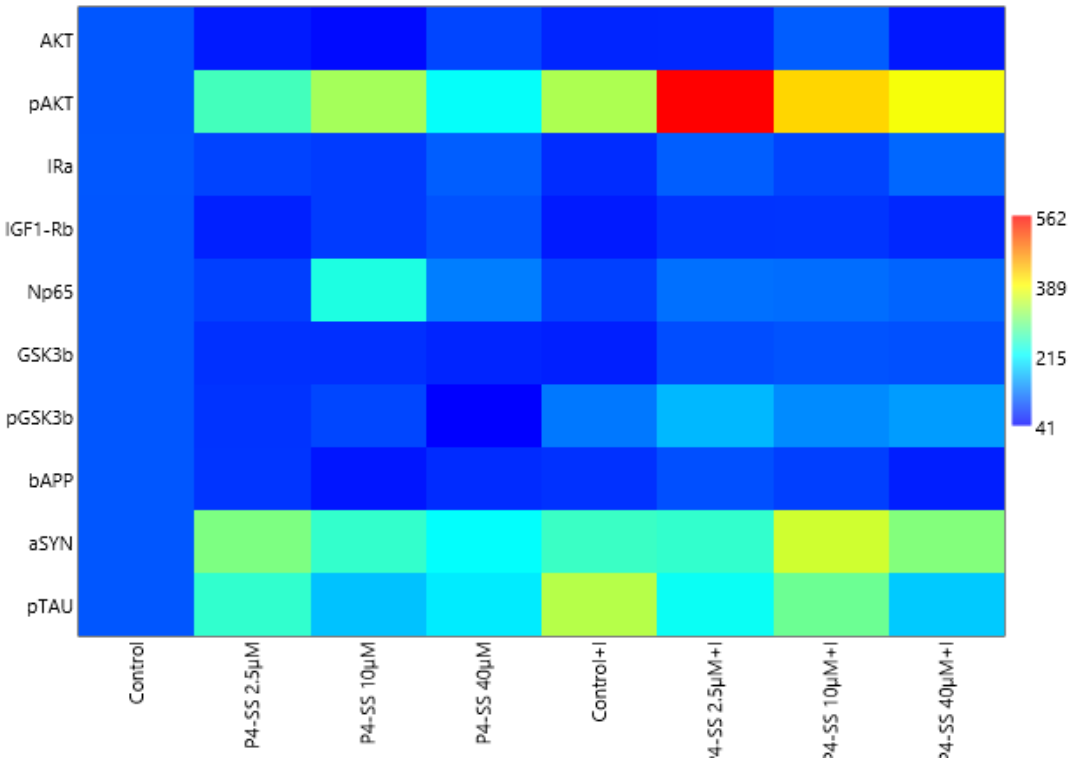

Figure 5.8. Matrix plot made from Western blots of differentiated SH-SY5Y human neuroblastoma cells treated with P4-SS a GlcCer synthesis inhibitor for 48 hours; data are presented as percentage of intensity calculated against the control group; + I = with insulin; P4-SS=(*S, S*) D, L-threo-phenyl-2-hexadecanoylamino-3-pyrrolidino-1-propanol; Akt = protein kinase B; pAkt = protein kinase b phosphorylated at tyrosine 473; IRα = insulin receptor alpha subunit; IGF1-Rβ = beta subunit of receptor for insulin like growth factor; NP65 = neuroplastin 65; GSK3β = glycogen synthase kinase beta; GSK3α = glycogen synthase kinase alpha; pGSK3β = glycogen synthase kinase beta phosphorylated at tyrosine 216; βAPP = beta amyloid precursor protein; αSyn = alpha synuclein; pTAU = tau protein phosphorylated at Ser202 and Thr 205.

Table 5.80. Protein signal intensity calculated as a percentage against the control group from Western blot for differentiated SH-SY5Y human neuroblastoma cells treated 48 hours with P4-SS, a GlcCer synthesis inhibitor.

Epitope	w/o insulin				w/ insulin				Two-way ANOVA					
	Control	P4-SS 2.5 µM	P4-SS 10 µM	P4-SS 40 µM	Control	P4-SS 2.5 µM	P4-SS 10 µM	P4-SS 40 µM	F values; (degrees of freedom)			p-values		
	Mean; SD	Mean; SD	Mean; SD	Mean; SD	Mean; SD	Mean; SD	Mean; SD	Mean; SD	Insulin	SS	Insulin × SS	Insulin	SS	Insulin × SS
AKT	100.00; 7.25	59.06; 6.92	48.42; 5.38	88.29; 10.64	66.18; 10.91	67.24; 6.59	104.17; 8.66	56.97; 4.99	0.00 (1,24)	2.18 (3,24)	13.99 (3,24)	0.9574	0.1155	<0.0001
pAKT	100.00; 17.56	260.68; 32.82	327.15; 34.58	218.65; 45.45	332.94; 23.76	562.43; 71.08	416.99; 30.30	382.35; 8.49	55.20 (1,24)	10.46 (3,24)	2.944 (3,24)	<0.0001	0.0001	0.0533
IRα	100.00; 7.52	87.02; 6.32	81.24; 5.08	105.19; 7.31	71.54; 5.16	105.00; 5.47	87.57; 6.69	111.43; 9.05	0.01 (1,24)	5.44 (3,24)	4.55 (3,24)	0.9221	0.0053	0.0116
IGF1-Rβ	100.00; 2.32	63.29; 6.65	81.16; 5.07	96.93; 0.47	58.67; 4.49	76.07; 3.75	76.98; 2.85	67.48; 2.68	32.43 (1,24)	3.91 (3,24)	19.84 (3,24)	<0.0001	0.0209	<0.0001
Np65	100.00; 2.26	84.00; 1.96	234.56; 8.51	126.79; 3.68	84.75; 2.84	117.20; 1.48	115.10; 2.60	109.19; 1.22	125.13 (1,24)	194.83 (3,24)	145.47 (3,24)	<0.0001	<0.0001	<0.0001
GSK3β	100.00; 0.98	74.18; 2.93	73.06; 2.29	65.90; 2.26	62.60; 5.22	93.76; 2.89	97.48; 1.85	95.47; 2.43	20.20 (1,24)	1.16 (3,24)	60.20 (3,24)	0.0003	0.3533	<0.0001
pGSK3β	100.00; 14.97	75.68; 3.71	88.93; 12.16	40.99; 5.76	122.92; 8.87	166.58; 15.78	135.68; 8.35	146.98; 14.68	68.86 (1,24)	2.00 (3,24)	5.74 (3,24)	<0.0001	0.1403	0.0041
βAPP	100.00; 5.02	76.45; 8.01	55.44; 3.32	70.48; 4.83	74.67; 9.19	95.05; 13.21	83.94; 9.48	61.84; 7.87	0.32 (1,24)	3.53 (3,24)	4.56 (3,24)	0.5778	0.0390	0.0170
αSyn	100.00; 7.83	299.78; 22.41	249.59; 20.42	216.75; 15.76	254.35; 22.53	249.37; 4.03	355.78; 10.92	303.91; 27.56	33.59 (1,24)	17.70 (3,24)	11.72 (3,24)	<0.0001	<0.0001	<0.0001
pTAU	100.00; 14.01	248.44; 25.63	172.85; 23.77	201.47; 32.50	338.67; 62.26	221.79; 26.25	288.66; 48.34	178.20; 24.60	13.80 (1,24)	0.99 (3,24)	9.61 (3,24)	0.0018	0.4222	0.0007

w/o insulin = without insulin; w insulin = with insulin; P4-SS = (*S, S*) D, L-threo-phenyl-2-hexadecanoylamino-3-pyrrolidino-1-propanol; Akt = protein kinase B; pAkt = protein kinase b phosphorylated at tyrosine 473; IRα = insulin receptor alpha subunit; IGF1-Rβ = beta subunit of receptor for insulin like growth factor; NP65 = neuroplastin 65; GSK3β = glycogen synthase kinase beta; GSK3α = glycogen synthase kinase alpha; pGSK3β = glycogen synthase kinase beta phosphorylated at tyrosine 216; βAPP = beta amyloid precursor protein; αSyn = alpha synuclein; pTAU = tau protein phosphorylated at Ser202 and Thr 205.

Table 5.81. Post hoc Tukey HSD test of two-way ANOVA results for Western blot against Akt epitope on differentiated SH-SY5Y human neuroblastoma cells treated 48 hours with P4-SS, a GlcCer synthesis inhibitor. Data are presented as a percentage calculated against the control group.

The first set of variables (A)		The second set of variables (B)		Post hoc Tukey HSD p-value A vs B
Insulin treatment	The concentration of P4 - SS	Insulin treatment	The concentration of P4 - SS	
w/o insulin	P4-SS 10 μM	w insulin	P4-SS 10 μM	0.0011

w/o insulin = without insulin; w insulin = with insulin; P4-SS = (*S, S*) D, L-threo-phenyl-2-hexadecanoylamino-3-pyrrolidino-1-propanol.

Table 5.82. Post hoc Tukey HSD test of two-way ANOVA results for Western blot against pAkt epitope on differentiated SH-SY5Y human neuroblastoma cells treated 48 hours with P4-SS, a GlcCer synthesis inhibitor. Data are presented as a percentage calculated against the control group.

The first set of variables (A)		The second set of variables (B)		Post hoc Tukey HSD p-value A vs B
Insulin treatment	The concentration of P4 - SS	Insulin treatment	The concentration of P4 - SS	
w/o insulin	Control	w/o insulin	P4-SS 10 μM	0.0054
w/o insulin	Control	w insulin	Control	0.0041
w/o insulin	Control	w insulin	P4-SS 40 μM	0.0005
w/o insulin	Control	w insulin	P4-SS 10 μM	0.0002
w/o insulin	Control	w insulin	P4-SS 2.5 μM	0.0001

w/o insulin = without insulin; w insulin = with insulin; P4-SS = (*S, S*) D, L-threo-phenyl-2-hexadecanoylamino-3-pyrrolidino-1-propanol.

Table 5.83. Post hoc Tukey HSD test of two-way ANOVA results for Western blot against IRα epitope on differentiated SH-SY5Y human neuroblastoma cells treated 48 hours with P4-SS, a GlcCer synthesis inhibitor. Data are presented as a percentage calculated against the control group.

The first set of variables (A)		The second set of variables (B)		Post hoc Tukey HSD p-value A vs B
Insulin treatment	The concentration of P4 - SS	Insulin treatment	The concentration of P4 – SS	
w/o insulin	P4-SS 40 μM	w insulin	Control	0.0295
w insulin	Control	w insulin	P4-SS 40 μM	0.0064
w insulin	Control	w insulin	P4-SS 2.5 μM	0.0308

w/o insulin = without insulin; w insulin = with insulin; P4-SS = (*S, S*) D, L-threo-phenyl-2-hexadecanoylamino-3-pyrrolidino-1-propanol.

Table 5.84. Post hoc Tukey HSD test of two-way ANOVA results for Western blot against IGF1-Rβ epitope on differentiated SH-SY5Y human neuroblastoma cells treated 48 hours with P4-SS, a GlcCer synthesis inhibitor. Data are presented as a percentage calculated against the control group.

The first set of variables (A)		The second set of variables (B)		Post hoc Tukey HSD p-value A vs B
Insulin treatment	The concentration of P4 - SS	Insulin treatment	The concentration of P4 - SS	
w/o insulin	Control	w/o insulin	P4-SS 10 µM	0.0138
w/o insulin	Control	w/o insulin	P4-SS 2.5 µM	0.0001
w/o insulin	Control	w insulin	Control	0.0001
w/o insulin	Control	w insulin	P4-SS 40 µM	0.0001
w/o insulin	Control	w insulin	P4-SS 10 µM	0.0025
w/o insulin	Control	w insulin	P4-SS 2.5 µM	0.0017
w/o insulin	P4-SS 40 µM	w/o insulin	P4-SS 2.5 µM	0.0002
w/o insulin	P4-SS 40 µM	w insulin	Control	0.0001
w/o insulin	P4-SS 40 µM	w insulin	P4-SS 40 µM	0.0008
w/o insulin	P4-SS 40 µM	w insulin	P4-SS 10 µM	0.0366
w/o insulin	P4-SS 40 µM	w insulin	P4-SS 2.5 µM	0.0258
w/o insulin	P4-SS 10 µM	w insulin	Control	0.0134

w/o insulin = without insulin; w insulin = with insulin; P4-SS = (*S, S*) D, L-threo-phenyl-2-hexadecanoylamino-3-pyrrolidino-1-propanol.

Table 5.85. Post hoc Tukey HSD test of two-way ANOVA results for Western blot against NP65 epitope on differentiated SH-SY5Y human neuroblastoma cells treated 48 hours with P4-SS, a GlcCer synthesis inhibitor. Data are presented as a percentage calculated against the control group.

The first set of variables (A)		The second set of variables (B)		Post hoc Tukey HSD p-value A vs B
Insulin treatment	The concentration of P4 - SS	Insulin treatment	The concentration of P4 - SS	
w/o insulin	Control	w/o insulin	P4-SS 40 µM	0.0009
w/o insulin	Control	w/o insulin	P4-SS 10 µM	0.0001
w/o insulin	Control	w/o insulin	P4-SS 2.5 µM	0.0001
w/o insulin	Control	w insulin	Control	0.0001
w/o insulin	P4-SS 10 µM	w/o insulin	P4-SS 2.5 µM	0.0001
w/o insulin	P4-SS 10 µM	w insulin	Control	0.0001
w/o insulin	P4-SS 10 µM	w insulin	P4-SS 40 µM	0.0001
w/o insulin	P4-SS 10 µM	w insulin	P4-SS 10 µM	0.0001
w/o insulin	P4-SS 10 µM	w insulin	P4-SS 2.5 µM	0.0001
w/o insulin	P4-SS 2.5 µM	w insulin	P4-SS 40 µM	0.0019
w/o insulin	P4-SS 2.5 µM	w insulin	P4-SS 10 µM	0.0002
w/o insulin	P4-SS 2.5 µM	w insulin	P4-SS 2.5 µM	0.0001
w insulin	Control	w insulin	P4-SS 40 µM	0.0026
w insulin	Control	w insulin	P4-SS 10 µM	0.0002
w insulin	Control	w insulin	P4-SS 2.5 µM	0.0001

w/o insulin = without insulin; w insulin = with insulin; P4-SS = (*S, S*) D, L-threo-phenyl-2-hexadecanoylamino-3-pyrrolidino-1-propanol.

Table 5.86. Post hoc Tukey HSD test of two-way ANOVA results for Western blot against GSK3β epitope on differentiated SH-SY5Y human neuroblastoma cells treated 48 hours with P4-SS, a GlcCer synthesis inhibitor. Data are presented as a percentage calculated against the control group.

The first set of variables (A)		The second set of variables (B)		Post hoc Tukey HSD p-value A vs B
Insulin treatment	The concentration of P4 - SS	Insulin treatment	The concentration of P4 – SS	
w/o insulin	Control	w insulin	Control	0.0001
w/o insulin	P4-SS 40 µM	w insulin	P4-SS 40 µM	0.0001
w/o insulin	P4-SS 10 µM	w insulin	P4-SS 10 µM	0.0004
w/o insulin	P4-SS 10 µM	w insulin	P4-SS 2.5 µM	0.0020
w/o insulin	P4-SS 2.5 µM	w insulin	P4-SS 2.5 µM	0.0034
w insulin	Control	w insulin	P4-SS 40 µM	0.0001
w insulin	Control	w insulin	P4-SS 10 µM	0.0001
w insulin	Control	w insulin	P4-SS 2.5 µM	0.0001

w/o insulin = without insulin; w insulin = with insulin; P4-SS = (*S, S*) D, L-threo-phenyl-2-hexadecanoylamino-3-pyrrolidino-1-propanol.

Table 5.87. Post hoc Tukey HSD test of two-way ANOVA results for Western blot against pGSK3β epitope on differentiated SH-SY5Y human neuroblastoma cells treated 48 hours with P4-SS, a GlcCer synthesis inhibitor. Data are presented as a percentage calculated against the control group.

The first set of variables (A)		The second set of variables (B)		Post hoc Tukey HSD p-value A vs B
Insulin treatment	The concentration of P4 - SS	Insulin treatment	The concentration of P4 – SS	
w/o insulin	P4-SS 40 µM	w insulin	P4-SS 40 µM	0.0001
w/o insulin	P4-SS 2.5 µM	w insulin	P4-SS 2.5 µM	0.0003

w/o insulin = without insulin; w insulin = with insulin; P4-SS = (*S, S*) D, L-threo-phenyl-2-hexadecanoylamino-3-pyrrolidino-1-propanol.

Table 5.88. Post hoc Tukey HSD test of two-way ANOVA results for Western blot against βAPP epitope on differentiated SH-SY5Y human neuroblastoma cells treated 48 hours with P4-SS, a GlcCer synthesis inhibitor. Data are presented as a percentage calculated against the control group.

The first set of variables (A)		The second set of variables (B)		Post hoc Tukey HSD p-value A vs B
Insulin treatment	The concentration of P4 - SS	Insulin treatment	The concentration of P4 – SS	
w/o insulin	Control	w/o insulin	P4-SS 10 µM	0.0237

w/o insulin = without insulin; w insulin = with insulin; P4-SS = (*S, S*) D, L-threo-phenyl-2-hexadecanoylamino-3-pyrrolidino-1-propanol.

Table 5.89. Post hoc Tukey HSD test of two-way ANOVA results for Western blot against αSyn epitope on differentiated SH-SY5Y human neuroblastoma cells treated 48 hours with P4-SS, a GlcCer synthesis inhibitor. Data are presented as a percentage calculated against the control group.

The first set of variables (A)		The second set of variables (B)		Post hoc Tukey HSD p-value A vs B
Insulin treatment	The concentration of P4 - SS	Insulin treatment	The concentration of P4 – SS	
w/o insulin	Control	w/o insulin	P4-SS 40 µM	0.0028
w/o insulin	Control	w/o insulin	P4-SS 10 µM	0.0002
w/o insulin	Control	w/o insulin	P4-SS 2.5 µM	0.0001
w/o insulin	Control	w insulin	Control	0.0002
w/o insulin	Control	w insulin	P4-SS 40 µM	0.0001
w/o insulin	Control	w insulin	P4-SS 10 µM	0.0001
w/o insulin	Control	w insulin	P4-SS 2.5 µM	0.0002
w/o insulin	P4-SS 40 µM	w insulin	P4-SS 40 µM	0.0415
w/o insulin	P4-SS 40 µM	w insulin	P4-SS 10 µM	0.0004
w/o insulin	P4-SS 10 µM	w insulin	P4-SS 10 µM	0.0075
w insulin	Control	w insulin	P4-SS 10 µM	0.0117
w insulin	P4-SS 10 µM	w insulin	P4-SS 2.5 µM	0.0074

w/o insulin = without insulin; w insulin = with insulin; P4-SS = (*S, S*) D, L-threo-phenyl-2-hexadecanoylamino-3-pyrrolidino-1-propanol.

Table 5.90. Post hoc Tukey HSD test of two-way ANOVA results for Western blot against pTAU epitope on differentiated SH-SY5Y human neuroblastoma cells treated 48 hours with P4-SS, a GlcCer synthesis inhibitor. Data are presented as a percentage calculated against the control group.

The first set of variables (A)		The second set of variables (B)		Post hoc Tukey HSD p-value A vs B
Insulin treatment	The concentration of P4 - SS	Insulin treatment	The concentration of P4 – SS	
w/o insulin	Control	w insulin	Control	0.0006

w/o insulin = without insulin; w insulin = with insulin; P4-SS = (*S, S*) D, L-threo-phenyl-2-hexadecanoylamino-3-pyrrolidino-1-propanol.

5.6.3. Western blot analysis for MIG inhibitor

Treatment of the cells with MIG had a significant effect on the levels of all epitopes (AKT, pAKT, IRα, IGF1-Rβ, Np65, pGSK3β, βAPP, α Syn) except GSK3β and pTAU. Insulin treatment affected the levels of almost all epitopes except Akt, pAkt and pTAU. The combined effect of insulin and inhibitor treatment was observed for all epitopes except for three exceptions IRα, GSK3β and pTAU (Table 5.91., Figure 5.9., Figure 5.10.).

Post hoc analysis of AKT expression data showed an effect only on the reduction of epitope amount when comparing the control group and the high concentration treatment (Table 5.91., Table 5.92.).

The pAkt level was significantly upregulated in the low concentration treatment group compared to the control group. The same effect was observed with insulin application – most pronounced in the insulin treated control group. Treatment with high and medium inhibitor concentrations caused a significant downregulation of pAkt compared to the insulin-treated control group (Table 5.91., Table 5.93.).

IRα levels were significantly reduced by the treatment, even halved at low MIG concentrations. No other effects were observed (Table 5.91., Table 5.94.).

IGF1-Rβ levels were primarily affected by the combination of inhibitor treatment and insulin, which caused a reduction of half compared to the non-insulin treated groups. Differences were observed between the insulin and inhibitor treated groups, with the highest concentration of inhibitor resulting in significantly higher IGF1-Rβ levels than the medium and low concentration treated groups (Table 5.91., Table 5.95.).

The level of Np65 varied depending on the treatment. Application of high concentration of MIG caused a significant increase in Np65 levels, whereas the opposite effect was observed with low concentrations. In general, the combination of insulin and MIG significantly reduced Np65 levels compared to the non-insulin treated control group. The same effect was observed when the combined inhibitor and insulin treated, and untreated groups were compared. The highest significant effect on Np65 reduction among the insulin-treated groups was to the d high concentration of the inhibitor, which resulted in a nearly twofold reduction compared to the other groups (Table 5.91., Table 5.96.).

Application of insulin significantly reduced pGSK3β levels, especially when combined with MIG treatment. This reduction was significant between the groups treated with insulin and all inhibitors and the untreated control. The same significant effect was observed when groups treated with both inhibitor and insulin were compared with groups treated with inhibitor alone. The combination of inhibitor and insulin significantly reduced epitope levels compared to insulin alone (Table 5.91., Table 5.97.).

Application of insulin significantly reduced βAPP levels, with a fourfold effect in the control group. In the samples treated with MIG inhibitor alone, a significant increase

in βAPP levels was observed in medium concentration treated group and a significant decrease in epitope levels was observed in the low concentration compared to the untreated control and high concentration groups (Table 5.98.).

α Syn levels were significantly decreased by insulin and even more so when combined with inhibitor treatment. This was observed when all insulin untreated groups were compared with all insulin treated groups. When only the insulin-treated groups were observed, the application of a high concentration of inhibitor caused a significant increase in α Syn levels compared to the other groups (Table 5.99.).

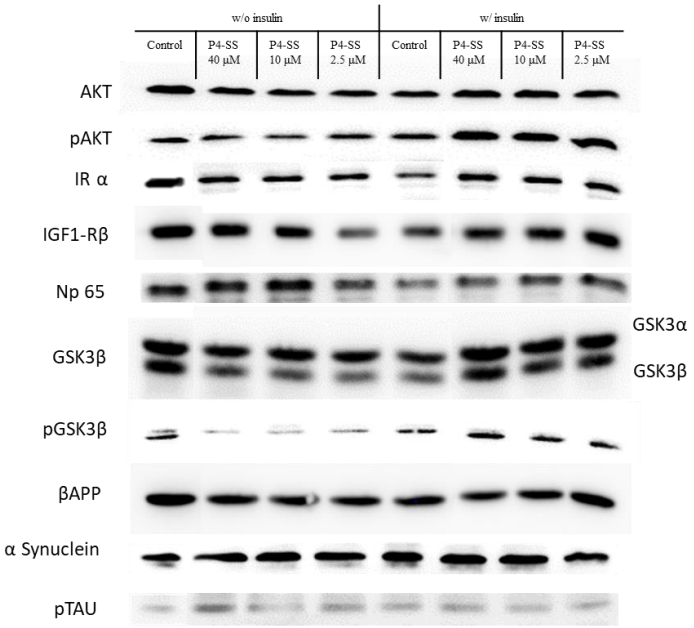

Figure 5.9. Western blots of differentiated SH-SY5Y human neuroblastoma cells treated with MIG a GlcCer synthesis inhibitor for 48 hours; w/o insulin = without insulin; w insulin = with insulin; MIG = miglustat; Akt = protein kinase B; pAkt = protein kinase b phosphorylated at tyrosine 473; IRα = insulin receptor alpha subunit; IGF1-Rβ = beta subunit of receptor for insulin like growth factor; NP65 = neuroplastin 65; GSK3β = glycogen synthase kinase beta; GSK3α = glycogen synthase kinase alpha; pGSK3β = glycogen synthase kinase beta phosphorylated at tyrosine 216; βAPP = beta amyloid precursor protein; αSyn = alpha synuclein; pTAU = tau protein phosphorylated at Ser202 and Thr 205.

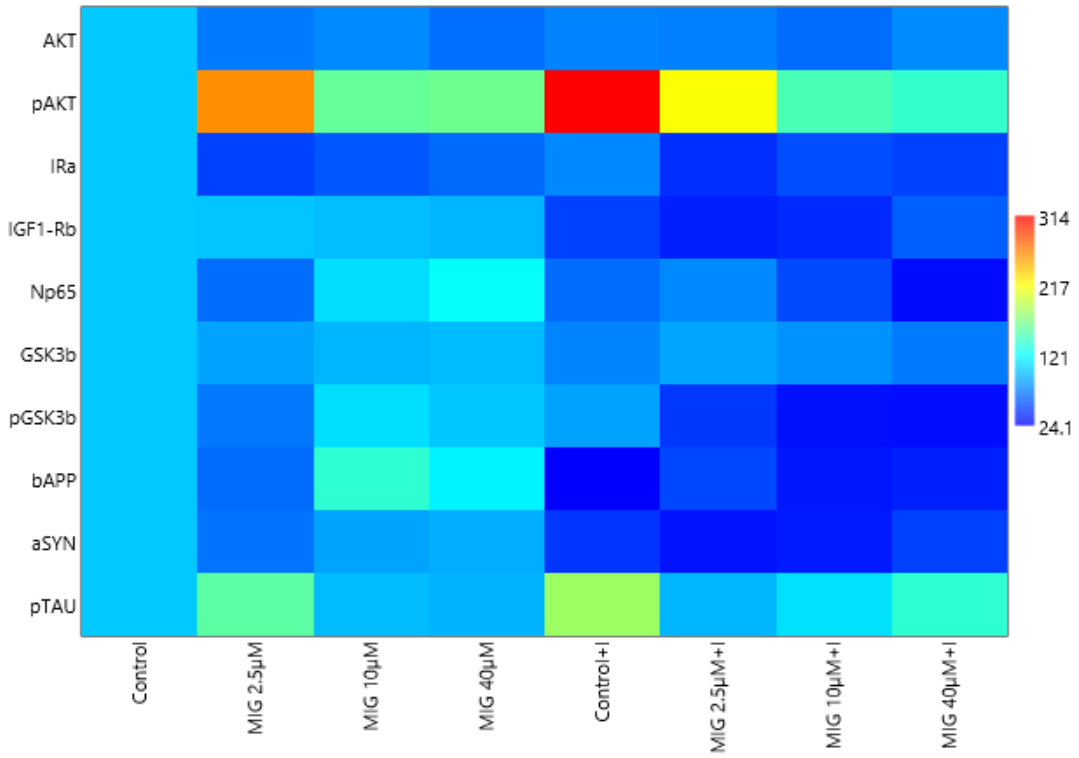

Figure 5.10. Matrix plot made from Western blots of differentiated SH-SY5Y human neuroblastoma cells treated with MIG a GlcCer synthesis inhibitor for 48 hours; data are presented as percentage of intensity calculated against the control group; + I = with insulin; MIG = miglustat; Akt = protein kinase B; pAkt = protein kinase b phosphorylated at tyrosine 473; IRα = insulin receptor alpha subunit; IGF1-Rβ = beta subunit of receptor for insulin like growth factor; NP65 = neuroplastin 65; GSK3β = glycogen synthase kinase beta; GSK3α = glycogen synthase kinase alpha; pGSK3β = glycogen synthase kinase beta phosphorylated at tyrosine 216; βAPP = beta-amyloid precursor protein; αSyn = alpha-synuclein; pTAU = tau protein phosphorylated at Ser202 and Thr 205.

Table 5.91. Protein signal intensity calculated as a percentage against the control group from Western blot for differentiated SH-SY5Y human neuroblastoma cells treated 48 hours with MIG, a GlcCer synthesis inhibitor.

Epitope	w/o insulin				w/ insulin				Two-way ANOVA					
	Control	MIG 2.5 µM	MIG 10 µM	MIG 40 µM	Control	MIG 2.5 µM	MIG 10 µM	MIG 40 µM	F values; (degrees of freedom)			p-values		
	Mean; SD	Mean; SD	Mean; SD	Mean; SD	Mean; SD	Mean; SD	Mean; SD	Mean; SD	Insulin	MIG	Insulin × MIG	Insulin	MIG	Insulin × MIG
Akt	100.00; 16.24	70.55; 2.45	76.50; 2.79	66.02; 2.37	74.27; 1.92	72.35; 4.17	65.27; 3.74	76.70; 2.06	1.85 (1,24)	3.14 (3,24)	3.12 (3,24)	0.1853	0.0438	0.0445
pAkt	100.00; 17.07	259.6; 42.12	159.0; 26.62	162.3; 25.39	313.9; 19.05	215.61; 12.95	148.40; 15.70	139.90; 20.88	4.04 (1,24)	6.16 (3,24)	12.56 (3,24)	0.0557	0.0029	<0.0001
IRα	100.00; 11.75	48.48; 3.27	56.96; 3.46	64.21; 5.01	75.62; 4.77	41.44; 2.27	53.67; 4.24	48.94; 1.88	10.61 (1,24)	23.29 (3,24)	1.49 (3,24)	0.0036	<0.0001	0.2419
IGF1-Rβ	100.00; 5.96	98.65; 0.17	96.05; 0.72	92.61; 2.33	48.31; 1.19	35.70; 5.40	39.75; 2.08	60.17; 1.25	530.58 (1,24)	4.28 (3,24)	8.82 (3,24)	<0.0001	0.0148	0.0004
Np65	100.00; 1.12	65.30; 3.53	107.58; 3.34	122.25; 2.96	64.99; 1.90	75.76; 7.21	51.70; 5.17	28.17; 2.82	245.92 (1,24)	3.53 (3,24)	61.32 (3,24)	<0.0001	0.0297	<0.0001
GSK3β	100.00; 11.67	85.92; 3.11	92.88; 2.23	94.80; 3.83	74.28; 2.31	86.46; 1.03	79.39; 0.45	70.68; 8.26	16.39 (1,24)	0.24 (3,24)	2.43 (3,24)	0.0009	0.8619	0.1021
pGSK3β	100.00; 4.56	69.71; 5.91	108.47; 10.06	99.71; 4.34	85.95; 5.72	44.90; 14.60	30.42; 11.17	28.40; 3.01	59.04 (1,24)	7.01 (3,24)	7.20 (3,24)	<0.0001	0.0009	0.0007
βAPP	100.00; 5.39	65.17; 5.76	137.82; 6.45	116.41; 4.92	24.05; 1.07	51.11; 1.51	32.66; 0.79	35.83; 0.93	571.86 (1,24)	18.98 (3,24)	45.21 (3,24)	<0.0001	<0.0001	<0.0001
αSyn	100.00; 8.97	67.99; 2.73	86.30; 6.88	89.94; 8.69	43.87; 13.98	30.93; 7.86	34.19; 9.43	48.92; 14.73	646.76 (1,24)	12.40 (3,24)	21.79 (3,24)	<0.0001	<0.0001	<0.0001
pTAU	100.00; 20.29	155.50; 37.60	94.86; 24.71	91.74; 20.20	179.77; 31.00	93.52; 27.16	109.28; 40.16	137.69; 41.31	0.77 (1,24)	0.51 (3,24)	1.86 (3,24)	0.3867	0.6734	0.1625

w/o insulin = without insulin; w insulin = with insulin; MIG = miglustat; Akt = protein kinase B; pAkt = protein kinase b phosphorylated at tyrosine 473; IRα = insulin receptor alpha subunit; IGF1-Rβ = beta subunit of receptor for insulin like growth factor; NP65 = neuroplastin 65; GSK3β = glycogen synthase kinase beta; GSK3α = glycogen synthase kinase alpha; pGSK3β = glycogen synthase kinase beta phosphorylated at tyrosine 216; βAPP = beta amyloid precursor protein; αSyn = alpha synuclein; pTAU = tau protein phosphorylated at Ser202 and Thr 205.

Table 5.92. Post hoc Tukey HSD test of two-way ANOVA results for Western blot against Akt epitope on differentiated SH-SY5Y human neuroblastoma cells treated 48 hours with MIG, a GlcCer synthesis inhibitor. Data are presented as a percentage calculated against the control group.

The first set of variables (A)		The second set of variables (B)		Post hoc Tukey HSD p-value A vs B
Insulin treatment	The concentration of MIG	Insulin treatment	The concentration of MIG	
w/o insulin	Control	w/o insulin	MIG-40 µM	0.0174

w/o insulin = without insulin; w insulin = with insulin; MIG = miglustat.

Table 5.93. Post hoc Tukey HSD test of two-way ANOVA results for Western blot against pAkt epitope on differentiated SH-SY5Y human neuroblastoma cells treated 48 hours with MIG, a GlcCer synthesis inhibitor. Data are presented as a percentage calculated against the control group.

The first set of variables (A)		The second set of variables (B)		Post hoc Tukey HSD p-value A vs B
Insulin treatment	The concentration of MIG	Insulin treatment	The concentration of MIG	
w/o insulin	Control	w/o insulin	MIG-2.5 µM	0.0020
w/o insulin	Control	w insulin	Control	0.0001
w insulin	Control	w insulin	MIG-40 µM	0.0008
w insulin	Control	w insulin	MIG-10 µM	0.0014

w/o insulin = without insulin; w insulin = with insulin; MIG = miglustat

Table 5.94. Post hoc Tukey HSD test of two-way ANOVA results for Western blot against IRα epitope on differentiated SH-SY5Y human neuroblastoma cells treated 48 hours with MIG, a GlcCer synthesis inhibitor. Data are presented as a percentage calculated against the control group.

The first set of variables (A)		The second set of variables (B)		Post hoc Tukey HSD p-value A vs B
Insulin treatment	The concentration of MIG	Insulin treatment	The concentration of MIG	
w/o insulin	Control	w/o insulin	MIG-40 µM	0.0022
w/o insulin	Control	w/o insulin	MIG-10 µM	0.0003
w/o insulin	Control	w/o insulin	MIG-2.5 µM	0.0001

w/o insulin = without insulin; w insulin = with insulin; MIG = miglustat

Table 5.95. Post hoc Tukey HSD test of two-way ANOVA results for Western blot against IGF1-Rβ epitope on differentiated SH-SY5Y human neuroblastoma cells treated 48 hours with MIG, a GlcCer synthesis inhibitor. Data are presented as a percentage calculated against the control group.

The first set of variables (A)		The second set of variables (B)		Post hoc Tukey HSD p-value A vs B
Insulin treatment	The concentration of MIG	Insulin treatment	The concentration of MIG	
w/o insulin	Control	w insulin	Control	0.0001
w/o insulin	Control	w insulin	MIG-40 µM	0.0001
w/o insulin	Control	w insulin	MIG-10 µM	0.0001
w/o insulin	Control	w insulin	MIG-2.5 µM	0.0001
w/o insulin	MIG-40 µM	w insulin	Control	0.0001
w/o insulin	MIG-40 µM	w insulin	MIG-40 µM	0.0001
w/o insulin	MIG-40 µM	w insulin	MIG-10 µM	0.0001
w/o insulin	MIG-40 µM	w insulin	MIG-2.5 µM	0.0001
w/o insulin	MIG-10 µM	w insulin	Control	0.0001
w/o insulin	MIG-10 µM	w insulin	MIG-40 µM	0.0001
w/o insulin	MIG-10 µM	w insulin	MIG-10 µM	0.0001
w/o insulin	MIG-10 µM	w insulin	MIG-2.5 µM	0.0001
w/o insulin	MIG-2.5 µM	w insulin	Control	0.0001
w/o insulin	MIG-2.5 µM	w insulin	MIG-40 µM	0.0001
w/o insulin	MIG-2.5 µM	w insulin	MIG-10 µM	0.0001
w/o insulin	MIG-2.5 µM	w insulin	MIG-2.5 µM	0.0001
w insulin	MIG-40 µM	w insulin	MIG-10 µM	0.0024
w insulin	MIG-40 µM	w insulin	MIG-2.5 µM	0.0003

w/o insulin = without insulin; w insulin = with insulin; MIG = miglustat

Table 5.96. Post hoc Tukey HSD test of two-way ANOVA results for Western blot against NP65 epitope on differentiated SH-SY5Y human neuroblastoma cells treated 48 hours with MIG, a GlcCer synthesis inhibitor. Data are presented as a percentage calculated against the control group.

The first set of variables (A)		The second set of variables (B)		Post hoc Tukey HSD p-value A vs B
Insulin treatment	The concentration of MIG	Insulin treatment	The concentration of MIG	
w/o insulin	Control	w/o insulin	MIG-40 µM	0.0105
w/o insulin	Control	w/o insulin	MIG-2.5 µM	0.0001
w/o insulin	Control	w insulin	Control	0.0001
w/o insulin	Control	w insulin	MIG-40 µM	0.0001
w/o insulin	Control	w insulin	MIG-10 µM	0.0001
w/o insulin	Control	w insulin	MIG-2.5 µM	0.0045
w/o insulin	MIG-40 µM	w/o insulin	MIG-2.5 µM	0.0001
w/o insulin	MIG-40 µM	w insulin	Control	0.0001
w/o insulin	MIG-40 µM	w insulin	MIG-40 µM	0.0001
w/o insulin	MIG-40 µM	w insulin	MIG-10 µM	0.0001
w/o insulin	MIG-40 µM	w insulin	MIG-2.5 µM	0.0001
w/o insulin	MIG-10 µM	w/o insulin	MIG-2.5 µM	0.0001
w/o insulin	MIG-10 µM	w insulin	Control	0.0001
w/o insulin	MIG-10 µM	w insulin	MIG-40 µM	0.0001
w/o insulin	MIG-10 µM	w insulin	MIG-10 µM	0.0001
w/o insulin	MIG-10 µM	w insulin	MIG-2.5 µM	0.0002
w/o insulin	MIG-2.5 µM	w insulin	MIG-40 µM	0.0001
w insulin	Control	w insulin	MIG-40 µM	0.0001
w insulin	MIG-40 µM	w insulin	MIG-10 µM	0.0061

The first set of variables (A)		The second set of variables (B)		Post hoc Tukey HSD p-value A vs B
Insulin treatment	The concentration of MIG	Insulin treatment	The concentration of MIG	
w insulin	MIG-40 µM	w insulin	MIG-2.5 µM	0.0001
w insulin	MIG-10 µM	w insulin	MIG-2.5 µM	0.0049

w/o insulin = without insulin; w insulin = with insulin; MIG = miglustat.

Table 5.97. Post hoc Tukey HSD test of two-way ANOVA results for Western blot against pGSK3β epitope on differentiated SH-SY5Y human neuroblastoma cells treated 48 hours with MIG, a GlcCer synthesis inhibitor. Data are presented as a percentage calculated against the control group.

The first set of variables (A)		The second set of variables (B)		Post hoc Tukey HSD p-value A vs B
Insulin treatment	The concentration of MIG	Insulin treatment	The concentration of MIG	
w/o insulin	Control	w insulin	MIG-40 µM	0.0001
w/o insulin	Control	w insulin	MIG-10 µM	0.0001
w/o insulin	Control	w insulin	MIG-2.5 µM	0.0013
w/o insulin	MIG-40 µM	w insulin	MIG-40 µM	0.0001
w/o insulin	MIG-40 µM	w insulin	MIG-10 µM	0.0001
w/o insulin	MIG-40 µM	w insulin	MIG-2.5 µM	0.0008
w/o insulin	MIG-10 µM	w insulin	MIG-40 µM	0.0001
w/o insulin	MIG-10 µM	w insulin	MIG-10 µM	0.0001
w/o insulin	MIG-10 µM	w insulin	MIG-2.5 µM	0.0004
w/o insulin	MIG-2.5 µM	w insulin	MIG-40 µM	0.0298
w/o insulin	MIG-2.5 µM	w insulin	MIG-10 µM	0.0231
w insulin	Control	w insulin	MIG-40 µM	0.0005
w insulin	Control	w insulin	MIG-10 µM	0.0004
w insulin	Control	w insulin	MIG-2.5 µM	0.0099

w/o insulin = without insulin; w insulin = with insulin; MIG = miglustat

Table 5.98. Post hoc Tukey HSD test of two-way ANOVA results for Western blot against βAPP epitope on differentiated SH-SY5Y human neuroblastoma cells treated 48 hours with MIG, a GlcCer synthesis inhibitor. Data are presented as a percentage calculated against the control group.

The first set of variables (A)		The second set of variables (B)		Post hoc Tukey HSD p-value A vs B
Insulin treatment	The concentration of MIG	Insulin treatment	The concentration of MIG	
w/o insulin	Control	w/o insulin	MIG-10 µM	0.0002
w/o insulin	Control	w/o insulin	MIG-2.5 µM	0.0004
w/o insulin	Control	w insulin	Control	0.0001
w/o insulin	Control	w insulin	MIG-40 µM	0.0001
w/o insulin	Control	w insulin	MIG-10 µM	0.0001
w/o insulin	Control	w insulin	MIG-2.5 µM	0.0001
w/o insulin	MIG-40 µM	w/o insulin	MIG-10 µM	0.0312
w/o insulin	MIG-40 µM	w/o insulin	MIG-2.5 µM	0.0001
w/o insulin	MIG-40 µM	w insulin	Control	0.0001
w/o insulin	MIG-40 µM	w insulin	MIG-40 µM	0.0001
w/o insulin	MIG-40 µM	w insulin	MIG-10 µM	0.0001
w/o insulin	MIG-40 µM	w insulin	MIG-2.5 µM	0.0001
w/o insulin	MIG-10 µM	w/o insulin	MIG-2.5 µM	0.0001

The first set of variables (A)		The second set of variables (B)		Post hoc Tukey HSD p-value A vs B
Insulin treatment	The concentration of MIG	Insulin treatment	The concentration of MIG	
w/o insulin	MIG-10 µM	w insulin	Control	0.0001
w/o insulin	MIG-10 µM	w insulin	MIG-40 µM	0.0001
w/o insulin	MIG-10 µM	w insulin	MIG-10 µM	0.0001
w/o insulin	MIG-10 µM	w insulin	MIG-2.5 µM	0.0001
w/o insulin	MIG-2.5 µM	w insulin	Control	0.0002
w/o insulin	MIG-2.5 µM	w insulin	MIG-40 µM	0.0022
w/o insulin	MIG-2.5 µM	w insulin	MIG-10 µM	0.0008
w insulin	Control	w insulin	MIG-2.5 µM	0.0047

w/o insulin = without insulin; w insulin = with insulin; MIG = miglustat

Table 5.99. Post hoc Tukey HSD test of two-way ANOVA results for Western blot against αSyn epitope on differentiated SH-SY5Y human neuroblastoma cells treated 48 hours with MIG, a GlcCer synthesis inhibitor. Data are presented as a percentage calculated against the control group.

The first set of variables (A)		The second set of variables (B)		Post hoc Tukey HSD p-value A vs B
Insulin treatment	The concentration of MIG	Insulin treatment	The concentration of MIG	
w/o insulin	Control	w insulin	Control	0.0001
w/o insulin	Control	w insulin	MIG-40 µM	0.0001
w/o insulin	Control	w insulin	MIG-10 µM	0.0001
w/o insulin	Control	w insulin	MIG-2.5 µM	0.0001
w/o insulin	MIG-40 µM	w insulin	Control	0.0001
w/o insulin	MIG-40 µM	w insulin	MIG-40 µM	0.0001
w/o insulin	MIG-40 µM	w insulin	MIG-10 µM	0.0001
w/o insulin	MIG-40 µM	w insulin	MIG-2.5 µM	0.0001
w/o insulin	MIG-10 µM	w insulin	Control	0.0001
w/o insulin	MIG-10 µM	w insulin	MIG-40 µM	0.0001
w/o insulin	MIG-10 µM	w insulin	MIG-10 µM	0.0001
w/o insulin	MIG-10 µM	w insulin	MIG-2.5 µM	0.0001
w/o insulin	MIG-2.5 µM	w insulin	Control	0.0001
w/o insulin	MIG-2.5 µM	w insulin	MIG-40 µM	0.0001
w/o insulin	MIG-2.5 µM	w insulin	MIG-10 µM	0.0001
w/o insulin	MIG-2.5 µM	w insulin	MIG-2.5 µM	0.0001
w insulin	Control	w insulin	MIG-40 µM	0.0001
w insulin	MIG-40 µM	w insulin	MIG-10 µM	0.0001
w insulin	MIG-40 µM	w insulin	MIG-2.5 µM	0.0001

w/o insulin = without insulin; w insulin = with insulin; MIG = miglustat.

5.6.4. Western blot analysis for CBE inhibitor

Treatment of the cells with CBE caused significant changes in the levels of pAkt, IRα, IGF1-Rβ, pGSK3β, βAPP and αSyn. Insulin treatment affected the levels of Akt,, pAkt,, IRα, IGF1-Rβ, βAPP and αSyn. The combined effect of insulin and inhibitor treatments was observed in almost all groups except pGSK3β (Table 5.100., Figure 5.11., Figure 5.12.).

Post hoc analysis of Akt levels showed only one significant result, where the application of insulin in the group treated with the medium concentration of inhibitor caused a significant increase in Akt levels compared to the group without insulin (Table 5.100., Table 5.101.).

For pAKT, the application of high concentration of CBE caused a significant threefold increase in pAkt levels compared to the untreated control group and a twofold increase compared to the medium and low concentration treated groups. The same pattern was observed in all insulin-treated groups compared to the untreated control. Within the insulin-treated group, low concentration of the inhibitor caused a one and half fold increase in pAkt levels compared to the insulin-treated control and the high concentration of inhibitor (Table 5.100., Table 5.102.).

IRα levels were significantly reduced by inhibitor application compared to the untreated control, regardless of concentration. This was also observed in the insulin and inhibitor treated groups compared to the untreated control. Application of insulin to the cells treated with the highest inhibitor concentration caused a significant decrease compared to the insulin-treated control, but there was no difference between the high concentration insulin treated and untreated groups (Table 5.100., Table 5.103.).

The application of CBE inhibitor caused a decrease in IGF1-Rβ levels, independent of concentration and insulin treatment, but no significant changes were observed within the groups (Table 5.100., Table 5.104.).

CBE and insulin treatment had a correlated effect on Np 65 levels, but not distinctive enough to be detected by post hoc tests. The same could be said for GSK3β (Table 5.100.).

Post hoc analysis of pGSK3β did not reveal any significant difference (Table 5.100.).

βAPP levels decreased with the treatment regardless of concentration of inhibitor. A fourfold decrease in epitope levels was only observed with application of insulin. Cells treated with inhibitors showed significantly lower βAPP levels than their counterparts treated with both insulin and inhibitor, regardless of concentration. When insulin-treated groups were observed, control groups had significantly lower βAPP than treated groups.

The medium concentration of inhibitor caused a significant decrease in epitope levels compared to the high and low concentrations (Table 5.100., Table 5.105.).

Treatment of the cells with high and low concentrations of CBE significantly reduced αSyn levels below those of the control group. The same effect occurred with the application of insulin in the control and inhibitor-treated groups, regardless of the inhibitor concentration. Treatment of the cells only with CBE resulted in an inverse dose-dependent effect, with the highest concentration causing the smallest reduction and significantly less reduction than that observed in cells treated with medium and low inhibitor concentrations. When the treatment was combined with insulin, it caused an increase in epitope levels: a significant increase was observed at medium and low inhibitor concentrations compared to the control (Table 5.100., Table 5.106.).

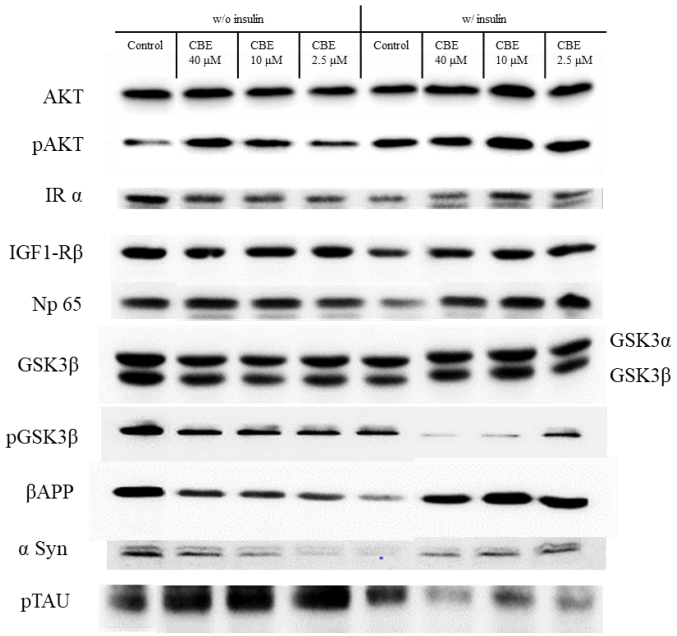

Figure 5.11. Western blots of differentiated SH-SY5Y human neuroblastoma cells treated with CBE a glycolipid metabolism inhibitor for 48 hours; w/o insulin = without insulin; w insulin = with insulin; CBE = conduritol B epoxide; Akt = protein kinase B; pAkt = protein kinase b phosphorylated at tyrosine 473; IRα = insulin receptor alpha subunit; IGF1-Rβ = beta subunit of receptor for insulin like growth factor; NP65 = neuroplastin 65; GSK3β = glycogen synthase kinase beta; GSK3α = glycogen synthase kinase alpha; pGSK3β = glycogen synthase kinase beta phosphorylated at tyrosine 216; βAPP = beta amyloid precursor protein; αSyn = alpha synuclein; pTAU = tau protein phosphorylated at Ser202 and Thr 205.

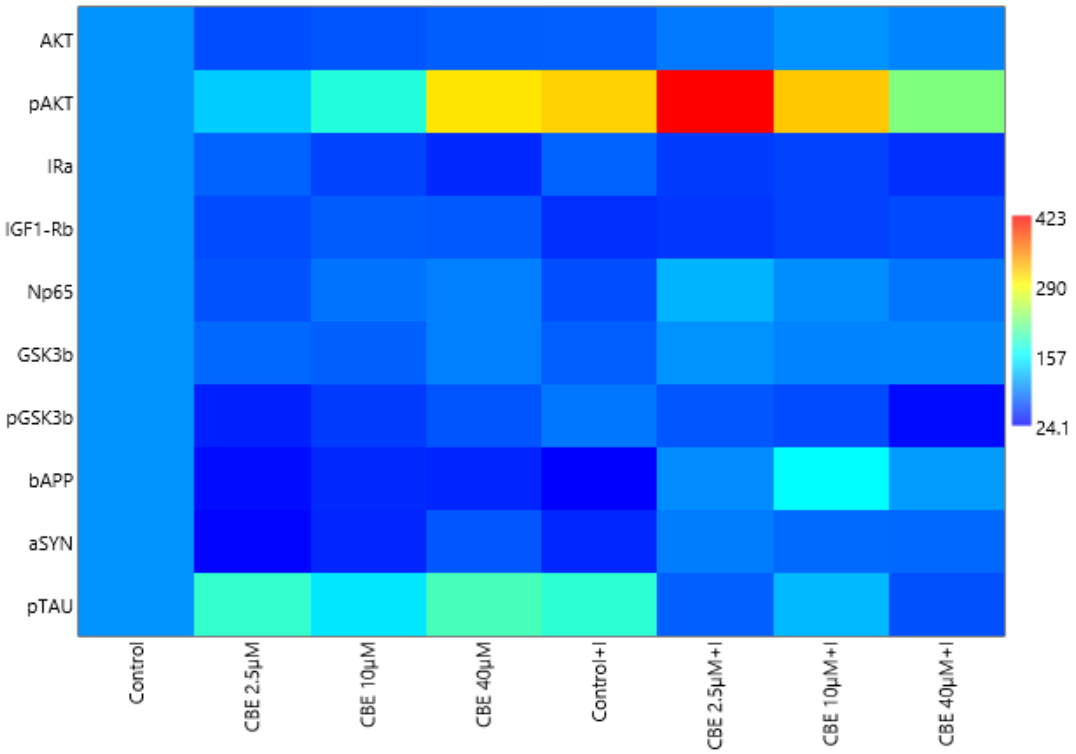

Figure 5.12. Matrix plot made from Western blots of differentiated SH-SY5Y human neuroblastoma cells treated with CBE a glycolipid metabolism inhibitor for 48 hours; data are presented as percentage of intensity calculated against the control group; + I = with insulin; CBE = conduritol B epoxide; Akt = protein kinase B; pAkt = protein kinase b phosphorylated at tyrosine 473; IRα = insulin receptor alpha subunit; IGF1-Rβ = beta subunit of receptor for insulin like growth factor; NP65 = neuroplastin 65; GSK3β = glycogen synthase kinase beta; GSK3α = glycogen synthase kinase alpha; pGSK3β = glycogen synthase kinase beta phosphorylated at tyrosine 216; βAPP = beta amyloid precursor protein; αSyn = alpha synuclein; pTAU = tau protein phosphorylated at Ser202 and Thr 205.

Table 5.100. Protein signal intensity calculated as a percentage against the control group from Western blot for differentiated SH-SY5Y human neuroblastoma cells treated 48 hours with CBE, a glycolipid metabolism inhibitor synthesis inhibitor.

Epitope	w/o insulin				w/ insulin				Two-way ANOVA					
	Control	CBE 2.5 µM	CBE 10 µM	CBE 40 µM	Control	CBE 2.5 µM	CBE 10 µM	CBE 40 µM	F values; (degrees of freedom)			p-values		
	Mean; SD	Mean; SD	Mean; SD	Mean; SD	Mean; SD	Mean; SD	Mean; SD	Mean; SD	Insulin	CBE	Insulin × CBE	Insulin	CBE	Insulin × CBE
Akt	100.00; 16.24	64.80; 6.92	67.87; 5.38	72.81; 10.64	74.27; 10.91	87.04; 6.59	100.87; 8.66	92.62; 4.99	7.29 (1,24)	1.09 (3,24)	8.11 (3,24)	0.0125	0.3716	0.0006
pAkt	100.00; 17.07	130.35; 17.28	174.91; 21.86	302.97; 35.45	313.93; 19.05	422.60; 20.52	318.36; 22.04	223.38; 19.13	82.05 (1,24)	3.67 (3,24)	25.87 (3,24)	<0.0001	0.0262	<0.0001
IRα	100.00; 11.75	74.94; 5.58	59.01; 3.04	45.64; 2.01	75.62; 4.77	54.92; 2.77	58.21; 3.07	48.59; 1.67	7.92 (1,24)	20.85 (3,24)	3.30 (3,24)	0.0095	<0.0001	0.0373
IGF1-Rβ	100.00; 5.96	62.94; 4.00	71.97; 6.54	70.19; 3.54	48.31; 1.19	52.51; 2.93	57.59; 6.93	62.17; 4.44	38.71 (1,24)	3.93 (3,24)	9.14 (3,24)	<0.0001	0.0204	0.0003
Np65	100.00; 1.12	66.91; 4.38	84.69; 5.08	90.11; 4.20	64.99; 1.90	117.92; 5.13	97.92; 8.58	85.39; 7.88	2.61 (1,24)	1.39 (3,24)	22.52 (3,24)	0.1186	0.2695	<0.0001
GSK3β	100.00; 11.67	77.63; 1.79	74.69; 1.00	90.71; 1.71	74.28; 2.31	100.43; 4.55	92.28; 0.34	94.29; 0.89	1.94 (1,24)	1.32 (3,24)	11.11 (3,24)	0.1817	0.2999	0.0003
pGSK3β	100.00; 4.56	40.57; 7.60	54.75; 4.51	67.94; 11.82	85.95; 5.72	68.81; 18.27	62.89; 27.83	28.87; 11.62	0.23 (1,24)	6.03 (3,24)	2.18 (3,24)	0.6284	0.0022	0.1093
βAPP	100.00; 5.39	30.15; 1.66	45.04; 2.69	42.98; 4.52	24.05; 1.07	96.68; 6.13	156.96; 3.62	105.25; 3.08	224.60 (1,24)	43.21 (3,24)	218.53 (3,24)	<0.0001	<0.0001	<0.0001
αSyn	100.00; 8.97	26.58; 6.09	43.49; 12.29	69.38; 2.74	43.87; 13.98	88.87; 8.25	79.58; 0.79	77.65; 15.37	128.80 (1,24)	23.00 (3,24)	132.98 (3,24)	<0.0001	<0.0001	<0.0001
pTAU	100.00; 20.29	183.48; 45.15	144.33; 35.34	193.48; 50.61	179.77; 31.00	73.45; 3.82	119.98; 4.71	65.76; 8.78	4.53 (1,24)	0.05 (3,24)	4.91 (3,24)	0.0437	0.9814	0.0083

w/o insulin = without insulin; w insulin = with insulin; CBE = conduritol B epoxide; Akt = protein kinase B; pAkt = protein kinase b phosphorylated at tyrosine 473; IRα = insulin receptor alpha subunit; IGF1-Rβ = beta subunit of receptor for insulin like growth factor; NP65 = neuroplastin 65; GSK3β = glycogen synthase kinase beta; GSK3α = glycogen synthase kinase alpha; pGSK3β = glycogen synthase kinase beta phosphorylated at tyrosine 216; βAPP = beta amyloid precursor protein; αSyn = alpha synuclein; pTAU = tau protein phosphorylated at Ser202 and Thr 205.

Table 5.101. Post hoc Tukey HSD test of two-way ANOVA results for Western blot against Akt epitope on differentiated SH-SY5Y human neuroblastoma cells treated 48 hours with CBE glycolipid metabolism inhibitor. Data are presented as a percentage calculated against the control group.

The first set of variables (A)		The second set of variables (B)		Post hoc Tukey HSD p-value A vs B
Insulin treatment	The concentration of CBE	Insulin treatment	The concentration of CBE	
w/o insulin	CBE-10 μM	w insulin	CBE-10 μM	0.0257

w/o insulin = without insulin; w insulin = with insulin; CBE = conduritol B epoxide

Table 5.102. Post hoc Tukey HSD test of two-way ANOVA results for Western blot against pAkt epitope on differentiated SH-SY5Y human neuroblastoma cells treated 48 hours with CBE glycolipid metabolism inhibitor. Data are presented as a percentage calculated against the control group.

The first set of variables (A)		The second set of variables (B)		Post hoc Tukey HSD p-value A vs B
Insulin treatment	The concentration of CBE	Insulin treatment	The concentration of CBE	
w/o insulin	Control	w/o insulin	CBE-40 μM	0.0001
w/o insulin	CBE-40 μM	w/o insulin	CBE-10 μM	0.0089
w/o insulin	CBE-40 μM	w/o insulin	CBE-2.5 μM	0.0003
w/o insulin	Control	w insulin	Control	0.0001
w/o insulin	Control	w insulin	CBE-40 μM	0.0127
w/o insulin	Control	w insulin	CBE-10 μM	0.0001
w/o insulin	Control	w insulin	CBE-2.5 μM	0.0001
w/o insulin	CBE-10 μM	w insulin	Control	0.0039
w/o insulin	CBE-10 μM	w insulin	CBE-10 μM	0.0028
w/o insulin	CBE-10 μM	w insulin	CBE-2.5 μM	0.0001
w/o insulin	CBE-2.5 μM	w insulin	Control	0.0002
w/o insulin	CBE-2.5 μM	w insulin	CBE-10 μM	0.0002
w/o insulin	CBE-2.5 μM	w insulin	CBE-2.5 μM	0.0001
w insulin	Control	w insulin	CBE-2.5 μM	0.0367
w insulin	CBE-40 μM	w insulin	CBE-2.5 μM	0.0001

w/o insulin = without insulin; w insulin = with insulin; CBE = conduritol B epoxide.

Table 5.103. Post hoc Tukey HSD test of two-way ANOVA results for Western blot against IRα epitope on differentiated SH-SY5Y human neuroblastoma cells treated 48 hours with CBE glycolipid metabolism inhibitor. Data are presented as a percentage calculated against the control group.

The first set of variables (A)		The second set of variables (B)		Post hoc Tukey HSD p-value A vs B
Insulin treatment	The concentration of CBE	Insulin treatment	The concentration of CBE	
w/o insulin	Control	w/o insulin	CBE-40 μM	0.0001
w/o insulin	Control	w/o insulin	CBE-10 μM	0.0004
w/o insulin	Control	w/o insulin	CBE-2.5 μM	0.0471
w/o insulin	CBE-40 μM	w/o insulin	CBE-2.5 μM	0.0132
w/o insulin	Control	w insulin	CBE-40 μM	0.0001
w/o insulin	Control	w insulin	CBE-10 μM	0.0003

The first set of variables (A)		The second set of variables (B)		Post hoc Tukey HSD p-value A vs B
Insulin treatment	The concentration of CBE	Insulin treatment	The concentration of CBE	
w/o insulin	Control	w insulin	CBE-2.5 µM	0.0002
w/o insulin	CBE-40 µM	w insulin	Control	0.0106
w/o insulin	CBE-2.5 µM	w insulin	CBE-40 µM	0.0323
w insulin	Control	w insulin	CBE-40 µM	0.0263

SD=standard deviation w/o insulin = without insulin; w insulin = with insulin; CBE = conduritol B epoxide.

Table 5.104. Post hoc Tukey HSD test of two-way ANOVA results for Western blot against IGF1-Rβ epitope on differentiated SH-SY5Y human neuroblastoma cells treated 48 hours with CBE glycolipid metabolism inhibitor. Data are presented as a percentage calculated against the control group.

The first set of variables (A)		The second set of variables (B)		Post hoc Tukey HSD p-value A vs B
Insulin treatment	The concentration of CBE	Insulin treatment	The concentration of CBE	
w/o insulin	Control	w/o insulin	CBE-40 µM	0.0042
w/o insulin	Control	w/o insulin	CBE-10 µM	0.0078
w/o insulin	Control	w/o insulin	CBE-2.5 µM	0.0004
w/o insulin	Control	w insulin	Control	0.0001
w/o insulin	Control	w insulin	CBE-40 µM	0.0003
w/o insulin	Control	w insulin	CBE-10 µM	0.0001
w/o insulin	Control	w insulin	CBE-2.5 µM	0.0001

w/o insulin = without insulin; w insulin = with insulin; CBE = conduritol B epoxide.

Table 5.105. Post hoc Tukey HSD test of two-way ANOVA results for western blot against βAPP epitope on differentiated SH-SY5Y human neuroblastoma cells treated 48 hours with CBE glycolipid metabolism inhibitor. Data are presented as a percentage calculated against the control group.

Expression of βAPP				
The first set of variables (A)		The second set of variables (B)		Post hoc Tukey HSD p-value A vs B
Insulin treatment	The concentration of CBE	Insulin treatment	The concentration of CBE	
w/o insulin	Control	w/o insulin	CBE-40 µM	0.0001
w/o insulin	Control	w/o insulin	CBE-10 µM	0.0001
w/o insulin	Control	w/o insulin	CBE-2.5 µM	0.0001
w/o insulin	Control	w insulin	Control	0.0001
w/o insulin	CBE-40 µM	w insulin	CBE-40 µM	0.0001
w/o insulin	CBE-40 µM	w insulin	CBE-10 µM	0.0001
w/o insulin	CBE-40 µM	w insulin	CBE-2.5 µM	0.0001
w/o insulin	CBE-10 µM	w insulin	Control	0.0254
w/o insulin	CBE-10 µM	w insulin	CBE-40 µM	0.0001
w/o insulin	CBE-10 µM	w insulin	CBE-10 µM	0.0001
w/o insulin	CBE-10 µM	w insulin	CBE-2.5 µM	0.0001
w/o insulin	CBE-2.5 µM	w insulin	CBE-40 µM	0.0001
w/o insulin	CBE-2.5 µM	w insulin	CBE-10 µM	0.0001
w/o insulin	CBE-2.5 µM	w insulin	CBE-2.5 µM	0.0001
w insulin	Control	w insulin	CBE-40 µM	0.0001
w insulin	Control	w insulin	CBE-10 µM	0.0001
w insulin	Control	w insulin	CBE-2.5 µM	0.0001

Expression of βAPP				
The first set of variables (A)		The second set of variables (B)		Post hoc Tukey HSD p-value A vs B
Insulin treatment	The concentration of CBE	Insulin treatment	The concentration of CBE	
w insulin	CBE-40 μM	w insulin	CBE-10 μM	0.0001
w insulin	CBE-10 μM	w insulin	CBE-2.5 μM	0.0001

w/o insulin = without insulin; w insulin = with insulin; CBE = conduritol B epoxide.

Table 5.106. Post hoc Tukey HSD test of two-way ANOVA results for Western blot against αSyn epitope on differentiated SH-SY5Y human neuroblastoma cells treated 48 hours with CBE glycolipid metabolism inhibitor. Data are presented as a percentage calculated against the control group.

The first set of variables (A)		The second set of variables (B)		Post hoc Tukey HSD p-value A vs B
Insulin treatment	The concentration of CBE	Insulin treatment	The concentration of CBE	
w/o insulin	Control	w/o insulin	CBE-40 μM	0.0478
w/o insulin	Control	w/o insulin	CBE-2.5 μM	0.0001
w/o insulin	Control	w insulin	Control	0.0001
w/o insulin	Control	w insulin	CBE-40 μM	0.0001
w/o insulin	Control	w insulin	CBE-10 μM	0.0073
w/o insulin	Control	w insulin	CBE-2.5 μM	0.0128
w/o insulin	CBE-40 μM	w/o insulin	CBE-10 μM	0.0004
w/o insulin	CBE-40 μM	w/o insulin	CBE-2.5 μM	0.0001
w/o insulin	CBE-40 μM	w insulin	Control	0.0001
w/o insulin	CBE-40 μM	w insulin	CBE-40 μM	0.0001
w/o insulin	CBE-40 μM	w insulin	CBE-10 μM	0.0001
w/o insulin	CBE-40 μM	w insulin	CBE-2.5 μM	0.0001
w/o insulin	CBE-10 μM	w/o insulin	CBE-2.5 μM	0.0001
w/o insulin	CBE-10 μM	w insulin	Control	0.0001
w/o insulin	CBE-10 μM	w insulin	CBE-40 μM	0.0001
w/o insulin	CBE-2.5 μM	w insulin	CBE-10 μM	0.0001
w/o insulin	CBE-2.5 μM	w insulin	CBE-2.5 μM	0.0001
w insulin	Control	w insulin	CBE-10 μM	0.0001
w insulin	Control	w insulin	CBE-2.5 μM	0.0001

w/o insulin = without insulin; w insulin = with insulin; CBE = conduritol B epoxide.

6. DISCUSSION

6.1. Cell viability after inhibitor treatments

Determining the survival rate of experimental models in a dose-dependent manner is crucial to properly monitor the response to treatment with different compounds and provides a preliminary measure of how to proceed further with the experiments. Three of the four inhibitors (P4-RR, P4-SS, MIG) target and inhibit, to varying degrees, a specific enzyme important in the synthesis of gangliosides – GlcCer (EC: 2.4.1.80). The fourth compound (CBE) acts as an inhibitor of the β-Glucosidase enzyme (EC: 3.2.1.21) responsible for the degradation of gangliosides. When cells were treated with P4 inhibitors, the dose-dependent effect on survival was strongest after 24 hours, with little or no effect after a further 24 hours. Most of the cells likely died within the first 24 hours of incubation, and the survivors were kept in metabolic stasis by the inhibitors. The addition of insulin, mainly due to the cytokine effect of insulin and its overall effect on cell metabolism, has brought cells out of metabolic stasis. This was best observed at low and medium concentrations after 24 hours of treatment, suggesting that cells are still able to compensate for the loss of glycolipids and partially restore metabolic activity after stimulation with insulin. After an additional day of inhibitor treatment, the cells were able to restore metabolic activity at least partially. At this point, insulin challenge caused the death of cells treated with low and medium concentrations and was reversed in cells treated with the highest concentration. The toxicity is cumulative over time and dose, and cells treated with medium and low doses were able to compensate for this metabolic nuisance and recover. Until insulin entered the experiment. At high concentrations of the inhibitor, ceramide accumulation probably occurred and may be the main cause of cell death, as it participates as a second messenger in the apoptotic signaling cascade.

However, too much ceramide can affect insulin signaling. It has been previously described that ceramides affect insulin signaling, but the result is a partial cessation and shutdown of the insulin signaling pathway in skeletal muscle cells and adipocytes (164). This would indicate an even poorer survival rate as the concentration increases due to the lack of antiapoptotic effects of insulin.

MIG is a drug used to treat Gaucher disease type 1 and its mechanism of action may be slightly different, although it acts on the same enzyme as the P4 inhibitors. Treatment of the cells with MIG and insulin had no significant effect on the cells until 48 hours after

treatment when the effect of insulin treatment was detectable and cells began to die, but not significantly enough to detect this by statistical analysis. Since MIG is a sugar derivative, more specifically a glucose derivative, it has fewer metabolic by-products than more complex P4 inhibitors. This may be one reason why their effects on survival were different.

CBE did not have such a dramatic effect on cell viability as the first two compounds. Overloading cells with gangliosides and its precursors also induces cell death, but only after 48 hours and without insulin treatment. This implies that altered lipid environment and ganglioside overload usually lead to mitochondrial death mediated by increased calcium ion influx through overactive IP3 sensitive calcium channel held open by GM1 (165,166). Insulin is a cytokine that is also able to bind to and partially activate the IGF1 receptor, which is sufficient to induce an antiapoptotic effect of IGF signaling in mitochondria (167,168). This can partially explain the survival dynamics of the cells. It is important to note that the solvent itself, in this case DMSO, did not affect the cell viability.

The MTT method is widely used, but it has limitations, mainly it requires a well-calibrated experimental setup with minimal variation between experiments and good laboratory technique. In addition, it relies heavily on mitochondria to metabolize yellow tetrazolium bromide into purple formazan. Because, in apoptosis, mitochondria will undergo fragmentation, thus reducing dye formation (169). There is always the question of whether the compound under investigation has any effect on mitochondrial survival and therefore this method needs to be tested by other methods that do not rely solely on the proper functioning of mitochondria, such as Annexin staining or other vital stains where the cell population is presented by absolute numbers (170).

Annexin V is a quite sensitive method for determining the status of the cells after treatment. Treatment of the cells with P4 inhibitors gave somewhat similar results to treatment with MTT. A dose-dependent response was observed, but in this case, the response of cells to insulin treatment was not as dramatic as it was with MTT. Insulin treatment of the P4-RR treated cells did not rescue cells from apoptosis as in the SS isoform, where both early and late apoptosis were reduced to some extent. The same pattern was observed with MIG. This observation may suggest that disruption of glycolipid synthesis first affects the mitochondria and then the cell as a whole unit.

Alteration of glycolipid composition usually leads to local instabilities within either mitochondrial or cell membranes. Garofalo et al. described a role for GD3-enriched microdomains in mitochondria in mitochondrial apoptosis (171). These disruptions strongly affect mitochondria due to their role in the synthesis of ATP and the maintenance of tight membrane composition. On the other hand, an excess of gangliosides usually leads to induction of cell death, which has been observed in astrocytes (172). What was observed when cells were treated with CBE? At higher concentrations, cells die. Since gene expression was not blocked by P4 and MIG inhibitors, the cells were likely trying to compensate for the lack of gangliosides by overexpressing GlcCer and all other ganglioside synthases in an attempt to patch holes in the membranes, causing mitochondria death, but keeping the cell more or less intact. To further examine the extent of mitochondrial involvement, treated cells should be stained for mitochondrial membrane potential (TMRE).

It should be mentioned that mechanical manipulation of cells also caused a certain level of cell death and apoptosis. This effect was reduced after insulin administration, which correlates with the previously observed effect of insulin, which increases the mechanical strength of the cells and also reduces apoptosis. The lack of the effect of DMSO on the cells was expected, due to the concentrations used in the experiments being much lower than those previously reported to have any effect on cell metabolism and viability, which was the reason why it was not further examined (173,174).

To put these results into perspective, glycosphingolipid synthesis inhibitors are also used in clinical practice, however, limited to the treatment of genetic disorders such as Gaucher disease. Recently, it was found that the application of D-PDMP, a GlcCer inhibitor similar to P4, caused a marked reduction in the size of mice renal tumors with a glycolipid profile (175). Functionally, if P4 and similar analogs were administered, they only acted on tissues outside the CNS, as they were unable to cross the blood-brain barrier due to their size and charge. High metabolic turnover is regularly found in tumors and the observed apoptotic effect of inhibitors may be useful in their treatment.

6.2. Immunocytochemical staining of the cells

Immunocytochemical analysis of cells treated with P4 inhibitors showed the opposite effect of the expected, i.e an increase in the levels of gangliosides, in particular GM1 and GD1a. Furthermore, it appears that the metabolic effect of insulin resulted in

further changes in the upregulation of ganglioside levels. This effect was expected as it promotes gene expression and subsequent increases in epitope levels, but only in the insulin-treated control groups. What is consolidating is the expected response to IR stimulation with insulin, where IR levels are reduced. This is observed in all treatment groups but is only significant in the group treated with both insulin and the lowest concentration of inhibitor. For the SS isoform of the inhibitor, the metabolic changes were not significant from a treatment point of view, but they caused a shift of the IR into the non-raft area of the membrane, especially when the lowest dose of treatment was applied. This type of response usually occurs when there is more ganglioside in the membrane which displaces IR from the caveolae association, rendering it inert, as observed in transgenic mice with sialidase overexpression (176). At the same time, GM1 shifted from rafts to non-rafts upon P4-SS treatment, and the reverse effect was observed when cells were treated with P4-RR. Again, the sterical specificity of the two isomers is shown. When GM1 is displaced in or out of the lipid rafts, it certainly causes an imbalance of all proteins that resides within the lipid rafts. It should be noted that both IR and GM1 are out of lipid rafts. Whether this GM1 is bound to IR or is in free form remains a question. Taking the study further, it is interesting to note that IGF1-receptor levels did not change significantly *in situ*, but rather shifted to the non-raft part of the membrane, especially when cells were treated with a low concentration of P4-RR inhibitor. This was not observed for the SS inhibitor isoform. Displacement of the IGF1-receptor from the lipid rafts probably renders it inactive and causes partial or complete signaling cascade arrest, as observed in mouse fibroblasts (177). Again, the exit of the IGF1-receptor from the lipid raft coincides with the exit of GM1. The question is whether this shift within the membrane is the result of a change in glycolipid levels, or an attempt to preserve cell metabolism.

Np65 is significantly decreased by the treatment with or without insulin. NPs are sensitive to changes in the metabolic environment, and any nudge will cause NP levels to decrease or increase (178). The loss of Np is likely to have an impact on the neuroplasticity of the cells and the overall ability to form new synapses or grow new neurites. The colocalization analysis showed no shifts around the membrane, which might indicate an overall decrease in Np65 levels rather than a knockout of the epitope from the lipid rafts, rendering it non-functional.

There was an interesting change with βAPP and still with sterical specificity. In cells treated with the SS isoform, the epitope shifted to the non-raft areas of the membrane, with the largest shift occurring at the lowest concentration. The RR isoform affected the efflux of βAPP from the rafts, but no accumulation into the rest of the membrane was observed. Proper recycling of the βAPP involves its entry into the lipid raft domain, where it is cleaved by secretase enzymes and endocytosed for further degradation. If something interferes with this process or the enzymes involved in the degradation of βAPP, Alzheimer's disease is likely to develop over time (179). This suggests that the SS isoform has a long-lasting amyloidogenic effect, unlike the RR isoform. This should be confirmed by exposure to low concentrations of inhibitors for at least 10 days to allow sufficient time for cells to develop the appropriate phenotype. For other epitopes, no significant changes were found, which may be due to the high susceptibility of the cells to buffer changes or poor antibody response, especially for flotillin, as the epitope is inside the cell and the use of membrane disrupting detergents to improve accessibility would likely disrupt all other epitopes and cause chaos (180).

Treatment of cells with MIG caused changes in some gangliosides, namely GD1b and GT1b. Still, it had a somewhat unexpected effect. The decrease in GD1b levels only occurred when insulin was added, whereas GT1b levels changed as expected in the absence of insulin, i.e levels decreased compared to the control. As with P4 inhibitors, the addition of insulin caused an increase in ganglioside levels, but with the difference that the treatment effectively reduced ganglioside levels. No significant changes were found in the position of these two gangliosides within the membrane. The reduction of GT1b and GD1a levels within the membrane may have a strong metabolic impact in the brain, where interactions with myelin-associated glycoprotein (MAG), myelin oligodendrocyte glycoprotein (MOG), and Nogo receptor can be achieved, but not in monocultures of differentiated neuroblastoma cells, so this information more likely to demonstrate of the efficacy of inhibiting ganglioside synthesis (181,182). On the other hand, even if the level of GM1 did not change, its position did. GM1 entered the non-raft domain independently of inhibitor concentration or insulin treatment. This GM1 exodus leaves the lipid raft crippled for proper function. The same was observed with P4 inhibitors, βAPP entered the non-raft domain after treatment with the highest concentration and insulin, but no significant change in entry into the lipid raft domain was detected. It is known that βAPP binds to the GM1 ganglioside, and its positioning

outside the lipid rafts causes alterations in its degradation, as β and γ secretase enzymes are located within the lipid rafts, leading to toxic amyloidosis (106,120,183). This drug has not been reported to cause long-term pathological changes in the brain of patients, but it has been found to cause lymphocyte depletion from lymph nodes and spleen (142,146). Although it does not affect the level of the IGF1-receptor, at the lowest concentration in the presence of insulin the receptor is translocated to the non-raft part of the cell membrane. This renders the receptor unfunctional and should cause the downstream tuning of the Akt signaling pathway. NP levels were reduced by inhibitor treatment and insulin, which should result in a reduction in the ability of cells to form neurite networks and neurite outgrowth (184). The concentration or position of other epitopes within the membrane was not significantly affected.

The effect of CBE can be detected as ganglioside accumulation, which may cause impaired insulin signaling and stability of lipid rafts due to glycolipid overload. the levels of GM1 and GD1a were affected by the treatment, with a trend of an increase in GM1 ganglioside levels but no statistical significance. Other gangliosides did not even show a trend. As previously with ganglioside synthesis inhibitors, the addition of insulin caused an increase in GD1a levels, but not to a great extent compared to the insulin-treated control, indicating that there is a limit to the extent to which this GD1a ganglioside can be accumulated by the cells. Other gangliosides showed no significant increase or decrease, but GT1b was statistically prone to leave lipid rafts after treatment with CBE. Since GT1b has previously demonstrated a strong avidity to affiliate with lipid rafts, cholesterol, and amyloid proteins, several factors may contribute to this (185). The first is that overload with GT1b within lipid rafts forces GT1b to leave rafts as a rescue mechanism to maintain raft stability. The second is that overflow into the non-raft region due to a stronger diffusion gradient than the interaction forces that hold the ganglioside within the lipid rafts. Functionally, this would probably affect the interaction between the neuron and glial cells, but in this case, this interaction was not possible as this is a cell monoculture. The association of GT1b with IR indicates it plays some role in the stabilization of lipid rafts. It is important to note that IR levels decreased across the membrane after treatment of the cells with CBE, with no shifts between lipid rafts and non-rafts, regardless of concentration or insulin treatment. In human endothelial cells, overexpression of GM1 caused a shift in the IR signaling pathway and thus increased the rate of cell death (186). Treatment of cells with inhibitors caused a decrease in IR levels,

regardless of concentration. This effect may be because the conduritol molecule binds to the IR and forces it to recycle, as demonstrated in previous research studies with conduritol derivatives (187). The same effect was seen with insulin itself, which is to be expected because insulin binding to the IR eventually forces it to recycle. IGF1-Rβ levels were elevated with the treatment. Colocalization analysis showed that the receptor moved into the raft area of the membrane upon treatment. This might indicate that the cell is primed for activation of the IGF1 signaling cascade, given the removal of the insulin receptor from the membrane. This pattern may be a countermeasure against insulin leaving the lipid rafts, keeping cytokine signaling functional. The concentrations of CBE used in these experiments are sub-effective and have been shown to have the effects of repositioning the IR in the membrane.

6.3. Histochemical staining of the cells

Treatment of cells with P4 inhibitors reduced the length of neurites. This was more pronounced for the RR isoform when insulin was applied, but when the SS isoform was challenged with insulin, the opposite happened compared to the controls. Blocking ganglioside synthesis, especially of complex gangliosides such as GD1a and GT1b, promotes the growth of neurites in cell cultures of primary cortical neurons and mouse models of traumatic brain injury (188–190). Complex gangliosides, when present, reduce neurite outgrowth *in vitro* due to their interaction with the Nogo receptor (191). Autoactivation of the Nogo receptor or the production of ligand for the receptor by the SH-SY5Y cell line has not been previously described. Inokuchi demonstrated that two different isomers of GlcCer inhibitors have opposite effects, where the L-isoform stimulated the production of GSL, but D-isoform caused inhibition (192). The steric-specific effect was also observed between P4-RR and P4-SS, only when insulin was added to P4-SS, suggesting that cytokine stimulation is required for neurite outgrowth. Another study demonstrated that after 3 days of treatment with PDMP, a compound with a structure and function similar to P4 caused a reduction in neurite outgrowth and a reduction in axonal networks of cultured hippocampal neurons (193). In both cases (P4-RR and P4-SS), the expected result was neurite outgrowth, regardless of insulin due to the inhibition of ganglioside synthesis, but since the effect was not or was only partially achieved by the addition of insulin, it can be assumed that these isoforms have an activating effect on GSL enzymes or that the cells can overcome the inhibition.

Previously, it was described how different concentrations of insulin stimulate neurite outgrowth, where it had a positive effect on neurons in dorsal root ganglia. That effect was only observed at extremely low concentrations ranging from 1 to 10 nM, and no effect was observed around 1 μM (190). In this experiment, 2 μM of insulin were used for 2 hours to stimulate insulin signaling briefly but strongly. It may be that overstimulation of already disrupted insulin pathways caused regression of neurites to protect the cell from death. A better effect might be achieved by prolonged exposure to low concentrations of insulin where cells would have sufficient time to adjust to the metabolic changes.

MIG had the expected effect on the length of neurites at the highest concentrations of 40 μM. The lowest concentration of 2.5 μM caused a reduction in neurite length, while 10 μM had no significant effect. The same was observed with insulin stimulation. As mentioned earlier, MIG is a less complex compound and its metabolic byproducts are easier to handle by the cell. The reason why the inverse effect is present at low concentrations can be explained by the cellular compensatory mechanisms, where the cell is still able to overcome the inhibitory effect of GSL by upregulating the gene expression of the missing gangliosides synthesizing enzymes and pumping out the inhibitor by efflux pumps. This peak concentration at which the cell is still able to compensate is around 10 μM, and the decrease in length is attributed to the overshooting during compensation.

The shortening of neurites was observed at 2.5 and 10 μM concentrations of CBE, with the highest concentration of 40 μM having an inverse effect. The effect on neurite outgrowth was observed by doubling or tripling the length of neurite after treatment with insulin. The effect on neurite outgrowth was expected, as blocking the β-Galactosidase enzyme stimulates the accumulation of endogenous GM1, which stimulates the growth of neurites through several mechanisms, one related to an increased influx of calcium ions into the cell, and others through the induction of MAP kinases and tau proteins. This has been observed both in the cultures of primary neurons and in established cell lines (193–195). The efficacy of the treatment was best with the addition of insulin and correlates with the previously described IC_{50} value for glucocerebrosidase A (IC_{50}=44.1 μM), which corresponds to the highest concentrations used. This is most likely due to the effect of insulin on transcription and gene expression, which converts the low effect of GM1 accumulation into a significant effect. The reasons why CBE had the opposite effect on neurites are not yet clear, but studies of the effect of higher concentrations without insulin

show that the hypothesized effects are correct. This may well be an inverse hormonal effect of weak ganglioside accumulation (196).

Having said this, to better understand what is happening when P4 inhibitors are applied, enzyme kinetic studies should be performed to determine the extent to which they inhibit the enzyme of interest, especially since there are no studies available for these two isomers. These results may have practical applications in brain injuries when both MIG and CBE are used together. It should reduce the total amount of complex gangliosides such as GD1a and GT1b, while preventing the degradation of existing gangliosides, leaving only these as targets for the endogenous neuraminidase Neu3. This, in turn, should theoretically decouple Nogo receptor inhibition from axon and dendrite growth and stimulate the formation of new neuronal networks. CBE itself has been successfully used to preserve the motor network in a mouse model of amyotrophic lateral sclerosis (197). Further *in vitro* and *in vivo* investigations are necessary to better understand how the combination might work.

6.4. MALDI-TOF MS lipidome analysis

Before analyzing the differences between cells treated with inhibitors and untreated cells in-depth, it is important to establish which changes in the lipidome are caused by insulin treatment and to extend the observed changes from there. The main biochemical modules affected by the application of insulin are ones involved in the biosynthesis of cholesterol sphingosine and ceramide, and from the observation of molecules involved in these pathways, it can be deduced that the reduction in biosynthesis has occurred. A decrease in cholesterol biosynthesis has previously been observed in brain tissue in both neurons and astroglia and is regulated through downregulation of SREBP2 following activation of the insulin signaling cascade (198). Sphingosine and ceramide have an interesting effect on the insulin signaling pathway. It has been previously observed that overload of ceramide usually leads to inhibition of Akt phosphorylation at serine 473, thus cutting off cytokine effect of the insulin, stimulating apoptosis and programmed cell death (199). It was also found that an increase in ceramide levels in skeletal muscle cells occurred after 16 hours of insulin stimulation, leading to a decoupling of insulin signalization (200). The opposite effect was observed in this experiment in neuroblastoma cells after 2-hour treatment with insulin. This is due to the short-term effects of insulin,

where spiking in the transcription of proteins and enzymes also leads to a depletion of accumulated biological material, without sufficient time to accommodate the shortage through negative feedback loops. Interestingly, the reduction in neurite length after insulin application and the previously discussed non-significant change in cell viability are not consistent with this observation and hypothesis.

Treatment of cells with P4-RR inhibitor in all three concentrations affected ceramide and sphingosine biosynthesis. Medium concentration affected the biosynthesis of cholesterol and ergocalciferol, while high concentration affected the biosynthesis of bile acid, triacylglycerol, and inosine. As expected, the addition of insulin to the experimental groups resulted in additional changes, namely in tetrahydrobiopterin metabolism and in thyroid hormone biosynthesis. If we go through the identified compounds, it gives us an interesting insight into the cellular metabolism changes. The degradation of ATRA, a compound used for differentiation of the SH-SY5Y cells is somehow inhibited in cells treated with the highest concentration of P4-RR. This is interesting because the medium used for the treatment did not contain any retinoic acid, only the ATRA that has been introduced into the cells before the treatment. The mechanism by which the processing of retinoic acid was stopped is still unclear. One possibility is that the treatment blocked the cytochrome CYP26B1 enzyme involved in the degradation of ATRA, thus keeping the levels of the compound high (201,202). If examined, one of the commonly used inhibitors for this enzyme has little to no similarity to the P4 compound (203). Also, it is important to note that the elevated concentration of ATRA metabolites implies that other enzymes are affected as well, primarily retinoic acid dehydrogenases that produce 11 and 9-cis retinal, which is only observed at the highest concentrations. No increase in ATRA concentrations was found after insulin administration. The addition of P4-RR independently of concentration reduces the levels of phosphoethanolamine (PE), more specifically 1-Octadecanoyl-2-(5Z,8Z,11Z,14Z-eicosatetraenoyl)-sn-glycero-3-phosphoethanolamine. The group of compounds is an important building block of the cell membrane. According to the Kyoto Encyclopedia of Genes and Genomes (KEGG) database, it is involved in a process of cell death different from apoptosis called ferroptosis, where the accumulation of iron causes cascade oxidation of lipids, which ends in cell death (204,205). A reduction in the level of PE may indicate that it is utilized in the process of ferroptosis, which correlates with the findings of the MTT test, where cell viability is reduced, and with the general lack of Annexin V stain (205). On the other hand, ferroptosis is characterized by the accumulation of toxic

polyunsaturated fatty acids (PUFA), which, once created, propagate further oxidation and subsequent mitochondria-induced cell death (206). It is also possible that the cells either further metabolized this compound during the process of ferroptosis, or the compound was released into the cell growth medium by exocytosis. Another interesting note about this PE isoform is that its levels are elevated in the plasma of morbidly obese people, which links it to the development of insulin resistance and its absence may cause hyperactivation of the insulin signaling cascade (207). This hypothesis needs to be tested *in vitro* in the same cell model to determine the role of PE in insulin signaling. Interestingly, cholesterol precursor, not cholesterol itself, biosynthesis is upregulated. The compound in question is 4 alpha-Methyl zymosterol and it is quite low in the Blotch pathway of cholesterol biosynthesis, seven steps away from the final molecule (208,209). Cholesterol and its precursors are difficult to ionize by MALDI-TOF-MS and usually require a special procedure involving silver or other heavy metals (210). This cholesterol precursor has a methyl group that makes it more susceptible for ionization and it is most likely the reason why it was detected. No data were found on why affecting glycolipid biosynthesis affects cholesterol biosynthesis. Application of insulin reduced the levels of this cholesterol precursor by twelvefold, but this was only observed at the lowest concentration of P4-RR. This correlates with the effect of insulin on cholesterol biosynthesis and with the previous observation using insulin alone, but in this case cholesterol levels were reduced even more. The observed pattern shows that cells are able to compensate for the disruption in cholesterol metabolism caused by the inhibitor up to the point where only the medium concentration showed an effect by itself, and the highest most likely caused enough damage to overload these mechanisms. Going further in analysis of metabolic disruptions, we come to the porphyrins. Porphyrins are molecules integral in building the hem molecule, where only changes that cause the accumulation of porphyrins are of importance as they cause a wide range of symptoms affecting the nervous system such as anxiety, confusion, breathing problems and others organ systems causing constipation, vomiting, general nausea or skin redness and blistering (211,212). Since the first and last three steps of porphyrin synthesis occur inside the mitochondria, it could be that the dysfunction of the mitochondria caused the decrease in porphyrin levels in the cells. This is not a standard molecule readily found in cells, but rather a metabolic intermediate. It has also been found to be a ligand for the mitochondrial translocator protein (TSPO) located in the outer mitochondrial membrane, which serves as a transporter molecule for cholesterol into mitochondria (213). In patients with

Alzheimer's disease, TSPO levels have been elevated and its overactivation was protective against high amyloid protein levels (214). This does not explain why the levels of porphyrin dropped as during the sample preparation, mitochondria were kept in homogenate and no recorded further changes in the metabolism of porphyrin were found in the samples, with the same observed after the insulin was applied to the treated cells. Other molecules strongly tied to the glycolipid metabolism such as sphingosine, dehydrosphinganine, or N-glycolylneuraminate were changed in levels. The change was even more pronounced with the addition of insulin, and when cherry picked molecules are observed, the results correlate as expected. Each of these molecules can be identified as other molecule by examining the mass-to-charge ratio only, so fragmentation analysis is necessary to determine with sufficient confidence which exact molecule was affected by the treatment. Upon insulin addition, changes in the tetrahydrobiopterin (BH4) biosynthesis occurred, and an increase in the levels of precursors and final molecules was found. At the lowest concentrations of the P4-RR inhibitor, the upregulation was the highest and vice versa. BH4 is an important cofactor in the biosynthesis of dopamine (DA), which is one of the hallmarks of the differentiated SH-SY5Y cells (215). The overproduction and accumulation of BH4 lead to auto-oxidation of the molecule and the production of hydrogen peroxide and nitrous oxide, which in the end causes oxidative damage (216,217). It is also important to note that when BH4 is present in higher than usual concentrations, it activates MAPK, p38, and Erk1/2, which are downstream molecules in the insulin signaling pathway. In combination with the activation of the insulin pathway, the production of reactive oxygen radicals usually causes cell death (216). This correlated with MTT, where cells started to die after the addition of insulin, most likely as a result of the overactivation of the insulin signaling pathway. It was observed that BH4 increases insulin sensitivity, this way creating a closed circuit signaling with limited ability to regulate it once cells were challenged with insulin (218). Metabolism of pyruvate was altered and upregulated after the addition of insulin, and this is visible in rising levels of (R)-S-Lactoylglutathione (SLG) with the highest difference in cells treated with medium concentrations. The accumulation of the metabolite could be the result of blockage of the enzyme hydroxy-acyl-glutathione hydrolase (EC:3.1.2.6.), which metabolizes it into D-Lactate and glutathione, or it is the result of excess in its synthesis. The enzyme is located inside mitochondria and accumulation of this metabolite could be an indicator of disfunction linked to the oxidative status. It could be argued this is an attempt of mitochondria to repair oxidative damage and prevent further damage, as

SLG can serve as a backup for regenerating glutathione, which is important for preservation of protein structure and function during times of high oxidative stress (219). Further studies of mitochondrial metabolic changes are necessary to provide a definitive answer. Another effect observed with addition of insulin is the accumulation of iodine. This phenomenon is difficult to explain as cells should have iodine sensitive transporters on the cell membrane that facilitate iodine uptake and the medium should contain a certain amount of the element, but this is not the case. The only source of iodine could be the fetal bovine serum (FBS) used to culture the cells, which is also the source of thyroid hormones, but no FBS was used during experimental procedures, so it begs the questions of wheather the treatment causes a disruption in iodine metabolism in the cells, and why is this only obvious after the insulin application. This could be due to the higher metabolic turnover rate caused by insulin, which accelerates the breakdown of iodine-containing compounds. Further research is necessary to properly address this question.

Treatment of the cells with P4-SS, the second isoform of this inhibitor, caused a similar response to treatment with P4-RR, but with several important differences. The treatment alone caused a decrease in cholesterol biosynthesis and an increase in the production of BH4, and the effect of the treatment was amplified by the addition of insulin, with a sixteenfold decrease in cholesterol levels when cells were treated with the highest inhibitor concentration. Previous studies indicated that inhibition of cholesterol biosynthesis caused neurite outgrowth both *in vitro* and *in vivo* (220). In the experiment where neurite length was measured, a significant neurite outgrowth was recorded after the addition of insulin to the treated cells. The cells did not reach pre-treatment levels, but the increase was significant compared to the insulin-treated control. The reason why the cells could not fully compensate may be due to the large metabolic effect on the cell itself. When only cholesterol levels are affected, the cells can compensate, in contrast to blocking the synthesis of large amounts of glycolipids. As with the RR-isomer, treatment of cells with the SS-isomer is likely to cause ferroptosis, which is observable in PE closely related to this process. The addition of insulin caused an accumulation of SLG in cells treated with a low concentration of the inhibitor, indicating that mitochondria could compensate for oxidative damage up to that point and that with more concentrated treatment mitochondria probably underwent mitochondrial apoptosis, as shown by the MTT results. No observable changes in retinoic acid metabolism were found. The biosynthesis of ceramide and sphingosine was affected by all three concentrations of the compound, both without and with insulin. As with the previous inhibitor, fragmentation

is necessary to draw the correct conclusions to determine exactly which molecule is affected.

Treatment of cells with MIG caused somewhat similar effects in the cells as P4 inhibitors. This is expected due to the effects on the same enzyme. There are some differences, mainly in the effects on second messengers, such as the induction of changes in energy metabolism through modulation of second messenger levels such as cyclo-adenosine monophosphate (cAMP), nicotinamide, and nicotinamide riboside. These changes were not detected in the insulin-treated group. In previous studies, when SH-SY5Y cells overexpressed nicotinamide N-methyltransferase (E.C. 2.1.1.1), thus overproducing N-methyl-nicotinamide (NMNA), neurite outgrowth was recorded and the insulin signaling pathway was modified through alteration of pAkt levels (221,222). In this experiment, neurite outgrowth was observed at the highest concentration of the treatment, and this was the only concentration where the precursor of NMNA, nicotinamide, was three times higher than in the control. In the same treatment group, cAMP levels increased fourfold, indicating several different possibilities. One is that the activity of adenylyl cyclase was upregulated in the same way. This enzyme normally binds to transmembrane receptors and acts as a point of signal transduction in the cell. The second possibility is the inactivation of an enzyme that degrades cAMP – phosphodiesterase due to the role of GM1 in protecting the enzyme from inactivation (223,224). In this experiment, the levels of all gangliosides should decrease after the application of the inhibitor, and the results indicate that effect. Insulin, as a cytokine may affect gene expression in cells and increase the level of the inhibited enzyme, counteracting the effect of the inhibitor and partially compensating for the increase in ganglioside levels. Cholesterol levels are also affected by the low concentration itself. The inhibitory effect increases severalfold when insulin is added, regardless of concentration, and the effect is most pronounced at high concentrations of the inhibitor. The upregulation of tetrahydrobiopterin is present and, as discussed earlier, is likely to affect the sensitization of the insulin signaling pathway in the cells. Despite being a commercially available and clinically approved drug, it has not shown dramatic effects on the cells. If the drug structure is examined, it is a glucose analog that enters the GlcCer synthase enzyme and blocks the synthesis of this GlcCer metabolite. However, there is about 4 g/L of glucose in the cell growth medium that may compete for the position within the enzyme. Nevertheless, a better effect can be expected in cell growth medium with 1

g/L of glucose, which reduces the number of metabolic competitors, and this way simulates the physiological conditions in the body.

Up to this point, the cells have inhibited a point of glycosphingolipid biosynthesis. Treatment with CBE causes blockade of glycolipid degradation and effects of intracellular overload was observed. Ceramide and sphingosine biosynthesis were affected by the addition of CBE, regardless of concentration or insulin treatment. Cholesterol level was downregulated with medium and high concentrations without insulin and in cells treated with insulin regardless of CBE concentration. Previous research has demonstrated that cholesterol glycosylation was downregulated after CBE administration via direct enzyme inhibition (225). This was not observed in the series of experiments, most likely due to a decrease in the sensitivity of the instrument when imaging samples in a broad range, and the change was most likely subtle due to the CBE concentrations used. Other effects on cholesterol levels and CBE treatment have not been recorded in the literature. As previously observed with biosynthesis inhibitors, changes in sphingosine, palmitoyl-ethanolamine, and 3-dehydrosphinganine levels were also detected. The effect was amplified by insulin treatment, most likely due to its effects on gene transcription and activation of cell metabolism. Fragmentation analysis is necessary to determine the true nature of the change, especially due to the opposite result for these compounds at different masses. PE associated with ferroptosis decreased with the application of CBE and insulin. Application of low concentrations of CBE without insulin caused a sevenfold increase in PE, indicating that cells accumulate toxic PUFAs and ferroptosis should progress. It remains a question as to what is the threshold of glycolipid metabolic disruption that triggers one or the other mechanism of compensation, and how cells measure the extent of disruption. However, when cells are treated with a low concentration of CBE and the accumulation of PE is induced by the addition of insulin, a significant increase in BH4 metabolites is induced, suggesting an upregulation of its biosynthesis. Research by Kraft et al. has demonstrated an anti-ferroptosis effect of BH4 excess on the cells, indicating that cells at a low CBE treatment require metabolic stimulation to effectively counteract ferroptosis processes (226). It is important to note that CBE at high concentration caused N-acetylneuraminate accumulation. This is most likely the result of a rescue mechanism of the cell to battle the ganglioside overload, which can be deleterious to the cell. Complete ganglioside degradation is blocked by inhibition of the glucosidase enzyme, and one of the remaining molecular solutions is to cleave sialic acids from the ganglioside structure with the sialidase enzyme to reduce the

effect of the overload. The byproducts of these reactions are N-acetylneuraminate and the less complex ganglioside. This can be further repeated until all sialic acids are clipped off, all the way to the lactosyl ceramide (227,228). This is good proof that the high concentration of CBE inhibitor was high enough to trigger glycolipid accumulation.

6.5. Western blot protein analysis

When the effects of the four compounds on the cells are observed, regardless of them being inhibitors of ganglioside synthesis or inhibitors of degradation of gangliosides, they all share a similar pattern regarding the levels of Akt, pAkt, IRα, and IGF1-Rβ. With each treatment, Akt levels have decreased below untreated levels, mostly regardless of concentration, while pAkt levels increased, sometimes three to fourfold compared to untreated cells. The addition of insulin caused the expected increase in pAkt levels, but this was more pronounced when treatment is combined with insulin. At the same time, IR and IGF1-Rβ levels decreased, indicating either binding of the compounds to the receptors or internally activating them, either way reducing the total levels of receptors through lysosomal degradation. This indicates that treatment by itself causes a shift in the activity of downstream signaling molecules of insulin. Np65 levels had various response regarding the treatment. Insulin alone reduced the Np65 levels, as did the P4-RR and CBE treatments. P4-SS and MIG caused an increase in Np65 levels. Combining treatment with both inhibitor and insulin had an inverse effect in the MIG and CBE treated groups. GSK3β levels generally dropped when cells were treated only with the inhibitors, except for P4-RR, where a decrease was first observed at low concentrations, and more GSK3β was present at higher inhibitor concentrations. The addition of insulin caused a decrease in epitope levels in the control group, and even more so when cells were treated with MIG or P4-RR. Treatment of cells with P4-SS and CBE with the addition of insulin caused an increase in epitope levels. The phosphorylated form of GSK3β was either reduced by treatment or nothing significant happened to its levels. MIG and CBE caused a decrease in epitope levels, which was most pronounced in MIG-treated cells. Treatment of cells with P4-RR caused no change, while P4-SS increased epitope levels, which strengthens the isomer-specific activity. For all compounds, βAPP levels decreased upon treatment, and the same was observed with insulin itself. Combining treatment with insulin resulted in an interesting shift. With P4-RR, the drop in βAPP levels was even more pronounced, and with all other treatments, epitope levels increased above the insulin-treated control,

with the greatest increase in the CBE-treated group. Alpha-synuclein showed an interesting pattern, where both isoforms of P4 inhibitors caused an increase in epitope levels, whereas treatment of cells with CBE and MIG caused a drop in epitope levels. This might indicate additional metabolic stress caused by P4 inhibitors. The addition of insulin caused a drop in epitope levels in cells treated with P4-RR and MIG, a rise in epitope levels in cells treated with CBE, while in cells treated with P4-SS no significant change was observed compared to the insulin-treated control. Changes in pTAU levels were more indicative than statistically significant. The treatments caused a rise in epitope levels, while the addition of insulin alone caused a rise in epitope levels. The combination of inhibitor treatment and insulin usually dropped epitope levels, but the standard deviation was too large for statistical significance.

Before in-depth analysis, it is important to note that many epitopes are directly related to insulin signaling and certain behavior is to be expected from them after insulin hormone application. These molecules are Akt, or pAkt in its activated form, GSK3β, or pGSK3β in its phosphorylated form, and two receptors to which insulin can bind – the IR and the IGF1-receptor. After insulin binds to the receptor, the signaling cascade propagates through the IRS to Akt and phosphorylates it at serine 473, activating it, which was observed in the insulin-treated control group, where a four to sixfold increase in pAkt levels was observed, with a concomitant decrease in AKT levels. The decrease in Akt levels is the result of its dephosphorylation, as the negative feedback loop consisting of lipid phosphatase and protein phosphatase A2 cleaves phosphate groups from pAkt, rendering it inactive (229). Dephosphorylation of pAkt also accelerates its degradation, as the removal of phosphates increases ubiquitination and proteasomal degradation (230). For all inhibitors, the effect of activation of Akt via phosphorylation was observed. The inhibitors activated the insulin signaling pathway to a different extent. For the P4 and MIG inhibitors, it is expected that blocking of GlcCer synthase upregulates ceramide levels and blocks the phosphorylation cascade between IRS and Akt, as previously described in several papers . The reasons why this was not observed in this study is due to the fact that no ceramide overload was found in the MALDI-TOF MS analysis and the cells were able to sufficiently shift the metabolism to avoid ceramide overload. Considering the level of cell death measured by MTT, it could be discussed that cells used this pathway activation to survive by preserving the metabolic structure of the cells and sacrificing the mitochondria. Binding of insulin to the IR itself or the IGF1-receptor causes activation, followed by recycling and partial degradation of the receptor to

maintain downstream cascade regulation (59). It was also previously described that CBE and its variants can bind to and similarly activate the insulin receptor as the hormone itself (187). Since insulin receptor and IGF1-receptor levels were reduced differently, and the insulin signaling cascade was activated, it could be argued that either the GlcCer inhibitors themselves or metabolic byproducts released into the cell medium via exocytosis bound to and activated the receptors. The IR levels were reduced in CBE-treated cells as expected, but no effect was observed with the IGF1-receptor. Another interesting point is that Gb3 globoside and GlcCer can enter lipid raft microdomains and the cell membrane themselves, causing a spatial redistribution of proteins within the membrane, altering their activity, and activating Akt in a receptor-independent pathway (231). This was observed when the GlcCer synthase was overexpressed, and it remains to be seen whether and how the cells in this experiment were able to compensate for the inhibitory effects of P4 and MIG. Challenging cells with insulin in the case of P4-RR caused a significant change in pAkt only in cells treated with the highest concentration of the inhibitor. At the same time, IR levels remained the same or higher and IGF1-receptor levels decreased compared to the control. The opposite effect was observed for the SS isoform, where the highest activation was at low concentrations, but interestingly IR levels raised and IGF1-receptor levels dropped but not below the insulin-treated control. This effect was not observed when cells were MIG-treated and challenged with insulin. The levels of pAkt remained similar to those without insulin. The same could be said for the IR, but not for the IGF1-receptor, whose levels dropped as it was activated. Previous investigations have demonstrated that activation of the IGF1-receptor usually leads to the activation and phosphorylation of Akt (232). Treatment with CBE affected IGF1-receptor levels, and with the addition of insulin, the effect was more than obvious. It could be argued that CBE can also similarly bind to IGF1-receptors to how it binds to and activates the IR, as previously described. This could explain the observed behavior that treatments either destabilize or alter the IGF1-receptor, forcing it to activate without a physiological stimulus i.e without insulin or insulin-like growth factor.

Continuing with the molecules of the insulin signaling cascade, we arrive at GSK3β and its active form which is phosphorylated at tyrosine 216. GSK3β is highly expressed in the CNS and has a regulatory function in modulating mitochondrial activity, apoptotic processes, and cell morphology. Phosphorylation of GSK3β at tyrosine 216 keeps it constitutively active or even enhances its enzymatic activity, only phosphorylation at serine 9 shuts down the enzyme. Interestingly, a twofold increase in

phosphorylation does not significantly affect the level of the non-phosphorylated form, so the ratio of the two may not be necessary to approach the analysis (233). Notably, the application of insulin itself reduced total GSK3β levels, which has not been previously recorded. The use of insulin usually reduces the activity of the kinase but does not reduce the level of the enzyme itself. The combination of treatment and insulin reverted kinase levels to those found in the control group. Also, previous reports have shown that gangliosides did not affect the levels of the kinase itself. This behavior may be because in other experiments cells have been exposed to insulin for a longer period, and kinase levels can bounce back via induced gene expression. However, the effect of glucocorticoids on the degradation of GSK3β via ubiquitin 26S proteasome has been described, but only after 72 hours of exposure and in mammalian epithelial tumor cells (234). The SH-SY5Y line is of tumor origin and similar behavior may occur when differentiated cells are exposed to the insulin for short periods. The extension of the effects of short insulin exposure needs to be further investigated as it may provide insight into how tumor cells respond to short bursts of insulin and provide a focal point for possible treatments. The GSK3β enzyme plays a crucial role in several metabolic pathways, it can be expected that a reduction in its total levels should have a significant impact on the β-catenin signaling pathway, the regulation of apoptosis, and cell survival in general (232,233,235,236). This may explain the low survival rate and the change in cellular behavior when insulin was added to the treated groups, where the cells detached from the bottom of the flask. Treatment of cells with P4-SS but not RR isoform reduced total levels of pGSK3β, but not statistically significantly. However, the addition of insulin had a slightly opposite effect, and the level of the active molecule was higher than in control groups or in inhibitor-treated groups. Since phosphorylation on tyrosine 216 is an autocatalytic event, it could be argued that the gene expression induced by the addition of insulin caused a rise in total GSK3β levels followed by an increase in the levels of the active form. It should be mentioned that in this research the levels of GSK3β phosphorylated at serine 9 were not measured, which would greatly aid to determine which segment of the activity regulation was affected: the kinases that inactivate GSK3β or the autophosphorylation activity itself. The activity pattern observed would be expected if the Akt molecule was inactive due to ceramide overload, which is not the case, because pAkt is four times higher than in the insulin untreated groups, and still there is a rise in GSK3β activity.

Treatment of cells with MIG showed a slightly different story, even though it should affect the same enzyme as P4. The effect on the active form of GSK3β was inhibitory when insulin was applied. This is consistent with current knowledge, and there was no significant effect on baseline levels of GSK3β and the treatment itself did not alter levels of the phosphorylated form (233). CBE had an inhibitory effect on the activity of GSK3β. Since there is an accumulation of glycolipid metabolic byproducts, it is likely that ceramide also accumulates. It was found that the specific C2 ceramide activates the PI3K/Akt signaling pathway, thus deactivating GSK3β, allowing cell anabolic activity, pushing it into cell division, stimulating gene expression regulated by the cAMP response element-binding protein (CREB), and reorganizing the cell metabolic needs (237,238). The effect of individual compounds on the activity and stability of GSK3β needs to be further investigated, as modulation of energy metabolism is possible in both metabolic diseases and cancerous tissue. If the compounds are successful in acting on any of these, it would be of great importance for people suffering from these diseases.

NP is not a newly discovered molecule, but its role is still somewhat unclear, and research to discover most of its roles is gaining traction. Its main role is to regulate neuroplasticity, maintain intracellular calcium levels and facilitate the formation of new synapses. Treatment of cells with inhibitors of GlcCer synthase has generally caused an increase in Np65 levels and it can be argued that this should cause dendrite outgrowth or at least significant changes in cell morphology. If we observe the results pertaining to dendrite length, it is obvious that the increase in Np65 did not aid in the elongation of neurites. The application of insulin reduced the total levels of Np65 if we observed the total length of neurites. The answer to why this happened may be found in the position of the Np65 molecule. The majority of the active molecule is localized inside the lipid rafts, and a small part is localized outside (178). The application of inhibitors and insulin caused a shift of Np65 outside of the rafts thus rendering it inactive. The reason why the shift happened when cells are treated with insulin alone is still unclear. Why are higher levels of Np65 observed in GlcCer inhibitor-treated cells? One answer could be that the cells are trying to compensate for functional loss of the Np65 and have started to produce more molecules. To give a more definitive answer gene expression analysis should be performed. However, Mlinac et al. have described that mice lacking complex gangliosides have several times higher levels of Np mRNA and altered spatial distribution and immunoreactivity towards Np65 in the hippocampus complex gangliosides which are necessary for proper synapse formation (239). MIG had a similar but different effect on

the cell metabolism again. Length of neurites and Np65 levels increased, and even though the addition of insulin caused a sharp drop in Np65 levels, the effect on the length of neurites was not dramatic. The reason why this happens is still unknown. On the other hand, overloading the cells with gangliosides had no significant effect on Np65 levels, and as expected, more gangliosides caused the elongation of neurites. These experiments regarding NPs should be performed on primary neuronal cell culture because in that case direct observation of synaptogenesis would be possible and the real extent of the effects of altered glycolipid levels on NPs could be observed.

Treatment of cells with GlcCer synthase inhibitors almost always led to a reduction in APP levels, and even more so after the application of insulin. It is known that gangliosides play an important role in the regulation of amyloid protein splicing, oligomerization, and propagation of toxic amyloid aggregates. Previous studies have demonstrated that the excess of GM1 leads to the accumulation of amyloid-beta and leads to a reduction in the production of soluble APP through modulation of gamma-secretase activity (240). Experiments utilizing an inhibitor of GlcCer synthesis should reduce total levels of all gangliosides including GM1 thus it is safe to argue that reduction of ganglioside levels leads to a reduction in the total amount of APP as observed in Western blots. The application of insulin also upregulates the activity of the insulin-degrading enzyme, which is a small metalloprotease that cleaves APP and propagates its degradation (241). CBE-treated cells had a different response regarding APP. Levels should have risen because CBE induces the accumulation of glycolipids rather than their depletion. It could also be argued that due to the lack of insulin stimulatory effect there was not enough gene expression activity for the response to the created overload. At the same time, levels of pAKT were several times higher than those of the control group, thus AKT-regulated gene expression should not be impaired. The insulin-degrading enzyme is upregulated by PI3K activity, the same enzyme that activates AKT. Since activity and levels of PI3K were not measured, it is hard to deduce the extent of the treatment effects. There were several described human cases suffering from Gaucher disease and amyloidosis, but no detailed genetic studies have been performed (241–243). A possible explanation is that the activity of the insulin-degrading enzyme was modified after CBE and insulin administration and thus became inactive. Further kinetic studies are necessary to determine the effect of glycolipid overload on enzyme activity.

The TAU protein is a microtubule-associated protein that serves as a stabilizer of microtubule structure and consequently cytoarchitectonics. It has been determined that

1% of total brain proteins are tau proteins. Since phosphorylation of any protein would change its 3D structure and function, the level of phosphorylation of the tau protein is important. In the late stages of AD, phosphorylation levels of serine 202 and threonine 205 positions are increased (244). Treatment of cells with GlcCer inhibitors caused a rise in levels of pTAU and the application of insulin exacerbated this effect. This was even more prominent with P4 type inhibitors. The accumulation of hyperphosphorylated tau protein is somewhat correlated with cell inability to create new neurites but is also related to the level of activity of GSK3β. Previously was described the correlation between increased GSK3β activity and increased phosphorylation of TAU protein (245). Based on this, it is safe to argue that the increased levels of pGSK3β-Tyr206 are part of the reason for the higher phosphorylation of tau protein than in the control group. It has also been found that peripheral hyperinsulinemia promotes hyperphosphorylation of tau protein *in vivo* (246,247). Also, the complex ganglioside GQ1b reduces the level of tau phosphorylation and that is most likely true for other complex gangliosides (248). Since there is the treatment-mediated rise in Akt activity and the decrease in levels of gangliosides, it should be argued that upregulating the activity of Akt and modifying the activity of GSK3β caused a spike in pTAU levels in the cells. CBE treatment causes a spike in the level of pTAU, which is most likely not related to GSK3β due to its lower levels and activity. No data were found for Gaucher disease, CBE, and accumulation of pTAU. This may be because ganglioside and glycolipid overload do not produce pathological changes in the form of neurofibrillary tangles and synucleopathies are the predominant neurodegenerative pathology in patients suffering from Gaucher disease (113,249–251). Further investigation is necessary to determine the exact mechanism of pTAU accumulation and whether this is a potential problem i.e. whether it would lead to the development of pathological neurofibrillary tangles.

Regarding the alpha-synuclein (αSyn), there is a large discrepancy in epitope levels between the control groups of different inhibitors. CBE did not have the expected effects and induced the accumulation of αSyn, especially since this has been previously observed in both *in vitro* and *in vivo* models (252–255). The experiments regarding αSyn should be repeated with higher concentrations of CBE and if higher concentrations of CBE produce the expected effects, then this low dose CBE effect should be re-examined to determine the mechanism of low-level glycolipid accumulation on αSyn. The same can be said for other inhibitors. For now, the discrepancy between literature data and observed effects is too large and it should not be considered valid.

6.6. Prospects of the study

In this study, the inhibitory effects of P4 isoforms and MIG on cell growth were demonstrated. This could be utilized in treating certain tumors with a high glycan profile, such as prostate cancers and certain types of breast cancers. In those types of cancers, it was found that the dysregulation of cell death is due to the inactivation of the PI3K/Akt pathway (256,257). Since treatment with inhibitors theoretically causes a spike in Akt activity, it should activate an apoptotic cascade. Treatment of cell cultures of these tumors should be the first step in assessing the efficiency of this, if the results are promising, research should be extended into animal models. Since the entire insulin signaling cascade was only turned on by the treatment itself, and there were no drastic changes in the positions of the proteins in the membrane, it could be utilized at low concentrations as a modifier of insulin metabolism in people with type 2 diabetes, which could potentially reduce or delay the need for the use of antidiabetic medications (258).

6.7. Limitations of the study

This study has been performed in a cell model that mimics neuronal phenotype when differentiated. It is also a cancerous cell line and the responses to different metabolic challenges do not necessarily correspond to those of the healthy cells lines such as the human fibroblast cell line such as BJ (ATCC-CRL 2522) or primary cell cultures. Repeating these experiments in healthy cell lines and primary cultures of cortical neurons should provide more accurate insights into the extent of the effect of GlcCer inhibition on metabolism. Lipid raft isolation should also be done and subsequent western blot analysis of lipid rafts to determine subtle changes in lipid raft composition that cannot be detected by immunocytochemistry. Fragmentation analysis with molecular standards should also be performed in the analysis of lipid profile by MALT-TOF-MS.

7. CONCLUSIONS

- Treating cells with P4 inhibitors will cause cell death with the effect being aggravated by the addition of insulin, most likely killing off the mitochondria. Miglustat and conduritol B epoxide in given concentrations did not affect cell capability to survive.

- Immunocytochemical staining revealed that P4 inhibitor isoforms have a stereospecific effect. P4 and MIG inhibitors cause the redistribution of βAPP reducing the cell's ability to properly metabolize it, creating long-term cell damage. GM1 ganglioside and IGF1-Rβ shifted into the non-raft part of the cell membrane because of ganglioside synthesis disruption, while CBE did not affect the redistribution of GM1 and IGF1-Rβ.

- Treating cells with GlcCer inhibitor reduced their capability to grow neurites, and only the glycolipid overload has induced neurite growth.

- Lipidome analysis indicated that mitochondrial metabolism was affected with treatment, observed in the change of levels of molecules included in ferroptosis.

- Treatment-induced changes in levels of sphingosine, dehydrosphinganine, and palmitoyl-ethanolamine were as expected. Treatment with GlcCer inhibitors caused downregulated cholesterol biosynthesis via unknown metabolic regulation.

- Disrupting glycolipid biosynthesis causes hyperactivation of the insulin signaling cascade observable in increased levels of pAkt, pGSK3β, and reduced levels of insulin receptor and IGF1-Rβ. CBE in sub-effective concentrations had an unexpected effect on the insulin signaling cascade, causing its hyperactivation.

8. SUMMARY

Objectives: Gangliosides are essential for stabilizing and organization of the membrane microdomains, which serve as communication hubs for relaying insulin signaling into the cell. Interfering with ganglioside synthesis should disrupt insulin signaling by downregulation or upregulation, depending on which enzyme is disrupted. This, in turn, should cause changes in cell neuroplasticity, morphology, and tolerance to insulin challenge.

Study design: SH-SY5Y human neuroblastoma cell line was differentiated for 10 days with retinoic acid and treated for 48 hours with two isoforms of P4 inhibitor of ganglioside synthesis, miglustat inhibitor of ganglioside synthesis, and inhibitor of glycolipid degradation – conduritol B epoxide.

Material and methods: For MTT, cells were grown, differentiated, and treated in collagen-coated 96 healthy plates. After treatment, cell viability was determined. Cells were grown and differentiated on collagen-coated glass slides for immunocytochemistry and morphology and stained with specific antibodies for epitopes of interest, and FITC dye for morphology. For Annexin V, Western blots, and MALDI-TOF, cells were grown in six biological replicas for each treatment concentration and protocol in 6-well plates. After treatment cells were scraped, homogenated, and prepared for further analysis by flow cytometry, Western blot, or MALDI-TOF MS.

Results: Interfering with glycolipid biosynthesis caused dose-dependent cell death and change in morphology. Miglustat caused expected morphology changes in the form of neurite elongation, whilst CBE in sub-effective concentrations had the reverse effect on cell morphology. The insulin signaling pathway was upregulated with all treatments. Cells demonstrated changes in neuroplasticity and different responses to induced metabolic stress depending on which inhibitor was applied.

Conclusion: Disrupting glycolipid composition will interfere with insulting signaling, cause morphological changes, and disrupt the neuroplasticity of the cells.

Keywords: SH-SY5Y, miglustat, conduritol B epoxide, insulin, neuroplasticity.

SAŽETAK

Cilj: Gangliozidi su važni za stabilizaciju i organizaciju membranskih mikrodomena koji služe kao komunikacijska središta za prenošenje inzulinske signalizacije u stanicu. Ometanje sinteze gangliozida trebalo bi poremetiti inzulinsku signalizaciju pojačavajući je ili snižavajući, ovisno o tome koji je enzim poremećen. To bi pak trebalo uzrokovati promjene u staničnoj neuroplastičnosti, morfologiji i toleranciji na inzulin.

Ustroj studije: Stanična linija humanog neuroblastoma SH-SY5Y diferencirana je 10 dana retinoičnom kiselinom i tretirana 48 sati s dvije izoforme P4 inhibitora sinteze gangliozida, miglustat inhibitorom sinteze gangliozida i inhibitorom razgradnje glikolipida - conduritol B epoksidom.

Materijali i metode: Za MTT stanice su uzgajane, diferencirane i tretirane u pločicama s 96 jažica presvučenih kolagenom. Nakon tretmana utvrđena je održivost stanica. Stanice su uzgajane i diferencirane na pokrovnim staklima presvučenim kolagenom za imunocitokemiju i morfologiju i obojane specifičnim antitijelima za epitope od interesa te FITC bojom za morfologiju. Za Aneksin V, western blot i MALDI-TOF analize, stanice su uzgajane u šest bioloških replika za svaku koncentraciju u pločicama sa 6 jažica, nakon što su tretirane stanice sastrugane, homogenirane i pripremljene za daljnju analizu protočnom citometrijom, western blotom ili MALDI- TOF MS.

Rezultati: ometanje biosinteze glikolipida uzrokuje o dozi ovisnu staničnu smrt i promjenu morfologije. Miglustat je uzrokovao očekivane morfološke promjene u obliku produljenja neurita, dok je CBE u sufektivnim koncentracijama imao reverzni učinak na staničnu morfologiju. Put signalizacije inzulina bio je pojačan u svim tretmanima. Stanice su pokazale promjene u neuroplastičnosti i različit odgovor na inducirani metabolički stres, ovisno o tome koji je inhibitor primijenjen.

Zaključak: Ometanje sastava glikolipida ometat će inzulinsku signaliziraciju, uzrokovati morfološke promjene i poremetiti neuroplastičnost stanica.

Ključne riječi: SH-SY5Y, miglustat, conduritol B epoksid, inzulin, neuroplastičnost.

9. REFERENCES

1. Plasma Membrane (Cell Membrane) [Internet]. Genome.gov. [cited 2020 Feb 1]. Available from: https://www.genome.gov/genetics-glossary/Plasma-Membrane

2. Griffiths G. Cell evolution and the problem of membrane topology. Nat Rev Mol Cell Biol. 2007 Dec;8(12):1018–24.

3. Gould SB. Membranes and evolution. Curr Biol. 2018 Apr;28(8):R381–5.

4. Evolutionary Remodeling of the Cell Envelope in Bacteria of the Planctomycetes Phylum | Genome Biology and Evolution | Oxford Academic [Internet]. [cited 2021 Jan 6]. Available from: https://academic.oup.com/gbe/article/12/9/1528/5882020

5. Vollmer W. Bacterial outer membrane evolution via sporulation? Nat Chem Biol. 2012 Jan;8(1):14–8.

6. Frontiers | Does Cholesterol Play a Role in the Bacterial Selectivity of Antimicrobial Peptides? | Immunology [Internet]. [cited 2021 Jan 6]. Available from: https://www.frontiersin.org/articles/10.3389/fimmu.2012.00195/full

7. Lipid map of the mammalian cell | Journal of Cell Science [Internet]. [cited 2021 Jan 6]. Available from: https://jcs.biologists.org/content/124/1/5

8. Li H, Lykotrafitis G. Erythrocyte Membrane Model with Explicit Description of the Lipid Bilayer and the Spectrin Network. Biophys J. 2014 Aug 5;107(3):642–53.

9. Casares D, Escribá PV, Rosselló CA. Membrane Lipid Composition: Effect on Membrane and Organelle Structure, Function and Compartmentalization and Therapeutic Avenues. Int J Mol Sci [Internet]. 2019 May 1 [cited 2021 Jan 6];20(9). Available from: https://www.ncbi.nlm.nih.gov/pmc/articles/PMC6540057/

10. Merrill AH, Vu MN. Glycolipids. In: Bradshaw RA, Stahl PD, editors. Encyclopedia of Cell Biology [Internet]. Waltham: Academic Press; 2016 [cited 2021 Jan 3]. p. 180–93. Available from: http://www.sciencedirect.com/science/article/pii/B9780123944474100227

11. Maxfield FR, van Meer G. Cholesterol, the central lipid of mammalian cells. Curr Opin Cell Biol. 2010 Aug;22(4):422–9.

12. Goluszko P, Nowicki B. Membrane Cholesterol: a Crucial Molecule Affecting Interactions of Microbial Pathogens with Mammalian Cells. Infect Immun. 2005 Dec;73(12):7791–6.

13. Moulton ER, Hirsche KJ, Hobbs ML, Schwab JM, Bailey EG, Bell JD. Examining the effects of cholesterol on model membranes at high temperatures: Laurdan and Patman see it differently. Biochim Biophys Acta BBA - Biomembr. 2018 Aug 1;1860(8):1571–9.

14. Schön A, Clarkson BR, Jaime M, Freire E. Temperature stability of proteins: Analysis of irreversible denaturation using isothermal calorimetry. Proteins. 2017 Nov;85(11):2009–16.

15. Else PL, Turner N, Hulbert AJ. The Evolution of Endothermy: Role for Membranes and Molecular Activity. Physiol Biochem Zool Ecol Evol Approaches. 2004;77(6):950–8.

16. Hassett RP, Crockett EL. Habitat temperature is an important determinant of cholesterol contents in copepods. J Exp Biol. 2009 Jan 1;212(1):71–7.

17. Reynolds AM, Lee RE, Costanzo JP. Membrane adaptation in phospholipids and cholesterol in the widely distributed, freeze-tolerant wood frog, Rana sylvatica. J Comp Physiol B. 2014 Apr 1;184(3):371–83.

18. Alberts B, Johnson A, Lewis J, Raff M, Roberts K, Walter P. The Lipid Bilayer. Mol Biol Cell 4th Ed [Internet]. 2002 [cited 2021 Jan 6]; Available from: https://www.ncbi.nlm.nih.gov/books/NBK26871/

19. Bhattacharya A, Brea RJ, Niederholtmeyer H, Devaraj NK. A minimal biochemical route towards de novo formation of synthetic phospholipid membranes. Nat Commun. 2019 Jan 17;10(1):300.

20. History of Sialic Acids, Gangliosides, and GM3 | SpringerLink [Internet]. [cited 2021 Jan 30]. Available from: https://link.springer.com/chapter/10.1007/978-981-15-5652-4_1

21. Hakomori S. Structure, organization, and function of glycosphingolipids in membrane. Curr Opin Hematol. 2003 Jan;10(1):16–24.

22. Hölzl G, Dörmann P. Structure and function of glycoglycerolipids in plants and bacteria. Prog Lipid Res. 2007 Sep 1;46(5):225–43.

23. Bandet CL, Tan-Chen S, Bourron O, Le Stunff H, Hajduch E. Sphingolipid Metabolism: New Insight into Ceramide-Induced Lipotoxicity in Muscle Cells. Int J Mol Sci. 2019 Jan;20(3):479.

24. Hanafusa K, Hotta T, Iwabuchi K. Glycolipids: Linchpins in the Organization and Function of Membrane Microdomains. Front Cell Dev Biol [Internet]. 2020 [cited 2021 Jan 23];8. Available from: https://www.frontiersin.org/articles/10.3389/fcell.2020.589799/full

25. Honke K. Biosynthesis and biological function of sulfoglycolipids. Proc Jpn Acad Ser B. 2013;89(4):129–38.

26. Schnaar RL. Gangliosides of the vertebrate nervous system. J Mol Biol. 2016 Aug 14;428(16):3325–36.

27. Sandhoff K, Kolter T. Biosynthesis and degradation of mammalian glycosphingolipids. Philos Trans R Soc B Biol Sci. 2003 May 29;358(1433):847–61.

28. Kolter T, Proia RL, Sandhoff K. Combinatorial ganglioside biosynthesis. J Biol Chem. 2002 Jul 19;277(29):25859–62.

29. Eckhardt M. The role and metabolism of sulfatide in the nervous system. Mol Neurobiol. 2008 Jun;37(2–3):93–103.

30. Substantial sulfatide deficiency and ceramide elevation in very early Alzheimer's disease: potential role in disease pathogenesis - Han - 2002 - Journal of Neurochemistry - Wiley Online Library [Internet]. [cited 2021 Jan 30]. Available from: https://onlinelibrary.wiley.com/doi/full/10.1046/j.1471-4159.2002.00997.x

31. Regina Todeschini A, Hakomori S. Functional role of glycosphingolipids and gangliosides in control of cell adhesion, motility, and growth, through glycosynaptic microdomains. Biochim Biophys Acta. 2008 Mar;1780(3):421–33.

32. Jackson SN, Colsch B, Egan T, Lewis EK, Schultz JA, Woods AS. Gangliosides' analysis by MALDI-ion mobility MS. The Analyst. 2011 Feb 7;136(3):463–6.

33. Mlinac K, Fabris D, Vukelić Z, Rožman M, Heffer M, Bognar SK. Structural analysis of brain ganglioside acetylation patterns in mice with altered ganglioside biosynthesis. Carbohydr Res. 2013 Dec 15;382:1–8.

34. Davies LRL, Varki A. Why Is N-Glycolylneuraminic Acid Rare in the Vertebrate Brain? Top Curr Chem. 2015;366:31–54.

35. Schnaar RL. Animal Glycolipids. In: eLS [Internet]. American Cancer Society; 2015 [cited 2021 Feb 21]. p. 1–13. Available from: https://onlinelibrary.wiley.com/doi/abs/10.1002/9780470015902.a0000706.pub3

36. Schnaar RL, Kinoshita T. Glycosphingolipids. In: Varki A, Cummings RD, Esko JD, Stanley P, Hart GW, Aebi M, et al., editors. Essentials of Glycobiology [Internet]. 3rd ed. Cold Spring Harbor (NY): Cold Spring Harbor Laboratory Press; 2015 [cited 2021 Feb 21]. Available from: http://www.ncbi.nlm.nih.gov/books/NBK453016/

37. Rahmann H, Rösner H, Sonnentag U, Esders S. Gangliosides and regeneration of the goldfish optic nerve in vivo and in vitro. Neurochem Int. 1992 Apr 1;20(3):371–83.

38. Atomic-resolution conformational analysis of the GM3 ganglioside in a lipid bilayer and its implications for ganglioside–protein recognition at membrane surfaces [Internet]. [cited 2021 Feb 21]. Available from: https://www.ncbi.nlm.nih.gov/pmc/articles/PMC2733776/

39. Aureli M, Mauri L, Ciampa MG, Prinetti A, Toffano G, Secchieri C, et al. GM1 Ganglioside: Past Studies and Future Potential. Mol Neurobiol. 2016 Apr 1;53(3):1824–42.

40. Ong RL, Yu RK. 1H-NMR assignments of GM1-oligosaccharide in deuterated water at 500 MHz by two-dimensional spin-echo J-correlated spectroscopy. Arch Biochem Biophys. 1986 Feb 15;245(1):157–66.

41. Sonnino S, Prinetti A. Membrane domains and the "lipid raft" concept. Curr Med Chem. 2013;20(1):4–21.

42. The mystery of membrane organization: composition, regulation and roles of lipid rafts | Nature Reviews Molecular Cell Biology [Internet]. [cited 2021 Feb 22]. Available from: https://www.nature.com/articles/nrm.2017.16

43. Prinetti A, Chigorno V, Prioni S, Loberto N, Marano N, Tettamanti G, et al. Changes in the lipid turnover, composition, and organization, as sphingolipid-enriched membrane domains, in rat cerebellar granule cells developing in vitro. J Biol Chem. 2001 Jun 15;276(24):21136–45.

44. L C, E DF, S S, A P. Gangliosides and the multiscale modulation of membrane structure. Chem Phys Lipids. 2011 Sep 19;164(8):796–810.

45. Levental I, Levental KR, Heberle FA. Lipid Rafts: Controversies Resolved, Mysteries Remain. Trends Cell Biol. 2020 May 1;30(5):341–53.

46. Klymchenko AS, Kreder R. Fluorescent Probes for Lipid Rafts: From Model Membranes to Living Cells. Chem Biol. 2014 Jan 16;21(1):97–113.

47. van Deventer S, Arp AB, van Spriel AB. Dynamic Plasma Membrane Organization: A Complex Symphony. Trends Cell Biol. 2021 Feb 1;31(2):119–29.

48. Petersen EN, Chung H-W, Nayebosadri A, Hansen SB. Kinetic disruption of lipid rafts is a mechanosensor for phospholipase D. Nat Commun. 2016 Dec 15;7(1):13873.

49. Lee I-H, Imanaka MY, Modahl EH, Torres-Ocampo AP. Lipid Raft Phase Modulation by Membrane-Anchored Proteins with Inherent Phase Separation Properties. ACS Omega. 2019 Apr 30;4(4):6551–9.

50. Da Silva JS, Hasegawa T, Miyagi T, Dotti CG, Abad-Rodriguez J. Asymmetric membrane ganglioside sialidase activity specifies axonal fate. Nat Neurosci. 2005 May;8(5):606–15.

51. Kappagantula S, Andrews MR, Cheah M, Abad-Rodriguez J, Dotti CG, Fawcett JW. Neu3 Sialidase-Mediated Ganglioside Conversion Is Necessary for Axon Regeneration and Is Blocked in CNS Axons. J Neurosci. 2014 Feb 12;34(7):2477–92.

52. Miyagi T, Yamaguchi K. Mammalian sialidases: physiological and pathological roles in cellular functions. Glycobiology. 2012 Jul;22(7):880–96.

53. Kabayama K, Sato T, Saito K, Loberto N, Prinetti A, Sonnino S, et al. Dissociation of the insulin receptor and caveolin-1 complex by ganglioside GM3 in the state of insulin resistance. Proc Natl Acad Sci U S A. 2007 Aug 21;104(34):13678–83.

54. Farooqui T, Franklin T, Pearl DK, Yates AJ. Ganglioside GM1 enhances induction by nerve growth factor of a putative dimer of TrkA. J Neurochem. 1997 Jun;68(6):2348–55.

55. Prendergast J, Umanah GKE, Yoo S-W, Lagerlöf O, Motari MG, Cole RN, et al. Ganglioside regulation of AMPA receptor trafficking. J Neurosci Off J Soc Neurosci. 2014 Sep 24;34(39):13246–58.

56. Boccuto L, Aoki K, Flanagan-Steet H, Chen C-F, Fan X, Bartel F, et al. A mutation in a ganglioside biosynthetic enzyme, ST3GAL5, results in salt & pepper syndrome, a neurocutaneous disorder with altered glycolipid and glycoprotein glycosylation. Hum Mol Genet. 2014 Jan 15;23(2):418–33.

57. DeFronzo RA, Mandarino LJ. Insulin Actions. In: Henry HL, Norman AW, editors. Encyclopedia of Hormones [Internet]. New York: Academic Press; 2003 [cited 2021 Jan 3]. p. 333–47. Available from: http://www.sciencedirect.com/science/article/pii/B0123411033001765

58. Chan S. Insulin Receptor. In: Enna SJ, Bylund DB, editors. xPharm: The Comprehensive Pharmacology Reference [Internet]. New York: Elsevier; 2007 [cited 2021 Jan 3]. p. 1–5. Available from: http://www.sciencedirect.com/science/article/pii/B9780080552323603605

59. Haeusler RA, McGraw TE, Accili D. Biochemical and cellular properties of insulin receptor signalling. Nat Rev Mol Cell Biol. 2018 Jan;19(1):31–44.

60. Uchikawa E, Choi E, Shang G, Yu H, Bai X. Activation mechanism of the insulin receptor revealed by cryo-EM structure of the fully liganded receptor–ligand complex. Brunger AT, Cole PA, Grigorieff N, editors. eLife. 2019 Aug 22;8:e48630.

61. Kabayama K, Sato T, Saito K, Loberto N, Prinetti A, Sonnino S, et al. Dissociation of the insulin receptor and caveolin-1 complex by ganglioside GM3 in the state of insulin resistance. Proc Natl Acad Sci. 2007 Aug 21;104(34):13678–83.

62. Ceresa BP, Kao AW, Santeler SR, Pessin JE. Inhibition of Clathrin-Mediated Endocytosis Selectively Attenuates Specific Insulin Receptor Signal Transduction Pathways. Mol Cell Biol. 1998 Jul;18(7):3862–70.

63. Araki E, Lipes MA, Patti ME, Brüning JC, Haag B, Johnson RS, et al. Alternative pathway of insulin signalling in mice with targeted disruption of the IRS-1 gene. Nature. 1994 Nov 10;372(6502):186–90.

64. Mardilovich K, Pankratz SL, Shaw LM. Expression and function of the insulin receptor substrate proteins in cancer. Cell Commun Signal. 2009 Jun 17;7(1):14.

65. Delahaye L, Mothe-Satney I, Myers MG, White MF, Van Obberghen E. Interaction of insulin receptor substrate-1 (IRS-1) with phosphatidylinositol 3-kinase: effect of substitution of serine for alanine in potential IRS-1 serine phosphorylation sites. Endocrinology. 1998 Dec;139(12):4911–9.

66. Mitotic regulators and the SHP2-MAPK pathway promote IR endocytosis and feedback regulation of insulin signaling | Nature Communications [Internet]. [cited 2021 Mar 7]. Available from: https://www.nature.com/articles/s41467-019-09318-3

67. He W, O'Neill TJ, Gustafson TA. Distinct Modes of Interaction of SHC and Insulin Receptor Substrate-1 with the Insulin Receptor NPEY Region via Non-SH2 Domains. J Biol Chem. 1995 Oct 6;270(40):23258–62.

68. Lee S, Lynn EG, Kim J, Quon MJ. Protein Kinase C-ζ Phosphorylates Insulin Receptor Substrate-1, -3, and -4 But Not -2: Isoform Specific Determinants of Specificity in Insulin Signaling. Endocrinology. 2008 May;149(5):2451–8.

69. Ali M, Bukhari SA, Ali M, Lee H-W. Upstream signalling of mTORC1 and its hyperactivation in type 2 diabetes (T2D). BMB Rep. 2017 Dec;50(12):601–9.

70. Yoon M-S. The Role of Mammalian Target of Rapamycin (mTOR) in Insulin Signaling. Nutrients [Internet]. 2017 Oct 27 [cited 2021 Mar 7];9(11). Available from: https://www.ncbi.nlm.nih.gov/pmc/articles/PMC5707648/

71. The X-Linked Inhibitor of Apoptosis Protein Enhances Survival of Murine Islet Allografts | Diabetes [Internet]. [cited 2021 Mar 7]. Available from: https://diabetes.diabetesjournals.org/content/54/9/2533

72. Jolivalt CG, Lee CA, Beiswenger KK, Smith JL, Orlov M, Torrance MA, et al. Defective insulin signaling pathway and increased GSK-3 activity in the brain of diabetic mice: parallels with Alzheimer's disease and correction by insulin. J Neurosci Res. 2008 Nov 15;86(15):3265–74.

73. Wada A. GSK-3 inhibitors and insulin receptor signaling in health, disease, and therapeutics. Front Biosci Landmark Ed. 2009 Jan 1;14:1558–70.

74. Dupont J, Karas M, LeRoith D. The Potentiation of Estrogen on Insulin-like Growth Factor I Action in MCF-7 Human Breast Cancer Cells Includes Cell Cycle Components*. J Biol Chem. 2000 Nov 17;275(46):35893–901.

75. Lai A, Sarcevic B, Prall OWJ, Sutherland RL. Insulin/Insulin-like Growth Factor-I and Estrogen Cooperate to Stimulate Cyclin E-Cdk2 Activation and Cell Cycle Progression in MCF-7 Breast Cancer Cells through Differential Regulation of Cyclin E and p21WAF1/Cip1*. J Biol Chem. 2001 Jul 13;276(28):25823–33.

76. Serine 332 Phosphorylation of Insulin Receptor Substrate-1 by Glycogen Synthase Kinase-3 Attenuates Insulin Signaling [Internet]. [cited 2020 Dec 25]. Available from: https://www.jbc.org/content/280/6/4422.long

77. Andreozzi F, Laratta E, Sciacqua A, Perticone F, Sesti G. Angiotensin II impairs the insulin signaling pathway promoting production of nitric oxide by inducing phosphorylation of insulin receptor substrate-1 on Ser312 and Ser616 in human umbilical vein endothelial cells. Circ Res. 2004 May 14;94(9):1211–8.

78. Luo M, Langlais P, Yi Z, Lefort N, De Filippis EA, Hwang H, et al. Phosphorylation of human insulin receptor substrate-1 at Serine 629 plays a positive role in insulin signaling. Endocrinology. 2007 Oct;148(10):4895–905.

79. Sparatore B, Patrone M, Passalacqua M, Pedrazzi M, Pontremoli S, Melloni E. Human Neuroblastoma Cell Differentiation Requires Protein Kinase C-θ. Biochem Biophys Res Commun. 2000 Dec 20;279(2):589–94.

80. Li Y, Soos TJ, Li X, Wu J, DeGennaro M, Sun X, et al. Protein Kinase C θ Inhibits Insulin Signaling by Phosphorylating IRS1 at Ser1101. J Biol Chem. 2004 Oct 29;279(44):45304–7.

81. Bernstein H-G, Smalla K-H, Bogerts B, Gordon-Weeks PR, Beesley PW, Gundelfinger ED, et al. The immunolocalization of the synaptic glycoprotein neuroplastin differs substantially between the human and the rodent brain. Brain Res. 2007 Feb 23;1134(1):107–12.

82. Maness PF, Schachner M. Neural recognition molecules of the immunoglobulin superfamily: signaling transducers of axon guidance and neuronal migration. Nat Neurosci. 2007 Jan;10(1):19–26.

83. Hill IE, Selkirk CP, Hawkes RB, Beesley PW. Characterization of novel glycoprotein components of synaptic membranes and postsynaptic densities, gp65 and gp55, with a monoclonal antibody. Brain Res. 1988 Sep 27;461(1):27–43.

84. Desrivières S, Lourdusamy A, Tao C, Toro R, Jia T, Loth E, et al. Single nucleotide polymorphism in the neuroplastin locus associates with cortical thickness and intellectual ability in adolescents. Mol Psychiatry. 2015 Feb;20(2):263–74.

85. Carrott L, Bowl MR, Aguilar C, Johnson SL, Chessum L, West M, et al. Absence of Neuroplastin-65 Affects Synaptogenesis in Mouse Inner Hair Cells and Causes Profound Hearing Loss. J Neurosci. 2016 Jan 6;36(1):222–34.

86. Amuti S, Tang Y, Wu S, Liu L, Huang L, Zhang H, et al. Neuroplastin 65 mediates cognitive functions via excitatory/inhibitory synapse imbalance and ERK signal pathway. Neurobiol Learn Mem. 2016 Jan 1;127:72–83.

87. Empson RM, Buckby LE, Kraus M, Bates KJ, Crompton MR, Gundelfinger ED, et al. The cell adhesion molecule neuroplastin-65 inhibits hippocampal long-term potentiation via a mitogen-activated protein kinase p38-dependent reduction in surface expression of GluR1-containing glutamate receptors. J Neurochem. 2006 Nov;99(3):850–60.

88. Herrera-Molina R, Mlinac-Jerkovic K, Ilic K, Stöber F, Vemula SK, Sandoval M, et al. Neuroplastin deletion in glutamatergic neurons impairs selective brain functions and calcium regulation: implication for cognitive deterioration. Sci Rep. 2017 Aug 4;7(1):7273.

89. Ilic K, Mlinac-Jerkovic K, Jovanov-Milosevic N, Simic G, Habek N, Bogdanovic N, et al. Hippocampal expression of cell-adhesion glycoprotein neuroplastin is altered in Alzheimer's disease. J Cell Mol Med. 2019 Feb;23(2):1602–7.

90. Kheiri G, Dolatshahi M, Rahmani F, Rezaei N. Role of p38/MAPKs in Alzheimer's disease: implications for amyloid beta toxicity targeted therapy. Rev Neurosci. 2019 Jan 1;30(1):9–30.

91. Lipid Rafts: Controversies Resolved, Mysteries Remain: Trends in Cell Biology [Internet]. [cited 2020 Oct 26]. Available from: https://www.cell.com/trends/cell-biology/fulltext/S0962-8924(20)30031-3

92. Simons K, Ikonen E. Functional rafts in cell membranes. Nature. 1997 Jun;387(6633):569–72.

93. Functions of lipid raft membrane microdomains at the blood–brain barrier | SpringerLink [Internet]. [cited 2021 Feb 22]. Available from: https://link.springer.com/article/10.1007/s00109-009-0488-6

94. Simons K, Toomre D. Lipid rafts and signal transduction. Nat Rev Mol Cell Biol. 2000 Oct;1(1):31–9.

95. Yu RK, Tsai Y-T, Ariga T, Yanagisawa M. Structures, biosynthesis, and functions of gangliosides--an overview. J Oleo Sci. 2011;60(10):537–44.

96. Ariga T, Wakade C, Yu RK. The Pathological Roles of Ganglioside Metabolism in Alzheimer's Disease: Effects of Gangliosides on Neurogenesis. Int J Alzheimers Dis [Internet]. 2011 Jan 9 [cited 2021 Mar 21];2011. Available from: https://www.ncbi.nlm.nih.gov/pmc/articles/PMC3025365/

97. Zhang Y, Zhao Y, Zhang L, Yu W, Wang Y, Chang W. Cellular Prion Protein as a Receptor of Toxic Amyloid-β42 Oligomers Is Important for Alzheimer's Disease. Front Cell Neurosci [Internet]. 2019 Jul 30 [cited 2021 Mar 24];13. Available from: https://www.ncbi.nlm.nih.gov/pmc/articles/PMC6682659/

98. Rushworth JV, Hooper NM. Lipid Rafts: Linking Alzheimer's Amyloid-β Production, Aggregation, and Toxicity at Neuronal Membranes. Int J Alzheimers Dis [Internet]. 2010 Dec 27 [cited 2019 May 11];2011. Available from: https://www.ncbi.nlm.nih.gov/pmc/articles/PMC3014710/

99. Gonzalez-Perez O. Neural stem cells in the adult human brain. Biol Biomed Rep. 2012;2(1):59–69.

100. Seki T, Hori T, Miyata H, Maehara M, Namba T. Analysis of proliferating neuronal progenitors and immature neurons in the human hippocampus surgically removed from control and epileptic patients. Sci Rep. 2019 Dec 3;9(1):18194.

101. Goldman SA, Sim F. Neural progenitor cells of the adult brain. Novartis Found Symp. 2005;265:66–80; discussion 82-97.

102. Drouin E, Drouin G. The first report of Alzheimer's disease. Lancet Neurol. 2017 Sep 1;16(9):687.

103. Braak H, Braak E. Alzheimer's disease affects limbic nuclei of the thalamus. Acta Neuropathol (Berl). 1991;81(3):261–8.

104. Hardy J. A Hundred Years of Alzheimer's Disease Research. Neuron. 2006 Oct 5;52(1):3–13.

105. 2018 Alzheimer's disease facts and figures. Alzheimers Dement. 2018 Mar 1;14(3):367–429.

106. de Paula V de JR, Guimarães FM, Diniz BS, Forlenza OV. Neurobiological pathways to Alzheimer's disease: Amyloid-beta, TAU protein or both? Dement Neuropsychol. 2009;3(3):188–94.

107. Goedert M. NEURODEGENERATION. Alzheimer's and Parkinson's diseases: The prion concept in relation to assembled Aβ, tau, and α-synuclein. Science. 2015 Aug 7;349(6248):1255555.

108. Müller UC, Deller T, Korte M. Not just amyloid: physiological functions of the amyloid precursor protein family. Nat Rev Neurosci. 2017 May;18(5):281–98.

109. O'Brien RJ, Wong PC. Amyloid Precursor Protein Processing and Alzheimer's Disease. Annu Rev Neurosci. 2011;34:185–204.

110. Ikeda K, Yamaguchi T, Fukunaga S, Hoshino M, Matsuzaki K. Mechanism of amyloid β-protein aggregation mediated by GM1 ganglioside clusters. Biochemistry. 2011 Jul 26;50(29):6433–40.

111. Ferreira ST, Lourenco MV, Oliveira MM, De Felice FG. Soluble amyloid-β oligomers as synaptotoxins leading to cognitive impairment in Alzheimer's disease. Front Cell Neurosci [Internet]. 2015 May 26 [cited 2021 Mar 7];9. Available from: https://www.ncbi.nlm.nih.gov/pmc/articles/PMC4443025/

112. Cline EN, Bicca MA, Viola KL, Klein WL. The Amyloid-β Oligomer Hypothesis: Beginning of the Third Decade. J Alzheimers Dis. 64(Suppl 1):S567–610.

113. Role of tau protein in both physiological and pathological conditions - PubMed [Internet]. [cited 2021 Mar 7]. Available from: https://pubmed.ncbi.nlm.nih.gov/15044677/

114. Frontiers | Hyperphosphorylation of Tau Associates With Changes in Its Function Beyond Microtubule Stability | Cellular Neuroscience [Internet]. [cited 2021 Mar 7]. Available from: https://www.frontiersin.org/articles/10.3389/fncel.2018.00338/full

115. Yamazaki Y, Zhao N, Caulfield TR, Liu C-C, Bu G. Apolipoprotein E and Alzheimer disease: pathobiology and targeting strategies. Nat Rev Neurol. 2019 Sep;15(9):501–18.

116. Liu C-C, Kanekiyo T, Xu H, Bu G. Apolipoprotein E and Alzheimer disease: risk, mechanisms, and therapy. Nat Rev Neurol. 2013 Feb;9(2):106–18.

117. Gómez-Benito M, Granado N, García-Sanz P, Michel A, Dumoulin M, Moratalla R. Modeling Parkinson's Disease With the Alpha-Synuclein Protein. Front Pharmacol [Internet]. 2020 Apr 23 [cited 2021 Mar 7];11. Available from: https://www.ncbi.nlm.nih.gov/pmc/articles/PMC7191035/

118. Sveinbjornsdottir S. The clinical symptoms of Parkinson's disease. J Neurochem. 2016;139(S1):318–24.

119. Klein C, Westenberger A. Genetics of Parkinson's Disease. Cold Spring Harb Perspect Med [Internet]. 2012 Jan [cited 2021 Mar 7];2(1). Available from: https://www.ncbi.nlm.nih.gov/pmc/articles/PMC3253033/

120. Kakio A, Nishimoto S, Yanagisawa K, Kozutsumi Y, Matsuzaki K. Interactions of amyloid beta-protein with various gangliosides in raft-like membranes: importance of GM1 ganglioside-bound form as an endogenous seed for Alzheimer amyloid. Biochemistry. 2002 Jun 11;41(23):7385–90.

121. Matsuzaki K, Kato K, Yanagisawa K. Abeta polymerization through interaction with membrane gangliosides. Biochim Biophys Acta. 2010 Aug;1801(8):868–77.

122. Ariga T. Pathogenic role of ganglioside metabolism in neurodegenerative diseases. J Neurosci Res. 2014 Oct;92(10):1227–42.

123. Yanagisawa K. Role of gangliosides in Alzheimer's disease. Biochim Biophys Acta. 2007 Aug;1768(8):1943–51.

124. Chiricozzi E, Lunghi G, Di Biase E, Fazzari M, Sonnino S, Mauri L. GM1 Ganglioside Is A Key Factor in Maintaining the Mammalian Neuronal Functions Avoiding Neurodegeneration. Int J Mol Sci [Internet]. 2020 Jan 29 [cited 2021 Mar 24];21(3). Available from: https://www.ncbi.nlm.nih.gov/pmc/articles/PMC7037093/

125. Forsayeth J, Hadaczek P. Ganglioside Metabolism and Parkinson's Disease. Front Neurosci [Internet]. 2018 [cited 2021 Mar 24];12. Available from: https://www.frontiersin.org/articles/10.3389/fnins.2018.00045/full

126. Wu G, Lu Z-H, Kulkarni N, Ledeen RW. Deficiency of ganglioside GM1 correlates with Parkinson's disease in mice and humans. J Neurosci Res. 2012;90(10):1997–2008.

127. Agholme L, Lindström T, Kågedal K, Marcusson J, Hallbeck M. An in vitro model for neuroscience: differentiation of SH-SY5Y cells into cells with morphological and biochemical characteristics of mature neurons. J Alzheimers Dis JAD. 2010;20(4):1069–82.

128. Avola R, Graziano ACE, Pannuzzo G, Albouchi F, Cardile V. New insights on Parkinson's disease from differentiation of SH-SY5Y into dopaminergic neurons: An involvement of aquaporin4 and 9. Mol Cell Neurosci. 2018;88:212–21.

129. Ross RA, Biedler JL. Presence and regulation of tyrosinase activity in human neuroblastoma cell variants in vitro. Cancer Res. 1985 Apr;45(4):1628–32.

130. Påhlman S, Ruusala AI, Abrahamsson L, Mattsson ME, Esscher T. Retinoic acid-induced differentiation of cultured human neuroblastoma cells: a comparison with phorbolester-induced differentiation. Cell Differ. 1984 Jun;14(2):135–44.

131. Gusel'nikova VV, Korzhevskiy DE. NeuN As a Neuronal Nuclear Antigen and Neuron Differentiation Marker. Acta Naturae. 2015;7(2):42–7.

132. Rebhan M, Vacun G, Bayreuther K, Rösner H. Altered ganglioside expression by SH-SY5Y cells upon retinoic acid-induced neuronal differentiation. Neuroreport. 1994 Apr 14;5(8):941–4.

133. Krishna A, Biryukov M, Trefois C, Antony PM, Hussong R, Lin J, et al. Systems genomics evaluation of the SH-SY5Y neuroblastoma cell line as a model for Parkinson's disease. BMC Genomics. 2014 Dec 20;15(1):1154.

134. Boyle JP, Hettiarachchi NT, Wilkinson JA, Pearson HA, Scragg JL, Lendon C, et al. Cellular consequences of the expression of Alzheimer's disease-causing presenilin 1 mutations in human neuroblastoma (SH-SY5Y) cells. Brain Res. 2012 Mar 14;1443:75–88.

135. Constantinescu R, Constantinescu AT, Reichmann H, Janetzky B. Neuronal differentiation and long-term culture of the human neuroblastoma line SH-SY5Y. In: Gerlach M, Deckert J, Double K, Koutsilieri E, editors. Neuropsychiatric Disorders An Integrative Approach [Internet]. Vienna: Springer Vienna; 2007 [cited 2019 May 11]. p. 17–28. Available from: http://link.springer.com/10.1007/978-3-211-73574-9_3

136. Mustapić M, Glumac Z, Heffer M, Zjalić M, Prološčić I, Masud M, et al. AC/DC magnetic device for safe medical use of potentially harmful magnetic nanocarriers. J Hazard Mater. 2021 May 5;409:124918.

137. Inokuchi J, Kuroda Y, Kosaka S, Fujiwara M. L-threo-1-phenyl-2-decanoylamino-3-morpholino-1-propanol stimulates ganglioside biosynthesis, neurite outgrowth and synapse formation in cultured cortical neurons, and ameliorates memory deficits in ischemic rats. Acta Biochim Pol. 1998;45(2):479–92.

138. Chujor CSN, Feingold KR, Elias PM, Holleran WM. Glucosylceramide synthase activity in murine epidermis: quantitation, localization, regulation, and requirement for barrier homeostasis. J Lipid Res. 1998 Feb 1;39(2):277–85.

139. Lee L, Abe A, Shayman JA. Improved Inhibitors of Glucosylceramide Synthase. J Biol Chem. 1999 May 21;274(21):14662–9.

140. Lewis AC, Wallington-Beddoe CT, Powell JA, Pitson SM. Targeting sphingolipid metabolism as an approach for combination therapies in haematological malignancies. Cell Death Discov. 2018 Jun 28;4(1):1–11.

141. Yamane M. Palmitoyl-ceramide accumulation with necrotic cell death in A549 cells, followed by a steep increase in sphinganine content. Biochim Open. 2015 Jan 1;1:11–27.

142. Miglustat [Internet]. [cited 2021 Mar 14]. Available from: https://go.drugbank.com/drugs/DB00419

143. Weinreb NJ, Barranger JA, Charrow J, Grabowski GA, Mankin HJ, Mistry P. Guidance on the use of miglustat for treating patients with type 1 Gaucher disease. Am J Hematol. 2005 Nov;80(3):223–9.

144. Ficicioglu C. Review of miglustat for clinical management in Gaucher disease type 1. Ther Clin Risk Manag. 2008 Apr;4(2):425–31.

145. Schueler UH, Kolter T, Kaneski CR, Zirzow GC, Sandhoff K, Brady RO. Correlation between enzyme activity and substrate storage in a cell culture model system for Gaucher disease. J Inherit Metab Dis. 2004 Sep 1;27(5):649–58.

146. Zavesca (Miglustat): Uses, Dosage, Side Effects, Interactions, Warning [Internet]. RxList. [cited 2021 Mar 14]. Available from: https://www.rxlist.com/zavesca-drug.htm

147. Hiremath P, Nuguru K, Agrahari V. Chapter 8 - Material Attributes and Their Impact on Wet Granulation Process Performance. In: Narang AS, Badawy SIF, editors. Handbook of Pharmaceutical Wet Granulation [Internet]. Academic Press; 2019 [cited 2021 Mar 14]. p. 263–315. Available from: https://www.sciencedirect.com/science/article/pii/B9780128104606000129

148. Kurakula M, Rao GSNK. Pharmaceutical assessment of polyvinylpyrrolidone (PVP): As excipient from conventional to controlled delivery systems with a spotlight on COVID-19 inhibition. J Drug Deliv Sci Technol. 2020 Dec;60:102046.

149. Polyvinylpyrrolidone Undefined, K 30 | 9003-39-8 | Sigma-Aldrich [Internet]. [cited 2021 Mar 14]. Available from: https://www.sigmaaldrich.com/catalog/product/sial/81420?lang=en&region=HR

150. PubChem. Magnesium stearate [Internet]. [cited 2021 Mar 14]. Available from: https://pubchem.ncbi.nlm.nih.gov/compound/11177

151. Pandey VN, Tiwari N, Pandey VS, Rao A, Das I. Chapter 13 - Targeted drug delivery and gene therapy through natural biodegradable nanostructures in pharmaceuticals. In: Grumezescu AM, editor. Nanoarchitectonics in Biomedicine [Internet]. William Andrew Publishing; 2019 [cited 2021 Mar 14]. p. 437–72. Available from: https://www.sciencedirect.com/science/article/pii/B9780128162002000128

152. PubChem. Titanium dioxide [Internet]. [cited 2021 Mar 14]. Available from: https://pubchem.ncbi.nlm.nih.gov/compound/26042

153. Koopman G, Reutelingsperger CP, Kuijten GA, Keehnen RM, Pals ST, van Oers MH. Annexin V for flow cytometric detection of phosphatidylserine expression on B cells undergoing apoptosis. Blood. 1994 Sep 1;84(5):1415–20.

154. Annexin V staining assay protocol for apoptosis | Abcam [Internet]. [cited 2019 May 9]. Available from: https://www.abcam.com/protocols/annexin-v-detection-protocol-for-apoptosis

155. Ziomek CA. The use of fluorescein isothiocyanate (FITC) as a short-term cell lineage marker in the peri-implantation mouse embryo. Wilhelm Rouxs Arch Dev Biol. 1982 Jan 1;191(1):37–41.

156. Rueden CT, Schindelin J, Hiner MC, DeZonia BE, Walter AE, Arena ET, et al. ImageJ2: ImageJ for the next generation of scientific image data. BMC Bioinformatics. 2017 Nov 29;18(1):529.

157. Home — Spyder IDE [Internet]. [cited 2021 Mar 10]. Available from: https://www.spyder-ide.org/

158. Ho S-Y, Chao C-Y, Huang H-L, Chiu T-W, Charoenkwan P, Hwang E. NeurphologyJ: An automatic neuronal morphology quantification method and its application in pharmacological discovery. BMC Bioinformatics. 2011 Jun 8;12(1):230.

159. Bligh EG, Dyer WJ. A RAPID METHOD OF TOTAL LIPID EXTRACTION AND PURIFICATION. Can J Biochem Physiol [Internet]. 2011 Feb 2 [cited 2021 Mar 11]; Available from: https://cdnsciencepub.com/doi/abs/10.1139/o59-099

160. R: a language and environment for statistical computing [Internet]. [cited 2020 Jul 29]. Available from: https://www.gbif.org/tool/81287/r-a-language-and-environment-for-statistical-computing

161. Bradford MM. A rapid and sensitive method for the quantitation of microgram quantities of protein utilizing the principle of protein-dye binding. Anal Biochem. 1976 May 7;72(1):248–54.

162. Ladner CL, Yang J, Turner RJ, Edwards RA. Visible fluorescent detection of proteins in polyacrylamide gels without staining. Anal Biochem. 2004 Mar 1;326(1):13–20.

163. Fluorescent Protein Visualization Immediately After Gel Electrophoresis Using an In-Gel Trichloroethanol Photoreaction with Tryptophan | Springer Nature Experiments [Internet]. [cited 2021 Mar 2]. Available from: https://experiments.springernature.com/articles/10.1007/978-1-4939-8745-0_22

164. Chavez JA, Siddique MM, Wang ST, Ching J, Shayman JA, Summers SA. Ceramides and Glucosylceramides Are Independent Antagonists of Insulin Signaling. J Biol Chem. 2014 Jan 10;289(2):723–34.

165. Sano R, Annunziata I, Patterson A, Moshiach S, Gomero E, Opferman J, et al. GM1-ganglioside accumulation at the mitochondria-associated ER membranes links ER stress to Ca2+-dependent mitochondrial apoptosis. Mol Cell. 2009 Nov 13;36(3):500–11.

166. d'Azzo A, Tessitore A, Sano R. Gangliosides as apoptotic signals in ER stress response. Cell Death Differ. 2006 Mar;13(3):404–14.

167. Peruzzi F, Prisco M, Morrione A, Valentinis B, Baserga R. Anti-apoptotic Signaling of the Insulin-like Growth Factor-I Receptor through Mitochondrial Translocation of c-Raf and Nedd4 *. J Biol Chem. 2001 Jul 13;276(28):25990–6.

168. Cai W, Sakaguchi M, Kleinridders A, Gonzalez-Del Pino G, Dreyfuss JM, O'Neill BT, et al. Domain-dependent effects of insulin and IGF-1 receptors on signalling and gene expression. Nat Commun [Internet]. 2017 Mar 27 [cited 2021 Apr 7];8. Available from: https://www.ncbi.nlm.nih.gov/pmc/articles/PMC5378997/

169. Suen D-F, Norris KL, Youle RJ. Mitochondrial dynamics and apoptosis. Genes Dev. 2008 Jun 15;22(12):1577–90.

170. Strober W. Trypan Blue Exclusion Test of Cell Viability. Curr Protoc Immunol. 2015 Nov 2;111:A3.B.1-A3.B.3.

171. Garofalo T, Giammarioli AM, Misasi R, Tinari A, Manganelli V, Gambardella L, et al. Lipid microdomains contribute to apoptosis-associated modifications of mitochondria in T cells. Cell Death Differ. 2005 Nov;12(11):1378–89.

172. Hwang J, Lee S, Lee JT, Kwon TK, Kim DR, Kim H, et al. Gangliosides induce autophagic cell death in astrocytes. Br J Pharmacol. 2010 Feb 1;159(3):586–603.

173. De Abreu Costa L, Henrique Fernandes Ottoni M, Dos Santos MG, Meireles AB, Gomes de Almeida V, De Fátima Pereira W, et al. Dimethyl Sulfoxide (DMSO) Decreases Cell Proliferation and TNF-α, IFN-γ, and IL-2 Cytokines Production in Cultures of Peripheral Blood Lymphocytes. Molecules. 2017 Nov;22(11):1789.

174. Tunçer S, Gurbanov R, Sheraj I, Solel E, Esenturk O, Banerjee S. Low dose dimethyl sulfoxide driven gross molecular changes have the potential to interfere with various cellular processes. Sci Rep. 2018 Oct 4;8(1):14828.

175. Chatterjee S, Alsaeedi N, Hou J, Bandaru VVR, Wu L, Halushka MK, et al. Use of a Glycolipid Inhibitor to Ameliorate Renal Cancer in a Mouse Model. PLOS ONE. 2013 May 9;8(5):e63726.

176. Sasaki A, Hata K, Suzuki S, Sawada M, Wada T, Yamaguchi K, et al. Overexpression of Plasma Membrane-associated Sialidase Attenuates Insulin Signaling in Transgenic Mice*. J Biol Chem. 2003 Jul 25;278(30):27896–902.

177. Huo H, Guo X, Hong S, Jiang M, Liu X, Liao K. Lipid rafts/caveolae are essential for insulin-like growth factor-1 receptor signaling during 3T3-L1 preadipocyte differentiation induction. J Biol Chem. 2003 Mar 28;278(13):11561–9.

178. Beesley PW, Herrera-Molina R, Smalla K-H, Seidenbecher C. The Neuroplastin adhesion molecules: key regulators of neuronal plasticity and synaptic function. J Neurochem. 2014;131(3):268–83.

179. Cho YY, Kwon O-H, Chung S. Preferred endocytosis of amyloid precursor protein from cholesterol-enriched lipid raft microdomains. bioRxiv. 2020 Jun 26;2020.06.26.172874.

180. Heffer-Lauc M, Viljetiæ B, Vajn K, Schnaar RL, Lauc G. Effects of Detergents on the Redistribution of Gangliosides and GPI-anchored Proteins in Brain Tissue Sections. J Histochem Cytochem Off J Histochem Soc. 2007 Aug;55(8):805–12.

181. Myelin oligodendrocyte glycoprotein antibody-associated disease: an immunopathological study | Brain | Oxford Academic [Internet]. [cited 2021 Apr 11]. Available from: https://academic.oup.com/brain/article-abstract/143/5/1431/5837518

182. Williams G, Wood A, Williams E-J, Gao Y, Mercado ML, Katz A, et al. Ganglioside inhibition of neurite outgrowth requires Nogo receptor function: identification of interaction sites and development of novel antagonists. J Biol Chem. 2008 Jun 13;283(24):16641–52.

183. GM1 ganglioside-bound amyloid beta-protein (A beta): a possible form of preamyloid in Alzheimer's disease - PubMed [Internet]. [cited 2021 Mar 7]. Available from: https://pubmed.ncbi.nlm.nih.gov/7489364/

184. Vemula SK, Malci A, Junge L, Lehmann A-C, Rama R, Hradsky J, et al. The Interaction of TRAF6 With Neuroplastin Promotes Spinogenesis During Early Neuronal Development. Front Cell Dev Biol [Internet]. 2020 [cited 2021 Apr 11];8. Available from: https://www.frontiersin.org/articles/10.3389/fcell.2020.579513/full

185. Ahyayauch H, de la Arada I, Masserini ME, Arrondo JLR, Goñi FM, Alonso A. The Binding of Aβ42 Peptide Monomers to Sphingomyelin/Cholesterol/Ganglioside Bilayers Assayed by Density Gradient Ultracentrifugation. Int J Mol Sci. 2020 Jan;21(5):1674.

186. Sasaki N, Itakura Y, Toyoda M. Ganglioside GM1 Contributes to the State of Insulin Resistance in Senescent Human Arterial Endothelial Cells. J Biol Chem. 2015 Oct 16;290(42):25475–86.

187. Hossain MU, Khan MA, Rakib-Uz-Zaman SM, Ali MT, Islam MS, Keya CA, et al. Treating Diabetes Mellitus: Pharmacophore Based Designing of Potential Drugs from Gymnema sylvestre against Insulin Receptor Protein. BioMed Res Int. 2016 Feb 28;2016:e3187647.

188. Usuki S, Hamanoue M, Kohsaka S, Inokuchi J. Induction of Ganglioside Biosynthesis and Neurite Outgrowth of Primary Cultured Neurons by l-threo-1-Phenyl-2-Decanoylamino-3-Morpholino-1-Propanol. J Neurochem. 1996;67(5):1821–30.

189. Benady A, Freidin D, Pick CG, Rubovitch V. GM1 ganglioside prevents axonal regeneration inhibition and cognitive deficits in a mouse model of traumatic brain injury. Sci Rep. 2018 Sep 6;8(1):13340.

190. Lázár BA, Jancsó G, Pálvölgyi L, Dobos I, Nagy I, Sántha P. Insulin Confers Differing Effects on Neurite Outgrowth in Separate Populations of Cultured Dorsal Root Ganglion Neurons: The Role of the Insulin Receptor. Front Neurosci [Internet]. 2018 Oct 10 [cited 2021 Apr 8];12. Available from: https://www.ncbi.nlm.nih.gov/pmc/articles/PMC6191510/

191. Lingwood CA. Glycosphingolipid Functions. Cold Spring Harb Perspect Biol [Internet]. 2011 Jul [cited 2021 Apr 8];3(7). Available from: https://www.ncbi.nlm.nih.gov/pmc/articles/PMC3119914/

192. Inokuchi J, Usuki S, Jimbo M. Stimulation of glycosphingolipid biosynthesis by L-threo-1-phenyl-2-decanoylamino-1-propanol and its homologs in B16 melanoma cells. J Biochem (Tokyo). 1995 Apr;117(4):766–73.

193. Schwarz A, Rapaport E, Hirschberg K, Futerman AH. A Regulatory Role for Sphingolipids in Neuronal Growth: INHIBITION OF SPHINGOLIPID SYNTHESIS AND DEGRADATION HAVE OPPOSITE EFFECTS ON AXONAL BRANCHING *. J Biol Chem. 1995 May 5;270(18):10990–8.

194. Ferreira A, Busciglio J, Landa C, Caceres A. Ganglioside-enhanced neurite growth: evidence for a selective induction of high-molecular-weight MAP-2. J Neurosci. 1990 Jan 1;10(1):293–302.

195. Fang Y, Wu G, Xie X, Lu Z-H, Ledeen RW. Endogenous GM1 Ganglioside of the Plasma Membrane Promotes Neuritogenesis by Two Mechanisms. Neurochem Res. 2000 Jul 1;25(7):931–40.

196. Lushchak VI. Dissection of the Hormetic Curve: Analysis of Components and Mechanisms. Dose-Response. 2014 Apr 11;12(3):466–79.

197. Henriques A, Huebecker M, Blasco H, Keime C, Andres CR, Corcia P, et al. Inhibition of β-Glucocerebrosidase Activity Preserves Motor Unit Integrity in a Mouse Model of Amyotrophic Lateral Sclerosis. Sci Rep. 2017 Jul 12;7(1):5235.

198. Suzuki R, Lee K, Jing E, Biddinger SB, McDonald JG, Montine TJ, et al. Diabetes and Insulin in Regulation of Brain Cholesterol Metabolism. Cell Metab. 2010 Dec 1;12(6):567–79.

199. Sokolowska E, Blachnio-Zabielska A. The Role of Ceramides in Insulin Resistance. Front Endocrinol [Internet]. 2019 Aug 21 [cited 2021 Apr 11];10. Available from: https://www.ncbi.nlm.nih.gov/pmc/articles/PMC6712072/

200. Hansen ME, Tippetts TS, Anderson MC, Holub ZE, Moulton ER, Swensen AC, et al. Insulin Increases Ceramide Synthesis in Skeletal Muscle. J Diabetes Res. 2014 May 18;2014:e765784.

201. Ocaya PA, Elmabsout AA, Olofsson PS, Törmä H, Gidlöf AC, Sirsjö A. CYP26B1 Plays a Major Role in the Regulation of All-trans-Retinoic Acid Metabolism and Signaling in Human Aortic Smooth Muscle Cells. J Vasc Res. 2011;48(1):23–30.

202. Armstrong JL, Ruiz M, Boddy AV, Redfern CPF, Pearson ADJ, Veal GJ. Increasing the intracellular availability of all-trans retinoic acid in neuroblastoma cells. Br J Cancer. 2005 Feb 28;92(4):696–704.

203. Pasquali D, Chieffi P, Deery WJ, Nicoletti G, Bellastella A, Sinisi AA. Differential effects of all-trans-retinoic acid (RA) on Erk1/2 phosphorylation and cAMP accumulation in normal and malignant human prostate epithelial cells: Erk1/2 inhibition restores RA-induced decrease of cell growth in malignant prostate cells. Eur J Endocrinol. 2005 Apr 1;152(4):663–9.

204. KEGG PATHWAY: Ferroptosis - Reference pathway [Internet]. [cited 2021 Apr 18]. Available from: https://www.genome.jp/kegg-bin/show_pathway?map04216+C21480

205. Shen L, Lin D, Li X, Wu H, Lenahan C, Pan Y, et al. Ferroptosis in Acute Central Nervous System Injuries: The Future Direction? Front Cell Dev Biol [Internet]. 2020 [cited 2021 Apr 18];8. Available from: https://www.frontiersin.org/articles/10.3389/fcell.2020.00594/full

206. Yan H, Zou T, Tuo Q, Xu S, Li H, Belaidi AA, et al. Ferroptosis: mechanisms and links with diseases. Signal Transduct Target Ther. 2021 Feb 3;6(1):1–16.

207. Donovan EL, Pettine SM, Hickey MS, Hamilton KL, Miller BF. Lipidomic analysis of human plasma reveals ether-linked lipids that are elevated in morbidly obese humans compared to lean. Diabetol Metab Syndr. 2013 May 14;5(1):24.

208. Singh DK, Porter TD. Inhibition of Sterol 4α-Methyl Oxidase Is the Principal Mechanism by Which Garlic Decreases Cholesterol Synthesis. J Nutr. 2006 Mar 1;136(3):759S-764S.

209. KEGG MODULE: M00101 [Internet]. [cited 2021 Apr 18]. Available from: https://www.genome.jp/kegg-bin/show_module?M00101+C05103

210. Angelini R, Yutuc E, Wyatt MF, Newton J, Yusuf FA, Griffiths L, et al. Visualising Cholesterol in Brain by On-Tissue Derivatisation and Quantitative Mass Spectrometry Imaging. bioRxiv. 2020 Nov 7;2020.11.06.369447.

211. Porphyria - Symptoms and causes [Internet]. Mayo Clinic. [cited 2021 Apr 18]. Available from: https://www.mayoclinic.org/diseases-conditions/porphyria/symptoms-causes/syc-20356066

212. Nishida K, Tojo T, Kondo T, Yuasa M. Evaluation of the correlation between porphyrin accumulation in cancer cells and functional positions for application as a drug carrier. Sci Rep. 2021 Jan 21;11(1):2046.

213. Lejri I, Grimm A, Hallé F, Abarghaz M, Klein C, Maitre M, et al. TSPO Ligands Boost Mitochondrial Function and Pregnenolone Synthesis. J Alzheimers Dis. 72(4):1045–58.

214. Arbo BD, Marques CV, Ruiz-Palmero I, Ortiz-Rodriguez A, Ghorbanpoor S, Arevalo MA, et al. 4′-Chlorodiazepam is neuroprotective against amyloid-beta through the modulation of survivin and bax protein expression in vitro. Brain Res. 2016 Feb 1;1632:91–7.

215. Hasegawa T, Matsuzaki M, Takeda A, Kikuchi A, Furukawa K, Shibahara S, et al. Increased dopamine and its metabolites in SH-SY5Y neuroblastoma cells that express tyrosinase. J Neurochem. 2003;87(2):470–5.

216. Chongthammakun V, Sanvarinda Y, Chongthammakun S. Reactive oxygen species production and MAPK activation are implicated in tetrahydrobiopterin-induced SH-SY5Y cell death. Neurosci Lett. 2009 Jan 16;449(3):178–82.

217. Choi HJ, Kim SW, Lee SY, Hwang O. Dopamine-dependent cytotoxicity of tetrahydrobiopterin: a possible mechanism for selective neurodegeneration in Parkinson's disease. J Neurochem. 2003;86(1):143–52.

218. Ishi M, Shimizu S, Nagai T, Kiuchi Y, Yamamoto T. Insulin Stimulates Tetrahydrobiopterin Synthesis in Mouse Brain Microvascular Endothelial Cells. Pteridines. 1999 Nov 1;10(4):213–6.

219. Armeni T, Cianfruglia L, Piva F, Urbanelli L, Luisa Caniglia M, Pugnaloni A, et al. S-D-Lactoylglutathione can be an alternative supply of mitochondrial glutathione. Free Radic Biol Med. 2014 Feb 1;67:451–9.

220. Moutinho M, Nunes MJ, Correia JC, Gama MJ, Castro-Caldas M, Cedazo-Minguez A, et al. Neuronal cholesterol metabolism increases dendritic outgrowth and synaptic markers via a concerted action of GGTase-I and Trk. Sci Rep. 2016 Aug 5;6(1):30928.

221. Parsons RB, Aravindan S, Kadampeswaran A, Evans EA, Sandhu KK, Levy ER, et al. The expression of nicotinamide N-methyltransferase increases ATP synthesis and protects SH-SY5Y neuroblastoma cells against the toxicity of Complex I inhibitors. Biochem J. 2011 Apr 27;436(1):145–55.

222. Thomas MG, Saldanha M, Mistry RJ, Dexter DT, Ramsden DB, Parsons RB. Nicotinamide N-methyltransferase expression in SH-SY5Y neuroblastoma and N27 mesencephalic neurones induces changes in cell morphology via ephrin-B2 and Akt signalling. Cell Death Dis. 2013 Jun;4(6):e669.

223. Tyurina YY, Tyurin VA, Avrova NF. Ganglioside GM1 protects cAMP 3′ 5′: Phosphodiesterase from inactivation caused by lipid peroxidation in brain synaptosomes of rats. Mol Chem Neuropathol. 1993 Aug 1;19(3):205–17.

224. Bergeron A, Guillemette C, Sirard M-A, Richard FJ, Bergeron A, Guillemette C, et al. Active 3′–5′ cyclic nucleotide phosphodiesterases are present in detergent-resistant membranes of mural granulosa cells. Reprod Fertil Dev. 2017 Apr 10;29(4):778–90.

225. Marques ARA, Mirzaian M, Akiyama H, Wisse P, Ferraz MJ, Gaspar P, et al. Glucosylated cholesterol in mammalian cells and tissues: formation and degradation by multiple cellular β-glucosidases. J Lipid Res. 2016 Mar;57(3):451–63.

226. Kraft VAN, Bezjian CT, Pfeiffer S, Ringelstetter L, Müller C, Zandkarimi F, et al. GTP Cyclohydrolase 1/Tetrahydrobiopterin Counteract Ferroptosis through Lipid Remodeling. ACS Cent Sci. 2020 Jan 22;6(1):41–53.

227. Monti E, Miyagi T. Structure and Function of Mammalian Sialidases. In: Gerardy-Schahn R, Delannoy P, von Itzstein M, editors. SialoGlyco Chemistry and Biology I: Biosynthesis, structural diversity and sialoglycopathologies [Internet]. Berlin, Heidelberg: Springer; 2015 [cited 2021 Apr 26]. p. 183–208. (Topics in Current Chemistry). Available from: https://doi.org/10.1007/128_2012_328

228. Rashed AA, Ahmad H, Abdul Khalid SK, Rathi D-NG. The Potential Use of Sialic Acid From Edible Bird's Nest to Attenuate Mitochondrial Dysfunction by In Vitro Study. Front Pharmacol [Internet]. 2021 [cited 2021 Apr 26];12. Available from: https://www.frontiersin.org/articles/10.3389/fphar.2021.633303/full

229. Manning BD, Toker A. AKT/PKB Signaling: Navigating the Network. Cell. 2017 Apr 20;169(3):381–405.

230. Wei Y, Zhou J, Yu H, Jin X. AKT phosphorylation sites of Ser473 and Thr308 regulate AKT degradation. Biosci Biotechnol Biochem. 2019 Mar 4;83(3):429–35.

231. Wegner M-S, Schömel N, Gruber L, Örtel SB, Kjellberg MA, Mattjus P, et al. UDP-glucose ceramide glucosyltransferase activates AKT, promoted proliferation, and doxorubicin resistance in breast cancer cells. Cell Mol Life Sci. 2018 Sep 1;75(18):3393–410.

232. Yang L, Wang H, Liu L, Xie A. The Role of Insulin/IGF-1/PI3K/Akt/GSK3β Signaling in Parkinson's Disease Dementia. Front Neurosci [Internet]. 2018 [cited 2021 Apr 30];12. Available from: https://www.frontiersin.org/articles/10.3389/fnins.2018.00073/full

233. Krishnankutty A, Kimura T, Saito T, Aoyagi K, Asada A, Takahashi S-I, et al. In vivo regulation of glycogen synthase kinase 3β activity in neurons and brains. Sci Rep. 2017 Aug 17;7(1):8602.

234. Failor KL, Desyatnikov Y, Finger LA, Firestone GL. Glucocorticoid-Induced Degradation of Glycogen Synthase Kinase-3 Protein Is Triggered by Serum- and Glucocorticoid-Induced Protein Kinase and Akt Signaling and Controls β-Catenin Dynamics and Tight Junction Formation in Mammary Epithelial Tumor Cells. Mol Endocrinol. 2007 Oct 1;21(10):2403–15.

235. Hoffmeister L, Diekmann M, Brand K, Huber R. GSK3: A Kinase Balancing Promotion and Resolution of Inflammation. Cells. 2020 Apr;9(4):820.

236. Robertson H, Hayes JD, Sutherland C. A partnership with the proteasome; the destructive nature of GSK3. Biochem Pharmacol. 2018 Jan 1;147:77–92.

237. Noel A, Ingrand S, Barrier L. Inhibition of GSK3β by pharmacological modulation of sphingolipid metabolism occurs independently of ganglioside disturbance in a cellular model of Alzheimer's disease. Exp Neurol. 2015 Sep 1;271:308–18.

238. Plotegher N, Bubacco L, Greggio E, Civiero L. Ceramides in Parkinson's Disease: From Recent Evidence to New Hypotheses. Front Neurosci [Internet]. 2019 [cited 2021 May 1];13. Available from: https://www.frontiersin.org/articles/10.3389/fnins.2019.00330/full

239. Mlinac K, Jovanov Milošević N, Heffer M, Smalla K-H, Schnaar RL, Kalanj Bognar S. Neuroplastin Expression in the Hippocampus of Mice Lacking Complex Gangliosides. J Mol Neurosci. 2012 Sep 1;48(1):161–6.

240. Zha Q, Ruan Y, Hartmann T, Beyreuther K, Zhang D. GM1 ganglioside regulates the proteolysis of amyloid precursor protein. Mol Psychiatry. 2004 Oct;9(10):946–52.

241. Leissring MA, González-Casimiro CM, Merino B, Suire CN, Perdomo G. Targeting Insulin-Degrading Enzyme in Insulin Clearance. Int J Mol Sci. 2021 Jan;22(5):2235.

242. Hřebíček M, Hodaňová K, Ledvinová J, Sokolová J, Elleder M, Zeman J, et al. A case of type I Gaucher disease with cardiopulmonary amyloidosis and chitotriosidase deficiency. Virchows Arch. 1996 Nov 1;429(4):305–9.

243. Hanash SM, Rucknagel DL, Heidelberger KP, Radin NS. Primary Amyloidosis Associated with Gaucher's Disease. Ann Intern Med. 1978 Nov 1;89(5_Part_1):639–41.

244. Neddens J, Temmel M, Flunkert S, Kerschbaumer B, Hoeller C, Loeffler T, et al. Phosphorylation of different tau sites during progression of Alzheimer's disease. Acta Neuropathol Commun. 2018 Jun 29;6(1):52.

245. Toral-Rios D, Pichardo-Rojas PS, Alonso-Vanegas M, Campos-Peña V. GSK3β and Tau Protein in Alzheimer's Disease and Epilepsy. Front Cell Neurosci [Internet]. 2020 [cited 2021 May 2];14. Available from: https://www.frontiersin.org/articles/10.3389/fncel.2020.00019/full

246. Freude S, Plum L, Schnitker J, Leeser U, Udelhoven M, Krone W, et al. Peripheral Hyperinsulinemia Promotes Tau Phosphorylation In Vivo. Diabetes. 2005 Dec 1;54(12):3343–8.

247. Gonçalves RA, Wijesekara N, Fraser PE, De Felice FG. The Link Between Tau and Insulin Signaling: Implications for Alzheimer's Disease and Other Tauopathies. Front Cell Neurosci [Internet]. 2019 Feb 5 [cited 2021 May 2];13. Available from: https://www.ncbi.nlm.nih.gov/pmc/articles/PMC6371747/

248. Shin M-K, Choi M-S, Chae H-J, Kim J-W, Kim H-G, Kim K-L. Ganglioside GQ1b ameliorates cognitive impairments in an Alzheimer's disease mouse model, and causes reduction of amyloid precursor protein. Sci Rep. 2019 Jun 11;9(1):8512.

249. Wei J, Takamatsu Y, Wada R, Fujita M, Ho G, Masliah E, et al. Therapeutic Potential of αS Evolvability for Neuropathic Gaucher Disease. Biomolecules. 2021 Feb;11(2):289.

250. Sardi SP, Clarke J, Viel C, Chan M, Tamsett TJ, Treleaven CM, et al. Augmenting CNS glucocerebrosidase activity as a therapeutic strategy for parkinsonism and other Gaucher-related synucleinopathies. Proc Natl Acad Sci U S A. 2013 Feb 26;110(9):3537–42.

251. Beck M. The Link Between Lysosomal Storage Disorders and More Common Diseases. J Inborn Errors Metab Screen. 2016 Jan 1;4:2326409816682767.

252. Schapira AHV, Gegg ME. Glucocerebrosidase in the pathogenesis and treatment of Parkinson disease. Proc Natl Acad Sci. 2013 Feb 26;110(9):3214–5.

253. Niederkofler V, Auer E, Amschl D, Neddens J, Hutter-Paier B. CBE treatment of alpha-synuclein over-expressing and wildtype mice models Gaucher disease pathology. Mol Genet Metab. 2019 Feb 1;126(2):S108–9.

254. Papadopoulos VE, Nikolopoulou G, Antoniadou I, Karachaliou A, Arianoglou G, Emmanouilidou E, et al. Modulation of β-glucocerebrosidase increases α-synuclein secretion and exosome release in mouse models of Parkinson's disease. Hum Mol Genet. 2018 May 15;27(10):1696–710.

255. McGlinchey RP, Lee JC. Emerging Insights into the Mechanistic Link between α-Synuclein and Glucocerebrosidase in Parkinson's Disease. Biochem Soc Trans. 2013 Dec;41(6):1509–12.

256. Matsumoto T, Hatakeyama S, Yoneyama T, Tobisawa Y, Ishibashi Y, Yamamoto H, et al. Serum N -glycan profiling is a potential biomarker for castration-resistant prostate cancer. Sci Rep. 2019 Nov 14;9(1):16761.

257. Peixoto A, Relvas-Santos M, Azevedo R, Santos LL, Ferreira JA. Protein Glycosylation and Tumor Microenvironment Alterations Driving Cancer Hallmarks. Front Oncol [Internet]. 2019 [cited 2021 May 3];9. Available from: https://www.frontiersin.org/articles/10.3389/fonc.2019.00380/full

258. Jensterle M, Kravos NA, Goričar K, Janez A. Short-term effectiveness of low dose liraglutide in combination with metformin versus high dose liraglutide alone in treatment of obese PCOS: randomized trial. BMC Endocr Disord. 2017 Jan 31;17(1):5.

10. BIOGRAPHY

Personal data

Name and surname: Milorad Zjalić

Date and place of birth: 13 September 1991.

Address: Petefi Šandora 40 Darda

Cell phone number: 0989146425

Email: mzjalic@mefos.hr

Education

2006-2010 – Nursing school Osijek

2010-2013 – Bachelor's degree in biology

2013-2016 – Master's degree in experimental biology

Work experience

2016 – Department for medical biology and genetics, Faculty of Medicine Osijek

Published scientific papers

1. Zjalić M, Mustapić M, Glumac Z, Prološčić I, Blažetić S, Vuković A, i ostali. Construction of AC/DC magnetic syringe device for stimulated drug release, injection and ejection of nanocarriers and testing cytotoxicity in vitro. MethodsX. 01. siječanj 2021.;8:101312.

2. Mlinac-Jerkovic K, Ilic K, Zjalić M, Mandić D, Debeljak Ž, Balog M, i ostali. Who's in, who's out? Re-evaluation of lipid raft residents. J Neurochem; DOI 10.1111/jnc.15446

3. Mustapić M, Glumac Z, Heffer M, Zjalić M, Prološčić I, Masud M, i ostali. AC/DC magnetic device for safe medical use of potentially harmful magnetic nanocarriers. J Hazard Mater. 2021.;409:124918.

4. Fenrich M, Mrdenovic S, Balog M, Tomic S, Zjalic M, Roncevic A, i ostali. SARS-CoV-2 Dissemination Through Peripheral Nerves Explains Multiple Organ Injury. Front. Cell. Neurosci., August 2020 | https://doi.org/10.3389/fncel.2020.00229

5. Debeljak Ž, Niehoff A-C, Bandjak A, Mandić D, Bošnjak B, Heffer M, Stefan Mrđenović, Ivana Marković, Milorad Zjalić, Vatroslav Šerić. MALDI TOF Mass Spectrometry Imaging of Blood Smear: Method Development and Evaluation. Int J Mol Sci. siječanj 2021.;22(2):585.

6. Labak I, Pavić V, Zjalić M, Blažetić S, Viljetić B, Merdić E, i ostali. PSA-NCAM expression in the teleost optic tectum is related to ecological niche and use of vision in finding food. J Fish Biol. 2017.;91(2):473–89.